Universidade de São Paulo
Instituto de Biociências
Departamento de Genética e Biologia Evolutiva

By: **Renato M. Domingos**

Conserved structural and dynamic aspects behind Ohr enzymatic catalysis: Ohr as potential drug targets

"Aspectos estruturais e dinâmicos envolvidos na catálise enzimática das Ohr: Ohr como potenciais alvos de drogas"

São Paulo

2018

By: **Renato Mateus Domingos**

Conserved structural and dynamic aspects behind Ohr enzymatic catalysis: Ohr as potential drug targets

"Aspectos estruturais e dinâmicos envolvidos na catálise enzimática das Ohr: Ohr como potenciais alvos de drogas"

Dissertation submitted to the Institute of Biosciences of University of São Paulo, as a partial requirement to obtain the Doctoral degree in Biological Sciences, in the field of biology/genetics.

Supervisor: Prof. Dr. Luis Eduardo Soares Netto

São Paulo

2018

CATALOGUING DATA

Domingos, Renato Mateus
Conserved structural and dynamic aspects behind Ohr enzymatic catalysis : Ohr as potential drug targets / Renato Mateus Domingos ; orientador Luis Eduardo Soares Netto. – Sao Paulo, 2018.

154 f.

Tese (Doutorado) – Instituto de Biociências da Universidade de São Paulo, Departamento de Genética e Biologia Evolutiva

1. Ohr. 2. Organic hydroperoxide resistance protein. 3. Peroxidase 4. Thiol 5. Dihydrolipoamide. I. Netto, Luis Eduardo Soares, oriente. II. Título.

DISSERTATION COMMITTEE:

Prof. Dr.	Prof. Dr.
Prof. Dr.	Prof. Dr.

Prof. Dr. Luis Eduardo Soares Netto
Supervisor

CONSIDERATIONS

This thesis represents the work developed during 5 years (early 2014 to late 2018), mostly performed in the Laboratory of Proteins and Redox Biology (**PI – Luis E.S. Netto**) at Institute of Biosciences at University of Sao Paulo. Formal collaborations were established at Laboratory of QSAR and Molecular Modeling of Bioactive Compounds (**PI – Antonia T. Amaral**) at Institute of Chemistry; at Laboratory of Applied Structural Biology (**PI – Marcio V.B. Dias**) at Institute of Biomedical Sciences, both at University of Sao Paulo; and also at Laboratory of Theoretical & Computational Chemistry and Molecular Modeling (**PI – Dario A. Estrin**) at Institute of Physical Chemistry of Materials, Environment and Energy at University of Buenos Aires. Most of the crystallography experiments were performed in the crystallography facilities at the Laboratory of Functional and Structural Biology of Secretory Systems (**PI – Chuck S. Farah**) at Institute of Chemistry at University of Sao Paulo. This study was financed in part by the Coordenação de Aperfeiçoamento de Pessoal de Nível Superior – Brasil (CAPES-001); Conselho Nacional de Desenvolvimento Científico e Tecnológico – Brasil (CNPq); Fundação de Amparo à Pesquisa do Estado de São Paulo – Brasil (FAPESP), grant 2013/07937-8, Redox Process in Biomedicine – CEPID program; Center for Structural Biology of MERCOSUR – Mercosur (CeBEM) and Pró-Reitoria de Pós-Graduação da Universidade de São Paulo – Brasil (PRPG).

The thesis was written in the Chapter model in which were included two, already published peer review articles and one article which is still in preparation to be submitted. The manuscripts are presented in their original format as required by the scientific journals where they were submitted to. A fourth article is presented, however further experiments need to be performed in order to be published. Finally, all conference proceedings, courses, and workshops, which contributed to the divulgation of this work and improved the enthusiasm, technical and intellectual skills of the author are summarized in the **Appendix 2**.

This dissertation is dedicated to all of those who mostly shaped my life (family & close friends) and to all Brazilians who directly or indirectly (through public funds) provided me with the opportunity to professionally improve and work with such talented people

Considering the crucial Social Component of scientific research…

Anyone can become angry – that is easy. But to be angry with the right person, to the right degree, at the right time, for the right purpose, and in the right way – this is not easy.
ARISTOTLE, *The Nicomachean Ethics*

Science is made by human interactions – Humans are emotionally dependent and human interactions are not always emotionally desired – To perform cutting-edge science, emotional intelligence must, inevitably, be mastered.
Written while writing this thesis at São Paulo, 21st of June, 2018, sleep deprived, years of cultural shock shaping influences and caffeine inspired

ACKNOWLEDGMENTS

Professionally, these 5 years in Brazil were an incredible challenge and fed up two of the most addictive desires, my curiosity and the ambition of accomplishment. For that I feel that many people must be acknowledged. First, **Luis E.S. Netto** – Luis received an e-mail (2012) from the other side of the ocean, from a totally unknown person and enthusiastically answered. That enthusiasm and trust, touched me straight away. Later I realized it was a personal characteristic and it turned to be very important during the development of my work. Luis always supported and encouraged my scientific development and always let me have some freedom in the way I conducted my research. Professionally, it was a great experience. **Jose F. da Silva Neto** – I had the luck to arrive at the laboratory when he was concluding the last year of pos-doc. He is a such incredible research and academic professional, his way of calmly and deeply explaining the technical procedures involving the most important theoretical concepts totally impressed me when I arrived. Working my first three months with him was greatly inspiring. **Gabriela da Oliveira Silveira** – Professionally, life has no meaning when parallelly there is no investment in a healthy social network. Gabriela was the only true friend I had in Brazil and probably the only one who truly felt my essence. Sharing my time with her was incredibly crucial to provide some balance in the unbalanced life we all have living in São Paulo city. **Vanessa Simões** – Apart from the fact that Vanessa was my first running company she was also very important at the first years, facilitating my adaptation in the country as she always counted on me for several lesure activities, essential to allow me to know people and places. **Raphael Dias Teixeira** – He was crucial improving my learning curve related to X-ray crystallography and all structure related data I generated during my PhD. He always enthusiastically and calmly advised in specific technical procedures and suggesting courses which were essencial to accelerate my understanding and improvement at early stages of my PhD. **Lucas Gasparello Viviani –** Searching for inhibitor compounds was with no doubt one of the goals of my project which captivated me more, although we did not invest as much time as I would like, trying to improve our search, it was a great pleasure to learn with you. **Thiago G. Pires Alegria** – He was the person from my laboratory with who I discussed, practically all my experiments and strategies when trying to develop a publishable concise work. **Fernando Gomes** – He is one of the most outstanding researchers I have met, his high standard personal and professional ethics are amazing. Collaborating in some of his projects was a pleasure. I hope we could keep collaborating, even far apart. **Eduardo Tassoni Tsuchida** – his scientific maturity is natural and intellectually he has no limits. He has a great professional future ahead. It was a pleasure to share the laboratory bench with him and have the opportunity to know him and share several professional and personal thoughts. **Flavio Romero Palma** – He was one of the first persons I have met in Brazil. The most relevant thing I can pick up from my interaction with Flavio, was our daily coffee breaks, during long laboratory experiments, our discussions turned to be very interesting and challenging due to our distinct points of views. **Diogo de Abreu Meireles** – Diogo is a person to whom I must thank for all the professional impact he had due to some work collaborations we performed during my stay in the laboratory. **Rogério Aleixo** – We spent entire days at the Brazilian Synchrotron Light Laboratory performing x-ray experiments. It was a pleasure to share ideas and collaborating with him. **Federico Issoglio** – We met in 2015 in Montevideo in an international course. At the time he was about to begin his pos-doc at University of Buenos Aires with Dario Estrin. In 2017 I reencountered Federico in Rio de Janeiro in a congress. It happened that, during a break, Federico commented with Dario Estrin how interesting would it be if MM and QM-MM simulation were performed with some of my structure. Later, me and Luis Netto joined them and we agreed to try to apply for a studentship to allow my travel to Argentina to learn and perform MM and QM-MM simulations and improve the quality of my research. Five months later, I was arriving in Buenos Aires were Federico did not directly collaborate with me, but he was totally essencial to my instant adaptation to the city and laboratory, which was crucial in the development of my research. **William Agudelo**, **Ari Zeida** and **Dario A. Estrin** – Dario A. Estrin provided me with all conditions for a very productive stay at his laboratory. William and Ari were crucial providing all theoretical and technical basis to perform MM and QM-MM simulations and with their collaboration we were able to really take the most of three months of intense work in Buenos Aires. I must emphasize, William stayed with me until late in the day, several times, calmly explained me the basis of the QM-MM methodology and the computational concepts and it was a pleasure to me to share all the time we shared together. **Jademilson Santos** and **Marcio Dias** – Marcio Dias provided me with all the condition the perform the DSF experiments at his laboratory. Jademilson was responsible for the theoretical and technical training which allow-me to initiate some experiments with their library of fragment of molecules. **Andressa Y. Sakugawa**, **Waldir Caldeira**, **Derik**, **Julia**, **Amanda**, **Simone V. Alves** – The technicians who most, directly interacted in the development of my research providing the best conditions which allowed my work to be always performed efficiently. **Anita M.F. del Guercio, Guadalupe Neri** and **Priscila Santos e Verónica Santiago** – together with Thiago and Derik they were part of the group of people with who I used to run. This did not directly contribute to my research, but for sure, the moments we spent running and having random conversations, contributed to the essential mental relaxation every week. It was a pleasure to share those moments with you. **Cesar**, **Carlos** and **Joao** – Who together with Thiago and Eduardo, shared most of my lunch time when we randomly talked and shared opinions. **Jessica de Sousa –** for all the support and friendship from the very first day I arrived in Sao Paulo. **Danielle de Moura –** Danielle is a great friend of mine and she directly contributed allowing my stay in California during data collection in the SSRL and she has done the proofread of most the important written documents related to my Phd. **Paula Rita Pereira –** Rita is a great friend from my childhood who turned out to be very important during the last stressful months while writing the manuscript of my paper and the dissertation. Sharing relaxed conversation at the end of the days was incredibly important for me. All the **general staff** of Institute of Biosciences and USP who allow our university and institute to run every day. Finally, **CAPES**, **CNPq**, **FAPESP**, **CeBEM** and other funding agencies were essencial to support my living expenses in the city and to perform the work at the laboratory and participate in congresses and courses. CeBEM allowed my stay in Buenos Aires to work at Dario Estrin's laboratory.

INDEX

LIST OF FIGURES I
LIST OF TABLES III
CHAPTER 1 – GENERAL INTRODUCTION 1
1.1 – Oxidative atmosphere evolution 2
1.2 – Oxidative species generation 3
1.2.1 – Respiration *vs* ROS 3
1.2.2 – Lipid peroxidation *vs* ROS 3
1.2.3 – Endogenous mechanisms of ROS generation 4
1.2.4 – Antibiotic-mediated killing mechanisms and ROS generation 5
1.3 – Antioxidant defense 7
1.3.1 – General mechanisms 7
1.3.2 – Overview of specialized sensors of ROS 8
1.3.3 – Thiol dependent peroxidases 9
1.4 – Ohr/OsmC Superfamily of proteins 13
1.4.1 - Primary structure characteristics 13
1.4.2 - Overall structure characteristics 14
1.4.3 – Expression pattern and mutant phenotypes 15
1.4.4 – Phylogenetic distribution of Ohr/OsmC proteins. 17
1.5 - Organic Hydroperoxide Resistance Proteins (Ohr) 18
1.5.1 - Structure characteristics 18
1.5.2 - Proposed Enzymatic Mechanism 19
1.5.3 – Possible oxidant substrates of Ohr 20
1.5.4 – Ohr reductant substrates 21
1.5.5 – Ohr and virulence 21
1.5.6 - Ohr as a Potential Drug target 23
1.6 – References 24
CHAPTER 2 – FUNCTIONAL AND EVOLUTIONARY CHARACTERIZATION OF OHR PROTEINS IN EUKARYOTES REVEALS MANY ACTIVE HOMOLOGS AMONG PATHOGENIC FUNGI 28
2.1 – Main contribution by R.M. Domingos 29
2.2 – Abstract 30
2.3 – Introduction 31
2.4 – Material and methods 32
2.4.1 – Dataset source and sequence extraction 32
2.4.2 – Primary sequence clustering 32
2.4.3 – Phylogenetic analysis 32
2.4.4 – Strains and growth conditions 32
2.4.5 – Cloning procedures 33
2.4.6 – Protein purification 33
2.4.7 – Reduction of peroxidases with DTT 34
2.4.8 – Thiol dependent peroxidase activity assays 34
2.4.9 – Site directed mutagenesis 34
2.4.10 – Kinetics of linoleic acid hydroperoxide reduction by *Mf*Ohrdel - AhpE competition assay . 34
2.4.11 – pK_a determination of C_P residue from *Mf*Ohr_{del} WT 35
2.4.12 – Affinity purification of *X. fastidiosa* anti-Ohr serum 35
2.4.13 – Protoplastization of *M. fijiensis mycelia* 35
2.4.14 – Subcellular fractionation 36
2.4.15 – MfOhr subcellular localization 36
2.5 – Results 37
2.5.1 – Ohr/OsmC homologs data mining & their taxonomic distribution among eukaryote 37
2.5.2 – Distribution of Ohr, OsmC and Ohr-like subfamilies homologs among eukaryotes 39
2.5.3 – Genomic configurations of ohr/osmC genes in eukaryotic organisms 40
2.5.4 – Recombinant eukaryotic Ohr and OsmC have peroxidase activity 41
2.5.5 – MfOhr enzymatic properties are similar to the bacterial Ohrs 42
2.5.6 – Single Cys mutants of *Mf*Ohr do not have detectable peroxidase activity 43
2.5.7 – Determination of cysteine's pK_a values 44
2.5.8 – *Mf*Ohr intramolecular disulfide bond formation upon hydroperoxide treatment 44
2.5.9 – Is *Mf*Ohr targeted to mitochondria? 45
2.6 – Discussion 47
2.7 – References 49
CHAPTER 3 – STRUCTURAL INSIGHTS ON THE EFFICIENT CATALYSIS OF HYDROPEROXIDE REDUCTION BY OHR: CRYSTALLOGRAPHIC AND MOLECULAR DYNAMICS APPROACHES 51

3.1 – Main contribution by Renato M. Domingos 52
3.2 – Abstract 53
3.3 – Introduction 54
3.4 – Materials and methods 56
3.4.1 – Crystallization trials, data collection and processing 56
3.4.2 – Structure determination, model building and refinement 56
2.4.3 – Site-directed mutagenesis 56
2.4.4 – Lipoamide-lipoamide dehydrogenase peroxidase-coupled assay 57
2.4.5 – pK_a determination by monobromobimane alkylation assay 57
2.4.6 – Circular dichroism 57
2.4.7 – Morph conformations 57
2.4.8 – MD simulations 57
3.5 – Results 60
3.5.1 – Crystal structure of *Xf*Ohr as a disulfide in its open form 60
3.5.2 – Molecular dynamics of *Xf*Ohr: from closed to open states 62
2.5.3 – Molecular dynamics of *Xf*Ohr: from the open to closed states 69
2.5.4 – Biochemical Analysis of *Xf*Ohr mutants (R19A and E51A) 70
3.6 – Discussion 72
3.7 – References 75
CHAPTER 4 – UNIQUE STRUCTURAL SWITCHES ALONG THE CATALYTIC CYCLE OF OHR ARE ASSISTED BY SUBSTRATES AND PRODUCTS 78
4.1 – Main contribution by Renato M. Domingos 79
4.2 – Abstract 80
4.3 – Introduction 81
4.4 – Results 83
4.4.1 – Available Ohr structure conformations 84
4.4.2 – The Structure of Ohr in complex with its biological reductant (DHL) 85
4.4.3 – A hydrophobic collar is conserved and relevant for Ohr-substrates interactions 85
4.4.4 – Flexible regions surrounding Ohr active site 87
4.4.5 – Oxidized Ohr is more prone to undergo Arg loop opening 88
4.4.6 – Alcohol release assisted the Arg-loop opening 90
4.4.7 – DHL induces the fast closing switch 90
4.4.8 – Catalytic arginine is not required for the reduction of Ohr by DHL 90
4.4.9 – Catalytic triad disruption is crucial for Ohr reduction by DHL 92
4.5 – Discussion 94
4.6 – Methods 98
4.6.1 – Cloning procedures and site-directed mutations of *Cv*OhrA and *Cv*OhrB 98
4.6.2 – Protein expression and purification 98
4.6.3 – Protein quantification 98
4.6.4 – Lipoamide reduction to dihydrolipoamide 98
4.6.5 – Crystallization. 99
4.6.6 – Structural determination 99
4.6.7 – Crystallographic B-factors and structures superposition 99
4.6.7 – Parameterization of new molecules for MD simulations 100
4.6.8 – System preparation for classical MD 100
4.6.9 – Classical Molecular Dynamics Simulations 100
4.6.10 – Steered Molecular Dynamics (SMD) 101
4.6.11 – Kinetics of oleic acid hydroperoxide reduction by *Cv*OhrA 101
4.6.12 – Ohr specific activities for tBOOH reduction 102
4.6.13 – Hybrid Quantum Molecular Dynamics (QM-MM) 102
4.7 – References 103
CHAPTER 5 – ORGANIC HYDROPEROXIDE RESISTANCE PROTEIN AS A POTENTIAL DRUG TARGET – SEARCH FOR INHIBITOR COMPOUNDS 105
5.1 – Main contribution by Renato M. Domingos 106
5.2 – Abstract 107
5.3 – Introduction 108
5.4 – Results 110
5.4.1 – Pharmacophore Model 110
5.4.2 – Electrophilic ligand design 111
5.4.3 – Experimental conditions standardization of the inhibitor activity assay 112
5.4.4 – IC_{50} determination for the inhibitor compounds 114
5.4.5 – DSF approach 114
5.5 – Discussion 116
5.6 – Methods 118
5.6.1 – Pharmacophore model and virtual screening 118
5.6.2 – Peroxidatic activity assay for screening and IC_{50} determination 118

5.6.3 – DSF experiments ... 118
5.7 – References ... 119
CHAPTER 6 – DISCUSSION AND GENERAL CONCLUSIONS ... 120
6.1 – Discussion ... 120
6.2 – References ... 123
CHAPTER 7 – ABSTRACT ... 124
7.1 – Abstract ... 124
7.2 – Resumo ... 126
APPENDIX 1 – SUPPLEMENTARY DATA ... 128
$_{Ap}$1.1 – Chapter 4 (supplementary) ... 128
$_{Ap}$1.2 – Chapter 5 (supplementary) ... 134
APPENDIX 2 – CONFERENCE PROCEEDINGS, COURSES, INTERNSHIPS, & AWARDS ... 138
$_{Ap}$2.1 – Abstracts in Conference proceedings and workshops ... 138
$_{Ap}$2.2 – Specialized Courses ... 139
$_{Ap}$2.3 – Internships ... 140
$_{Ap}$2.4 – Awards ... 140

LIST OF FIGURES

CHAPTER 1 – GENERAL INTRODUCTION

Fig.1 – A phylogenetic tree of Nrf2 protein relative to atmospheric oxygen Earth's history. 2
Fig.2 – Generation of different oxidative species by energy transfer or sequential reduction of ground-state triplet oxygen. 3
Fig.3 – Lipid peroxidation process. 4
Fig.4 – ROS in antibiotic-mediated Killing. 6
Fig.5 – Hydrogen peroxide sensing by OxyR. 8
Fig.6 – Representation of a thiol. 9
Fig.7 – General mechanism for thiol oxidation. 9
Fig.8 – Structure of cysteinyl residue within protein. 10
Fig. 9 – Simplified reaction of the reduction of peroxides catalyzed by peroxidases. 10
Fig. 10 – Thiol-disulfide exchange. 10
Fig. 11 – Peroxiredoxins reaction mechanisms. 11
Fig. 12 – Catalytic cycle of glutathione peroxidases. 12
Fig. 13 – The mechanism of H_2O_2 reduction and GPX regeneration by thioredoxin for nonselenium GPx. 12
Fig. 14 – Schematic representation of glutaredoxin secondary structure. 13
Fig. 15 – Sequence comparison among Ohr/OsmC Superfamily. 13
Fig. 16 – Topology diagram of the Ohr dimer. 14
Fig. 17 – OsmC *vs* Ohr, structure considerations. 14
Fig. 18 – Effects of peroxide on growth and survival of X. campestris wt and ohr mutant. 15
Fig. 19 – Expression of ohr in response to various oxidants. 15
Fig. 20 – Expression analysis of ohr and osmC in response to stresses in *D. radiodurans* and *P. aeruginosa*. 15
Fig. 21 – Ohr and OsmC expression regulation. 16
Fig. 22 – Regulation of gene transcription by the redox sensor OhrR. 17
Fig. 23 – The two major conformational states found in Ohr crystal structures, the open and close conformations. 18
Fig. 24 – PEG binding in the X. fastidiosa Ohr active site. 19
Fig. 25 – Proposed mechanism of action of Ohr proteins. 19
Fig. 26 – Lipoylated moieties. 21
Fig. 27 – Model identifying where in the L. monocytogenes life cycle, Ohr is required. 22
Fig. 28 – Model of the OhrR and AphB reducing sensors action on Vibrio cholerae virulence. 23

CHAPTER 2 – FUNCTIONAL AND EVOLUTIONARY CHARACTERIZATION OF OHR PROTEINS IN EUKARYOTES REVEALS MANY ACTIVE HOMOLOGS AMONG PATHOGENIC FUNGI

Fig. 1 – Multiple sequence alignment of selected members from Ohr, OsmC and Ohr-like subfamilies. 37
Fig. 2 – RAxML maximum likelihood phylogenetic tree constructed using retrieved eukaryotic sequences from Ohr/OsmC family. 38
Fig. 3 – Genomic arrangements of genes from Ohr/OsmC family present in Eukaryotes. 40
Fig. 4 – Thiol dependent peroxidase activity of eukaryotic Ohr and OsmC enzymes. 41
Fig. 5 – Thiol specificity of MfOhr peroxidase activity. 41
Fig. 6 – Specific activities of MfOhr and MfOhrdel towards CuOOH, tBOOH and H_2O_2. 42
Fig. 7 – Kinetics of LAOOH reduction by MfOhr. 42
Fig. 8 – Comparison of the peroxidase activities of MfOhrdel and the C87S and C154S mutants. 43
Fig. 9 – pK_a value of C_p residue of MfOhrdel. 44
Fig. 10 – Non-reducing SDS-PAGE gels showing the effect of DTT and hydroperoxide treatments on MfOhrdel, MfOhrdel C154S and MfOhrdel C87S. 45
Fig. 11 – Western blots of total (TF), cytosolic (CF) and enriched mitochondria (EMF) fractions of protoplasts cells of M. fijiensis Mf_1. 45

CHAPTER 3 – STRUCTURAL INSIGHTS ON THE EFFICIENT CATALYSIS OF HYDROPEROXIDE REDUCTION BY OHR: CRYSTALLOGRAPHIC AND MOLECULAR DYNAMICS APPROACHES

Fig 1. Comparison of different crystal structures of Ohr 61
Fig 2. Morph conformations superimposed to the closed and open states of XfOhr. 62
Fig 3. Localized fluctuations for XfOhr in the reduced and oxidized states. 64
Fig 4. Distance values between Arg19-Cα and Glu51-Cα atoms and between Arg19-Cα and C_p-Cα atoms for the XfOhr-S- and XfOhr-SS trajectories. 65
Fig 5. Salt-bridge and Hbond interactions of Arg19 with Cp and with Glu51 during XfOhr-S^-, XfOhr-SS, XfOhr-SH and E51A XfOhr-S^- simulations. 66
Fig 6. XfOhr-S^- and XfOhr-SS representative structures from MD simulations. 67
Fig 7. Representative structures of XfOhr-SH, XfOhr mutants from MD simulations. 68

Fig 8. Comparative analyses of wild-type XfOhr and two mutants (R19A and E51A). 70
Fig 9. Proposed model for fatty acid hydroperoxide reduction by Ohr. 72
CHAPTER 4 – UNIQUE STRUCTURAL SWITCHES ALONG THE CATALYTIC CYCLE OF OHR ARE ASSISTED BY SUBSTRATES AND PRODUCTS
Fig. 1 – Six crystallographic structures, including the complexes of Ohr enzymes with DTT and DHL 84
Fig. 2 – Hydrophobic cradle underlies interactions between Ohr enzymes with their substrates..... 86
Fig. 3 – Insights into the Ohr dynamics by crystallography and molecular dynamics. 87
Fig. 4 – Free energy profiles for the transition from CS to OS. 89
Fig. 5 – Ohr Kinetics evaluating arginine role during hydroperoxide reduction and DHL oxidation. 91
Fig. 6 – Hybrid QM-MM analysis comparing the intramolecular disulfide bond attack by DHL (reaction III, figure 5) in open and close states. 92
Fig. 7 – Proposed detailed scheme for Ohr enzymatic mechanism..... 96
CHAPTER 5 – ORGANIC HYDROPEROXIDE RESISTANCE PROTEIN AS A POTENTIAL DRUG TARGET – SEARCH FOR INHIBITOR COMPOUNDS
Fig. 1 – Pharmacophore model design. 110
Fig. 2 – Electrophilic functional groups with susceptibility to attack the peroxidatic cysteine sulphur at Ohr active site. 111
Fig. 3 – Reaction system standardization for the evaluation of the potential inhibitor activity..... 112
Fig. 4 – IC_{50} standardization assay. 112
Fig. 5 – Screening of the Inhibitory capacity for the selected compounds. 113
Fig. 6 – IC_{50} determination. 113
Fig. 7 – DSF assay..... 114
Fig. 8 – DSF-derived compounds with substantial Tm shifts. 115
APPENDIX 1 – SUPPLEMENTARY DATA
Ap1.1 – Chapter 4 (supplementary)
Fig. S1 – Comparison of Arg-loop openings. 128
Fig. S2 – Flexibility of the Arg-loop in the IS present in the *Bs*OhrB (PDB_{ID}=2BJO). 130
Fig. S3 – Carbon chain release assisted the disruption of the R_ε and E_ε (R_{NH}-$E_{O\varepsilon}$) interaction. 131
Fig. S4 – Electrostatic surface during key stages of Ohr catalysis..... 132
Fig. S5 – Spatial representation of available molecular interactions at *Xf*Ohr active site (PDB_{ID}=1ZB9). 133

LIST OF TABLES

CHAPTER 1 – GENERAL INTRODUCTION

Table 1 – Parameters related to hydroperoxide reduction by Ohr 20

CHAPTER 3 – STRUCTURAL INSIGHTS ON THE EFFICIENT CATALYSIS OF HYDROPEROXIDE REDUCTION BY OHR: CRYSTALLOGRAPHIC AND MOLECULAR DYNAMICS APPROACHES

Table 1 **–** Data collection and refinement statistics parameters for the XfOhr open-state. 60

Table 2 – Average backbone RMSD (Å) and standard deviation values with respect to the corresponding starting structures calculated for each simulation. 63

CHAPTER 4 – UNIQUE STRUCTURAL SWITCHES ALONG THE CATALYTIC CYCLE OF OHR ARE ASSISTED BY SUBSTRATES AND PRODUCTS

Table 1 **-** Data collection and refinement statistics 83

APPENDIX 1 – SUPPLEMENTARY DATA

Ap1.1 – Chapter 4 (supplementary)

Table S1 **–** Ohr dimer interface hydrogen interactions 129

Table S2 **–** Primers for site-directed mutation 133

Table S3 **–** Expressing conditions of recombinant proteins 133

Ap1.2 – Chapter 5 (supplementary)

Table S1 – Molecules from Virtual screening 134

CHAPTER 1 – GENERAL INTRODUCTION

Permissions for the reuse of published figures in the thesis/dissertation

All the permissions for the reuse of published contents in: Free Radical Biology and Medicine, Trends in Microbiology, American Society for Microbiology, Biochimica et Biophysica Acta (BBA) - General Subjects, the EMBO Journal, the FEBS journal, the Microbiology journal, Journal of molecular biology, Journal of Biological Chemistry and Cell Press, were obtained through: http://www.copyright.com/. Permissions for the reuse of published contents in *Antioxidant Redox Signaling* was obtained by e-mail. (Authors were also notified).

List of Abbreviations:

GOE – Great Oxygenation Event

ROS – Reactive Oxygen Species

ATP – Adenosine Triphosphate

NADPH – Nicotinamide Adenine Dinucleotide Phosphate

NOX – NADPH Oxidases

COX – Cyclooxygenase

LOX – Lipoxygenase

TCA – Tricarboxylic Acid Cycle

GSH – Reduced Glutathione

GSSG – Oxidized Glutathione

GI – gastrointestinal

TSA – Thiol-Specific Antioxidant

SOD – Superoxide Dismutases

Trx – Thioredoxin

TrxR – Thioredoxin Reductase

TPx – Thioredoxin Peroxidases

Prx – Peroxiredoxins

GPx – Glutathione Peroxidase

ORP – Oxidoreduction Potentials

Co-IP – Co-Immunoprecipitation

Ohr – Organic hydroperoxide resistance proteins

OsmC – Osmotically inducible Protein C

OC – Open conformation

CC – Close Conformation

LMW – Low Molecular Weight

DHLA – Dihydrolipoic acid

OGDC – 2-oxo-acid dehydrogenase complex

OhrR – Organic hydroperoxide resistance Repressor

1.1 – Oxidative atmosphere evolution

Atmospheric molecular oxygen levels suffered dramatic variations along the geological history of planet Earth. Five major stages were proposed to represent the atmospheric history of the planet, which is tightly connected with the evolution of organisms (**Fig. 1**) (Gacesa *et al*, 2016). The transition

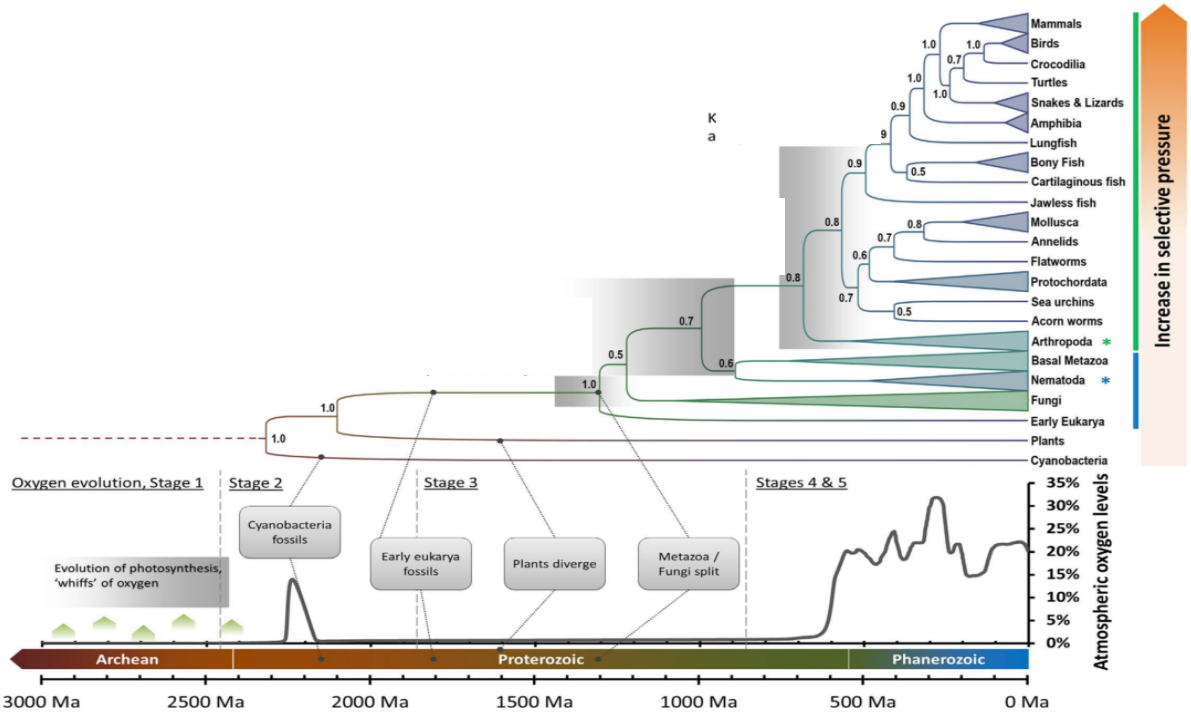

Fig.1 – A phylogenetic tree of Nrf2 protein (the master transcription regulator of antioxidant defenses in mammals) relative to atmospheric oxygen Earth's history. The chart presents the 5-stage model of oxygen evolution; Stage 1 – period when atmosphere and oceans were anoxic. Stage 2 – initiates the "Great oxygenation Event"; Stage 3 – period during which atmospheric oxygen levels remained low due to absorption by reduced environment and minerals; Stage 4 – period after saturation of previous global oxygen buffers, when oxygen levels raised, reaching present atmospheric levels in stage 5. Eukarya and cyanobacteria are pointed according the first confirmed fossil evidence. Selective pressure increases towards more recently evolved phyla (increasing orange hue). Image adapted from Gacesa *et al*, 2016.

from the anoxic "stage 1" to the highly oxygen saturated atmospheric levels of "stage 5" had the crucial intervention of oxygen-producing photosynthetic cyanobacteria during "stage 2", stipulating the beginning of the "Great Oxygenation Event" (GOE) at 2.45-1.85 Ga (**Fig. 1**) (Schirrmeister *et al*, 2013), when large amounts of oxygen were released to the atmosphere. Then, oxygen was uptaken due to oxidation of the reduced atmosphere and minerals, by the end of "stage 2" and during "stage 3". Only when minerals were highly oxidized, the atmospheric oxygen levels reached around 20% (stage 4) and remained like that until recent days (stage 5). From the origin of photosynthetic cyanobacteria in "stage 2" to the oxygen saturation of atmosphere in "stage 4 and 5" there was a lag-time, which was proposed to have lasted ~ 1 Ga (Gacesa *et al*, 2016; Holland, 2006). GOE is known as the highest impacting geologic environmental change associated to history of life on Earth (Holland, 2006). This event opened new opportunities for the bioenergetics of organisms. The accumulation of molecular oxygen in the atmosphere allowed the emergence of aerobic respiration, a much more efficient process to generate energy than the previous existing ones. Such increase in generating energy efficiency marked an evolutionary transition to the dominance of aerobe biota which continues to date (Gacesa *et al*, 2016).

Despite the efficiency associated to the aerobic metabolism in producing energy, the presence of high levels of molecular oxygen is concomitantly associated to the generation of reactive oxygen species (ROS). Distinct ROS display different degrees of reactivity, which in turn are linked to cell toxicity and damage of lipids, proteins, carbohydrates and DNA, all crucial components of biological systems (Gacesa *et al*, 2016). The dual, opposite sides of the molecular oxygen appearance is then, not only associated to the dominance of aerobic organisms but also to a great diversification of biological species due to the selective pressure applied by the increasing of toxicity of oxygen-derived reactive molecules (Gacesa *et al*, 2016; Rodriguez & Redman, 2005).

1.2 – Oxidative species generation

1.2.1 – Respiration *vs* ROS

Although increased oxidative state of the atmosphere is tightly associated to toxicity and damage of cellular components, molecular oxygen is relatively nonreactive (Rodriguez & Redman, 2005; Cadenas, 1989). However, oxygen can be converted to highly reactive chemical compounds when exposed to high energy (UV light) or to electron-transferring reactions. The sequential reduction of triplet oxygen can originate, among other chemical species, the superoxide radical ion, hydrogen peroxide and the most reactive of all: the hydroxyl radical (**Fig. 2**) (Rodriguez & Redman, 2005; Apel & Hirt, 2004). In eukaryotes, mitochondria is the main organelle associated with the production of ROS, where the electron transport chain is coupled to the translocation of protons across the inner membrane, generating an electrochemical gradient required for the adenosine triphosphate (ATP) synthesis (Chatre & Ricchetti, 2014; Rose & Sheahan, 2012; Murphy, 2009). Through the leakage of electrons along the respiratory chain, superoxide anion radical is generated in small amounts that can then be converted to other oxidants (Cadenas, 1989) Therefore, oxidants are unavoidable side-products in aerobic organisms. Therefore, to benefit from the higher energetic yields of respiration, living organisms had to deal with strong selective pressures such as the requirement of antioxidant systems as new adaptation strategies for the new environmental conditions (Lushchak, 2011; Rodriguez & Redman, 2005; Apel & Hirt, 2004).

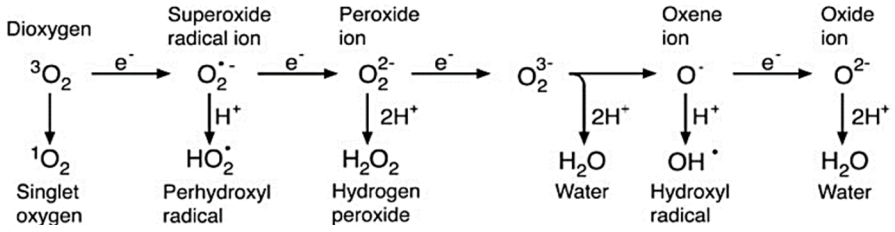

Fig.2 – Generation of different oxidative species by energy transfer or sequential univalent reduction of ground-state triplet oxygen. Image from Rodriguez & Redman, 2005.

1.2.2 – Lipid peroxidation *vs* ROS

Saturated and unsaturated fatty acids are critical components of cell membranes, which are essential to maintain cell structure and function both in bacteria and eukaryotic cells. Unsaturated fatty acid of membranes are the primary cell components which are subjected to damage caused by ROS

(**Fig. 2**) (Sultana *et al*, 2013; Parsons & Rock, 2013; Yin *et al*, 2011). The reaction between oxidants and these lipids is known as lipid peroxidation and it is highly associated to cell failure and development of diseases. Lipid peroxidation is a multi-step process (**Fig. 3**) (Sultana *et al*, 2013). The process initiates with the free radical (such as, hydroxyl HO•, alkoxyl RO•, peroxyl ROO•) attack towards the undamaged lipid, abstracting an allylic H from the methylene group in the methylene group of the lipid, forming a carbon-centered alkyl radical (Initiation **Fig. 3**). The alkyl radical reacts with molecular oxygen and a peroxyl radical is produced, which in turn can abstract another allylic H to initiate a self-perpetuating chain reaction (propagation step) leading to the formation of organic hydroperoxides (ROOH) (Propagation **Fig. 3**). This propagation chain of reactions can eventually terminate, when different types of radicals react with each other originating stable (non-radicals) products. Alternatively, when the radical encounters antioxidants such as enzymes (E) or vitamin E or C the propagation of lipid peroxidation is inhibited (Yin *et al*, 2011; Sultana *et al*, 2013).

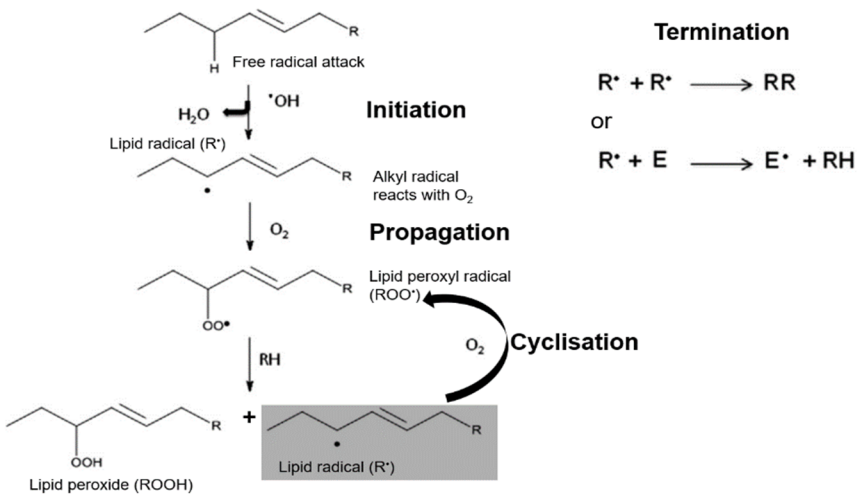

Fig.3 – Lipid peroxidation process. E = enzyme or LMW reductant. Image adapted from Yin *et al*, 2011, Sultana *et al*, 2013.

1.2.3 – Endogenous mechanisms of ROS generation

Along the great diversification of biological species, living organisms developed multiple other endogenous enzymatic systems which generate oxidant compounds with different degrees of reactivities (Yin *et al*, 2011). The production of oxidant molecules by biological organisms rapidly evolved to become an essential feature in cell signaling, through the redox regulation of gene expression, defense mechanisms against pathogen attacks, inflammatory response or metabolism of drugs and xenobiotics.

NADPH oxidases (NOX) are a family of heme-containing transmembrane enzymes that are mostly associated to the generation of an oxidative burst in macrophages and neutrophils in an attempt to fight pathogenic invasion (Franchini *et al*, 2013; Panday *et al*, 2015). These enzymes produce superoxide anion radicals by electron transference across biological membranes where oxygen is the electron acceptor (Bedard & Krause, 2007). Superoxide anion radicals (or hydrogen peroxide generated by dismutation of this free radical) generated by NOX can also act as second messenger in immune response related mechanisms, thus they are essential enzymes working as inflammatory mediators in mammals (Franchini *et al*, 2013; Panday *et al*, 2015). However, ROS produced by NOX enzymes has

been proposed to have many distinct roles, other than associated to immune response mechanisms (Bedard & Krause, 2007). Apart from mammals, NOX-derived generation of ROS is vastly conserved among multicellular organisms, such as protists, arthropods, fungi or plants (Gandara *et al*, 2017; Breitenbach *et al*, 2015; Bedard *et al*, 2007; Takemoto *et al*, 2007). Currently, the availability of compounds targeting NOX enzymes is lifting the possibility of new short-term therapeutics against ROS production, effectively protecting tissue damaging and inflammation, without incapacitating their anti-pathogen activity (Panday *et al*, 2015).

Lipoxygenase (LOX) and Cyclooxygenase (COX) enzymes are responsible for catalyzing the formation of the corresponding hydroperoxides from polyunsaturated fatty acids such as linoleic and arachidonic acid. This is the initial step in the formation of several lipid mediators involved in cellular homeostasis, proliferation and differentiations, and in pathophysiological processes such as inflammation and tumorgenesis (Mashima & Okuyama, 2015; Schneider *et al*, 2007; Brash, 1999). Drug Targeting LOX and COX are recognized therapeutic valuable options against inflammatory diseases such as arthritis, rheumatisms, asthma and as diary plain relievers (Mashima & Okuyama, 2015; Zarghi & Arfaei, 2011; Schneider *et al*, 2007). Furthermore, LOX and the peroxidation of fatty acids are essential for plant cell mechanisms of adaptation against many abiotic stressor effects such as, drought, frosts, temperature variation, high humidity, pesticide pollution and herbivory insects (Woldemariam *et al*, 2018; Babenko *et al*, 2017; Santino *et al*, 2013).

Nitric-oxide synthases (NOS) is another enzymatic system that generates oxidants as mediators in cell signaling in processes such as, regulation of vascular tone, neurotransmission and immunity. NOS are responsible for the production of nitric oxide ($^{\bullet}NO$) which in turn can react with superoxide anion and be converted into peroxynitrite ($ONOO^-$). This reaction occurs even in presence of superoxide dismutase, suggesting the peroxynitrite formation is extremely fast (Radi, 2013). When in excess, nitric oxide lead to cytotoxic events and can results in cell failure. However it is also known that mammals can benefit from peroxynitrite to resist the attacks of pathogenic microorganisms (Alvarez *et al*, 2011). Frequently, drugs administrated to treat patients have lipophilic nature and are converted into hydrophilic compounds by the organism during drug metabolism (Banerjee & Ghosh, 2016; Rowland *et al*, 2013). Drug and non-drug xenobiotics metabolism display three distinct phases (phase I II and III). Phase I has Cytochrome P450s (CYP families) as the main component responsible to oxidize lipophilic components into hydrophilic molecules in bacteria, plants and mammals (Banerjee & Ghosh, 2016; Powles & Yu, 2010; Lewis & Wiseman, 2005). This process is the major ROS generator during drug metabolism, contributing to oxidative stress (Banerjee & Ghosh, 2016).

1.2.4 – Antibiotic-mediated killing mechanisms and ROS generation

The involvement of oxidants in antibiotic-mediated killing of pathogens is still a debatable issue, which needs more investigation. Nevertheless, there are strong evidences on the involvement of the tricarboxylic acid cycle (TCA) in oxidant-mediated killing of several pathogenic bacterial species

by antibiotic´s treatment (**Fig. 4**). The mechanism involves the hyperactivation of the electron transport chain, caused by the released of reducing agents in the TCA cycle which induces the formation of superoxide and hydrogen peroxide. The increase of superoxide concentrations leads to damage on iron-sulphur clusters in proteins, which in turn destabilizes ferrous (Fe^{2+}) iron. Free ferrous iron could then react with hydrogen peroxide and generate hydroxyl radicals (Fenton reaction). As mentioned above, hydroxyl radicals are highly reactive and can by their own damage DNA, lipids (inducing lipid peroxidation) and proteins; or can indirectly damage DNA by oxidizing their precursors in the deoxyribonucleotide pool (Kohanski *et al*, 2007; Belenky *et al*, 2015; Van Acker & Coenye, 2017). Furthermore, studies in *Enterococcus faecalis* SOD-mutants showed that the antibiotic tolerance was dependent on the energy source present during the experiment. Treatment with different classes of bactericidal antibiotics (β-lactams, aminoglycosides, and quinolones) led to increased oxygen consumption for some energy source consumptions, agreeing with the hypothesis that these killing agents are redox-related (Dwyer *et al*, 2014; Belenky *et al*, 2015; Ladjouzi *et al*, 2015; Van Acker & Coenye, 2017). Other important considerations are the several defense mechanisms against oxidative damage and DNA repair owned by bacteria. Several studies showed the induction of OxyR (oxidative sensor) upon antibiotic treatment. The surviving ability strongly decreased in catalase deletion mutants and after addition of a SOD (superoxide anion dismutase) inhibitor (Van Acker *et al*, 2016; Van Acker & Coenye, 2017). In conclusion, manipulation ROS in the leaving systems or inhibiting defense mechanisms against oxidative damage may lead to the development of new antibiotics therapies. Nevertheless, studies indicate that sublethal doses of some antibiotics led to resistance through ROS-induced mutagenesis (Kohanski *et al*, 2010; Van Acker & Coenye, 2017).

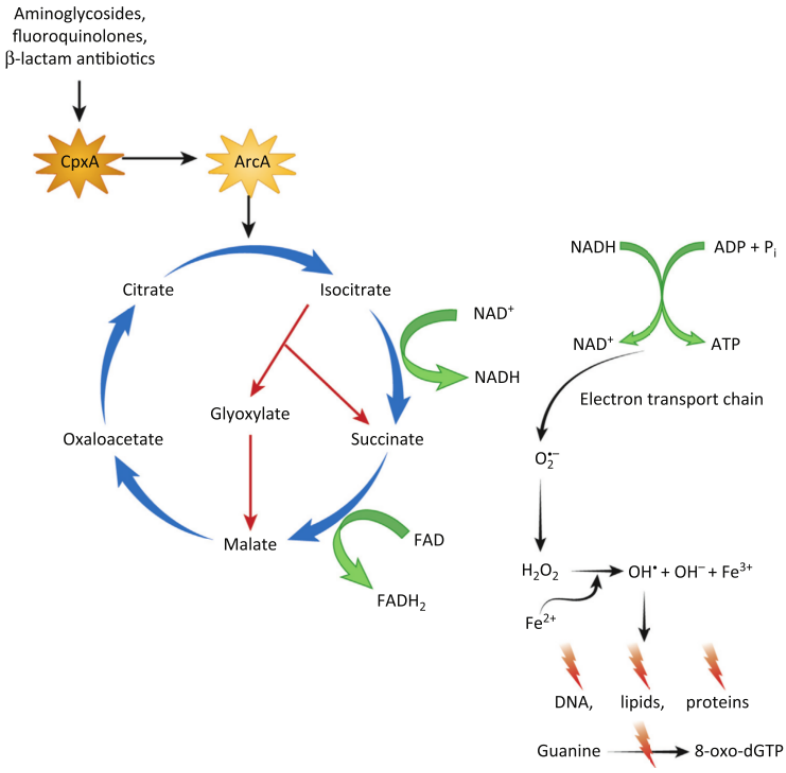

Fig.4 – ROS in antibiotic-mediated Killing. Antibiotics such as ampicillin, kanamycin and norfloxacin, activate TCA cycle through the envelope stress-response sensor (CpxA), which in turn would signal to ArcA (regulator of genes involved in aerobic and anaerobic pathways) to trigger a chain of events which lead to oxidative molecules generation. Image taken from Van Acker & Coenye, 2017.

1.3 – Antioxidant defense

1.3.1 – General mechanisms

As previously mentioned, oxidative species with different degrees of reactivity are unavoidable side-products of aerobic metabolism, which living organism have to cope with. Although, oxidative compounds are not always deleterious and can play physiological roles in cells, at controlled concentrations. Therefore, generation and degradation of oxidants must be under constant regulation in cells, keeping ROS at non-toxic concentrations (Lushchak, 2011). Several strategies were developed by living organisms to minimize ROS-related damage, among them:

Making less ROS – Organisms such as *Caenorhabditis elegans* can cluster together to regulate O_2 levels. Another way of preventing ROS formation is the existence of metal ions protein binders (such as transferrin, ferritins and metallothioneins), their interaction prevents Fenton reaction (formation of hydroxyl radical, $HO^{\bullet}$) and as consequence, preventing lipid peroxidation too (Halliwell, 2006).

Scavenging ROS – Superoxide dismutase (SOD) was one of the first identified powerful antioxidant enzymes. These enzymes catalyze the dismutation of two superoxide radical anion ($O_2^{\bullet-}$) molecules to hydrogen peroxide (H_2O_2) and molecular oxygen (O_2) (Ighodaro & Akinloye, 2017). Then, H_2O_2 can also be removed by enzymes such as catalases and peroxidases, such as glutathione peroxidases and peroxiredoxins (both thiol-enzymes, i.e. depending on peroxidatic cysteine (C_p) residues). Glutathione peroxidases (selenium-containing enzymes) also require two reduced glutathione (GSH) molecules to convert H_2O_2 into water, and forming oxidized glutathione (GSSG), which could then be reduced back to GSH by glutathione reductases. However, for some sulfur containing glutathione peroxidases, thioredoxin enzymes are preferably used instead of GSH as substrate. Peroxiredoxins are very important H_2O_2 removing systems due to their high concentration in cells as well as to their high reactivity. Peroxiredoxins are also able to detoxify organic hydroperoxides (Halliwell, 2006; Jacobson *et al*, 1989). These enzymes also need reduced partners for their reactivation after reacting with H_2O_2 (Halliwell, 2006), which in most cases is thioredoxin. Other very important enzymes are the main subject of our work, the organic hydroperoxide resistance proteins (Ohr), which are mainly present in bacteria and fungi. Ohr are Cys-based, lypoil-dependent peroxidases with extraordinary reactivity towards organic hydroperoxides (10^6–10^8 $M^{-1}.s^{-1}$), but not towards hydrogen peroxide (Mongkolsuk *et al*, 1998a; Alegria *et al*, 2017). Other type of ROS scavengers are non-proteinaceous agents, which are preferentially oxidized by oxidant molecules preserving more important biomolecules. Example of such molecules are, ascorbate, tocopherols (Tocs), carotenoids, urate, plasma albumin and GSH itself (Halliwell, 2006).

ROS-related DNA repairing – Oxidative molecules continuously damage DNA, affecting its structure and consequently its function. These structure modification can, frequently, be lethal,

thus cells evolved with enzymatic mechanisms of constant scanning, protection and repairing of DNA (Jena, 2012)

1.3.2 – Overview of specialized sensors of ROS

Escherichia coli is known to express at least nine enzymes (catalases or peroxidases) which among them, some are able to scavenge hydrogen peroxide or organic hydroperoxide (Mishra & Imlay, 2012). The expression of these enzymes is regulated through specialized oxidative sensors, such as, OxyR and OhrR. Together with SoxR, which induces the transcription of other important redox enzymes, they allow regulation of the expression of many important redox enzymes, allowing bacteria to trigger quick adaptive responses to oxidative stress (Sporer *et al*, 2017). *SoxR* Induces the transcription of several redox proteins, including antioxidant manganese-containing superoxide dismutase (Mn-SOD), endonuclease IV (radical-induces DNA damage repairing) and glucose-6-phosphate dehydrogenase (G6PDH). SoxR regulon is also associated to the reduction of the expression level of outer membrane protein F (OmpF) a purin which operates as non-specific transport channel and modifies the level of small ribosomal protein S6. Thus, this regulon operates as protector system against xenobiotics (Sporer et al, 2017; Lushchak, 2011; Greenberg et al, 1990). OxyR is a well characterized member of LysR family of transcription activators and acts as a sensor of increased levels of hydrogen peroxide. OxyR proteins exist in oxidized and reduced forms, however is the direct oxidation of a cysteine residue in OxyR the signal responsible for the activation of the OxyR regulon. After OxyR oxidation, a large conformational change takes places, increasing the affinity of this transcription factor for its target DNA sequence (Jo *et al*, 2015). The redox mechanism of OxyR activation involves two highly conserved cysteines. The Cys-199 is directly oxidized by hydrogen peroxide and a second cysteine (Cys-208) which is responsible for the formation of the intermolecular disulfide bond formation (**Fig. 5**). OxyR can activate the transcription of *katG* (catalase HPI) and *ahpC* (peroxiredoxin) in response of oxidative stress (Lushchak, 2011). Bacteria hold yet another oxidative stress sensor, the OhrR. This transcriptional regulator belongs to the MarR family of bacterial regulators and is directly involved in the control of the expression of the Ohr protein (subject of this study) when specifically activated by

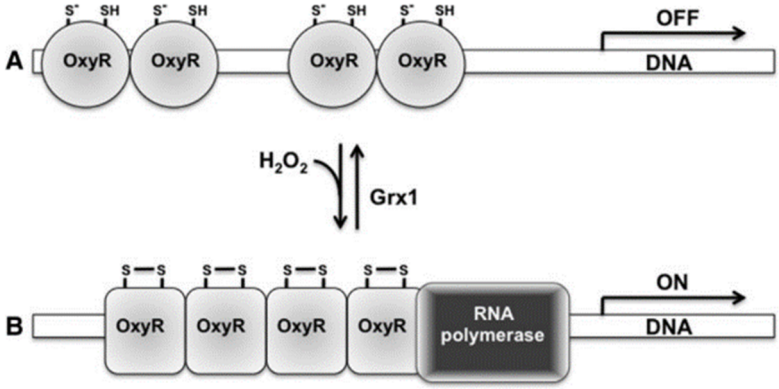

Fig.5 – Hydrogen peroxide sensing by OxyR. (A) Reduced OxyR would bind the DNA promotor regions, preventing transcription. (B) Oxidation of OxyR reactive cysteine by H_2O_2 leads to sulfenic acid formation which in turn would react with a second cysteine forming an intramolecular disulfide bridge. The biding of cysteines would drive structural changes in the OxyR protein which would allow the recruitment of RNA polymerase and consequent transcription activation. OxyR would be reduced by glutaredoxin 1, a member of the OxyR regulon. Image taken from Vázquez-Torres, 2012.

organic hydroperoxide (Mongkolsuk *et al*, 2002; Hong *et al*, 2005; Vázquez-Torres, 2012; Garnica *et al*, 2017). As it regulates the expression of Ohr protein, OhrR sensor mechanism will be further addressed below.

In fungi, the transcription factor, Yap1p is a well-known regulator, which binds specific DNA sequences localized within promoter regions of target genes. Many of these genes are known to respond to oxidative stress. However, Yap1p is not directly a sensor for H_2O_2, and this function is provided by Gpx3, a sulfur glutathione-dependent peroxidase (Lushchak, 2011). Some of the proteins, induced by Yap1p are: thioredoxin (Trx2), glutathione synthase (GSH2), thioredoxin reductase 1 (TrR), glutathione peroxidase (Gpx), thioredoxin peroxidases (Tsa) and alkylhydroperoxides 1 (Ahp1).

1.3.3 – Thiol dependent peroxidases

Among all the diverse antioxidant systems, our study will focus on a family of proteins (Ohr protein sub-family) which display thiol dependent peroxidase activity. Thiols are nucleophilic compounds containing a sulfhydryl group (**Fig. 6**) and can be present in small molecules or in proteins as part of the side chains of cysteine amino acids. Low-molecular-weight (LMW) thiols such as glutathione, lipoic acid and coenzyme A are also common in biological systems and frequently participate in mixed-disulfide bonds with proteins. Their structure and biophysical properties (such as p*Ka* and redox potential) are responsible for differential recognition by enzymes, making them essential molecules concerning regulatory and metabolic functions (Van Laer *et al*, 2012; Poole, 2015). In proteins, the cysteine residues are one of the least abundant but one of the four most frequently conserved amino acids (together with Gly, Pro, and Trp) and are frequently found within functional (regulatory, catalytic, or binding) sites in proteins (Poole, 2015). Cys residues are frequently found in highly buried regions of proteins, probably due to negative selective pressure to the occurrence of exposed cysteines which could performed non-physiological covalent interactions with a vast number of molecules (*i.e.*, proteins , LMW thiols and lipids) (Poole, 2015). Thiols are highly polarizable, becoming strong nucleophiles in their unprotonated state (thiolate), facilitating several redox modifications (S-sulfenylation (SOH), S-sulfinylation (SO_2H), S-sulfonylation (SO_3H), S-nitrosylation (SNO), glutathionylation (SSG) and S-sulfhydration (SSH)) (**Fig. 7**) (Nagy, 2013; Poole, 2015; Yang *et al*, 2016). Furthermore, thiol ionization of Cys residues (**Fig. 8**), depends

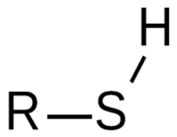

Fig.6 – Representation of a thiol.

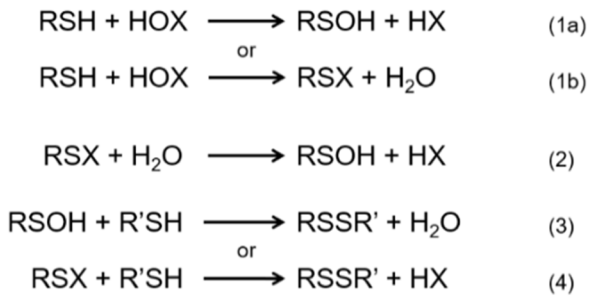

Fig.7 – General mechanism for thiol oxidation. Two-electron thiol oxidation to disulfide an occur via different mechanisms. The most common pathways are via sulfenic acid formation (RSOH in reaction 1a) or via an alternative sulfenyl (RSX, e.g., sulfenyl-halides, X=Cl, Br, or I in reaction 2b) intermediate. RSOH rapidly reacts with thiols turning into the corresponding disulfide species (reaction 3). RSX can hydrolyze to sulfenic acid (2) or it could react directly with another thiol to give the disulfide as in reaction 4. Adapted from Nagy, 2013.

on their location in the protein structure. In fact, Cys residues located at the N-terminal end of α-helices senses its positive dipole, which can decrease their p*Ka* values by up to 1.6 units (Kortemme & Creighton, 1995). However, p*Ka* is not the only single factor that contributes to enzyme efficiency. Actually, enzymes, such as peroxiredoxins, display specialized active site architectures, which provide adequate micro-environment not only for decreasing the thiol p*Ka* value, but also to stabilize the transition state with the substrate. Thereby, reaction rates of peroxiredoxins with peroxides can attain values as high as 10^7-10^8 M^{-1} s^{-1} (Hall *et al*, 2010; Ferrer-Sueta *et al*, 2011). Cysteine is then, the core player in thiol-dependent enzymes ability to reduce oxidant molecules to their respective alcohols (**Fig. 9**), without requiring any other cofactor or prosthetic group to complete their cycles. The control of the enzymatic switch between oxidized and reduced forms are biochemically crucial for life, not only in oxidative stress protection but also regulating signaling pathways (Parsonage *et al*, 2015; Stöcker *et al*, 2018). Additionally, the functionality of these systems and their turnover activity, frequently, depends on thiol-disulfide interchange (**Fig. 10**) which occurs spontaneously (slower) or is accelerated by LMW thiols interaction or through enzyme catalysis (Netto *et al*, 2016; Nagy, 2013; Winther & Thorpe, 2014).

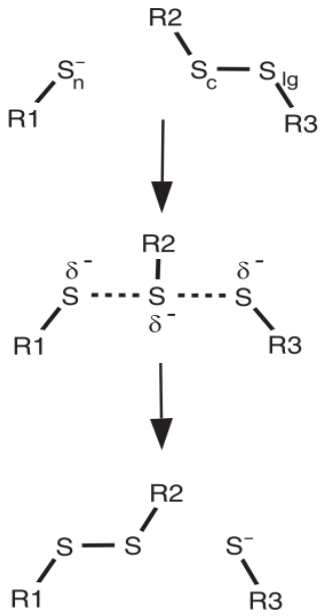

Fig. 10 – Thiol-disulfide exchange. The attack of a thiolate (the nucleophile, S-n) on a disulfide bond takes place through linear transition state where the central atom (Sc) will participate in a new disulfide bond and resolution of a new leaving group thiolate (S-lg). The sulfur of the two sulfur atoms participation in the disulfide bond will eventually act as leaving group, depending steric, electrostatic and intrinsic acidity of the thiolate species involved. Image taken from Winther & Thorpe, 2014.

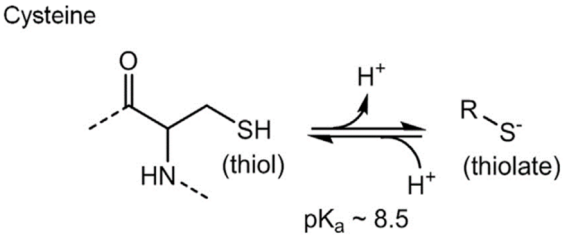

Fig.8 – Structure of cysteinyl residue within protein. Dotted lines represent neighbor residues. Both, protonated (left) and deprotonated (right) forms are dependent on average p*Ka* (which can vary according the particular protein microenvironments). Image taken from Poole, 2015.

The previous mentioned peroxiredoxins and glutathione peroxidases are examples of two very well studied thiol-dependent enzymes. Moreover, the Ohr proteins, the subject of study in our research, belong to the superfamily of Ohr/OsmC and they are also thiol-dependent enzymes which have been studied for the last two decades (Mongkolsuk *et al*, 1998a; Piccirillo *et al*, 2018) will be described below.

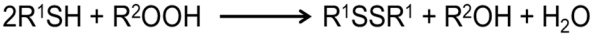

Fig. 9 – Simplified reaction of the reduction of peroxides catalyzed by peroxidases.

1.3.3.1 – Peroxiredoxins

Peroxiredoxins were first discovered in the late 1980s as a "protector protein", which inhibits enzyme inactivation (including glutamine synthetase activity) through a thiol/Fe(III)/O2 oxidation system (Kim *et al*, 1988). This "protector protein" had no sequence homology with other well-known antioxidant enzymes, such as catalases, superoxide dismutases (SOD) and glutathione peroxidase. This "protector protein" was first called as thiol-specific antioxidant (TSA) because it was able to provide antioxidant protection specifically against oxidants generated by thiol-containing systems (Chae *et al*, 1993). The oxidized form of TSA was proposed to be reduced by thioredoxin (Trx) and thioredoxin reductase (TrxR) systems, which mediate the electronic transference from NADPH to the oxidized TSA. Due to their dependency on the thioredoxin system to complete their turnover, these proteins were later renamed as thioredoxin peroxidases (TPx) (Chae *et al*, 1994a, 1994b). As several identified proteins showed homology to TPx and AhpC, it was proposed that all these enzymes would belong to a same family of proteins which was named as peroxiredoxin family (Chae *et al*, 1994a, 1994b).

As previously mentioned, peroxiredoxins are Cys-dependent peroxidases and during their catalytic cycle, a C_p thiolate (C_p-S^-) is part of a universal conserved Pxxx(T/S)xxC motif. Residues in this motif components of an architecture that make feasible an extremely efficient nucleophilic attack of C_p-S^- towards hydroperoxides. Then, C_p is oxidized to sulfenic acid (C_p-SOH). C_p-SOH frequently forms an inter or intrasubunit disulfide bond before being reduced by a reductant molecule back to its initial thiolate state (Perkins *et al*, 2015). These ubiquitous proteins were subjected to several kinetics studies, showing that peroxiredoxins can become oxidized by peroxides such as H_2O_2, lipid peroxides and peroxynitrite with a second order rate ranging from 10^6 to 10^8 $M^{-1}s^{-1}$. Considering their high concentration in mammalian cells, peroxiredoxins are considered the major targets for peroxides (Halliwell, 2006; Adimore *et al*, 2010; Perkins *et al*, 2015; Rhee, 2016). C_p is conserved throughout all the peroxiredoxin family and these enzymes can be further classified based on the location (or absence) of a second catalytic Cys residues (resolution cysteine, C_r). Thus, peroxiredoxins sub-groups are: typical 2-Cys Prx, atypical 2-Cys Prx and 1-Cys Prx subfamily. In the typical 2-Cys Prx, C_p-SOH reacts with C_r of the

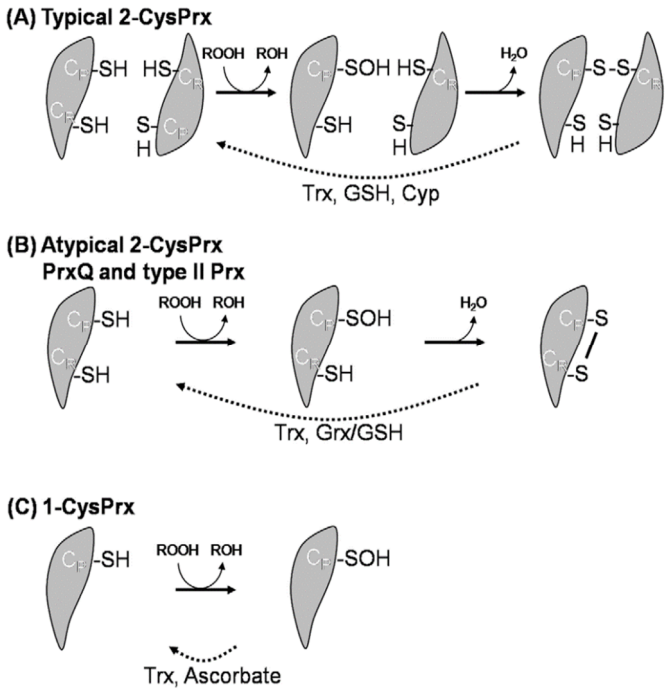

Fig. 11 – Peroxiredoxins reaction mechanisms. Scheme taken from Barranco-Medina *et al*, 2009.

other subunit to form an inter-disulfide bond, which would then be reduced by a reducing agent. In atypical 2-Cys Prx, C_p-SOH reacts with the Cr from the same subunit, forming an intra-disulfide bond, which is then reduced by a thiol compound. Finally, the 1-Cys Prx subfamily, C_p-SOH can only be resolved by forming a disulfide bond with other proteins or LMW-thiols (**Fig. 11**) (Rhee *et al*, 2001; Barranco-Medina *et al*, 2009). Alternatively, our group showed that ascorbate can also support the peroxidase activity of 1-Cys Prx (Monteiro *et al*, 2007).

Among other roles in a wide array of cell signaling processes, peroxiredoxins were identified to be involved in bacterial and fungi virulence, protecting the microorganisms against the oxidative burst caused by the host's immunity system (Kaihami *et al*, 2014; Perkins *et al*, 2015; Hillmann *et al*, 2016).

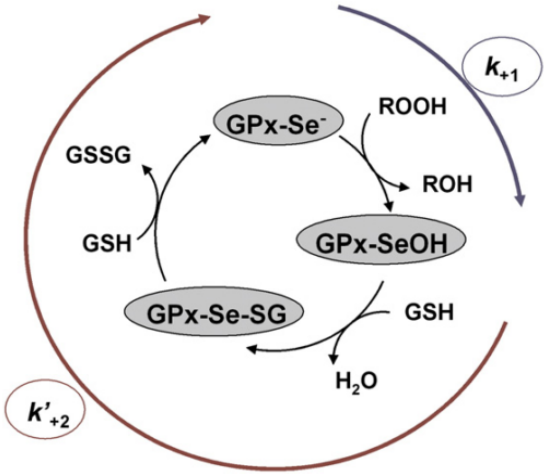

Fig. 12 – Catalytic cycle of glutathione peroxidases. These catalytic cycle in valid for GPx1, 3 and 4. First selenol becomes oxidized to selenic acid by a hydroperoxide. A first GSH would react with the selenic acid forming a selenadisulfide link which would be resolved by a second GSH molecules. Figure from Brigelius-flohé & Maiorino, 2013

1.3.3.2 – glutathione peroxidases

Another relevant thiol-dependent peroxidase family was first characterized during late-1950s as a peroxidase which would protect erythrocytes from oxidative damage and it was named as Glutathione peroxidase (GPx), as its activity, typically, depends on glutathione (GSH) (Mills, 1957). Glutathione peroxidases are ubiquitous proteins which, most frequently, have a C_p as peroxiredoxins. However, in mammal, it is more common the existence of a seleno-cysteine (Herbette *et al*, 2007; Toppo *et al*, 2008). A seleno-cysteine consists of a cysteine, which the sulphur atom is replaced by a selenium atom (R-SeH). Such characteristic is associated to an increase in efficiency in detoxifying either hydrogen peroxide or organic hydroperoxides in presence of glutathione (**Fig. 12**) (Brigelius-flohé & Maiorino, 2013). Non-selenium GPx shows much less efficiency in decomposing peroxides, however it was proposed that non-selenium GPx could play important roles in signal-transduction pathways such as in yeast and *Arabidopsis thaliana* (Delaunay *et al*, 2002; Miao *et al*, 2006). Some non-selenium GPx displays weak affinity for glutathione and thioredoxin system can reduction of these enzymes with higher efficiency (**Fig. 13**) (Herbette *et al*, 2007). Again, in line with the observation that the generation and release of oxidant

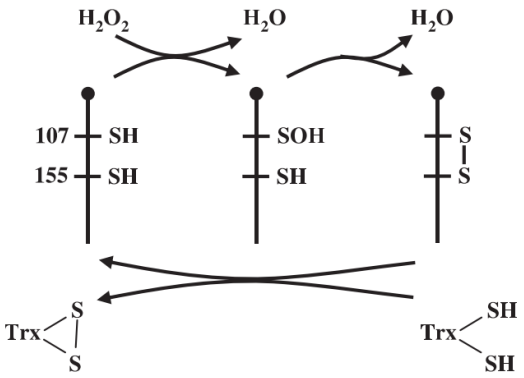

Fig. 13 – The mechanism of H2O2 reduction and GPX regeneration by thioredoxin for nonselenium GPx. Scheme from Herbette *et al*, 2007

molecules (oxidative burst) by phagocytic cells is one of the important component in host's defenses against bacterial pathogenicity, some indicated that glutathione peroxidase is involved with the virulence of pathogenic microorganisms (Brenot *et al*, 2004; Gardiner *et al*, 2015).

Peroxiredoxins and glutathione peroxidases are very well characterized enzymes and belong to a very large and diverse group of proteins which share a common structural architecture: the thioredoxin fold (Atkinson & Babbitt, 2009; Collet & Messens, 2010) (**Fig. 14**) .

1.4 – Ohr/OsmC Superfamily of proteins

1.4.1 - Primary structure characteristics

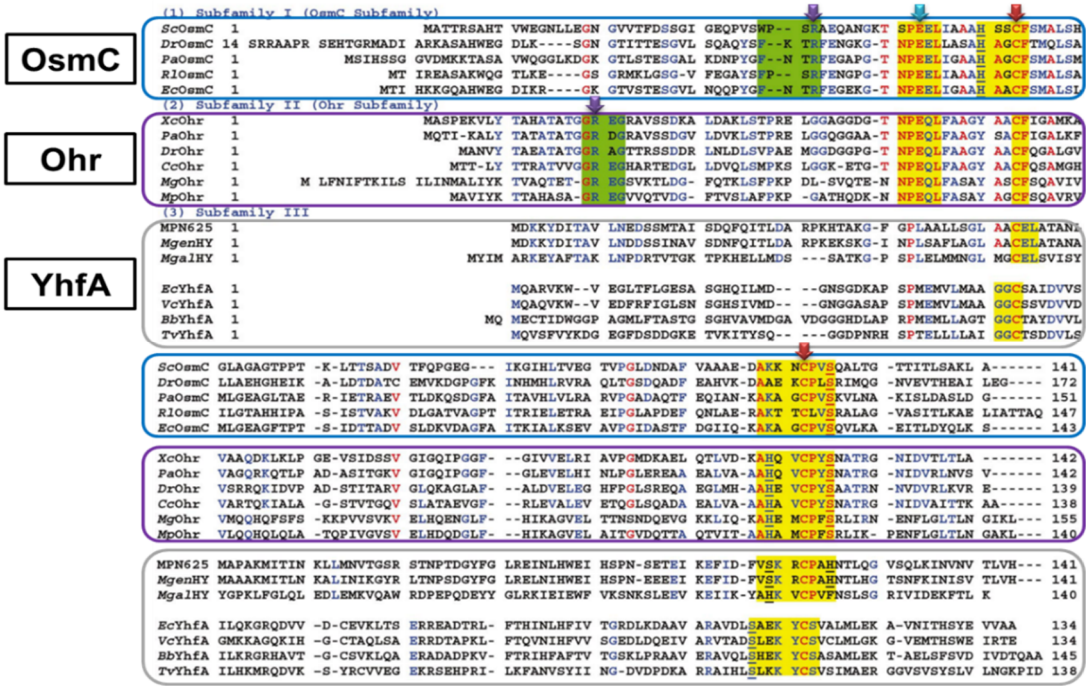

Fig. 15 – Sequence comparison among Ohr/OsmC Superfamily. Three sequence sub-families are aligned with several homologues, representing OsmC, Ohr and YhfA. Red arrows represent cysteines conserved in all subfamilies and purple and blue arrows represent catalytical arginine. Figure adapted from Shin *et al*, 2004

Ohr enzymes are also Cys-based peroxidases but they present very distinct structural and biochemical features, when compared with peroxiredoxins and glutathione peroxidases (Lesniak *et al*, 2002; Cussiol *et al*, 2003; Oliveira *et al*, 2006). These proteins belong to the Ohr/OsmC family, which includes three sub-families. Members of Ohr (Organic hydroperoxide resistance proteins) (blue box, **Fig. 15**) and (OsmC Osmotically inducible Protein C) (purple box, **Fig. 15**) sub-families display thiol-peroxidase activity. In contrast, the third large group of proteins do not shown any peroxidase activity and were named as YhfA (grey box, **Fig. 15**) (Gutierrez & Devedjian, 1991; Mongkolsuk *et al*, 1998a; Atichartpongkul *et al*, 2001; Shin *et al*, 2004).

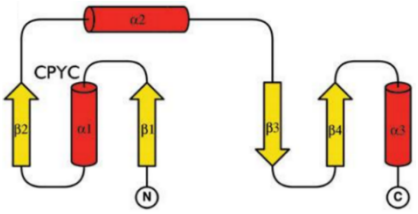

Fig. 14 – Schematic representation of glutaredoxin secondary structure. These proteins have Trx-fold consisting in the two Trx motifs connected by an extra α-helix. Collet & Messens, 2010

Recently, a study in our laboratory indicated that this third sub-family should be referred as Ohr-like (Meireles *et al*, 2017).

All the three groups contain two very conserved Cys: a N-terminal Cys that is directly responsible for the reduction of the peroxide (in the case of Ohr and OsmC) and a second C-terminal Cys that takes part of the disulfide bond (red arrows, **Fig. 15**). Furthermore, Ohr and OsmC also show a very conserved Glu (blue arrows, **Fig. 15**) in their primary sequence, which interacts with a very conserved Arg. This conserved Arg appears to increase the nucleophilicity of C_p. The location of this Arg in the primary within each of one the sub-families is distinct (purple arrows, **Fig. 15**), but in the tertiary structure they overlap quite well (Shin *et al*, 2004).

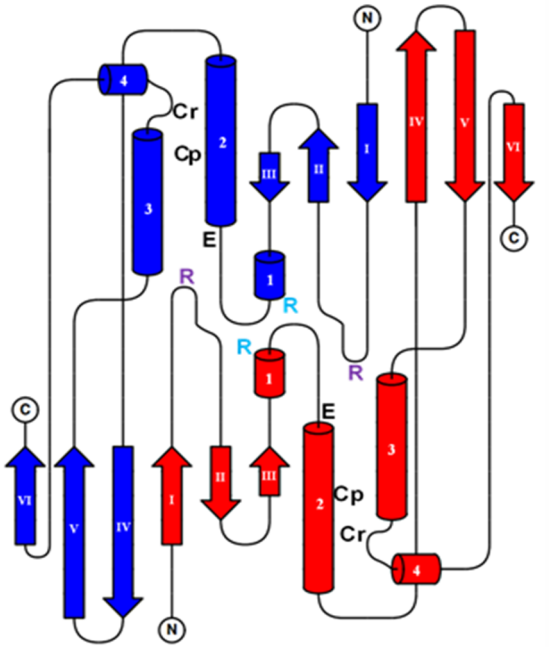

Fig. 16 – Topology diagram of the Ohr dimer. Blue represent chain A and red chain B. Catalytical Arg (R) are represented both for OsmC (light blue) and Ohr (purple). Figure adapted from Lesniak *et al*, 2002.

1.4.2 - Overall structure characteristics

The first tridimensional structures of Ohr (*P. aeruginosa*) and OsmC (*E. coli*) were released in 2002 and 2003, respectively, by Lesniak *et al*, and, for the first time was shown that OsmC, like its Ohr homolog presented peroxidatic activity (Lesniak *et al*, 2002, 2003). Together with YhfA sub-family, these proteins present a very distinct structure than the thioredoxin fold. The biologically active form of Ohr and OsmC is a homodimer with tightly intertwined

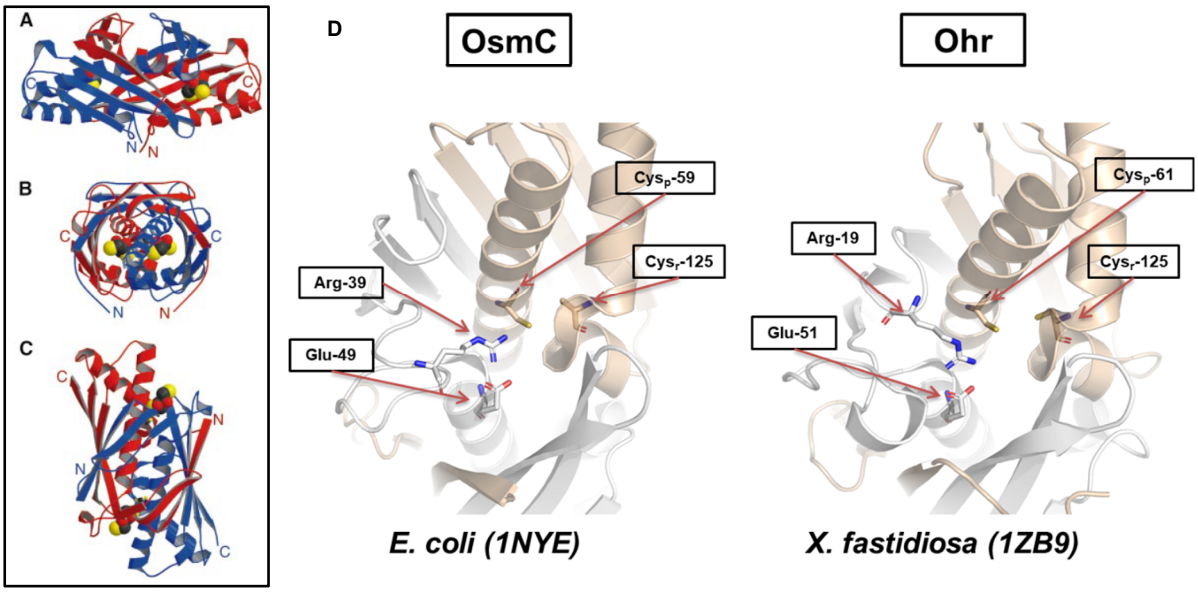

Fig. 17 – OsmC *vs* Ohr, structure considerations. From A to C there are represented three 90º views of the Ohr biological structure. Red and Blue represent the different monomers. DTT molecules is shown in spheres (red = oxygen, black = carbon, yellow = sulfur). D There is represented the tridimensional structure of an OsmC and an Ohr protein showing the positional different features of the catalytical triad residues (C_p, R_c and E). Adaptation from Lesniak *et al*, 2002

monomers in a head-to-tail orientation, originating an oval shape quaternary structure (**Fig 16 & 17**). Two antiparallel β-sheets, each composed of six strands (three from each monomer), wrap around four central short α-helices assembling two identical active pockets at opposite positions of the dimeric protein (Lesniak *et al*, 2002). The sum of all van der Waals helix-helix packing interactions at the center of the hydrophobic core of the dimeric enzyme is responsible for combining essential elements from both monomers, which fold together in an active Ohr (Lesniak *et al*, 2002, 2003; Shin *et al*, 2004). Either in Ohr or OsmC, the C_p is in the middle of the second α-helix, a central and buried region of the protein (**Fig. 16 & 17**). C_p together with the conserved Glu and the conserved Arg, constitute the catalytic triad in both sub-families (**Fig. 16 & 17**). Interestingly, the catalytic arginine (R_c) in Ohr proteins is placed in a loop between β-sheet I and II while R_c in OsmC proteins is placed in the short and flexible α-helix 1 (Lesniak *et al*, 2002, 2003; Shin *et al*, 2004).

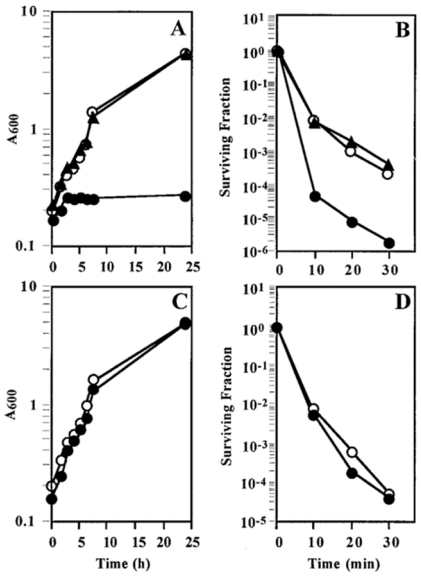

Fig. 18 – Effects of peroxide on growth and survival of X. campestris wt and ohr mutant. The effects on the growth of (A) t-BOOH (600 μM) and (C) H_2O_2 (200 μM) are shown on the left side. The effects on the survival of (B) t-BOOH (150 mM) and (D) H_2O_2 (30 mM) are shown on the right side. (○=wt, ●=*ohr* mutant and ▲=complementation with a vector expressing ohr). The figure was taken from Mongkolsuk *et al*, 1998

1.4.3 – Expression pattern and mutant phenotypes

Ohr was first described in late 1990's, when it was verified that the deletion of *ohr* gene rendered *Xanthomonas campestris* strongly sensitive to organic hydroperoxides (t-BOOH and CuOOH) but not hydrogen peroxide (Mongkolsuk *et al*, 1998a) (**Fig. 18**). Other evidences for the Ohr preference to organic hydroperoxides have been added since then, either by kinetic assays, employing various Ohr homologues or by viability evaluations employing mutant bacteria with *ohr* gene deletion (Ochsner *et al*, 2001; Cussiol *et al*, 2003, 2010; da Silva Neto *et al*, 2012; Si *et al*, 2015; Alegria *et al*, 2017).

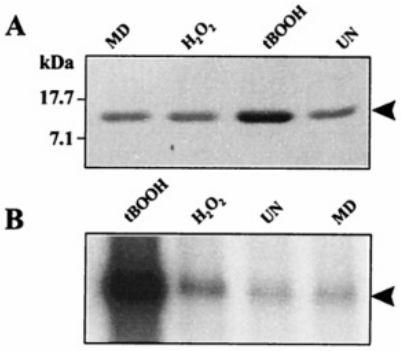

Fig. 19 – Expression of ohr in response to various oxidants. (A) represents Western analysis of Ohr levels in *X campestris*: (UN=uninduced, or induced with 100 μM of MD, H_2O_2 or tBOOH). (B) Northern blot of total RNA isolated from bacteria under the same conditions as the western blot. Image taken from Mongkolsuk *et al*, 1998

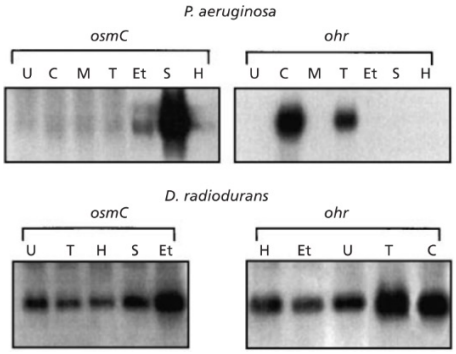

Fig. 20 – Expression analysis of ohr and osmC in response to stresses in *D. radiodurans* and *P. aeruginosa*. Northern blots from bacteria under different conditions. (U=untreated or treated with C= cumene hydroperoxide, H= H_2O_2, M= menadione, T= tBOOH or subjected to osmotic stress (S, salt) and ethanol stress (Et). Figure taken from Atichartpongkul *et al*, 2001, where experimental details can be found.

Furthermore, organic hydroperoxides (such as t-BOOH and CuOOH) strongly induce the expression of the *ohr* transcript as demonstrated in *X. campestris, P. aeruginosa* and *D. radiodurans* (Mongkolsuk *et al*, 1998a; Atichartpongkul *et al*, 2001) (**Fig. 19 & 20**).

OsmC was first characterized in 1991 by Gutierrez and Devedjian, however it took more than a decade to identify that enzymes belonging to the OsmC sub-family would also present peroxidatic activity as their homologue Ohr (Gutierrez & Devedjian, 1991; Lesniak *et al*, 2003). Interestingly, despite OsmC capability to reduce organic hydroperoxides, some these proteins were primarily associated to osmotic imbalance, since *OsmC* induction is triggered due to osmotic stress instead oxidative stress. In contrast of the pattern of *ohr* expression, *osmc* gene is induced by both increasing

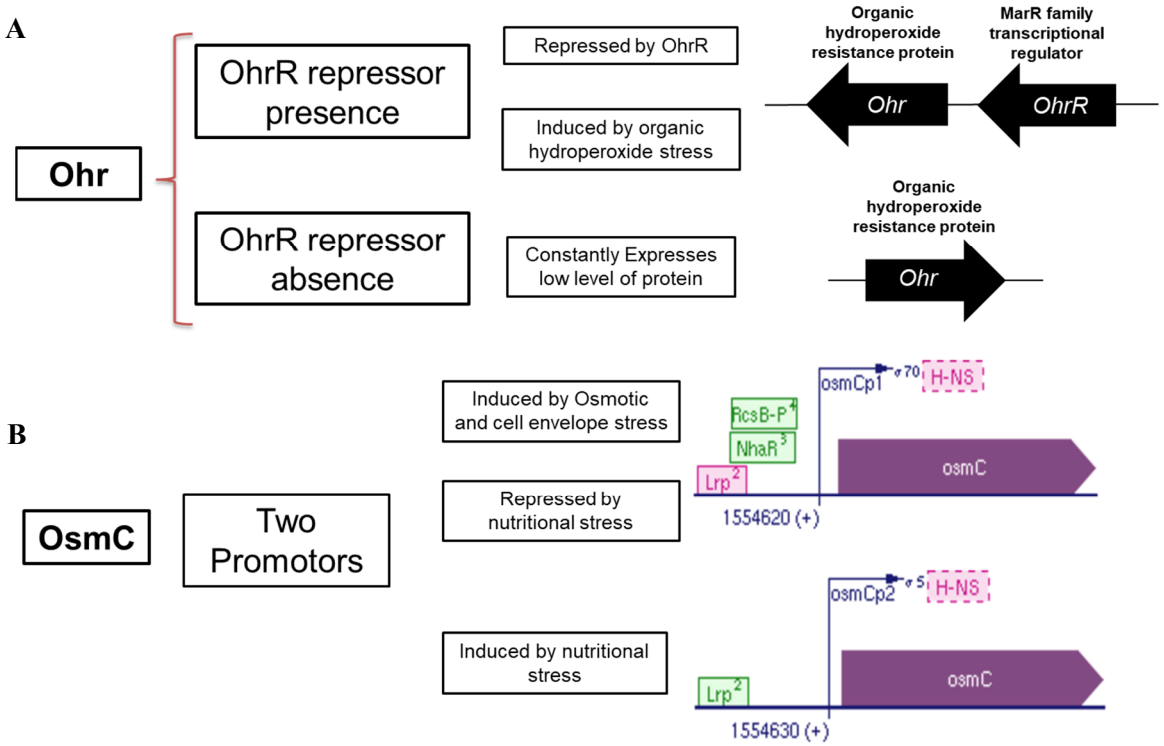

Fig. 21 – Ohr and OsmC expression regulation. (A) the *ohr* gene is frequently in close proximity to the *ohrR* gene, a transcription regulator which is responsible to control *ohr* expression. Still, *ohr* can also be found as a constitutive gene with no apparent regulation. (B) osmC gene expression is controlled by two different promoters, the OsmcP1 and OsmCp2. OsmcP1 is activated by dissection and osmotic shock and repressed by nutritional stress while OsmcP2 is induced by nutritional stress (Sledjeski & Gottesman, 1996; Bouvier *et al*, 1998; Davalos-garcia *et al*, 2001; Mongkolsuk *et al*, 2002; Cussiol *et al*, 2003; Oh *et al*. 2007).

of salt (S, **Fig. 20**) and ethanol concentrations (Et, **Fig. 20**) (Atichartpongkul *et al*, 2001).

As expected by their expression patterns, *ohr* and *osmC* genes are under very distinct regulatory machineries. For instance, two different promoters controlling *osmc* expression, OsmcP1 and OsmCp2, are present in the *E. coli* genome. It was first shown that leucine-responsive regulatory protein (Lrp) is associated to the repression of OsmCp1 and induction of OsmCp2 (Bouvier *et al*, 1998). Later, an additional regulatory system was identified: the two component-system *rcsB-rcsC,* which positively affects the OsmCp1 but not the OsmCp2. In *E.coli*, *rcsB-rcsC* regulation pathway is activated by dissection and osmotic shock (Sledjeski & Gottesman, 1996; Davalos-garcia *et al*, 2001) (**Fig. 21**).

In some bacteria, Ohr can be constitutively expressed, however, it is frequently controlled by OhrR regulators (**Fig. 21**) (Mongkolsuk *et al*, 2002; Cussiol *et al*, 2003; Oh *et al*, 2007). OhrR is functional as dimer and can operate either by 1-Cys or 2-Cys mechanisms, through which the regulator senses the oxidative stress induced by organic hydroperoxides. In both cases, a reactive cysteine is oxidized by organic hydroperoxides into –SOH. However, formation of C_P-SOH is not enough to trigger the conformational change required to dissociate this transcriptional repressor form DNA. In the case 1-Cys OhrR, C_P-SOH has to undergo nucleophilic substitution with endogenous low molecular-weight thiols and the formation of the mixed disulfide bond then trigger the dissociation of the repressor from the target DNA (**Fig. 22**) (Hong *et al*, 2005; Vázquez-Torres, 2012). In the case of 2-Cys OhrR, C_P-SOH condenses with the second Cys, originating an intermolecular disulfide in the homodimer, which then undergo a structural switch, leading to the repressor dissociation from the operator (Chuchue *et al*, 2006; Vázquez-Torres, 2012; da Silva Neto *et al*, 2012). In both cases, the oxidation processes are reversible. Our group showed that for *Chromobacterium violaceum* OhrR (2-cys OhrR), the thioredoxin system is the biological reducing agent of this thiol-based regulator (da Silva Neto *et al*, 2012). Furthermore, in some studies, OhrR, but not Ohr was associated to the virulence of *Pseudomonas aeruginosa*, *Vibrio cholerae* and *Chromobacterium violaceum* pathogenesis (Atichartpongkul *et al*, 2010; Liu *et al*, 2016; Previato-Mello *et al*, 2017). Some evidences suggest OhrR might be involved in other regulatory pathways, besides controlling *ohr* expression.

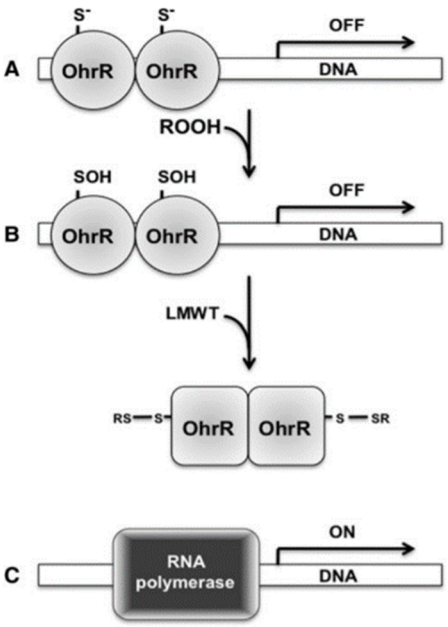

Fig. 22 – Regulation of gene transcription by the redox sensor OhrR. (A) The dimeric reduced OhrR protein represses the transcription of target genes. (B) Once Organic hydroperoxides oxidize OhrR reactive cysteine into a stable sulfenic acid state (SOH). This sulfenylated OhrR can then be thiolated by LMWT (represented in the figure) or by a second cysteine (when present) (not represented in the figure) driving the conformational changes associated with the dissociation of OhrR from RNA. (C) The dissociation of oxidized OhrR allows the recruitment of RNA polymerase to the ohr promoter. Image taken from Vázquez-Torres, 2012

1.4.4 – Phylogenetic distribution of Ohr/OsmC proteins.

Phylogenetic studies carried out in our group indicated that Ohr and OsmC are only present in microorganisms such as bacteria, fungi and some non-vascular plants (bryophytes). Specifically, Ohr homologues are present in several pathogenic microorganisms, and absent in mammals and plants which are hosts of microbial pathogens (Meireles *et al*, 2017). Such characteristic suggest that these proteins might represent convenient targets for drug design, when aiming to increase sensibility of pathogenic bacteria to the oxidative burst generated either by hosts immune system or by the mechanism of action from several antibiotics (Kohanski *et al*, 2007; Dwyer *et al*, 2009). Several results presented

in this thesis derived from internal collaborations within members of our lab. In one specific case, we showed the Ohr is presented in eukaryotic organisms, where these enzymes can be targeted to fungal mitochondria (**Chapter 2**).

1.5 - Organic Hydroperoxide Resistance Proteins (Ohr)

Proteins belonging to the Ohr sub-family present extraordinary efficiency towards organic hydroperoxides (10^6–10^8 M^{-1}. s^{-1}) (Cussiol *et al*, 2010; Alegria *et al*, 2017). Additionally, Ohr enzymes can be directly associated with their redox specialized sensor system, OhrR in operons, allowing cells to sense and increase their resistance towards oxidative stress through the induction of *ohr* expression (Mongkolsuk *et al*, 2002; Cussiol *et al*, 2003; da Silva Neto *et al*, 2012). These thiol-dependent peroxidases are, as previously mentioned, the main subject of interest in this study, thus we will focus the description of Ohr proteins.

1.5.1 - Structure characteristics

Ohr active site architecture is composed by two Cys residues (C_p and C_r), the C_p , which directly reacts with peroxides while Cr is essential for enzymatic turnover (**Fig. 23**). These two amino acids are present in the same subunit, while the other subunit is responsible to provide the catalytic Arg (R_c) and its positional partner, the catalytic Glu (E_c) (**Fig. 23, right**). In the so-called close state, the C_p, R_c and E_c interact through polar interactions, which stabilizes C_p in the thiolate state, thereby increasing its nucleophilicity. Analysis of Ohr (close conformation) from *Xylella fastidiosa* which was co-crystallized with a PEG molecule placed in its active pocket, allowed the identification of several hydrophobic interactions involved in the enzyme-ligand interactions (Oliveira *et al*, 2006). It was then proposed that PEG could be mimicking lipid hydroperoxides (putative substrates) and that these

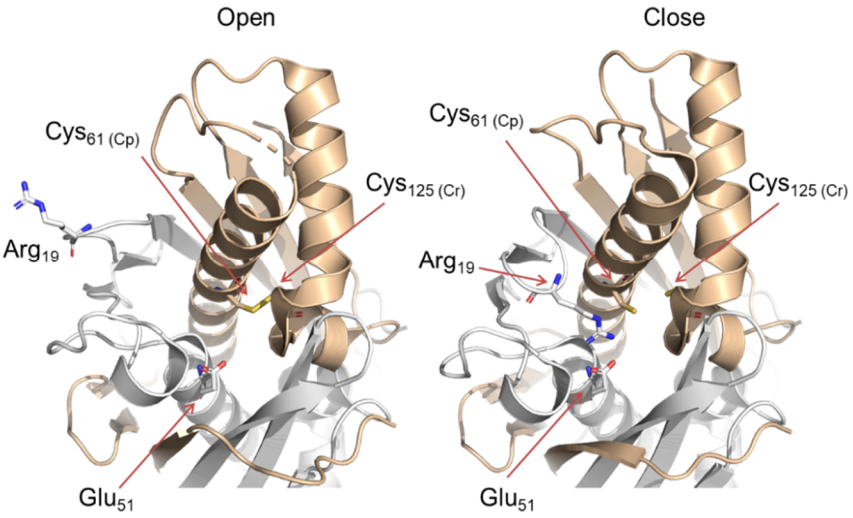

Fig. 23 – The two major conformational states found in Ohr crystal structures, the open and close conformations. (left) Open conformation is found when the catalytic triad (C_p, R and E) is disrupted. The loop containing the catalytical arginine loses stability at the active pocked when C_p and C_r are covalently bound. (right) Close conformation is found when the catalytical triad network interaction are intact where the catalytical arginine is facing the active site stabilized by the glutamate and the reduced C_p salt bridge interacting. Images generated from PDB_{ID}=4XX2 (left) and PDB_{ID}=1N2F (right).

interactions might be very important in enzyme-substrate interactions (Oliveira *et al*, 2006) (**Fig. 24**). Ohr could also assume an open state (OS), in which the loop containing R_c (Arg-loop) is far away from C_p, disrupting the C_p, R and E network of interactions (**Fig. 23, left**). This OS was previously suggested to be the most suitable to accommodate the reducing agent: the dihydrolipoic acid portion of lipoylated proteins (Lesniak *et al*, 2002; Cussiol *et al*, 2003; Meunier-Jamin *et al*, 2004; Oliveira *et al*, 2006; Cussiol *et al*, 2010).

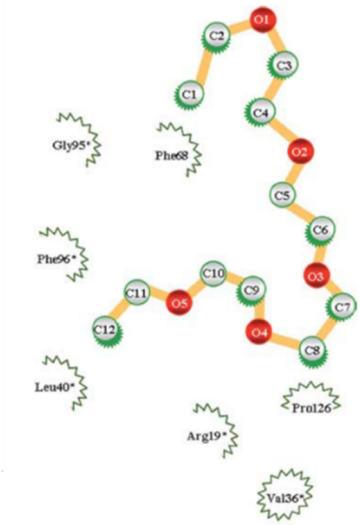

Fig. 24 – PEG binding in the X. fastidiosa Ohr active site. Protein–PEG hydrophobic interactions according to LIGPLOT analysis. Figure from Oliveira *et al*, 2006.

1.5.2 - Proposed Enzymatic Mechanism

The existence of these two different Ohr conformations (CS and OS) lead us to suggest that Ohr would depend on a major conformation changes to complete its catalytic cycle (Oliveira et at. 2006). Accordingly, the C_p, R_c and E_c network of interactions would be essential to assure Ohr reactivity towards lipid hydroperoxides (**Step I & II Fig. 25**) (Oliveira *et al*, 2006; Ta *et al*, 2011). Then C_p-SOH would condense with C_r, linking both sulfurs in a disulfide bond. The absence of a negative

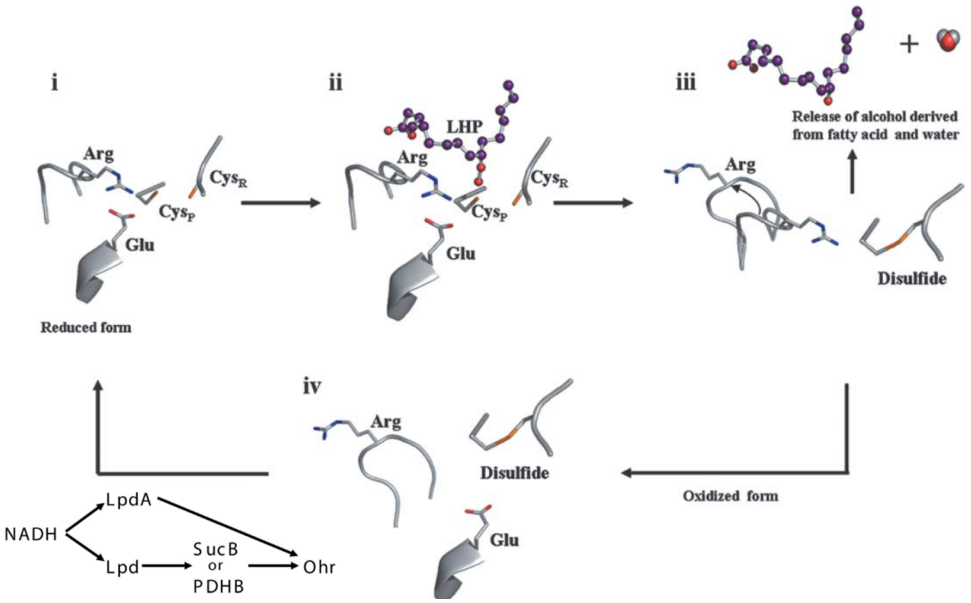

Fig. 25 – Proposed mechanism of action of Ohr proteins. (i) Reduced Ohr (Cp-S^-) together with a proximal glutamate allow the stabilization of the catalytical arginine in an inner position. These network interactions would be crucial for thiolate stabilization and the nucleophilicity of cysteine to attack the hydroperoxides. (ii) the lipid hydroperoxide (LHP) is attacked by Cp and Cp becomes oxidized into the sulfenic acid. (iii) The sulfenic acid from Cp is then quickly attacked by the sulfhydryl group of the resolution cysteine (Cr) forming an intramolecular disulfide bridge. The covalent bond would be responsible for the loss of stability of the catalytical arginine which would be detached and switch to the open conformation. (iv) The open conformation would better accommodate the biological reductant, lipoylated proteins (LpdA, SucB or PDHB) which would reduce Ohr inducing the rearrangement of the loop bringing the arginine back to an inner position. Image adapted from Oliveira *et al*, 2006 and Cussiol *et al*, 2010.

charge in C_P when Ohr is in the disulfide form would disrupt the network of interaction, allowing R_c to

leave the active site (**Step III, Fig.25**). Finally, Ohr would adopt the OC, which is expected to best accommodate the biological reductant, lipoylated proteins (ex. SucB or LpdA) (Cussiol *et al*, 2003; Meunier-Jamin *et al*, 2004; Oliveira *et al*, 2006; Cussiol *et al*, 2010). The importance of the R-loop dynamics for the Ohr turnover is another issue addressed during my PhD program towards which resulted in relevant achievements (**Chapter 3 & 4**).

1.5.3 – Possible oxidant substrates of Ohr

It is well known that Ohr enzymes display preference for organic hydroperoxides over hydrogen peroxide (Mongkolsuk *et al*, 1998a; Klomsiri *et al*, 2005; Oliveira *et al*, 2006; Alegria *et al*, 2017). However, in most of these studies, artificial compounds such as (t-BOOH or cumene hydroperoxide (CuOOH) were employed. Thus, the identification of the natural oxidizing substrates of Ohr was still a challenge. Then, studies on the induction of *ohr* expression by linoleic acid hydroperoxides indicated, for the first time, that fatty acid peroxides might be the biological substrates of Ohr (Klomsiri *et al*, 2005). Another additional evidence came from the previous mentioned, *Xf*Ohr crystallographic structure co-crystallized with a PEG molecule placed at its active pocket where it was evident that elongated hydroperoxides would fit very well into the electron density corresponding to the PEG molecule (Oliveira *et al*, 2006; Alegria *et al*, 2017). Furthermore, recently, several microbiological and biochemical/kinetic assays correlated and showed the systematic preference of Ohr to reduce elongated fatty acid hydroperoxides (**Table 1**) (Alegria *et al*, 2017). Ohr is also highly reactive towards peroxynitrite and the corresponding mutant strain is more sensitive to this oxidant than the wild type strain (Alegria *et al*, 2017). Further studies are required to understand the biochemical and structural basis for the Ohr-peroxynitrite interaction.

Table 1 – Parameters related to hydroperoxide reduction by Ohr

	k_{obs}, $M^{-1}.s^{-1}$	Oxidative inactivation, µM	$MIC_{wt}/MIC_{\Delta ohr}$*
Hydroperoxide	AhpE/Ohr competition	~IC_{10}†	Extent of inhibition
H_2O_2	$(3.0 \pm 0.6) \times 10^3$	>100	1
LAOOH	$(6.3 \pm 1.7) \times 10^7$	1	>10
OAOOH	$(4.5 \pm 3.5) \times 10^8$	1	>10
5(*S*)-HpETE	$(2.6 \pm 1.2) \times 10^7$	ND	ND
15(*S*)-HpETE	$(6.0 \pm 3.0) \times 10^7$	ND	ND
ChOOH	—	>100	1
t-BHP	$2.0 \times 10^{6‡}$	100	3
ONOOH	$(2 \pm 0.3) \times 10^7$	ND	—
CHP	ND	100	3

k_{obs}, observed rate constant; ND, not determined.
*Ratio of MIC_{wt} (minimal concentration of hydroperoxide that inhibits growth of wild-type strain) to $MIC_{\Delta ohr}$ (minimal concentration of hydroperoxide that inhibits growth of *Δohr* strain).
†Defined here as the amount of hydroperoxide that provokes 10% Ohr inactivation.
‡Because Ohr is several orders of magnitude more efficient than MtAhpE in the reduction of t-BHP, it was not possible to determine this rate constant through the competitive assay. Instead, data from the study by Cussiol *et al* 2010 were added here
Table from Alegria *et al.* 2017

1.5.4 – Ohr reductant substrates

As previously mentioned, the functionality of several thiol-dependent peroxidases and their turnover, frequently depends on thiol-disulfide exchange reactions. In highly efficient peroxidases, the reduction is dependent on LMW thiols or enzymatic reducing agents. Examples of reductants for peroxidases are monothiols such as the biological GSH or the synthetic 2-mercaptoethanol and enzymatic systems, such as thioredoxin (Nagy, 2013; Winther & Thorpe, 2014). Interestingly, differently to peroxiredoxins and glutathione reductases, neither the monothiols or the thioredoxin system can reduce Ohr (Cussiol *et al*, 2003). Nevertheless, dithiols such as DTT (a synthetic reducing agent), was able to recycle Ohr. Dihydrolipoic acid (DHLA) (**Fig. 26A**) a biological dithiol, similarly to DTT, could also support the peroxidase activity of Ohr (Cussiol *et al*, 2003). Although lipoylated proteins are mostly associated as electron acceptors in oxidative pathways (Cronan, 2016), they can also act as electron donors in some cases (**Fig. 26**) (Bryk *et al*, 2002; Eser *et al*, 2009; Cronan, 2016). Remarkably, the ability of lipoylated proteins to reduce Ohr enzymes was later described, both, by Co-Immunoprecipitation (Co-IP) and reconstitution of enzymatic systems (Cussiol *et al*, 2010). Furthermore, It was suggested that the reducing agents would interact with oxidized Ohr proteins in its open conformation (Meunier-Jamin *et al*, 2004; Oliveira *et al*, 2006). Before this work, there were no cohesive mechanistic studies on the Ohr dynamics, which could support the conformational exchange between OS and CS during enzymatic turnover. Furthermore, at this moment, it is still not any clear how lipoylated proteins would interact and reduce disulfides in Ohr enzymes. The results presented in **Chapter 4** represent an important contribution in this regard.

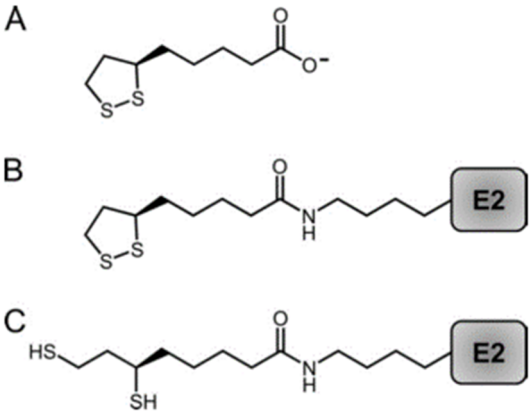

Fig. 26 – Lipoylated moieties. (A) *R* stereoisomer of lipoate (biologically active). (B) and (C) The oxidized and reduced lipoyl cofactor, lipoamide and dihydrolipoamide, respectively, bound to a conserved lysine residue of the E2 subunit of lipoylated complexes. Image taken from (Spalding & Prigge, 2010).

1.5.5 – Ohr and virulence

It is well accepted that Ohr peroxidase activity enhances cells' resistance against organic hydroperoxides insult. Among the several bacteria that can express the *ohr* gene, some are very relevant in terms of public health and agriculture, including *Pseudomonas aeruginosa*, *Xylella fastidiosa* and *Chromobacterium violaceum* (Mongkolsuk *et al*, 1998a; Chuchue *et al*, 2006; Atichartpongkul *et al*, 2010; Federici *et al*, 2012; da Silva Neto *et al*, 2012; Saikolappan *et al*, 2015). There are evidences of the involvement of Ohr in bacterial virulence, although this is still a controversial issue. For instance, *ohr* gene from *Actinobacillus pleuropneumoniae*, the causative agent of porcine pleuropneumonia, is specifically up- regulated during infection (Shea & Mulks, 2002; Wolfram *et al*, 2009). Moreover, studies in *Listeria monocytogenes*, a facultative intracellular bacterial pathogen and in *mycobacterium*

smegmatis, showed that Ohr plays a crucial role for bacteria survival within the phagosomes of the host macrophages (**Fig. 27**) (Saikolappan *et al*, 2015; Reniere *et al*, 2016). Other studies indicated that Ohr and its transcriptional repressor OhrR are crucial to the successful adaptation of *Bacillus cereus* to the gastrointestinal (GI) tract environment, which is characterized to have very distinct niches with different oxygen concentrations and different oxidoreduction potentials (ORP) (Clair *et al*, 2012). This study indicated that OhrA is important for pathogen adaptation during low ORP anaerobiosis and aerobiosis, however its importance was higher in aerobic respiratory conditions than in high reductive fermentative conditions. Nevertheless, it was shown that along OhrA expression, SucB was also highly expressed, under anaerobiosis. Then, it was hypothesized that OhrA could, possibly, be necessary to prevent excessive accumulation of the reduced form of lipoylated SucB (regenerating oxidative form) preventing the generation of oxidants from 2-oxo-acid dehydrogenase complex (OGDC) redox cycles under high reductive conditions (Clair *et al*, 2012).

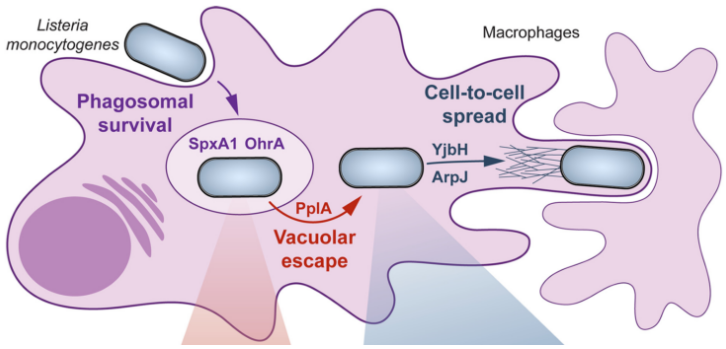

Fig. 27 – Model identifying where in the L. monocytogenes life cycle, Ohr is required. Once phagocytosed by a host macrophage, *L. monocytogenes* (light blue rods) requires the gene products of spxA1 and ohrA to survive in the phagosome. Image adapted from Reniere *et al*, 2016.

In spite all these lines of evidence, the Ohr involvement in virulence is still controversial. Contrarily to what was expected, the *ΔohrR* mutant (that express Ohr in large amounts) is some bacterial species was less virulent than the corresponding wild type strain. For instance, a great decrease in pathogenicity for a *Δohr Pseudomonas aeruginosa* strain was observed in a *Caenorhabditis elegans* model (Atichartpongkul *et al*, 2010). The authors raised the hypothesis that OhrR could not only control the expression of Ohr but could be also involved in the expression of other important genes for virulence (Atichartpongkul *et al*, 2010).

Vibrio cholerae is the causative agent of the diarrheal disease cholera. These bacteria have to face several life cycle transitions from oxygen-rich aquatic reservoirs to the oxygen-limiting conditions of human GI tract. Therefore, *V. cholerae* employs sophisticated signal-transduction networks to activate a set of virulence factors. Among them, OhrR was crucial as an additional anoxic sensor during the infection of this pathogen. At oxygen-limiting conditions, OhrR would attach to the promoter regions of target genes, including *tcpP*, a transmembrane regulator needed for the expression of *toxT*, the master virulence regulator of virulent genes in *Vibrio cholerae*. At aquatic and oxygen-rich environment OhrR would become oxidized and detached from the promoter region, preventing the tcpP expression (**Fig. 28**) (Liu *et al*, 2016).

These findings indicated that host-pathogen interactions are far more complex than initially anticipated. Ohr could also subvert complex host signaling processes, such as inflammatory processes

(Baxt *et al*, 2013). In fact, hydroperoxides of arachidonic acid are mediators of inflammatory processes in mammals, while hydroperoxide of linoleic acid plays equivalent roles in plants. As previously mentioned, Ohr efficiently reduces these hydroperoxides to the corresponding alcohols, thus the enzyme could play an important role in the bacterial response to oxidants and/or by disturbing host signaling processes (Baxt *et al*, 2013; Alegria *et al*, 2017).

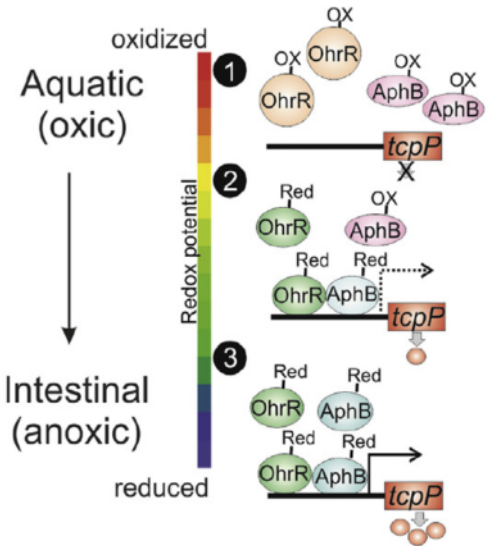

Fig. 28 – Model of the OhrR and AphB reducing sensors action on Vibrio cholerae virulence. AphB and OhrR respond to redox-potential changes differently. This results in differential regulation of tcpP so that promptly reduced OhrR jump-starts virulence during the transition from aquatic environments into the host. Image taken from Liu *et al*, 2016.

1.5.6 - Ohr as a Potential Drug target

Ohr presence in many pathogenic microorganisms; several evidences of its involvement in bacterial virulence; Ohr unique barrel shaped structural fold; and its absence in mammals and vascular plants (hosts in several important diseases), suggest that Ohr might be a potential target for drug development. Ohr inhibition could decreases bacteria chances in overcoming the host mechanisms of defense. Considering the probable involvement of oxidants in antibiotic-mediated killing of pathogens, the discovery of a bioactive compound with the ability to inhibit Ohr peroxidase activity could also work as a new antibiotic boosting molecule. Then, inhibiting Ohr could lead to a dual mechanism in fighting bacterial infections. Several results presented in this thesis represent initial steps regarding the search and design of molecules with potential to inhibit Ohr proteins (**Chapter 5**).

1.6 – References

Van Acker H & Coenye T (2017) The Role of Reactive Oxygen Species in Antibiotic-Mediated Killing of Bacteria. ***Trends Microbiol.*** 25**:** 456–466

Van Acker H, Gielis J, Acke M, Cools F, Cos P & Coenye T (2016) The role of reactive oxygen species in antibiotic-induced cell death in Burkholderia cepacia complex bacteria. ***PLoS One*** 11**:** 1–20

Adimore NJ, Jones DP & Kemp ML (2010) A Model of Redox Kinetics Implicates the Thiol Proteome in Cellular Hydrogen Peroxide Responses. ***Antioxid. Redox Signal.*** 13**:** 731–743

Alegria TGP, Meireles DA, Cussiol JRR, Hugo M, Trujillo M, de Oliveira MA, Miyamoto S, Queiroz RF, Valadares NF, Garratt RC, Radi R, Di Mascio P, Augusto O & Netto LES (2017) Ohr plays a central role in bacterial responses against fatty acid hydroperoxides and peroxynitrite. ***Proc. Natl. Acad. Sci.*** 114**:** E132–E141

Alvarez MN, Peluffo G, Piacenza L & Radi R (2011) Intraphagosomal peroxynitrite as a macrophage-derived cytotoxin against internalized Trypanosoma cruzi: Consequences for oxidative killing and role of microbial peroxiredoxins in infectivity. ***J. Biol. Chem.*** 286**:** 6627–6640

Apel K & Hirt H (2004) REACTIVE OXYGEN SPECIES: Metabolism, Oxidative Stress, and Signal Transduction. ***Annu. Rev. Plant Biol.*** 55**:** 373–399

Atichartpongkul S, Fuangthong M, Vattanaviboon P & Mongkolsuk S (2010) Analyses of the regulatory mechanism and physiological roles of Pseudomonas aeruginosa OhrR, a transcription regulator and a sensor of organic hydroperoxides. ***J. Bacteriol.*** 192**:** 2093–2101

Atichartpongkul S, Loprasert S, Vattanaviboon P, Whangsuk W, Helmann JD & Mongkolsuk S (2001) Bacterial Ohr and OsmC paralogues define two protein families with distinct functions and patterns of expression. ***Microbiology*** 147**:** 1775–82

Atkinson HJ & Babbitt PC (2009) An atlas of the thioredoxin fold class reveals the complexity of function-enabling adaptations. ***PLoS Comput. Biol.*** 5**:** 1–17

Babenko LM, Shcherbatiuk MM, Skaterna TD & Kosakivska I V. (2017) LIPOXYGENASES AND THEIR METABOLITES IN FORMATION OF PLANT STRESS TOLERANCE. ***Ukr Biochem. J.*** 89**:** 2409–4943

Banerjee S & Ghosh J (2016) Drug Metabolism and Oxidative Stress: Cellular Mechanism and New Therapeutic Insights. ***Biochem. Anal. Biochem.*** s3**:** 1–11

Barranco-Medina S, Lázaro JJ & Dietz KJ (2009) The oligomeric conformation of peroxiredoxins links redox state to function. ***FEBS Lett.*** 583**:** 1809–1816

Baxt LA, Garza-Mayers AC & Goldberg MB (2013) Bacterial subversion of host innate immune pathways. ***Science (80-.).*** 340**:** 697–701

Bedard K & Krause K-H (2007) The NOX Family of ROS-Generating NADPH Oxidases: Physiology and Pathophysiology. ***Physiol. Rev.*** 87**:** 245–313

Bedard K, Lardy B & Krause KH (2007) NOX family NADPH oxidases: Not just in mammals. ***Biochimie*** 89**:** 1107–1112

Belenky P, Ye JD, Porter CBM, Cohen NR, Lobritz MA, Ferrante T, Jain S, Korry BJ, Schwarz EG, Walker GC & Collins JJ (2015) Bactericidal Antibiotics Induce Toxic Metabolic Perturbations that Lead to Cellular Damage. ***Cell Rep.*** 13**:** 968–980

Bouvier J, Gordia S, Kampmann G, Lange R, Hengge-Aronis R & Gutierrez C (1998) Interplay between global regulators of Escherichia coli: Effect of RpoS, Lrp and H-NS on transcription of the gene osmC. ***Mol. Microbiol.*** 28**:** 971–980

Brash AR (1999) Lipoxygenases: Occurrence, Functions, Catalysis, and Acquisition of Substrate. ***J. Biol. Chem.*** 274**:** 23679–23682

Breitenbach M, Weber M, Rinnerthaler M, Karl T & Breitenbach-Koller L (2015) Oxidative stress in fungi: Its function in signal transduction, interaction with plant hosts, and lignocellulose degradation. ***Biomolecules*** 5**:** 318–342

Brenot A, King KY, Janowiak B, Caparon MG & Griffith O (2004) Contribution of Glutathione Peroxidase to the Virulence of Streptococcus pyogenes Contribution of Glutathione Peroxidase to the Virulence of Streptococcus pyogenes. ***Infect. Immun.*** 72**:** 408–413

Brigelius-flohé R & Maiorino M (2013) Biochimica et Biophysica Acta Glutathione peroxidases ☆. ***BBA - Gen. Subj.*** 1830**:** 3289–3303

Bryk R, Lima CD, Erdjument-Bromage H, Tempst P & Nathan C (2002) Metabolic enzymes of mycobacteria linked to antioxidant defense by a thioredoxin-like protein. ***Science (80-.).*** 295**:** 1073–1077

Cadenas E (1989) Biochemistry of Oxygen Toxicity. ***Annu. Rev. Biochem.*:** 79–110

Chae HZ, Chung SJ & Rhee SG (1994a) Thioredoxin-dependent peroxide reductase from yeast. ***J. Biol. Chem.*** 269**:** 27670–27678

Chae HZ, Kim IH, Kim K & Sue Goo Rhee (1993) Cloning, sequencing, and mutation of thiol-specific antioxidant gene of Saccharomyces cerevisiae. ***J. Biol. Chem.*** 268**:** 16815–16821

Chae HZ, Robison K, Poole LB, Church G, Storz G & Rhee SG (1994b) Cloning and sequencing of thiol-specific antioxidant from mammalian brain: alkyl hydroperoxide reductase and thiol-specific antioxidant define a large family of antioxidant enzymes. ***Proc. Natl. Acad. Sci.*** 91**:** 7017–7021

Chatre L & Ricchetti M (2014) Are mitochondria the Achilles' heel of the Kingdom Fungi? ***Curr. Opin. Microbiol.*** 20**:** 49–54

Chuchue T, Tanboon W, Prapagdee B, Dubbs JM, Vattanaviboon P & Mongkolsuk S (2006) ohrR and ohr Are the Primary Sensor / Regulator and Protective Genes against Organic Hydroperoxide Stress in Agrobacterium tumefaciens. 188**:** 842–851

Clair G, Armengaud J & Duport C (2012) Restricting Fermentative Potential by Proteome Remodeling: AN ADAPTIVE STRATEGY EVIDENCED IN BACILLUS CEREUS. ***Mol. Cell. Proteomics*** 11**:** M111.013102

Collet J-F & Messens J (2010) Structure, function, and mechanism of thioredoxin proteins. ***Antioxid. Redox Signal.*** 13**:** 1205–1216

Cronan JE (2016) Assembly of Lipoic Acid on Its Cognate Enzymes: an Extraordinary and Essential Biosynthetic Pathway. ***Microbiol. Mol. Biol. Rev.*** 80**:** 429–50

Cussiol JRR, Alegria TGP, Szweda LI & Netto LES (2010) Ohr (organic hydroperoxide resistance protein) possesses a previously undescribed activity, lipoyl-dependent peroxidase. ***J. Biol. Chem.*** 285**:** 21943–50

Cussiol JRR, Alves SV, de Oliveira MA & Netto LES (2003) Organic hydroperoxide resistance gene encodes a thiol-dependent peroxidase. ***J. Biol. Chem.*** 278**:** 11570–8

Davalos-garcia M, Conter A, Toesca I, Gutierrez C, Cam K, Davalos-garcia M, Conter A, Toesca I, Gutierrez C & Cam K (2001) Regulation of osmC Gene Expression by the Two-Component System rcsB-rcsC in Escherichia coli Regulation of osmC Gene Expression by the Two-Component System rcsB-rcsC in Escherichia coli. 183**:** 5870–5876

Delaunay A, Pflieger D, Barrault M-B, Vinh J & Toledano MB (2002) A Thiol Peroxidase Is an H2O2 Receptor and Redox-Transducer in Gene Activation. ***Cell*** 111**:** 471–481

Dwyer DJ, Belenky PA, Yang JH, MacDonald IC, Martell JD, Takahashi N, Chan CTY, Lobritz MA, Braff D, Schwarz EG, Ye JD, Pati M, Vercruysse M, Ralifo PS, Allison KR, Khalil AS, Ting AY, Walker GC & Collins JJ (2014) Antibiotics induce redox-related physiological alterations as part of their lethality. ***Proc. Natl. Acad. Sci.*** 111**:** E2100–E2109

Dwyer DJ, Kohanski MA & Collins JJ (2009) Role of reactive oxygen species in antibiotic action and resistance. **:** 482–489

Eser M, Masip L, Kadokura H, Georgiou G & Beckwith J (2009) Disulfide bond formation by exported glutaredoxin indicates glutathione's presence in the E. coli periplasm. ***Proc. Natl. Acad. Sci. U. S. A.*** 106**:** 1572–1577

Federici MT, Marcondes JA, Picchi SC, Stuchi ES, Fadel AL, Laia ML, Lemos MVF & Lemos EGM (2012) Xylella fastidiosa: An in vivo system to study possible survival strategies within citrus xylem vessels based on global gene expression analysis. ***Electron. J. Biotechnol.*** 15**:**

Ferrer-Sueta G, Manta B, Botti H, Radi R, Trujillo M & Denicola A (2011) Factors affecting protein thiol reactivity and specificity in peroxide reduction. ***Chem. Res. Toxicol.*** 24**:** 434–450

Franchini AM, Hunt D, Melendez JA & Drake JR (2013) Fc R-driven Release of IL-6 by Macrophages Requires NOX2-dependent Production of Reactive Oxygen Species. ***J. Biol. Chem.*** 288**:** 25098–25108

Gacesa R, Dunlap WC, Barlow DJ, Laskowski RA & Long PF (2016) Rising levels of atmospheric oxygen and evolution of Nrf2. ***Sci. Rep.*** 6**:** 27740

Gandara ACP, Torres A, Bahia AC, Oliveira PL & Schama R (2017) Evolutionary origin and function of NOX4-art, an arthropod specific NADPH oxidase. ***BMC Evol. Biol.*** 17**:** 1–16

Gardiner M, Thomas T & Egan S (2015) A glutathione peroxidase (GpoA) plays a role in the pathogenicity of Nautella italica strain R11 towards the red alga Delisea pulchra. ***FEMS Microbiol. Ecol.*** 91**:** 1–5

Garnica OA, Das K & Dhandayuthapani S (2017) OhrR of Mycobacterium smegmatis senses and responds to intracellular organic hydroperoxide stress. **:** 1–12

Greenberg JT, Monach P, Chou JH, Josephy PD & Demple B (1990) Positive control of a global antioxidant defense regulon activated by superoxide-generating agents in Escherichia coli. ***Proc. Natl. Acad. Sci. U. S. A.*** 87**:** 6181–6185

Gutierrez C & Devedjian JC (1991) Osmotic induction of gene osmC expression in Escherichia coli K12. ***J. Mol. Biol.*** 220**:** 959–73

Hall A, Parsonage D, Poole LB & Karplus PA (2010) Structural Evidence that Peroxiredoxin Catalytic Power is Based on Transition-State Stabilization. ***J. Mol. Biol.*** 402**:** 194–209

Halliwell B (2006) Reactive Species and Antioxidants. Redox Biology Is a Fundamental Theme of Aerobic Life. 141**:** 312–322

Herbette S, Roeckel-Drevet P & Drevet JR (2007) Seleno-independent glutathione peroxidases: More than simple antioxidant scavengers. ***FEBS J.*** 274**:** 2163–2180

Hillmann F, Bagramyan K, Straßburger M, Heinekamp T, Hong TB, Bzymek KP, Williams JC, Brakhage AA & Kalkum M (2016) The Crystal Structure of Peroxiredoxin ASP f3 Provides Mechanistic Insight into Oxidative Stress Resistance and Virulence of ASPergillus fumigatus. ***Sci. Rep.*** 6**:** 1–12

Holland HD (2006) The Oxygenation of the aAtmosphere and Oceans. ***Philos. Trans. R. Soc. Lond. B. Biol. Sci.*** 361**:** 903–915

Hong M, Fuangthong M, Helmann JD, Brennan RG & Herbig P (2005) Structure of an OhrR- ohrA Operator Complex Reveals the DNA Binding Mechanism of the MarR Family. 20**:** 131–141

Ighodaro OM & Akinloye OA (2017) First line defence antioxidants-superoxide dismutase (SOD), catalase (CAT) and glutathione peroxidase (GPX): Their fundamental role in the entire antioxidant defence grid. ***Alexandria J. Med.*****:** 1–7

Jacobson FS, Morgan RW, Christmanlf MF & Amesll BN (1989) An Alkyl Hydroperoxide Reductase from Salmonella typhimurium Involved in the Defense of DNA against Oxidative Damage.

Jena NR (2012) DNA damage by reactive species: Mechanisms, mutation and repair. ***J. Biosci.*** 37**:** 503–507

Jo I, Chung I-Y, Bae H-W, Kim J-S, Song S, Cho Y-H & Ha N-C (2015) Structural details of the OxyR peroxide-sensing mechanism. ***Proc. Natl. Acad. Sci.*** 112**:** 6443–6448

Kaihami GH, de Almeida JRF, dos Santos SS, Netto LES, de Almeida SR & Baldini RL (2014) Involvement of a 1-Cys Peroxiredoxin in Bacterial Virulence. ***PLoS Pathog.*** 10**:**

Kim K, Kim IH, Lee KY, Rhee SG & Stadtman ER (1988) The isolation and purification of a specific ‘protector’ protein which inhibits enzyme inactivation by a Thiol/Fe(III)/O2 mixed-function oxidation system. ***J. Biol. Chem.*** 263**:** 4704–4711

Klomsiri C, Panmanee W, Dharmsthiti S, Vattanaviboon P & Mongkolsuk S (2005) Novel roles of ohrR-ohr in Xanthomonas sensing, metabolism, and physiological adaptive response to lipid hydroperoxide. ***J. Bacteriol.*** 187**:** 3277–3281

Kohanski MA, DePristo MA & Collins JJ (2010) Sublethal Antibiotic Treatment Leads to Multidrug Resistance via Radical-Induced Mutagenesis. ***Mol. Cell*** 37**:** 311–320

Kohanski MA, Dwyer DJ, Hayete B & Lawrence CA (2007) A Common Mechanism of Cellular Death Induced by Bactericidal Antibiotics. **:** 797–810

Kortemme T & Creighton TE (1995) Ionisation of cysteine residues at the termini of model alpha-helical peptides. Relevance to unusual thiol pKa values in proteins of the thioredoxin family. ***J. Mol. Biol.*** 253**:** 799–812

Ladjouzi R, Bizzini A, van Schaik W, Zhang X, Rincï¿½ A, Benachour A & Hartke A (2015) Loss of antibiotic tolerance in sod-deficient mutants is dependent on the energy source and arginine catabolism in enterococci. ***J. Bacteriol.*** 197**:** 3283–3293

Van Laer K, Hamilton CJ & Messens J (2012) Low molecular weight thiols in thiol disulfide exchange

Lesniak J, Barton W a & Nikolov DB (2002) Structural and functional characterization of the Pseudomonas hydroperoxide resistance protein Ohr. ***EMBO J.*** 21**:** 6649–59

Lesniak J, Barton WA & Nikolov DB (2003) Structural and functional features of the Escherichia coli hydroperoxide resistance protein OsmC. ***Protein Sci.*** 12**:** 2838–43

Lewis DFV & Wiseman A (2005) A selective review of bacterial forms of cytochrome P450 enzymes. ***Enzyme Microb. Technol.*** 36**:** 377–384

Liu Z, Wang H, Zhou Z, Naseer N, Xiang F, Kan B, Goulian M & Zhu J (2016) Differential Thiol-Based Switches Jump-Start Vibrio cholerae Pathogenesis. ***Cell Rep.*** 14**:** 347–354

Lopachin RM & Gavin T (2017) Thiolate Sites : Relevance To Pathophysiological. 50**:** 195–205

Lushchak VI (2011) Adaptive response to oxidative stress: Bacteria, fungi, plants and animals. ***Comp. Biochem. Physiol. C. Toxicol. Pharmacol.*** 153**:** 175–190

Mashima R & Okuyama T (2015) The role of lipoxygenases in pathophysiology; new insights and future perspectives. ***Redox Biol.*** 6**:** 297–310

Meireles DA, Domingos RM, Gaiarsa JW, Ragnoni EG, Bannitz-Fernandes R, da Silva Neto JF, de Souza RF & Netto LES (2017) Functional and evolutionary characterization of Ohr proteins in eukaryotes reveals many active homologs among pathogenic fungi. ***Redox Biol.*** 12**:** 600–609

Meunier-Jamin C, Kapp U, Leonard G a & McSweeney S (2004) The structure of the organic hydroperoxide resistance protein from Deinococcus radiodurans. Do conformational changes facilitate recycling of the redox disulfide? ***J. Biol. Chem.*** 279**:** 25830–7

Miao Y, Lv D, Wang P, Wang X-C, Chen J, Miao C & Song C-P (2006) An Arabidopsis Glutathione Peroxidase Functions as Both a Redox Transducer and a Scavenger in Abscisic Acid and Drought Stress Responses. ***Plant Cell*** 18**:** 2749–2766

Mills GC (1957) Hemoglobin catabolism. I. Glutathione peroxidase, an erythrocyte enzyme which protects hemoglobin from oxidative breakdown. ***J. Biol. Chem.*** 229**:** 189–197

Mishra S & Imlay J (2012) Why do bacteria use so many enzymes to scavenge hydrogen peroxide? ***Arch. Biochem. Biophys.*** 525**:** 145–160

Mongkolsuk S, Panmanee W, Atichartpongkul S, Vattanaviboon P, Whangsuk W, Fuangthong M, Eiamphungporn W, Sukchawalit R & Utamapongchai S (2002) The repressor for an organic peroxide-inducible operon is uniquely regulated at multiple levels. ***Mol. Microbiol.*** 44**:** 793–802

Mongkolsuk S, Praituan W, Loprasert S, Fuangthong M & Chamnongpol S (1998a) Identification and Characterization of a New Organic Hydroperoxide Resistance (ohr) Gene with a Novel Pattern of Oxidative Stress Regulation from Xanthomonas campestrispv . phaseoli. ***J. Bacteriol.*** 180**:** 2636–2643

Mongkolsuk S, Praituan W, Loprasert S, Fuangthong M & Chamnongpol S (1998b) Identification and Characterization of a New Organic Hydroperoxide Resistance (ohr) Gene with a Novel Pattern of Oxidative Stress Regulation from Xanthomonas campestrispv . phaseoli Identification and Characterization of a New Organic Hydroperoxide Resi. ***J.***

Bacteriol. 180**:** 2636–2643
Monteiro G, Horta BB, Pimenta DC, Augusto O & Netto LES (2007) Reduction of 1-Cys peroxiredoxins by ascorbate changes the thiol-specific antioxidant paradigm, revealing another function of vitamin C. ***Proc. Natl. Acad. Sci.*** 104**:** 4886–4891
Murphy MP (2009) How mitochondria produce reactive oxygen species. ***Biochem. J.*** 417**:** 1–13
Nagy P (2013) Kinetics and Mechanisms of Thiol–Disulfide Exchange Covering Direct Substitution and Thiol Oxidation-Mediated Pathways. ***Antioxid. Redox Signal.*** 18**:** 1623–1641
Nelson KJ, Perkins A, Van Swearingen AED, Hartman S, Brereton AE, Parsonage D, Salsbury FR, Karplus PA & Poole LB (2017) Experimentally Dissecting the Origins of Peroxiredoxin Catalysis. ***Antioxid. Redox Signal.***: ars.2016.6922
Netto LES, de Oliveira MA, Tairum CA & da Silva Neto JF (2016) Conferring specificity in redox pathways by enzymatic thiol/disulfide exchange reactions. ***Free Radic. Res.*** 50**:** 206–245
Niesen FH, Berglund H & Vedadi M (2007) The use of differential scanning fluorimetry to detect ligand interactions that promote protein stability. ***Nat. Protoc.*** 2**:** 2212–2221
Ochsner UA, Hassett DJ & Vasil ML (2001) Genetic and Physiological Characterization ofohr , Encoding a Protein Involved in Organic Hydroperoxide Resistance in Pseudomonas aeruginosa. ***J. Bacteriol.*** 183**:** 773–778
Oh S, Shin J & Roe J (2007) Dual Role of OhrR as a Repressor and an Activator in Response to Organic Hydroperoxides in Streptomyces coelicolor □. 189**:** 6284–6292
Oliveira M a, Guimarães BG, Cussiol JRR, Medrano FJ, Gozzo FC & Netto LES (2006) Structural insights into enzyme-substrate interaction and characterization of enzymatic intermediates of organic hydroperoxide resistance protein from Xylella fastidiosa. ***J. Mol. Biol.*** 359**:** 433–45
Otto H-H & Schirmeister T (1997) Cysteine Proteases and Their Inhibitors. ***Chem. Rev.*** 97**:** 133–172
Panday A, Sahoo MK, Osorio D & Batra S (2015) NADPH oxidases: An overview from structure to innate immunity-associated pathologies. ***Cell. Mol. Immunol.*** 12**:** 5–23
Parsonage D, Nelson KJ, Ferrer-Sueta G, Alley S, Karplus PA, Furdui CM & Poole LB (2015) Dissecting Peroxiredoxin Catalysis: Separating Binding, Peroxidation, and Resolution for a Bacterial AhpC. ***Biochemistry*** 54**:** 1567–1575
Parsons JB & Rock CO (2013) Bacterial lipids: Metabolism and membrane homeostasis. ***Prog. Lipid Res.*** 52**:** 249–276
Perkins A, Nelson KJ, Parsonage D, Poole LB & Karplus PA (2015) Peroxiredoxins: guardians against oxidative stress and modulators of peroxide signaling. ***Trends Biochem. Sci.*** 40**:** 435–45
Pettersen EF, Goddard TD, Huang CC, Couch GS, Greenblatt DM, Meng EC & Ferrin TE (2004) UCSF Chimera - A visualization system for exploratory research and analysis. ***J. Comput. Chem.*** 25**:** 1605–1612
Piccirillo E, Alegria TGP, Discola KF, Cussiol JRR, Domingos RM, De Oliveira MA, de Rezende L, Netto LES & do Amaral AT (2018) Structural insights on the efficient catalysis of hydroperoxide reduction by Ohr: Crystallographic and molecular dynamics approaches. ***PLoS One*** 13**:** 1–23
Poole LB (2015) The basics of thiols and cysteines in redox biology and chemistry. ***Free Radic. Biol. Med.*** 80**:** 148–157
Powles SB & Yu Q (2010) Evolution in Action: Plants Resistant to Herbicides
Previato-Mello M, Meireles D de A, Netto LES & Neto JF da S (2017) Global transcriptional response to organic hydroperoxide and the role of OhrR in the control of virulence traits in Chromobacterium violaceum. ***Infect. Immun.*** 85**:** 1–18
R Core Team (2015) R: A Language and Environment for Statistical Computing.
Radi R (2013) Peroxynitrite, a stealthy biological oxidant. ***J. Biol. Chem.*** 288**:** 26464–26472
Reniere ML, Whiteley AT & Portnoy DA (2016) An In Vivo Selection Identifies Listeria monocytogenes Genes Required to Sense the Intracellular Environment and Activate Virulence Factor Expression. ***PLoS Pathog.*** 12**:** 1–27
Rhee SG (2016) Overview on Peroxiredoxin. ***Mol. Cells*** 39**:** 1–5
Rhee SG, Kang SW, Chang TS, Jeong W & Kim K (2001) Peroxiredoxin, a novel family of peroxidases. ***IUBMB Life*** 52**:** 35–41
Rodriguez R & Redman R (2005) Balancing the generation and elimination of reactive oxygen species. ***Proc. Natl. Acad. Sci.*** 102**:** 3175–3176
Rose RJ & Sheahan MB (2012) Plant Mitochondria. ***eLS***: 1–11
Rowland A, Miners JO & Mackenzie PI (2013) The UDP-glucuronosyltransferases: Their role in drug metabolism and detoxification. ***Int. J. Biochem. Cell Biol.*** 45**:** 1121–1132
Saikolappan S, Das K & Dhandayuthapani S (2015) Inactivation of the organic hydroperoxide stress resistance regulator OhrR enhances resistance to oxidative stress and isoniazid in Mycobacterium smegmatis. ***J. Bacteriol.*** 197**:** 51–62
Santino A, Taurino M, De Domenico S, Bonsegna S, Poltronieri P, Pastor V & Flors V (2013) Jasmonate signaling in plant development and defense response to multiple (a)biotic stresses. ***Plant Cell Rep.*** 32**:** 1085–1098
Schirrmeister BE, de Vos JM, Antonelli A & Bagheri HC (2013) Evolution of multicellularity coincided with increased diversification of cyanobacteria and the Great Oxidation Event. ***Proc. Natl. Acad. Sci.*** 110**:** 1791–1796
Schneider C, Pratt DA, Porter NA & Brash AR (2007) Control of Oxygenation in Lipoxygenase and Cyclooxygenase Catalysis. ***Chem. Biol.*** 14**:** 473–488
Shea RJ & Mulks MH (2002) ohr , Encoding an Organic Hydroperoxide Reductase , Is an In Vivo-Induced Gene in Actinobacillus pleuropneumoniae. 70**:** 794–802
Shin DH, Choi I-G, Busso D, Jancarik J, Yokota H, Kim R & Kim S-H (2004) Structure of OsmC from Escherichia coli: a salt-shock-induced protein. ***Acta Cryst.*** D60**:** 903–911
Si M, Wang J, Xiao X, Guan J, Zhang Y, Ding W, Chaudhry MT, Wang Y & Shen X (2015) Ohr Protects Corynebacterium glutamicum against Organic Hydroperoxide Induced Oxidative Stress. ***PLoS One*** 10**:** e0131634
da Silva Neto JF, Negretto CC & Netto LES (2012) Analysis of the Organic Hydroperoxide Response of Chromobacterium violaceum Reveals That OhrR Is a Cys-Based Redox Sensor Regulated by Thioredoxin. ***PLoS One*** 7**:**
Sledjeski DD & Gottesman S (1996) Osmotic shock induction of capsule synthesis in Escherichia coli K-12 . These include : Osmotic Shock Induction of Capsule Synthesis in Escherichia coli K-12. ***J. Bacteriol.*** 178**:** 1204–1206
Sporer AJ, Kahl LJ, Price-whelan A & Dietrich LEP (2017) Redox-Based Regulation of Bacterial Development and Behavior. ***Annu. Rev. Biochem.*** 86**:** 777–797
Stöcker S, Maurer M, Ruppert T & Dick TP (2018) A role for 2-Cys peroxiredoxins in facilitating cytosolic protein thiol oxidation. ***Nat. Chem. Biol.*** 14**:** 148–155
Sultana R, Perluigi M & Butterfield DA (2013) Lipid peroxidation triggers neurodegeneration: A redox proteomics view into the Alzheimer disease brain. ***Free Radic. Biol. Med.*** 62**:** 157–169
SYBYL (2013) SYBYL-X.
Ta P, Buchmeier N, Newton GL, Rawat M & Fahey RC (2011) Organic hydroperoxide resistance protein and ergothioneine compensate for loss of mycothiol in Mycobacterium smegmatis mutants. ***J. Bacteriol.*** 193**:** 1981–1990
Tairum CA, Santos MC, Breyer CA, Geyer RR, Nieves CJ, Portillo-Ledesma S, Ferrer-Sueta G, Toledo JC, Toyama MH, Augusto O, Netto LES & De Oliveira MA (2016) Catalytic Thr or ser Residue Modulates Structural Switches in 2-Cys Peroxiredoxin by Distinct Mechanisms. ***Sci. Rep.*** 6**:** 1–12
Takemoto D, Tanaka A & Scott B (2007) NADPH oxidases in fungi: Diverse roles of reactive oxygen species in fungal cellular differentiation. ***Fungal Genet. Biol.*** 44**:** 1065–1076
Toppo S, Vanin S, Bosello V & Tosatto SCE (2008) Evolutionary and Structural Insights Into the Multifaceted Glutathione Peroxidase (Gpx) Superfamily. ***Antioxid. Redox Signal.*** 10**:** 1501–1514
Vázquez-Torres A (2012) Redox Active Thiol Sensors of Oxidative and Nitrosative Stress. ***Antioxid. Redox Signal.*** 17**:** 1201–1214

Winther JR & Thorpe C (2014) Quantification of thiols and disulfides. ***Biochim. Biophys. Acta - Gen. Subj.*** 1840**:** 838–846

Woldemariam MG, Ahern K, Jander G & Tzin V (2018) A role for 9-lipoxygenases in maize defense against insect herbivory. ***Plant Signal. Behav.*** 13**:** e1422462

Wolfram TJ, LeVeque RM, Kastenmayer RJ & Mulks MH (2009) Ohr, an in vivo-induced gene in Actinobacillus pleuropneumoniae, is located on a genomic island and requires glutathione-S-transferase for activity. ***FEMS Immunol. Med. Microbiol.*** 57**:** 59–68

Yang J, Carroll KS & Liebler DC (2016) The Expanding Landscape of the Thiol Redox Proteome. ***Mol. Cell. Proteomics*** 15**:** 1–11

Yin H, Xu L & Porter N a. (2011) Free radical lipid peroxidation: Mechanisms and analysis. ***Chem. Rev.*** 111**:** 5944–5972

Zarghi A & Arfaei S (2011) Selective COX-2 Inhibitors: A Review of Their Structure-Activity Relationships. ***Iran. J. Pharm. Res.*** 10**:** 655–683

CHAPTER 2 – FUNCTIONAL AND EVOLUTIONARY CHARACTERIZATION OF OHR PROTEINS IN EUKARYOTES REVEALS MANY ACTIVE HOMOLOGS AMONG PATHOGENIC FUNGI

Functional and evolutionary characterization of Ohr proteins in eukaryotes reveals many active homologs among pathogenic fungi

D.A. Meireles[a,*], R.M. Domingos[a], J.W. Gaiarsa[a], E.G. Ragnoni[a], R. Bannitz-Fernandes[a], J.F. da Silva Neto[b], R.F. de Souza[c], L.E.S. Netto[a,*]

[a] Departmento de Genética e Biologia Evolutiva, Instituto de Biociências, Universidade de São Paulo, São Paulo, SP, Brazil
[b] Departamento de Biologia Celular e Molecular e Bioagentes Patogênicos, Faculdade de Medicina de Ribeirão Preto, Universidade de São Paulo, Ribeirão Preto, SP, Brazil
[c] Departmento de Microbiologia, Instituto de Ciências Biomédicas, Universidade de São Paulo, São Paulo, SP, Brazil

*To whom correspondence may be addressed. Email: nettoles@ib.usp.br or meireles@ib.usp.br

Key words: Ohr/OsmC; thiol-dependent peroxidases; phylogeny.

This Chapter was published in Redox Biology (Vol. 12) (Elsevier) in April 2017

https://doi.org/10.1016/j.redox.2017.03.026

2.1 – Main contribution by R.M. Domingos

I performed mostly of the kinetics of linoleic acid hydroperoxide (LAOOH) reduction by $MfOhr_{del}$-AhpE competition assays and the Thiol dependent peroxidase activity assays. I also participated in the cloning procedures, protein purification in the pK_a determination and also in the manuscript writing.

2.2 – Abstract

Ohr and OsmC proteins comprise two subfamilies within a large group of proteins that display Cys-based, thiol dependent peroxidase activity. These proteins were previously thought to be restricted to prokaryotes, but we show here, using iterated sequence searches, that Ohr/OsmC homologs are also present in 217 species of eukaryotes with a massive presence in Fungi (186 species). Many of these eukaryotic Ohr proteins possess an N-terminal extension that is predicted to target them to mitochondria. We obtained recombinant proteins for four eukaryotic members of the Ohr/OsmC family and three of them displayed lipoyl peroxidase activity. Further functional and biochemical characterization of the Ohr homologs from the ascomycete fungus *Mycosphaerella fijiensis* Mf_1 (MfOhr), the causative agent of Black Sigatoka disease in banana plants, was pursued. Similarly to what has been observed for the bacterial proteins, we found that: (i) the peroxidase activity of MfOhr was supported by DTT or dihydrolipoamide (dithiols), but not by β-mercaptoethanol or GSH (monothiols), even in large excess; (ii) MfOhr displayed preference for organic hydroperoxides (CuOOH and tBOOH) over hydrogen peroxide; (iii) MfOhr presented extraordinary reactivity towards linoleic acid hydroperoxides ($k=3.18 (\pm 2.13) \times 10^8\ M^{-1}\ s^{-1}$). Both Cys87 and Cys154 were essential to the peroxidase activity, since single mutants for each Cys residue presented no activity and no formation of intramolecular disulfide bond upon treatment with hydroperoxides. The pK_a value of the Cys_p residue was determined as 5.7 ± 0.1 by a monobromobimane alkylation method. Therefore, eukaryotic Ohr peroxidases share several biochemical features with prokaryotic orthologues and are preferentially located in mitochondria.

2.3 – Introduction

Organic hydroperoxide resistance (Ohr) proteins are Cys-based, thiol dependent peroxidases that belong to a family of proteins called Ohr/OsmC. OsmC (Osmotically inducible protein) are structurally related to Ohr enzymes [1] and together define two subfamilies that have their peroxidase activities well characterized within Ohr/OsmC family [2–4]. Members of a third group remain poorly characterized [1].

The physiological role played by Ohr and OsmC has been linked to the defense against organic hydroperoxide insults [1,5–11]. Ohr and OsmC are structurally distinct from peroxiredoxin (Prx) and glutathione-peroxidase (Gpx) enzymes [1,2], although all are Cys-based, thiol dependent peroxidases. While Prx and Gpx enzymes are ubiquitously distributed in all domains of life, Ohr/OsmC proteins were thought to be present only in Archaea and Eubacteria [2,6]. Contrary to Ohr enzymes, most Prx enzymes are highly reactive towards H_2O_2. One exception is Tpx from E. coli that similarly to Ohr enzymes also display higher specificity to organic peroxides over H_2O_2 [12], although the large majority of these peroxiredoxins are found in bacteria [13].

The catalytic mechanism of hydroperoxide reduction by Ohr and OsmC proteins is centered on a pair of redox-active cysteines, named peroxidatic (C_p) and resolving (C_r) cysteines, resembling that of the atypical 2-Cys Prxs. Ohr and OsmC are functionally dimeric and the cysteine residues are positioned in each monomer as part of two identical active sites located at opposing sides [2]. Two other residues of the active site also participate in catalysis: an arginine (Arg) and a glutamic acid (Glu) [3,14]. The peroxidase cycle starts with the nucleophilic attack of Cys_p towards the hydroperoxide. Upon hydroperoxide reduction to its corresponding alcohol, the Cp is oxidized to the sulfenic acid (Cys-SOH) intermediate, which readily reacts with Cr, giving rise to an intramolecular disulfide bond [14]. A new cycle begins when the disulfide bond is reduced back to the dithiolic form. Lipoyl groups covalently attached to some proteins are the biological reductants of these intramolecular disulfides [4]. Recently, we demonstrated that Ohr enzymes display high specificity for fatty acid hydroperoxides and peroxynitrite as oxidizing substrates [11].

Here, based on an in-depth sequence analysis, we describe the occurrence and distribution of Ohr and OsmC peroxidases in the Eukarya domain. OsmC proteins were only found in Dictyostelia, whereas Ohr members are predominantly present in Fungi (mainly Ascomycota and Basidiomycota). Four recombinant eukaryotic proteins from the Ohr/OsmC family were purified, three of which displayed thiol peroxidase activity. One of these, namely Ohr from the ascomycota fungus *Mychosphaerella fijiensis* Mf_1 (MfOhr), was further characterized, and its presence in the mitochondria of this fungus was demonstrated.

2.4 – Material and methods

2.4.1 – Dataset source and sequence extraction

The amino acid sequence from *Xylella fastidiosa* 9a5c strain was used as query for search against NCBI nr sequence database using deltaBLAST via NCBI website [15] (June of 2016) and the profile Hidden Markov Model (HMM) iterative method implemented in Jackhmmer 1.9 web server [16]. We conducted the search against NCBI nr sequence database using default options until convergence. The searches were restricted to the Eukarya Domain. Redundant entries and truncated sequences (less than 100 amino acids) were removed using CD-HIT software [17].

2.4.2 – Primary sequence clustering

We identified members of the Ohr and OsmC subfamilies in Eukarya using sequence motifs previously described [1,6]. Additional motifs were detected using alignments of eukaryotic Ohr sequences with structurally solved Ohr (PDB: 1ZB8, from X. fastidiosa; 1USP, from *Deinococcus radiodurans*; 3LUS, from Vibrio cholerae; 1N2F, from *Pseudomonas aeruginosa*) or OsmC (1NYE, from *Escherichia coli*) proteins. We curated the alignments manually, guided by successive multiple alignments runs generated by MAFFT operating with default sets [18]. The input sequences were collected by delta-blast and jackhmmer searches described in the previous section.

2.4.3 – Phylogenetic analysis

Maximum Likelihood (ML) inference of phylogenetic trees was based on the manually curated MAFFT alignment and the RAxML software [19] and applied to all non-redundant sequences retrieved or only sequences from the Ohr subfamily. For inference, we used WhelanGoldman (WAG) model of amino acid evolution with rate heterogeneity modeled by a GAMMA distribution and 1000 rapid bootstrap resampled estimates of log-likelihood (RELL bootstrap). The resulting phylogeny was prepared for visualization using Tree Editor from the MEGA 7 software [20].

2.4.4 – Strains and growth conditions

E. coli strains were grown in Lysogenic Broth (LB) medium at 37 °C supplemented with ampicillin (100 μg/mL). *Mycosphaerella fijiensis* Mf_1 was grown in Potato Dextrose Medium (PDB) at room temperature supplemented with streptomycin (100 μg/mL) and chloramphenicol (100 μg/mL). Dictyostelium discoideum AX4 cells were grown axenically in liquid maltose HL-5 modified medium [21] supplemented with ampicillin (100 μg/mL) and streptomycin (300 μg/mL) at 22 °C.

2.4.5 – Cloning procedures

To amplify ohr (MYCFIDRAFT_54770) and osmC (DDB_G0268884) genes without introns, samples of total RNA from germinated conidia of *M. fijiensis* Mf-1 and *D. discoideum* AX4 cells, respectively, were extracted using Trizol reagent (Ambion). RNA samples were treated with RNase-Free DNase I (Ambion) and submitted to reverse transcription (SuperScript II) using Oligo-dT to produce cDNA. To clone Mfohr into pET15b (Novagen®) and DdosmC into pPROEX expression vectors, sequences were amplified from appropriated cDNAs by PCR using the oligo pairs (5′→3′): Fow_TTAG**CATATG**GCTTCCGTAAGAGCATTC/rev_TTAG**GGATCC**CGTCCCGCTCTATCC AATAA and Fow_AGT**CATATG**AGCATTAGTAATAAAATTATTGGATCAGC/ Rev_AGT**GGATCC**CAAAAACAAATGGTGAGAAATCTG, respectively. The restriction sites for NdeI and BamHI are depicted by bold letters. Additionally, for Mfohr gene, a second PCR was performed using the same conditions described above using forward oligo (5′→3′) TTAG**CATATG**TCCCCGCCATTCTACACAGCCCAT, to produce a version of the protein MfOhr without the first 33 amino acid residues (*MfOhrdel*). The ohr gene from *Fusarium oxysporum f. sp. cubense* (*Foohr*) and Ohr-like (named as osmC gene by [22]) from *Trichomonas vaginalis* (*TvosmC)* were commercially synthesized by GenScript USA Inc., containing the sites for NheI and BamHI restriction enzymes in the flanking regions. The fragments that corresponded to the *Foohr* and *Tvosmc* genes were digested from pUC57 using *Nde*I and *Bam*HI restriction enzymes and subcloned into pET15b. Fidelity of all sequences was checked by chain termination sequencing method using T7 promoter and terminator oligonucleotides.

2.4.6 – Protein purification

Expression of recombinant MfOhr, $MfOhr_{del}$, FoOhr, DdOsmC or TvOsmC was induced by 0.1 mM of isopropyl 1-thio-β-D-galactopyranoside (IPTG) for 16 h at 20 °C in exponential culture (OD_{600} 0.5) of *E. coli* BL21 (*DE3*) CodonPlus (Agilent) harboring the appropriate expression vectors with moderate shaking. Then, cells were harvested by centrifugation and resuspended in the lysis buffer (500 mM NaCl, 20 mM sodium phosphate pH 7.4, 0.2 mg/mL lysozyme, 1 mM PMSF and 20 mM imidazole). Cells were disrupted by sonication (ten alternating cycles of 15 s of sonication 30% amplitude and 1 min on ice bath). Cell debris were separated from the supernatant by centrifugation at 15.000 rpm at 4 °C during 40 min. The supernatant was filtered using a 0.45 µm pore membrane and all expressed proteins were affinity purified (Ni-NTA Agarose column, Qiagen) with a peristaltic pump. The charged resin was washed sequentially with 3 column volumes of washing buffer (500 mM NaCl, 20 mM sodium phosphate pH 7.4) containing 50 mM and 100 mM imidazole and eluted with 3 column volumes of elution buffer (500 mM NaCl, 20 mM sodium phosphate pH 7.4 and 500 mM imidazole). Buffer exchange and concentration of purified proteins were performed in an Amicon Centrifugal 10 MW device (Millipore®). Protein purity was checked by SDS-PAGE and protein concentration was spectrophotometrically determined by its absorbance at 280 nm (for MfOhr, ε_{ox} =9970 and ε_{red}=10,095;

for MfOhrdel, ε_{ox}=4595 and ε_{red}=4470 M^{-1} cm^{-1}; for FoOhr, ε_{ox}=11,585 and ε_{red}=11,460 M^{-1} cm^{-1}, for DdOsmC, ε_{ox}=10,220 and ε_{red}=9970 and for TvOsmC, εox =15,720 and ε_{red}=15,470, according to ProtParam tool [23]).

2.4.7 – Reduction of peroxidases with DTT

In some assays, Cys-based peroxidases ($MfOhr_{del}$ or AhpE) were prereduced by 50 mM of DTT for 16 h at 4 °C, in the presence of 500 mM NaCl and 20 mM sodium phosphate pH 7.4. Excess of DTT was eliminated by two rounds of size-exclusion chromatography (HiTrap Dessalting, GE HealthCare) in a buffer (500 mM NaCl and 20 mM sodium phosphate pH 7.4) previously purged with N_2. The efficiency of this procedure was ascertained by the DTNB method [24].

2.4.8 – Thiol dependent peroxidase activity assays

Reductions of cumene hydroperoxide (CuOOH), tert-butyl hydroperoxide (tBOOH) or hydrogen peroxide (H_2O_2) were monitored by FOX assay [25] using DTT, dihydrolipoamide (DHLA), β-mercaptoethanol or glutathione as reductants.

Peroxidase activities were also analyzed by the lipoamide/lipoamide dehydrogenase coupled assay, following absorbance decay at 340 nm, as a consequence of NADH oxidation [4,26,27]. In this assay, the reaction was carried out at distinct concentrations of Ohr or OsmC enzymes as indicated in the legend of **Fig. 4**.

2.4.9 – Site directed mutagenesis

The oligo pairs (5′→3′) used to mutated Cp to serine (C87S) were C87SF TACGGAGCT**TCC**TTCCAAG and C87SR CTTGGAA**GGA**AGCTCCGTA and Cr to serine (C154S) were C154SF AAGGAGGTC**A**GTCCGTATAGC and C154SR GCTATACGGAC**T**GACCTCCTT, using the QuickChange II SiteDirected Mutagenesis Kit (Agilent Technologies). The bold letters indicate the mutate nucleotide(s).

2.4.10 – Kinetics of linoleic acid hydroperoxide (LAOOH) reduction by MfOhrdel - AhpE competition assay

The rate constant for the reduction of LAOOH by MfOhr was calculated according to a competitive assay previously described [11] that takes advantage of the redox-dependent changes in the intrinsic fluorescence of AhpE, a Cys-based peroxidase from *Mycobacterium tuberculosis* (MtAhpE) [6]. Briefly, Ohr and AhpE were pre-reduced with 50 mM of DTT as described above. Stopped-flow fluorescence measurements were performed using a commercially available stoppedflow device (SFA-20 Rapid Kinetics Spectrometer Accessory, TgK Scientific, United Kingdom, UK) coupled to a Varian Cary Eclipse Fluorescence Spectrophotometer (Agilent Technologies).

2.4.11 – pK_a determination of C_P residue from $MfOhr_{del}$ WT

The pK_a of the thiolate in C_p from $MfOhr_{del}$ was determined using the monobromobimane (mBrB) alkylation method that generates a fluorescent product detected at λ_{exc} 396 nm and λ_{em} 482 nm [29]. MfOhrdel was pre-reduced by DTT as described above. The assays were performed in flat-bottom white polystyrene 96-well plates (Costar) in triplicates, using Varian Cary Eclipse fluorescence spectrophotometer, operating at medium voltage with both emission and excitation slit of 5 nm. Immediately after the end of the reaction, the pH of samples was checked. An additional blank reaction was performed in absence of thiols, to determine if other components in buffers might interfere with the reaction. The angular coefficients were calculated using time points that included at least the initial 10 min of reaction that were fitted in a straight line. The curves displayed in **Fig. 9** were obtained by non-linear regression using Henderson-Hasselbalch equation and considering 95% of confidence using Prism 4 for Windows, GraphPad Software, San Diego, CA.

2.4.12 – Affinity purification of *X. fastidiosa* anti-Ohr serum

Since Ohr proteins present high structural similarity among themselves, we purified serum antibodies raised against Ohr from *X. fastidiosa* [4] to increase their specificity towards eukaryotic Ohr. Firstly, the His-tag from recombinant MfOhr was digested with thrombin following manufacturer instructions (Thrombin CleanCleave™ Kit, SIGMA Aldrich). The cleaved protein was covalently attached to a CNBr sepharose resin and stored in PBS pH 8.0. Then, the MfOhr sepharose beads were incubated with 2 mL of serum anti-XfOhr diluted in 8 mL of PBS pH 8.0 during 2 h at 4 °C. After, the beads were extensively washed with PBS pH 8.0 and antibodies were eluted from the resin with 2 mL of 0.2 M glycine pH 2.8. The samples eluted (500 µL fractions) were immediately neutralized with 20 µL of 3 M Tris-HCl pH 8.8 and 100 µL of 3 M KCl.

2.4.13 – Protoplastization of *M. fijiensis mycelia*

Approximately 10^6 conidia x mL^{-1} of *M. fijiensis* Mf_1 were inoculated in 100 mL of PDB medium supplemented with 34 µg/mL of chloramphenicol and incubated during 36 h at 30 °C under agitation (200 rpm). Cell walls of mycelia were digested with a mix of enzymes Lallzyme MMX (15g/L), lysing enzymes from *Trichoderma harzianum* (5g/L) (Sigma-Aldrich cat # L1412) and BSA (10g/L) in the presence of 50 mL of solution 1 (0.8 M ammonium sulfate, 0.1 M citric acid, pH 6), 50 mL of solution 2 (1% (w/v) yeast extract, 2% (w/v) sucrose, pH 6) and 26 mL of 1 M $MgSO_4$ and incubated during 5 h at 30 °C under gently agitation (100 rpm). Digested mycelia were filtered through a glass wool in order to separate protoplasts from cell debris and centrifuged 4000 rpm during 10 min at 4 °C.

2.4.14 – Subcellular fractionation

The subcellular fractionation was adapted from [30]. Briefly, to isolate mitochondria, protoplasts were suspended in 10 mL of SHE buffer (0.6 M sorbitol, 20 mM HEPES and 1 mM EDTA) supplemented with 1 mM PMSF and mechanical disrupted after 50 strokes on ice using a *dounce homogenizer*. The lysed protoplasts solution, that represented the total fraction (TF), was centrifuged at 3800 rpm for 7 min at 4 °C and the supernatant was reserved. The same procedure was repeated three times to wash away all cellular debris and some organelles like nuclei and the supernatant collected was submitted to a final centrifugation step at 16,000xg during 10 min at 4 °C to separate supernatant (cytoplasmic fraction, CF) from pellet (enriched mitochondrial fraction). The enriched mitochondrial fraction (EMF) was suspended in 200 µL of SHE buffer and all collected fractions were stored at −80 °C.

2.4.15 – MfOhr subcellular localization

To determine the subcellular localization of MfOhr, 15 or 30 µg of protein from extracts that correspond to the total fraction (TF), cytoplasmic fraction (CF) and enriched mitochondrial fraction (EMF) were separated by SDS-PAGE and the proteins were transferred to a nitrocellulose membrane. The membrane was stained with Ponceau S to check the amount of loaded proteins and incubated with antibodies that specifically target proteins from the cytoplasm (anti-PGK-1, phosphoglycerate kinase 1, Nordic BioSite cat. number BT-BS6691) or mitochondria (anti-COX IV, cytochrome c oxidase subunit IV, Abcam ab14744).

2.5 – Results

2.5.1 – Ohr/OsmC homologs data mining & their taxonomic distribution among eukaryote

Previously, Ohr and OsmC enzymes were thought to be present only in bacteria [2,6]. Our searches for homologs using delta-BLAST [15] and jackhmmer [16] in NCBI *nr* database revealed the existence of 392 eukaryotic proteins belonging to the Ohr/OsmC family (**Table S1**). Successive

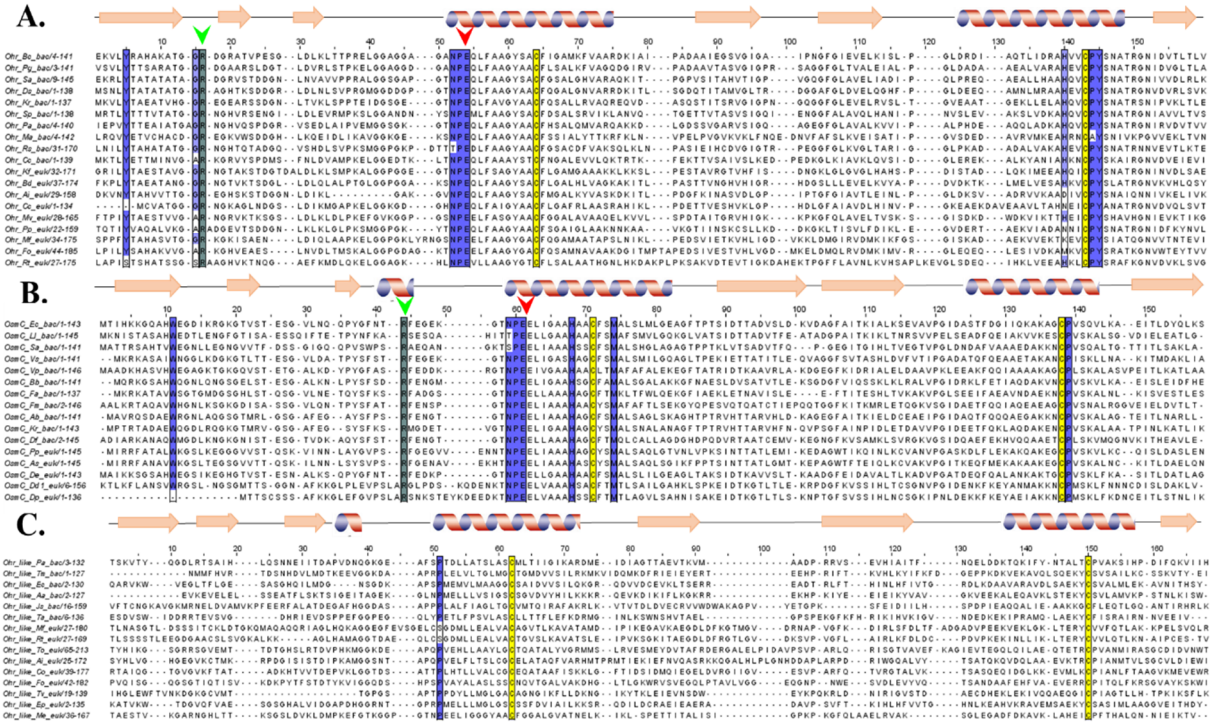

Fig. 1 – Multiple sequence alignment of selected members from Ohr, OsmC and Ohr-like subfamilies. The sequences were aligned using L-INS-I algorithm of MAFFT [13]. For each subfamily, sequences from different bacteria phyla were aligned with selected Ohr eukaryotic sequences. (A) For Ohr, 4NOZ secondary structure from *Burkholderia cenocepacia* J2315 (BcOhr) was used to guide the alignment. Green and red arrows denote catalytic Arg and Glu. The selected Ohr sequences of prokaryotes were: RsOhr from *Ralstonia solanacearum* UW551, SaOhr, from *Stigmatella aurantiaca*, PgOhr from *Polymorphum gilvum*, PaOhr from *Propionibacterium acnes*, CcOhr from *Clostridium carboxidivorans*, SpOhr from *Sphingobacterium paucimobilis*, DsOhr from *Deinococcus swuensis*, MrOhr from *Mastigocladopsis repens*, KrOhr from *Ktedonobacter racemifer* and MaOhr from *Mycoplasma alligatoris*. The selected Ohr sequences of eukaryotes were: PpOhr from *Physcomitrella patens*, KfOhr from *Klebsormidium flaccidum*, MfOhr from *Mychosphaerella fijiensis* CIRAD86, PmOhr from *Pseudocercospora musae*, FoOhr from *Fusarium oxysporum f. sp. cubense* race 4, Ai_Ohr from *Aphanomyces invadans*, BdOhr from *Batrachochytrium dendrobatidis* JEL423, CcOhr from *Calocera cornea* HHB12733 Cc_1, RtOhr from *Rhodotorula toruloides* ATCC 20409, MeOhr from *Mortierella elongata* AG-77, MvOhr from *Mortierella verticillata* NRRL 6337. (B) For OsmC, 1QLM secondary structure from *Escherichia coli* (EcOsmC) was used to guide the alignment. Green and red arrows denote catalytic Arg and Glu. The selected OsmC sequences of prokaryotes were: VpOsmC from *Variovorax paradoxus*, AbOsmC from *Azospirillum brasilense*, BbOsmC from *Bdellovibrio bacteriovorus*, SaOsmC from *Streptomyces avermitilis*, FaOsmC from *Flavobacterium aquatile*, KrOsmC from *Ktedonobacter racemifer*, DfOsmC from *Deinococcus frigens*, LlOsmC from *Lactococcus lactis*, FmOsmC from *Fischerella muscicola* and VsOsmC from *Verrucomicrobium spinosum*. The selected OsmC sequences of eukaryotes were: PpOsmC from *Polysphondylium pallidum* PN500, DpOsmC from *Dictyostelium purpureum*, AsOsmC from *Acytostelium subglobosum* LB1 and Dd1 OsmC from *Dictyostelium discoideum*. (C) Selected Ohr-like sequences deposited in PDB database were aligned with selected Ohr-like members from eukaryotic counterparts. For Ohr-like, secondary structure 2PN2 from *Psychrobacter arcticus* 273-4 (PaOhr-like) was used to guide the alignment. The selected OsmC sequences of prokaryotes were: AaOhr_like from *Aquifex aeolicus*, JsOhr_like from *Jannaschia sp.*, LlOhr_like from *Lactobacillus casei*, TmOhr_like from *Thermotoga maritima*, TaOhr_like from *Thermoplasma acidophilum*. The selected Ohr-like sequences of eukaryotes were: MpOhr like from *Micromonas pusilla* CCMP1545, EpOhr_like from *Exaiptasia pallida*, TvOhr_like from *Trichomonas vaginalis* G3, ToOhr_like from *Thalassiosira oceanica*, AiOhr_like from *Aphanomyces invadans*, MfOhr_like from *Mychosphaerella fijiensis* CIRAD86, FoOhr_like from *Fusarium oxysporum* f. sp. cubense race 4, CcOhr_like from *Calocera cornea* HHB12733, RtOhr_like from *Rhodotorula toruloides* ATCC 204091 and CoOhr_like from *Capsaspora owczarzaki* ATCC 30864.

alignments of all of these eukaryotic sequences allowed us to ascertain that 189 of these sequences belong to Ohr subfamily and 5 sequences belong to the OsmC subfamily. We also identified a third group of Ohr/OsmC sequences, named here as Ohr-like, that comprise 198 proteins from eukaryotic organisms (**Table S1**) and that await further characterization. Ohr, OsmC and Ohr-like proteins share a conserved pair of catalytic cysteines separated by approximately 60 amino acid residues in the primary sequence (**Fig. 1**) that, therefore, represents a hallmark feature of Ohr/OsmC of family proteins. Two additional residues (an Arg and a Glu) required for the peroxidatic activity [2,4,6,14] are both fully conserved in Ohr and OsmC subfamilies (**Fig. 1A** and **B**) but are absent in Ohr-like proteins (**Fig. 1C**). This conserved Glu residue is located at the same position in the primary sequences of Ohr and OsmC proteins, while the conserved Arg residue is located in the first loop between the 1st and 2nd β-sheets for Ohr proteins (**Fig. 1A**); and in the third loop between the 3rd β-sheet and the 1st α-helix for OsmC (**Fig. 1B**). Although the conserved Arg residue is present at different positions in the primary sequences of Ohr and OsmC enzymes, in the tertiary structures they occupy a similar orientation between the conserved Glu and Cp [1,12]. Members of Ohr/OsmC family were detected in all eukaryotic groups, except Metazoa (**Fig. 2A**), considering the Tree of Life and taxonomy proposed by [31]. The largest number of Ohr/OsmC homologs was observed in Fungi (76% or 300/392 of sequences), mainly in the Ascomycota and Basidiomycotate phyla. Other microbial eukaryotes from a wide range of clades

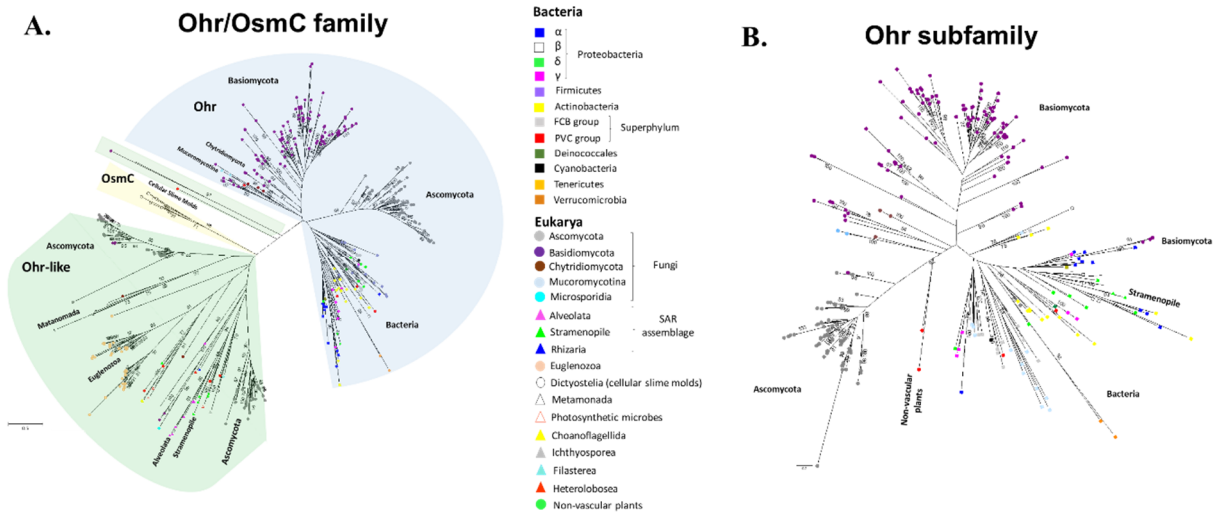

Fig. 2 – RAxML maximum likelihood phylogenetic tree constructed using retrieved eukaryotic sequences from Ohr/OsmC family. (A) Unrooted phylogenetic tree of 392 eukaryotic sequences plus 78 selected Ohr sequences from bacteria of distinct phyla. (B) Unrooted phylogenetic tree of 186 Ohr eukaryotic sequences plus 78 selected Ohr sequences from bacteria of distinct phyla.

contain about 16% (63/392 of sequences) of Ohr/OsmC homologs, such as Euglenozoa; Amebozoa; Metanomada (*Trichomonas vaginalis*); Heterolobosea (*Naegleria gruberi* strain NEG-M); and non-metazoan Holozoa, such as Choanoflagellida (*Salpingoeca, Monosiga*), Ichthyosporea (*Sphaeroforma*) and Filasterea (*Capsaspora*). Close to 5% (20/392) of all Ohr/OsmC sequences were found in the SAR (Stramenopiles, Alveolata and Rhizaria) clade, such as Alveolata (*Tetrahymena*, *Ichthyophthirius* and *Vitrella brassicaformis* CCMP3155), Stramenopiles (*Aphanomyces*, *Saprolegnia*, *Thalassiosira* and

Nannochloropsis) and Rhizaria (*Reticulomyxa filosa*) groups. Among the photosynthetic eukaryotes, Cryptista (*Guillardia theta* CCMP2712), Haptophyceae (*Emiliania huxleyi* CCMP1516), and non-vascular plants encode homologs of Ohr/OsmC genes in their genomes. Genes from non-vascular plants correspond to almost 2% of Ohr/OsmC homologs and were detected in the Chlorophyta (*Chlorella* and *Micromonas*), Bryophyta (*Physcomitrella patens*), Marchantiophyta (*Marchantia polymorpha*) and Streptophyta (*Klebsormidium flaccidum*). We also retrieved sequences from Metazoa, including sequences from nematode, *Trichuris trichiura* (GenBank accession CDW57322.1 and described in [22] as a member of Ohr/OsmC family), insect, *Drosophila eugracilis* (XP_017066882), crustacean, *Daphnia magna* (KZS01297) and sea *anemona Exaiptasia* pallida (KXJ04390). However, these sequences have extremely high amino acid identity to sequences from *Enterococcus* (100%), *Acetobacter* (100%), *Burkholderia* (98%) and *Oceanospirillum* (97%), respectively. Furthermore, there is no evidence of a signal peptide sequence in these animal proteins and it is most likely that these sequences are spurious, being derived from DNA from symbiotic bacteria or sample contamination [32,33]. Therefore, we did not include these sequences in our analysis.

2.5.2 – Distribution of Ohr, OsmC and Ohr-like subfamilies homologs among eukaryotes

To gain insights on the evolutionary relationships among Ohr, OsmC and Ohr-like sequences from different eukaryotic phyla, we analyzed the data retrieved using Maximum Likelihood (ML) phylogenetic inference. This resulted in a tree with well-defined clades bearing the signatures of each family (**Fig. 2A** and **B**). The occurrences of Ohr, OsmC and Ohr-like proteins among eukaryotic phylogenetic groups are quite distinct. While Ohr and OsmC homologs are more restricted to Fungi and cellular slime molds, respectively, Ohr-like homologs are widespread among various eukaryotic groups (**Fig. 2A**). The 189 sequences from Ohr subfamily compose a well-defined group that is isolated from bacterial counterparts and are mostly present in Fungi of the Ascomycota (87/189) and Basidiomycota (98/ 189 sequences) phyla (**Fig. 2B**). In contrast, the five members of the OsmC subfamily are grouped into a single monophyletic clade restricted to the Dictyostelia order (cellular slime molds) (**Fig. 2A**). Concerning the Ohr-like subfamily (198 sequences), most of them are present in Ascomycota (90 sequences), while only 16 sequences could be found in Basidiomycota. Ohr-like homologs are also abundant among Euglenozoa (48 sequences), but can also be found in nonmetazoan Holozoa, such as Sphaeroforma arctica JP610 (two Ohr-like paralogues) and Capsaspora owczarzaki (one Ohr-like), some of the closest unicellular relatives of multicellular animals [34]. Interestingly, a separated analysis that included only Ohr homologs and some selected bacterial Ohrs revealed that five eukaryotic Ohr homologs grouped within the bacterial Ohr group (**Fig. 2B**). These sequences were encoded by genes from different species of Basidiomycota, such as Calocera (C. cornea and C. viscosa) and Dacryopinax (represented by purple circles in the **Fig. 2B**) and *Stramenopiles Aphanomyces invadans* and *A. astaci* (represented by light green triangles in **Fig. 2B**). These latter sequences are likely examples of very

recent horizontal gene transfer events from bacterial lineages, given the absence of introns in organisms such as *Aphanomyces* and their low levels of similarity of sequences from organelles and organelle related bacterial lineages.

2.5.3 – Genomic configurations of ohr/osmC genes in eukaryotic organisms

Several eukaryotic genomes present more than one member of the Ohr/OsmC family, being arranged in highly variable configurations (**Fig. 3**). For instance, some fungi microorganisms present two or three ohr paralogues in their genomes (**Fig. 3A** and **B**), some located near to each other, in some cases the two gene are even neighbors (**Fig. 3A**), suggesting the occurrence of gene duplication events. Besides fungi, microorganisms that contain more than one gene of the Ohr/OsmC family are: *M. fijiensis* presenting one ohr and one ohr-like gene (**Fig. 3C**); *Trichomonas vaginalis* with four ohr-like genes (as also described by [22]) and *D. discoideum* AX4 containing one copy of osmC and one copy of an *ohr-like* gene (**Fig. 3D**). On the other hand, most of the other genomes encode only a single homolog of the ohr subfamily, as is the case of the moss *P. patens* (**Fig. 3E**).

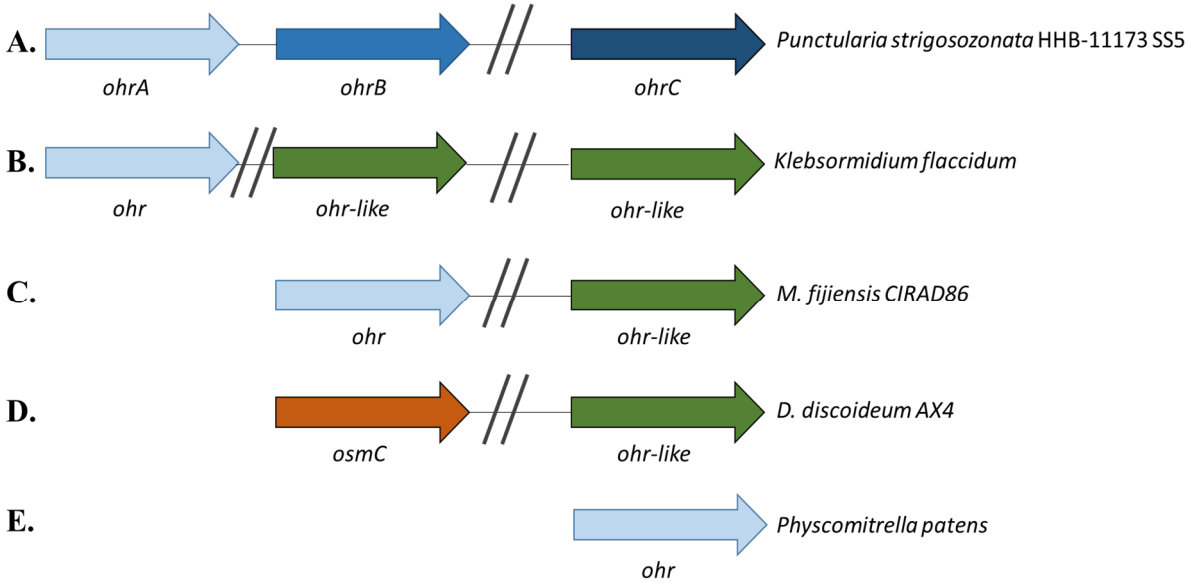

Fig. 3 – Genomic arrangements of genes from Ohr/OsmC family present in Eukaryotes.

We also observed that many eukaryotic *ohr/osmC* genes present introns, however their evolutionary significance is still elusive. The complete list of *ohr*, *osmC* or *ohr-like* genes (and their predicted introns), as well as their abundance in each specie, is presented in **table S1**.

2.5.4 – Recombinant eukaryotic Ohr and OsmC have peroxidase activity

To verify whether Ohr and OsmC homologs present in eukaryotic organisms also display lipoyl

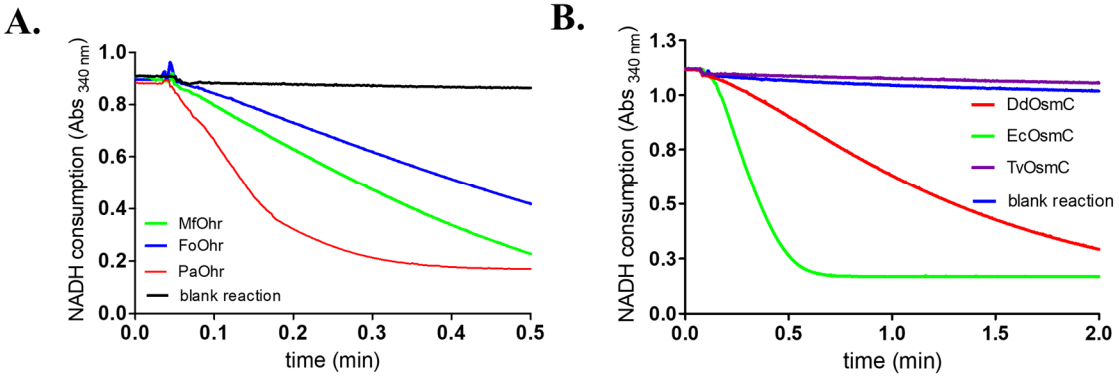

Fig. 4 – Thiol dependent peroxidase activity of eukaryotic Ohr and OsmC enzymes. Peroxidase activity assay of selected eukaryotic Ohr and OsmC proteins was assessed by the lipoamide/lipoamide dehydrogenase coupled assay. The reactions were performed with 0.625 µM of MfOhr and FoOhr (A) or 5 µM of DdOsmC (B) in the presence of 50 µM of reduced lipoamide, 100 µM of DTPA, 0.5 µM of Lpd (recombinant Dihydrolipoamide dehydrogenase from *X. fastidiosa*) and 200 µM of NADH in 50 µM of sodium phosphate pH 7.4. Reactions were initiated by addition of 200 µM of CuOOH. As positive controls, we also performed the same assay using bacterial recombinant enzymes 0.1 µM PaOhr (A) or 5 µM of EcOsmC (B).

peroxidase activity as their bacterial counterparts, we obtained recombinant Ohr proteins from *M. fijiensis* (MfOhr) and from F. oxysporium (FoOhr) and recombinant OsmC from *Dictyostelium discoideum* (DdOsmC), expressed in *E. coli*. All the selected fungal Ohr enzymes reduced tBOOH (**Fig. 4A**). The FoOhr reduced tBOOH at lower rates when compared with MfOhr and both proteins were

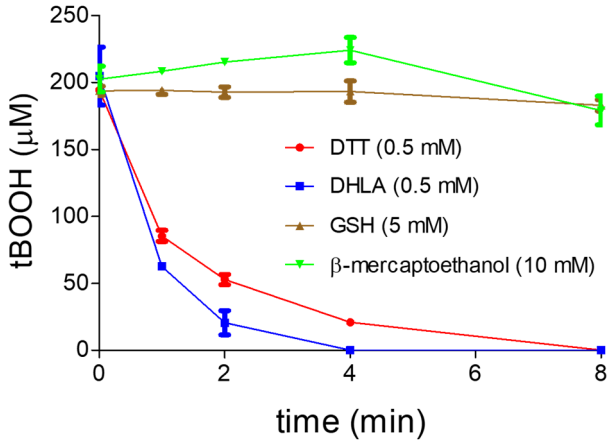

Fig. 5 – Thiol specificity of MfOhr peroxidase activity. The amount of tBOOH remaining in solution after reaction was determined by the FOX assay. Reactions were initiated by addition of thiol compounds and terminated by addition of 20 µl of HCl (5 M) into 100 µL reaction mixtures. Reactions were carried out in Tris-HCl buffer 50 mM, pH 7.4 in the presence of sodium azide (1 mM) and DTPA (0.1 mM). The tested reducing agents were: 5 mM of reduced glutathione (GSH), 10 mM of 2-mercaptoethanol, 0.5 mM of Dithiothreitol (DTT) or Dihydrolipoamide (DHLA).

less efficient peroxidases than their bacterial counterpart (PaOhr). Considering eukaryotic OsmC, DdOsmC presented about half of NADH consumption compared to the bacterial OsmC counterpart (*E. coli* BW25113) in the experimental conditions analyzed (**Fig. 4B**). We chose MfOhr for further characterization as it displayed the highest activity among the eukaryotic proteins studied.

2.5.5 – MfOhr enzymatic properties are similar to the bacterial Ohrs

Peroxidase activity of MfOhr was specifically supported by dithiols (DTT and DHLA) and not by monothiols (GSH and β-mercaptoethanol) (**Fig. 5**) and thus similar to bacterial Ohr enzymes [3]. We also analyzed MfOhr's specificity towards the oxidizing substrate, since it is well established that

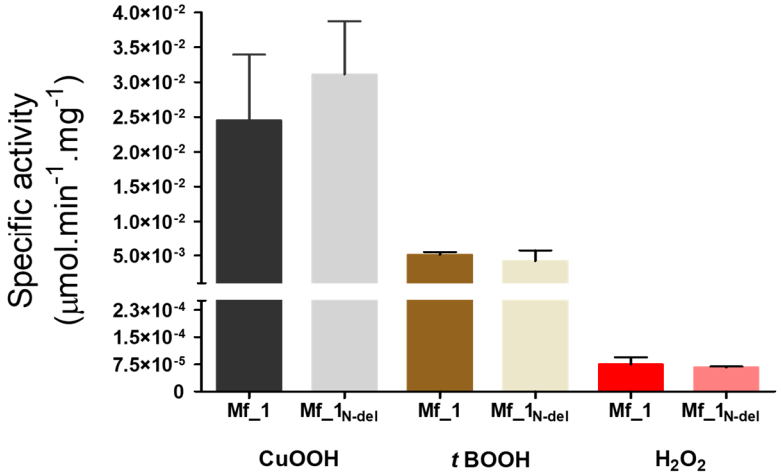

Fig. 6 – Specific activities of MfOhr and MfOhrdel towards CuOOH, tBOOH and H2O2. The values were calculated for the wild type (173 amino acids, MfOhr) or truncated (140 amino acids, $MfOhr_{del}$) versions of Mf_1 Ohr, using the lipoamide/lipoamide dehydrogenase coupled assay. Initial rates were obtained from the linear portion of the curves from reactions performed at 0.075, 0.1, 0.25 and 0.5 µM of enzyme, for tBOOH, 0.025, 0.05, 0.075 and 0.15 µM of enzyme, for CuOOH and 10, 12 and 15 µM of enzyme, for H_2O_2.

bacterial Ohr enzymes present higher preference for organic hydroperoxides over H_2O_2 [2–4,10]. Indeed, the specific activity of MfOhr for CuOOH was almost six times higher than the values presented for tBOOH and almost 500 times higher in comparison to H_2O_2 (**Fig. 6**). In conclusion, similarly to bacterial Ohr, MfOhr also displayed greater affinity for more hydrophobic substrates. We also evaluated the specific activities of a processed version of Ohr ($MfOhr_{del}$), in which the first 33 amino acids residues were removed, as it is well established that the N-terminal sequence is proteolytically cleaved

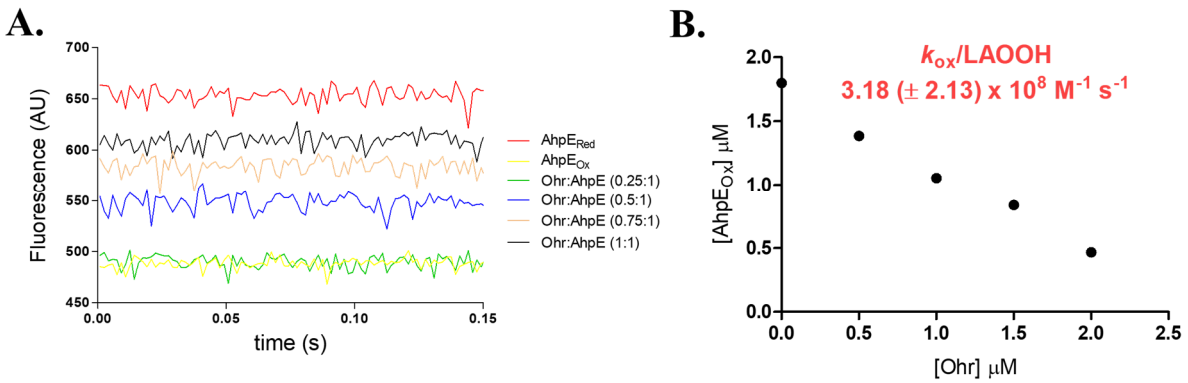

Fig. 7 – Kinetics of LAOOH reduction by MfOhr. **A.** Reaction of $MfOhr_{del}$ with LAOOH was investigated by a competitive assay following the Intrinsic tryptophan fluorescence emission (λ_{ex} =290 nm and λ_{em}=340 nm) of 2 µM AhpE [11]. Reduced AhpE was mixed with 0 (red line), 0.5 (green line), 1 (blue line), 1.5 (brown line) and 2 µM (black line) of reduced $MfOhr_{del}$ in the presence of 1.8 µM of LAOOH. The emission fluorescence of AhpE after oxidation by 1.8 µM of LAOOH, in the absence of MfOhr is shown as a yellow line. **B.** The fraction of oxidized AhpE ($AhpE_{Ox}$) decreases with increasing amount of $MfOhr_{del}$.

during import of the proteins into mitochondria. Both versions of the MfOhr (processed versus not processed) display similar specific activities values for each hydroperoxide tested (**Fig. 6**), suggesting that the N-terminal extension does not influence protein activity. In the following assays, we then chose to use the processed version of MfOhr ($MfOhr_{del}$). Since tBOOH and CuOOH are synthetic compounds, we decided to evaluate the ability of MfOhr to reduce more complex hydroperoxides, such as fatty acid hydroperoxides. In fact, we recently described that hydroperoxides derived from oleic, linoleic and arachidonic fatty acids are the biological substrates of bacterial Ohr, at least for enzymes from *P. aeruginosa* and *X. fastidiosa* [11]. Therefore, we determined the second order rate constant for the reaction between the reduced $MfOhr_{del}$ and linoleic acid hydroperoxide (LAOOH) by employing a competitive approach that follows redox dependent changes in the AhpE intrinsic fluorescence [11]. Like the bacterial enzymes, MfOhrdel displayed an extraordinarily high rate constant (3.2 (± 2.1)×10^8 M^{-1} s^{-1}) for LAOOH reduction (**Fig. 7A** and **B**).

2.5.6 – Single Cys mutants of MfOhr do not have detectable peroxidase activity

To evaluate the catalytic role of Cys residues of MfOhr, we generated single mutants for each residue.

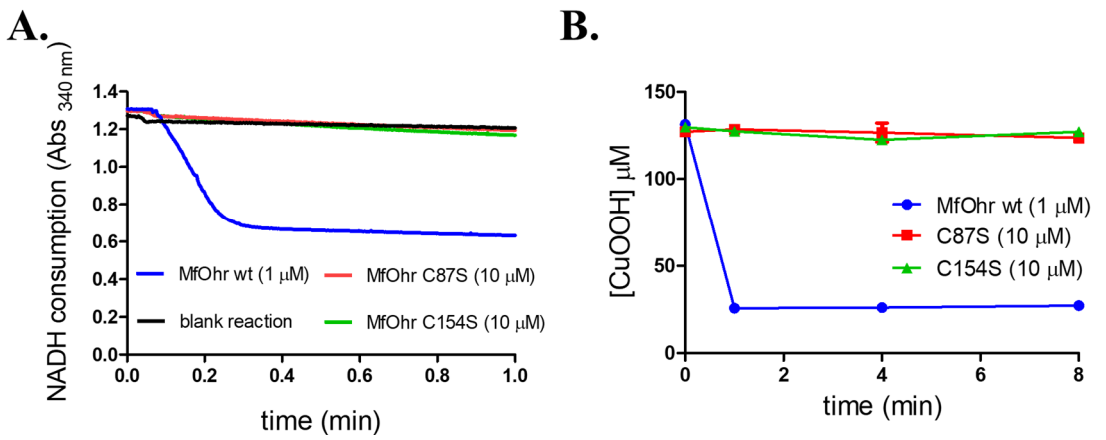

Fig. 8 – Comparison of the peroxidase activities of MfOhrdel and the C87S and C154S mutants. (A) Lipoamide/lipoamide dehydrogenase coupled assay. The reactions were performed at 37 ºC with 1 μM of $MfOhr_{del}$ (blue line) or 10 μM of mutant proteins (C87S, red line or C154S, green line), in the presence of 50 μM of reduced lipoamide, 100 μM of DTPA, 0.5 μM of XfLpd and 200 μM of NADH in 50 μM of sodium phosphate pH 7.4. Reactions were initiated by addition of 200 μM of CuOOH. Blank reaction (black line) was performed without enzyme. (B) The consumption of CuOOH was monitored during 8 minutes using FOX assay. The reactions were carried out in the presence of 1 μM ($MfOhr_{del}$) or 10 μM (C154S or C86S) enzymes. The control reactions for each tested hydroperoxide (enzyme + peroxide without DTT) and (hydroperoxide + DTT without enzyme) are not showed here. The figure is representative of at least two independent set of experiments.

Both mutants lost their peroxidase activity as assessed by lipoamide/lipoamide dehydrogenase coupled assay and FOX assay (**Fig. 8**). Similar results were observed for Ohr from *X. fastidiosa* [3]. These results suggest the C_r might have a role in activating C_p for hydroperoxide reduction.

2.5.7 – Determination of cysteine's p*K*$_a$ values

All thiol peroxidases so far described carry a reactive Cys, the so called C_p, whose thiolate group displays an acidic pK_a [35]. Therefore, we decided to determine the pKa value of C_p of $MfOhr_{del}$ by the monobromobimane alkylation method [29]. The curve that best fitted to the experimental data was

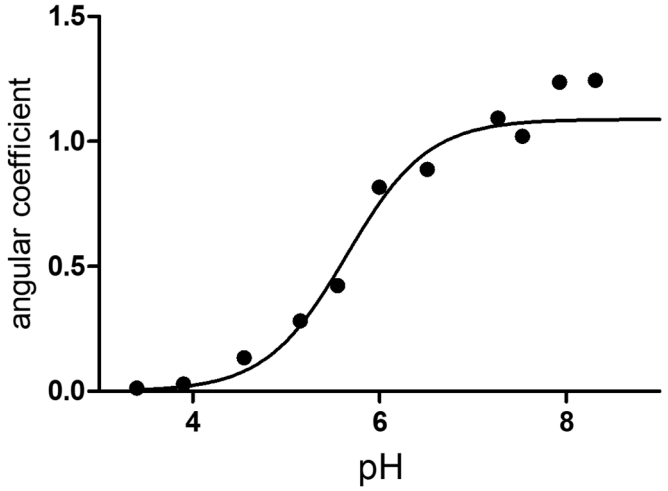

Fig. 9 – p*K*$_a$ value of C_p residue of MfOhrdel. Monobromobimane alkylation was performed using 4 µM of pre-reduced $MfOhr_{del}$ and 8 µM of monobromobimane in the presence of 15 mM of acetic acid, 15 mM of MES [2-(N-Morpholino Ethanesulfonic Acid] and 30 mM of Tris-HCl buffer adjusted to pH from 3.5 until 9.0. The determined pKa value of C_p from $MfOhr_{del}$ was 5.7 (± 0.1), according to non-linear regression using Henderson-Hasselbalch equation (GraphPad Software). This figure is representative of two independent set of experiments.

obtained by nonlinear regression (Handerson-Hasselbach equation) and resulted in a pK_a value of 5.7 ± 0.1 for the C_p residue (**Fig. 9**). This value is very similar to that previously described for bacterial type Ohr, 5.3 ± 0.1 [35]. We were unable to detect the pK_a of resolving Cys probably because this residue is deeply buried in the polypeptide backbone, as observed for bacterial Ohr enzymes, whose structures were elucidated [25]. Indeed, MfOhr C87S did not display any fluorescence upon mBrB treatment, supporting the hypothesis that C_r (Cys 154) is inaccessible to this alkylating agent under the experimental conditions employed here (data not shown).

2.5.8 – MfOhr intramolecular disulfide bond formation upon hydroperoxide treatment

We next studied the thiol redox state of Cys residue in response to hydroperoxides by non-reducing SDS-PAGE, since the intramolecular disulfide bond of Ohr enzymes can be detected due to its lower hydrodynamic volume as a band (band b) that migrates faster than the reduced state (band a) [14]. Wt, C87S and C154S MfOhr were exposed to reducing (10 mM of DTT) or oxidative conditions (0.1 mM of CuOOH, *t*BOOH or H_2O_2 and 0.017 mM of LAOOH) during 1 h at 37 °C. For the Wt MfOhr, we observed the appearance of band b upon oxidation as expected since it corresponds to the intramolecular disulfide (**Fig. 10A**). Band b was not observed when C_p or C_r residues were independently substituted by serine residues. In this case, a single band (band a) was observed that migrated equally regardless of

conditions (**Fig. 10B** and **C**). Therefore, again as bacterial enzymes, MfOhr is oxidized to a stable intramolecular disulfide upon oxidation by hydroperoxides.

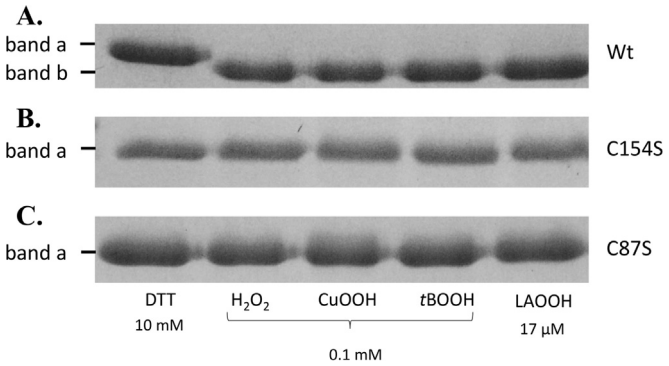

Fig. 10 – Non-reducing SDS-PAGE gels showing the effect of DTT and hydroperoxide treatments on MfOhrdel (A), MfOhrdel C154S (B) and MfOhrdel C87S (C). 10 µM of each protein were incubated during 1 h at 37 °C with 10 mM DTT, 0.1 mM H_2O_2, CuOOH or tBOOH or 17 µM linoleic acid hydroperoxide (LAOOH). All reactions were carried out in a buffer containing 0.5 M NaCl, 20 mM sodium phosphate pH 7.4 and 1 mM DTPA. Immediately after DTT or hydroperoxides treatments, all the samples were alkylated with NEM (100 mM) for 1 h at room temperature to avoid oxidation artefacts due

2.5.9 – Is MfOhr targeted to mitochondria?

Careful analysis of eukaryotic Ohr/OsmC sequences revealed that in most cases these sequences are longer than bacterial Ohr sequences (**Table S1**). The eukaryotic sequences contain an N-terminal extension that could harbor a signal peptide sequence for organellar localization or for extracellular secretion. Indeed, analysis of all 392 sequences by the TargetP and [28] and Mitofates [36] methods predicted that most of these proteins are addressed to mitochondria or another organelle (p > 90%) (**Table S1**). To experimentally verify if MfOhr is in fact a mitochondrial protein, we performed the

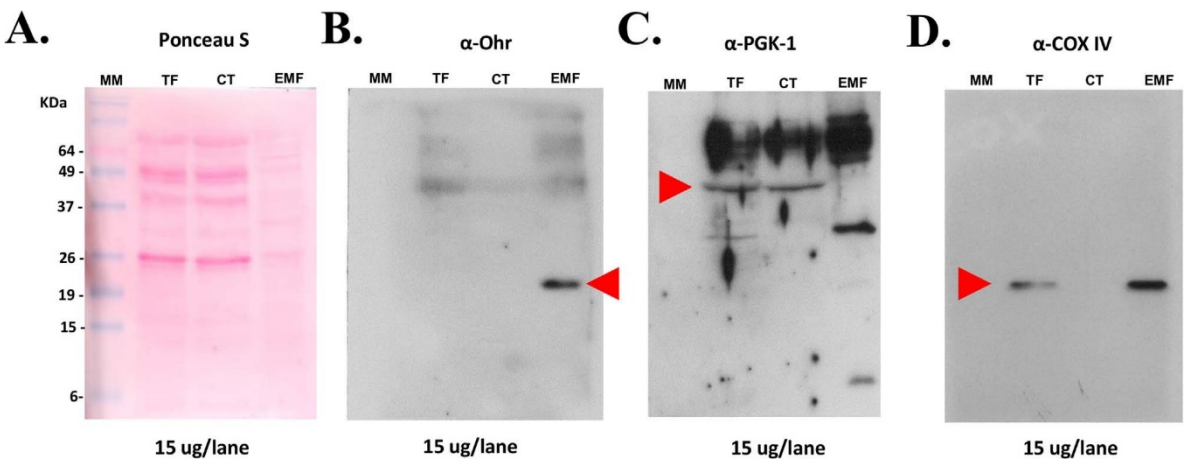

Fig. 11 – Western blots of total (TF), cytosolic (CF) and enriched mitochondria (EMF) fractions of protoplasts cells of M. fijiensis Mf_1. Fractions of M. fijiensis protoplasts are described in Material and Methods. A. Loading control (ponceau staining) of cellular fractions. After western blot, membrane was probed with affinity purified MfOhr polyclonal antibody (B); PGK-1, a cytoplasmic marker (C) and COX-IV, a mitochondrial marker (D), respectively.

subcellular fractionation of *M. fijiensis* protoplast cells, followed by western blot analysis. Initially, the affinity of purified Ohr antibody raised against bacterial Ohr was shown to be able to detect recombinant

$MfOhr_{del}$ (**Fig. S2**). However, MfOhr could not be detected in whole extracts of *M. fijiensis* mycelia grown in PDB medium, even when high amounts of total protein (200–300 µg) were employed. In contrast, a strong signal was observed in the enriched mitochondrial fraction (**Fig. 11B**). This is likely due to a dilution effect as the mitochondria occupy only a small fraction of the whole cellular mass. Indeed, COX IV, a well-established and abundant mitochondrial protein, was detected in whole extract at significantly lower levels than in the enriched mitochondrial fraction (**Fig. 11D**). As another control, the cytoplasmic protein PGK-1 was present in the total and cytoplasmic fraction but not in the mitochondrial fraction (**Fig. 11C**). Taken together, these results confirm the *in silico* prediction that MfOhr is a mitochondrial protein.

2.6 – Discussion

Initially thought to be exclusively found in prokaryotes, Ohr proteins have been described as the main enzymatic system involved in bacterial defense against organic hydroperoxides [5,7,9–11,35,37]. We show here that members of the Ohr/OsmC family are also present in several eukaryotic clades and are especially common among species of Fungi. To validate these *in silico* observations, biochemical characterization of selected proteins was carried out and our results indicated that these eukaryotic peroxidases are enzymatically similar to their bacterial counterparts.

Furthermore, we also demonstrated, not only for the Ohr subfamily but also for almost all eukaryotic Ohr/OsmC proteins, that the Nterminal signal sequence is predicted to localize to mitochondria or another organelle, such as the peroxisome or chloroplasts (**Table S1**). The presence of Ohr in mitochondria is in agreement with the fact that the proposed reducing system, *i. e*. lipoylated proteins from α-ketoacid dehydrogenase complexes [4], is also present in mitochondria. These findings are also consistent with the observation that mitochondria is a major source of endogenous oxidants [38,39]. It is reasonable to think that for eukaryotes, the peroxidase activity of Ohr may be related with detoxification of endogenous sources of hydroperoxides and might be not involved in defense towards exogenous insults of ROS, as it is currently proposed for bacteria [11,40,41].

It is noteworthy, that several species presenting Ohr homologs in eukaryotes are non-vascular plant or animal pathogens (**Table S1**), such as *M. fijiensis*, the causative agent of Black Sigatoka, the most important disease of banana and plants worldwide [42]. Remarkably, when we looked at the sequenced genomes currently available, we found that Ohr enzymes are completely absent in animals and vascular plants, although these organisms are hosts for microbial pathogens, thus making Ohr proteins a convenient target for drug development.

OsmC homologs also display thiol dependent peroxidase activity and show preference for organic hydroperoxides [43–46]. We also found OsmC enzymes in eukaryotes, but in this case the taxonomic distribution is restricted to some species within Dictyostelia. Interestingly, the *osmC* gene from *D. discoideum* AX4 was previously suggested to have been acquired via lateral gene transfer [47] but never had its peroxidase activity reported. To our knowledge, this is the first study that actually determined the peroxidase activity for an OsmC enzyme from *Dictyostelium* or any other eukaryotic organism.

Classification of proteins in the Ohr/OsmC family that do not belong to the Ohr and OsmC subfamilies were already described in the literature [1]. However, in these studies low numbers of sequences were analyzed. Here, Ohr-like sequences (not belonging to Ohr or OsmC subfamilies) were grouped together (**Fig. 2**), but we are aware that further studies are required for proper classification of these enzymes and an analysis including all available sequences of Ohr-like enzymes is currently under investigation in our laboratory.

Recently, the peroxidase activity of an Ohr-like enzyme from *T. vaginalis* was described [22] (Genbank accession no. XP_001323255). This protein was named TvOsmC, although it does not have the conserved Arg and Glu residues characteristic of the OsmC subfamily (**Fig. 1B** and **C**). In our experiments, TvOsmC did not display peroxidase activity (**Fig. 4B** and **S1**, respectively). In contrast, the peroxidase activity of TvOsmC was detected by Nývltová et al., [19]. Possibly, L and H (lipoylated) proteins from hydrogenossomes of *T. vaginalis* are required to support the peroxidase activity of this enzyme.

In summary, we showed that Ohr/OsmC proteins, mostly present in bacteria, also occur among eukaryotes, and are mostly targeted to organellar compartments. Although it is currently proposed that these genes were acquired from prokaryotes through lateral gene transfer events [22,47] and we did describe some cases for recent transfer events, our phylogeny cannot confirm nor negate the hypothesis of ancient transfers due to low bootstrap values in the deep branches of the Ohr/OsmC tree (**Fig. 2A**). On the other hand, to assume that members of the eukaryotic Ohr subgroup, which only includes genes from fungi, originate from endosymbiont-derived genes present in the last common ancestor of all eukaryotes would require multiple gene losses at the root of different eukaryotic lineages [48,49]. A more parsimonious explanation is that lateral gene transfer from bacteria to a lineage close to the common ancestor of extant fungal lineages was responsible for the unique presence of Ohr among fungi. As sequence databases grow and more sequences are added, further evolutionary studies will undoubtedly help improve our understanding of the origin and evolution of proteins from the Ohr/OsmC family across the many branches in the tree of life.

Acknowledgements

This work was supported by Fundação de Amparo à Pesquisa do Estado de São Paulo – FAPESP, process 2013/07937-8 (Redox Processes in Biomedicine -REDOXOMA). D.A.M was recipient of a fellowship from FAPESP, process 2012/21722-1. We thank Dr. Miguel J. Beltrán-García from Departamento de Química, Universidad Autónoma de Guadalajara, Guadalajara, Jalisco México and Dr. Aline Maria da Silva and Dr. Layla Farage Martins from Departamento de Bioquímica, Instituto de Química, Universidade de São Paulo, São Paulo, Brazil for kindly provide the *M. fijiensis* Mf_1 and *D. discoideum* AX4 strain, respectively.

Supplementary material

Supplementary data associated with this article can be found in the online version at doi:10.1016/j.redox.2017.03.026.

2.7 – References

[1] D.H. Shin, I.-G. Choi, D. Busso, J. Jancarik, H. Yokota, R. Kim, S.-H. Kim, Structure of OsmC from Escherichia coli: a salt-shock-induced protein, Acta Crystallogr. D. Biol. Crystallogr. 60 (2004) 903–911, http://dx.doi.org/10.1107/S0907444904005013.

[2] J. Lesniak, W.A. Barton, D.B. Nikolov, Structural and functional characterization of the Pseudomonas hydroperoxide resistance protein Ohr, EMBO J. 21 (2002) 6649–6659.

[3] J.R.R. Cussiol, S.V. Alves, M.A. de Oliveira, L.E.S. Netto, Organic hydroperoxide resistance gene encodes a thiol-dependent peroxidase, J. Biol. Chem. 278 (2003) 11570–11578, http://dx.doi.org/10.1074/jbc.M300252200.

[4] J.R.R. Cussiol, T.G.P. Alegria, L.I. Szweda, L.E.S. Netto, Ohr (organic hydroperoxide resistance protein) possesses a previously undescribed activity, lipoyl-dependent peroxidase, J. Biol. Chem. 285 (2010) 21943–21950, http://dx.doi.org/10.1074/ jbc.M110.117283.

[5] S. Mongkolsuk, W. Praituan, S. Loprasert, M. Fuangthong, S. Chamnongpol, Identification and characterization of a new organic hydroperoxide resistance (ohr) gene with a novel pattern of oxidative stress regulation from Xanthomonas campestrispv. Phaseoli Identification and characterization of a new organic hydroperoxide resi, J. Bacteriol. 180 (1998) 2636–2643.

[6] S. Atichartpongkul, S. Loprasert, P. Vattanaviboon, W. Whangsuk, J.D. Helmann,S. Mongkolsuk, Bacterial Ohr and OsmC paralogues define two protein families with distinct functions and patterns of expression, Microbiology 147 (2001) 1775–1782, http://www.ncbi.nlm.nih.gov/pubmed/11429455.

[7] T. Chuchue, W. Tanboon, J.M. Dubbs, P. Vattanaviboon, S. Mongkolsuk, B. Prapagdee, ohrR and ohr are the Primary Sensor/Regulator and Protective Genes Against Organic Hydroperoxide Stress in Agrobacterium Tumefaciens ohrR and ohr are the Primary Sensor/Regulator and Protective Genes against Organic Hydroperoxide Stress in Agrobacteria, 2006. doi: ⟨http://doi.org/10.1128/JB.188. 3.842⟩.

[8] A. Conter, C. Gangneux, M. Suzanne, C. Gutierrez, Survival of Escherichia coli during long-term starvation: effects of aeration, NaCl, and the rpoS and osmC gene products, Res. Microbiol. 152 (2001) 17–26, ⟨http://www.ncbi.nlm.nih.gov/ pubmed/11281321⟩.

[9] J.F. da Silva Neto, C.C. Negretto, L.E.S. Netto, Analysis of the organic hydroper- oxide response of chromobacterium violaceum reveals that OhrR is a cys-based redox sensor regulated by thioredoxin, PLoS One 7 (2012) e47090, http://dx.doi.org/10.1371/journal.pone.0047090.

[10] M. Si, J. Wang, X. Xiao, J. Guan, Y. Zhang, W. Ding, M.T. Chaudhry, Y. Wang, X. Shen, Ohr protects corynebacterium glutamicum against organic hydroperoxide induced oxidative stress, PLoS One 10 (2015) e0131634, http://dx.doi.org/10.1371/journal.pone.0131634.

[11] T.G.P. Alegria, D.A. Meireles, J.R.R. Cussiol, M. Hugo, M. Trujillo, M.A. de Oliveira,S. Miyamoto, R.F. Queiroz, N.F. Valadares, R.C. Garratt, R. Radi, P. Di Mascio, O. Augusto, L.E.S. Netto, Ohr plays a central role in bacterial responses against fatty acid hydroperoxides and peroxynitrite, Proc. Natl. Acad. Sci. USA 114 (2017) E132–E141, http://dx.doi.org/10.1073/pnas.1619659114.

[12] L.M.S. Baker, L.B. Poole, Catalytic mechanism of thiol peroxidase from Escherichia coli, J. Biol. Chem. 278 (2003) 9203–9211, http://dx.doi.org/10.1074/jbc.M209888200.

[13] K.J. Nelson, S.T. Knutson, L. Soito, C. Klomsiri, B. Leslie, J.S. Fetrow, Analysis of the Peroxiredoxin Family: Using Active Site Structure and Sequence Information for Global Classification and Residue Analysis, vol. 79, 2012, pp. 947–964. doi: ⟨http://doi.org/10.1002/prot.22936.analysis⟩.

[14] M. a. Oliveira, B.G. Guimarães, J.R.R. Cussiol, F.J. Medrano, F.C. Gozzo, L.E.S. Netto, Structural insights into enzyme-substrate interaction and character- ization of enzymatic intermediates of organic hydroperoxide resistance protein from Xylella fastidiosa, J. Mol. Biol. 359 (2006) 433–445, http://dx.doi.org/10.1016/j.jmb.2006.03.054.

[15] G.M. Boratyn, A. a. Schäffer, R. Agarwala, S.F. Altschul, D.J. Lipman, T.L. Madden, Domain enhanced lookup time accelerated BLAST, Biol. Direct 7 (2012) 12, http://dx.doi.org/10.1186/1745-6150-7-12.

[16] R.D. Finn, J. Clements, S.R. Eddy, HMMER web server: interactive sequence similarity searching, Nucleic Acids Res. 39 (2011) 29–37, http://dx.doi.org/10.1093/nar/gkr367.

[17] Y. Huang, B. Niu, Y. Gao, L. Fu, W. Li, CD-HIT Suite: a web server for clustering and comparing biological sequences, Bioinformatics 26 (2010) 680–682, http://dx.doi. org/10.1093/bioinformatics/btq003.

[18] K. Katoh, D.M. Standley, MAFFT multiple sequence alignment software version 7: improvements in performance and usability, Mol. Biol. Evol. 30 (2013) 772–780, http://dx.doi.org/10.1093/molbev/mst010.

[19] A. Stamatakis, Stamatakis – 2014 – RAxML Version 8 a Tool for Phylogenetic Analysis and Post-analysis of Large Phylogenies, 2014, pp. 2010–2011.

[20] S. Kumar, G. Stecher, K. Tamura, MEGA7: molecular evolutionary genetics analysis version 7.0 for bigger datasets, Mol. Biol. Evol. 33 (2016) msw054, http://dx.doi.org/10.1093/molbev/msw054.

[21] S. Cornillon, C. Foa, J. Davoust, N. Buonavista, J.D. Gross, P. Golstein, Programmed cell death in Dictyostelium, J. Cell Sci. 107 (1994) 2691–2704, http://dx.doi.org/10. 1016/j.bbamcr.2008.01.018.

[22] E. Nývltová, T. Smutná, J. Tachezy, I. Hrdý, OsmC and incomplete glycine decarboxylase complex mediate reductive detoxification of peroxides in hydro- genosomes of Trichomonas vaginalis, Mol. Biochem. Parasitol. (2015). http://dx.doi.org/10.1016/j.molbiopara.2016.01.006.

[23] B.A. Gasteiger E, C. Hoogland, A. Gattiker, S. Duvaud, M.R. Wilkins, R.D. Appel, Protein Identification and Analysis Tools on the ExPASy Server, Proteom. Protoc. Handb. (2005) 571–607, http://dx.doi.org/10.1385/1592598900.

[24] G.L. Ellman, Tissue sulfhydril groups, Arch. Biochem. Biophys. 82 (1959) 70–77.

[25] Z.Y. Jiang, J.V. Hunt, S.P. Wolff, Ferrous ion oxidation in the presence of xylenol orange for detection of lipid hydroperoxide in low density lipoprotein, Anal. Biochem. 202 (1992) 384–389, ⟨http://www.ncbi.nlm.nih.gov/pubmed/ 1519766⟩.

[26] K.F. Discola, M.A. de Oliveira, J.R. Rosa Cussiol, G. Monteiro, J.A. Barcena, P. Porras, C.A. Padilla, B.G. Guimaraes, L.E.S. Netto, Structural aspects of the distinct biochemical properties of glutaredoxin 1 and glutaredoxin 2 from Saccharomyces cerevisiae, J. Mol. Biol. 385 (2009) 889–901, http://dx.doi.org/10. 1016/j.jmb.2008.10.055.

[27] R. Bryk, Metabolic enzymes of mycobacteria linked to antioxidant defense by a thioredoxin-Like protein, Science 295 (80-.) (2002) 1073–1077, http://dx.doi.org/10.1126/science.1067798.

[28] M. Trujillo, G. Ferrer-Sueta, R. Radi, Chapter 10 kinetic studies on peroxynitrite reduction by peroxiredoxins, Methods Enzymol. 441 (2008) 173–196, http://dx.doi.org/10.1016/S0076-6879(08)01210-X.

[29] F. Sardi, B. Manta, S. Portillo-Ledesma, B. Knoops, M.A. Comini, G. Ferrer-Sueta, Determination of acidity and nucleophilicity in thiols by reaction with monobromobimane and fluorescence detection, Anal. Biochem. 435 (2013) 74–82, http:// dx.doi.org/10.1016/j.ab.2012.12.017.

[30] H. Schagger, W.A. Cramer, G. Vonjagow, Mitochondrial biogenesis and genetics Part A, Anal. Biochem. 217 (1994) 220–230, http://dx.doi.org/10.1016/0076-6879(95)60139-2.

[31] C.E. Hinchliff, S.A. Smith, J.F. Allman, J.G. Burleigh, R. Chaudhary, L.M. Coghill, K.A. Crandall, J. Deng, B.T. Drew, R. Gazis, K. Gude, D.S. Hibbett, L.A. Katz, H.D. Laughinghouse, E.J. McTavish, P.E. Midford, C.L. Owen, R.H. Ree, J.A. Rees, D.E. Soltis, T. Williams, K.A. Cranston, Synthesis of phylogeny and taxonomy into a comprehensive tree of life, Proc. Natl. Acad. Sci. USA 112 (2015) 201423041, http://dx.doi.org/10.1073/pnas.1423041112.

[32] G. Koutsovoulos, S. Kumar, D. Laetsch, L. Stevens, J. Daub, C. Conlon, No evidence for extensive horizontal gene transfer in the genome of the tardigrade Hypsibius dujardini, Pnas 113 (2016) 1–6, http://dx.doi.org/10.1073/pnas.1600338113.

[33] S.J. Salter, M.J. Cox, E.M. Turek, S.T. Calus, W.O. Cookson, M.F. Moffatt, P. Turner, J. Parkhill, N.J. Loman, A.W. Walker, Reagent and laboratory contamination can critically impact sequence-based microbiome analyses, BMC Biol. 12 (2014) 87, http://dx.doi.org/10.1186/s12915-014-0087-z.

[34] K. Schalchian-Tabrizi, M.A. Minge, M. Espelund, R. Orr, T. Ruden, K.S. Jakobsen, T. Cavalier-Smith, Multigene phylogeny of Choanozoa and the origin of animals, PLoS One 3 (2008) http://dx.doi.org/10.1371/journal.pone.0002098.

[35] D. de, A. Meireles, T.G. eronimo, P. Alegria, S.V. idigal Alves, C.R. ani, R. Arantes, L.E. duardo, S. Netto, A 14.7 kDa protein from Francisella tularensis subsp. novicida (named FTN_1133), involved in the response to oxidative stress induced by organic peroxides, is not endowed with thiol-dependent peroxidase activity, PLoS One 9 (2014) e99492, http://dx.doi.org/10.1371/journal.pone.0099492.

[36] Y. Fukasawa, J. Tsuji, S.-C. Fu, K. Tomii, P. Horton, K. Imai, MitoFates: improved prediction of mitochondrial targeting sequences and their cleavage sites, Mol. Cell. Proteom. 14 (2015) 1113–1126, http://dx.doi.org/10.1074/mcp.M114.043083.

[37] C. Fontenelle, C. Blanco, M. Arrieta, V. Dufour, A. Trautwetter, Resistance to organic hydroperoxides requires ohr and ohrR genes in Sinorhizobium meliloti, BMC Microbiol. 11 (2011) 100, http://dx.doi.org/10.1186/1471-2180-11-100.

[38] M.P. Murphy, How mitochondria produce reactive oxygen species, Biochem. J. 417 (2009) 1–13, http://dx.doi.org/10.1042/BJ20081386.

[39] C.L. Quinlan, R.L.S. Goncalves, M. Hey-Mogensen, N. Yadava, V.I. Bunik, M.D. Brand, The 2-oxoacid dehydrogenase complexes in mitochondria can produce superoxide/hydrogen peroxide at much higher rates than complex I, J. Biol. Chem. 289 (2014) 8312–8325, http://dx.doi.org/10.1074/jbc.M113.545301.

[40] J. Liu, Zhi Wang, Hui Zhou, Zhigang Sheng, Ying Naseer, Nawar Kan, Biao, Zhu, Thiol-based switch mechanism of virulence regulator AphB modulates oxidative stress response in Vibrio cholerae, Clin. Exp. Immunol. 102 (2016) 939–949, http:// dx.doi.org/10.1111/joms.12099.

[41] M.L. Reniere, A.T. Whiteley, D.A. Portnoy, An in vivo selection identifies Listeria monocytogenes Genes required to sense the intracellular environment and activate virulence factor expression, PLoS Pathog. 12 (2016) 1–27, http://dx.doi.org/10. 1371/journal.ppat.1005741.

[42] A.C.L. Churchill, Mycosphaerella fijiensis, the black leaf streak pathogen of banana: progress towards understanding pathogen biology and detection, disease develop- ment, and the challenges of control, Mol. Plant Pathol. 12 (2011) 307–328, http:// dx.doi.org/10.1111/j.1364-3703.2010.00672.x.

[43] S. Saikolappan, K. Das, S.J. Sasindran, C. Jagannath, S. Dhandayuthapani, OsmC proteins of Mycobacterium tuberculosis and Mycobacterium smegmatis protect against organic hydroperoxide stress, Tuberculosis 91 (Suppl 1) (2011) S119–S127, http://dx.doi.org/10.1016/j.tube.2011.10.021.

[44] W. Zhang, J.B. Baseman, Functional characterization of osmotically inducible protein C (MG_427) from Mycoplasma genitalium, J. Bacteriol. 196 (2014) 1012–1019, http://dx.doi.org/10.1128/JB.00954-13.

[45] J. Lesniak, W.A. Barton, D.B. Nikolov, Structural and functional features of the Escherichia coli hydroperoxide resistance protein OsmC, Protein Sci. 12 (2003) 2838–2843, http://dx.doi.org/10.1110/ps.03375603.

[46] S.-C. Park, B.P. Pham, L. Van Duyet, B. Jia, S. Lee, R. Yu, S.W. Han, J.-K. Yang, K.- S. Hahm, G.-W. Cheong, Structural and functional characterization of osmotically inducible protein C (OsmC) from Thermococcus kodakaraensis KOD1, Biochim. Biophys. Acta (2008) (1784) 783–788, http://dx.doi.org/10.1016/j.bbapap.2008.02.002.

[47] L. Eichinger, J.A. Pachebat, G. Glöckner, M. Rajandream, R. Sucgang, M. Berriman, J. Song, R. Olsen, K. Szafranski, Q. Xu, B. Tunggal, S. Kummerfeld, M. Madera, B.A. Konfortov, F. Rivero, A.T. Bankier, R. Lehmann, N. Hamlin, R. Davies, P. Gaudet, P. Fey, K. Pilcher, G. Chen, D. Saunders, E. Sodergren, P. Davis, A. Kerhornou, X. Nie, N. Hall, C. Anjard, L. Hemphill, N. Bason, P. Farbrother, B. Desany, E. Just, T. Morio, R. Rost, C. Churcher, J. Cooper, S. Haydock, N. van Driessche, A. Cronin, I. Goodhead, D. Muzny, T. Mourier, A. Pain, M. Lu, D. Harper, R. Lindsay, H. Hauser, K. James, M. Quiles, M. Madan Babu, T. Saito, C. Buchrieser, A. Wardroper, M. Felder, M. Thangavelu, D. Johnson, A. Knights, H. Loulseged, K. Mungall, K. Oliver, C. Price, M.A. Quail, H. Urushihara, J. Hernandez, E. Rabbinowitsch, D. Steffen, M. Sanders, J. Ma, Y. Kohara, S. Sharp, M. Simmonds, S. Spiegler, A. Tivey, S. Sugano, B. White, D. Walker, J. Woodward, T. Winckler, Y. Tanaka, G. Shaulsky, M. Schleicher, G. Weinstock, A. Rosenthal, E.C. Cox, R.L. Chisholm, R. Gibbs, W.F. Loomis, M. Platzer, R.R. Kay, J. Williams, P.H. Dear, A.A. Noegel, B. Barrell, A. Kuspa, The genome of the social amoeba Dictyostelium discoideum, Nature 435 (2005) 43–57, http://dx.doi.org/10.1038/nature03481.

[48] C. Ku, W.F. Martin, A natural barrier to lateral gene transfer from prokaryotes to eukaryotes revealed from genomes: the 70% rule, BMC Biol. 14 (2016) 89, http:// dx.doi.org/10.1186/s12915-016-0315-9.

[49] C. Ku, S. Nelson-sathi, M. Roettger, F.L. Sousa, P.J. Lockhart, D. Bryant, E. Hazkani- covo, J.O. Mcinerney, G. Landan, W.F. Martin, Endosymbiotic origin and differential loss of eukaryotic genes, Nature 524 (2015) 427–437, http://dx.doi.org/10. 1038/nature14963.

CHAPTER 3 – STRUCTURAL INSIGHTS ON THE EFFICIENT CATALYSIS OF HYDROPEROXIDE REDUCTION BY OHR: CRYSTALLOGRAPHIC AND MOLECULAR DYNAMICS APPROACHES

Structural Insights on the Efficient Catalysis of Hydroperoxide Reduction by Ohr: Crystallographic and Molecular Dynamics Approaches

Erika Piccirillo [1¶], Thiago G. P. Alegria [2¶], Karen F. Discola [2], José R. R. Cussiol [2], Renato M. Domingos [2], Marcos A. de Oliveira [3], Leandro de Rezende [1], Luis E. S. Netto [2*] and Antonia T-do Amaral [1*].

[1] Departamento de Química Fundamental, Instituto de Química, Universidade de São Paulo, São Paulo, SP, Brazil
[2] Departamento de Genética e Biologia Evolutiva, Instituto de Biociências, Universidade de São Paulo, São Paulo, SP, Brazil
[3] Instituto de Biociências, Campus do Litoral Paulista, Universidade Estadual Paulista Júlio de Mesquita Filho, São Vicente, SP, Brazil

* Corresponding authors E-mail: nettoles@ib.usp.br (LESN); atdamara@iq.usp.br (ATA)
¶ These authors contributed equally to this work.

This Chapter was published in PLoS ONE (Vol. 13) in May 2018

https://doi.org/10.1371/journal.pone.0196918

3.1 – Main contribution by Renato M. Domingos

I performed the crystallographic structure associated analysis. Participated in the molecular dynamics' interpretation and manuscript development.

3.2 – Abstract

Organic hydroperoxide resistance (Ohr) enzymes are highly efficient Cys-based peroxidases that play central roles in bacterial response to fatty acid hydroperoxides and peroxynitrite, two oxidants that are generated during host-pathogen interactions. In the active site of Ohr proteins, the conserved Arg (Arg19 in Ohr from *Xylella fastidiosa*) and Glu (Glu51 in Ohr from *Xylella fastidiosa*) residues, among other factors, are involved in the extremely high reactivity of the peroxidatic Cys (C_p) toward hydroperoxides. In the closed state, the thiolate of C_p is in close proximity to the guanidinium group of Arg19. Ohr enzymes can also assume an open state, where the loop containing the catalytic Arg is far away from C_p and Glu51. Here, we aimed to gain insights into the putative structural switches of the Ohr catalytic cycle. First, we describe the crystal structure of Ohr from *Xylella fastidiosa* (XfOhr) in the open state that, together with the previously described XfOhr structure in the closed state, may represent two snapshots along the coordinate of the enzyme-catalyzed reaction. These two structures were used for the experimental validation of molecular dynamics (MD) simulations. MD simulations employing distinct protonation states and *in silico* mutagenesis indicated that the polar interactions of Arg19 with Glu51 and C_p contributed to the stabilization of XfOhr in the closed state. Indeed, C_p oxidation to the disulfide state facilitated the switching of the Arg19 loop from the closed to the open state. In addition to the Arg19 loop, other portions of XfOhr displayed high mobility, such as a loop rich in Gly residues. In summary, we obtained a high correlation between crystallographic data, MD simulations and biochemical/enzymatic assays. The dynamics of the Ohr enzymes are unique among the Cys-based peroxidases, in which the active site Arg undergoes structural switches throughout the catalytic cycle, while C_p remains relatively static.

3.3 – Introduction

Oxidants such as fatty acid hydroperoxides are signaling molecules involved in host-pathogen interactions, and therefore, their levels are strictly controlled by peroxidases and other mechanisms [1–4]. Ohr (Organic hydroperoxide resistance) proteins are Cys-based, dithiol-dependent peroxidases that display unique biochemical and structural properties [5,6]. Ohr enzymes play central roles in the bacterial response to peroxynitrite and fatty acid hydroperoxides, two oxidants involved in host – pathogen interactions [1]. These enzymes are found in bacteria and fungi, and they are absent in their hosts (plants and animals) [7], making them promising targets for drug discovery. Some examples of pathogenic bacteria that express Ohr proteins are *Pseudomonas aeruginosa*, *Vibrio cholerae* and *Xyllela fastidiosa* [7]. *Xylella fastidiosa* is a plant pathogen with agronomic interest, causing disease in citrus, grapes and olives [8].

Ohr protein was first identified in *Xanthomonas campestris* pv. *phaseoli* due to its involvement in the bacterial response to organic hydroperoxides, but it is not involved in the H_2O_2 response [9]. This unusual organic hydroperoxide resistance phenotype is related to the ability of Ohr enzymes to reduce organic hydroperoxides with higher efficiency than H_2O_2 [5,6,10]. Ohr, Prxs (peroxiredoxins) and Gpx (GSH peroxidases) are all Cys-based, thiol-dependent peroxidases; however, Ohr and Prx/Gpx enzymes belong to distinct families, as their biochemical/enzymatic properties and structures are distinct [6, 11]. Instead, Ohr proteins share structural and amino acid sequence similarities with OsmC proteins, which were initially related to the bacterial response to osmotic stress [12]. Later, it was demonstrated that OsmC enzymes are also endowed with thiol peroxidase activity [13,14]. Therefore, Ohr/OsmC is a family of Cys-based proteins that also comprise proteins (such as YhfA from *Escherichia coli*) whose biochemical activity is still unknown [7,12,14].

Proteins belonging to the Ohr/OsmC family display a barrel-like structure formed by a tightly folded homodimer, in which two six-stranded β-sheets wrap around two central α-helices [6,11,15]. The two active sites are located at the dimer interface on opposite sides of the protein, and the reactive Cys, also called the peroxidatic Cys (C_p, Cys61 in Ohr from *Xylella fastidiosa* - XfOhr), is located in one of the central α-helices. C_p and two other residues (Arg19 and Glu51 in XfOhr) constitute the catalytic triad. The involvement of catalytic Arg in the ability of Ohr enzymes to reduce hydroperoxides was directly assessed by site-directed mutagenesis in Ohr from *Pseudomonas aeruginosa* (PaOhr) [6]. The carboxylic group of catalytic Glu orients the guanidinium group of Arg toward C_p in a configuration that appears to be optimal for the reduction of organic hydroperoxides [6,11]. Recently, we showed that fatty acid hydroperoxides are biological substrates of Ohr enzymes [1], displaying properties expected for ligands of these enzymes, such as an elongated shape and hydrophobicity. Peroxynitrite is also one of the biological oxidants of Ohr enzymes, but other features are associated with this catalysis [1]. In spite of all these advances, several aspects related to the extremely high efficiency of Ohr enzymes to

reduce hydroperoxides remains elusive, such as the possible occurrence of structural movements along the catalytic cycle.

The reaction of hydroperoxides with C_p generates a sulfenic acid (C_p-SOH), which undergoes condensation with the resolving Cys (C_r, which is Cys125 in XfOhr), generating an intramolecular disulfide bond [6,11]. Moreover, the loop that contains the catalytic Arg (herein named the Arg19 loop) was observed far away from C_p and the catalytic Glu in the crystal structure of Ohr from *Deinococcus radiodurans* (DrOhr) [15]. In this case, the two Cys residues form a disulfide bond [15]. Therefore, we previously hypothesized that Ohr enzymes in the so-called "closed state" [6,11] would present catalytic Arg in an orientation able to activate C_p for hydroperoxide reduction, whereas Ohr enzymes in the so-called "open configuration" [15] would be more prone to recycling by the reducing substrate. We have since shown that the reducing substrates of XfOhr are lipoylated proteins [10], in contrast to the Prx/Gpx counterparts that are mainly reduced by thioredoxin or GSH [16]. Here, for the first time, we present crystal structures for the same Ohr protein in the open and closed states, allowing for the validation of the *in silico* simulations. Additionally, to better understand the structural changes during the catalytic cycle, molecular dynamics (MD) simulations were applied to the XfOhr structure in its closed and open states, in distinct protonation and oxidation states, and after *in silico* mutagenesis. The same mutagenesis was also performed in the recombinant Ohr protein to evaluate its biochemical properties. Among other findings, our results indicate that polar interactions among the C_p, Arg19 and Glu51 residues are important to stabilize XfOhr in the closed state, and they are also required to activate the thiolate for hydroperoxide reduction. The disruption of any of these polar interactions releases some of the constraints on the Arg19 loop movement.

3.4 – Materials and methods

3.4.1 – Crystallization trials, data collection and processing

The procedures concerning XfOhr expression and purification have been previously reported [5]. XfOhr (10 mg/ml) was treated with 1.2 mM lipoamide at 310 K for 1 h and crystallized using the hanging-drop vapor diffusion method. The optimal crystallization condition was obtained using reservoir solution pH 6.0 (0.1 M sodium cacodylate and 0.4 M sodium citrate). The XfOhr crystal, cryoprotected by the mother liquor solution supplemented with 20 % glycerol, was cooled to 100 K in a nitrogen gas stream, and X-ray diffraction data were collected at protein crystallography beam line D03B-MX1 at the Brazilian Synchrotron Light Laboratory, LNLS. The data set was processed using the programs MOSFLM [17] and SCALA [18,19] from the CCP4i package [20].

3.4.2 – Structure determination, model building and refinement

The Matthews coefficient (2.18) revealed three Ohr chains per asymmetric unit, and the monomer structure of the XfOhr (1ZB8) was used as a search model in molecular replacement protocols using the program Phaser [21]. The model was constructed by consecutive cycles of manual modelling, using the program Coot [22], and refinement using Refmac [23]. The stereochemical parameters of the final model were evaluated using the programs PROCHECK [23] and WHATCHECK [25]. Cα superposition was performed using Coot [22], and molecular graphical representations were generated using PyMOL [26].

2.4.3 – Site-directed mutagenesis

The pET15b/XfOhr plasmid was used as a template to generate the individual Ohr mutants carrying mutations of Arg19 to Ala (R19A) and Glu51 to Ala (E51A). The mutagenesis protocols were performed according to the manufacturer's instructions (Quick Change II Kit; Stratagene) with the following primers: XfOhrR19A_F (5' CAACTGGTGGCGCCGATGGCAGC 3'), XfOhrR19A_R (5' GCTGCCATCGGCGCCACCAGTTG 3'), XfOhrE51A_F (5' GGTACCAATCCAGCGCAACTGTTTG 3') XfOhrE51A_R (5' CAAACAGTTGCGCTGGATTGGTACC 3'). The reaction products were treated with Dpn I to remove the parental methylated plasmids, and the *E. coli* XL1-Blue strain was used as the host and transformed by electroporation. Single colonies were selected and their plasmids were extracted and sequenced with the BigDye Terminator v3.1 Cycle Sequencing Kit using an automatic sequencer, the ABI 3730 DNA Analyzer (Thermo Scientific), to confirm the codon substitutions. The plasmids harboring the mutations were transformed into the *E. coli* BL21 (*DE3*) strain by electroporation. The procedures concerning XfOhr mutants expression and purification were the same as for the wild-type.

2.4.4 – Lipoamide-lipoamide dehydrogenase peroxidase-coupled assay

The lipoyl peroxidase activity levels of wild-type XfOhr and its mutants (R19A and E51A) were determined as previously described [10]. The reactions were followed by the decay of absorbance at 340 nm (e = 6,290 $M^{-1} \cdot cm^{-1}$) due to NADH oxidation.

2.4.5 – pK_a determination by monobromobimane alkylation assay

Wild-type XfOhr and its mutants (R19A and E51A) were reduced with 100 mM DTT (dithiothreitol) for 2 hours at room temperature. The DTT excess was then removed by gel filtration (PD-10 desalting column - GE), and the Ohr proteins (10 μM) were incubated with monobromobimane (2 μM) in buffers (50 mM) at different pH values (3.0 to 7.0) for 20 minutes at room temperature. The rates of alkylation by monobromobimane were determined by extrapolation of the maximum inclination of the curves [26]. Subsequently, the pK_a values were determined by the Henderson-Hasselbach equation in GraphPad®Prism4.

2.4.6 – Circular dichroism

All measurements were carried out in Tris buffer (10 mM) pH 7.4, and wild-type XfOhr and its mutants (R19A and E51A) were used at 15 μM. CD spectra were recorded from 180 to 320 nm using a JASCO spectropolarimeter, model J720 at the Central Analítica of IQUSP, SP.

2.4.7 – Morph conformations

Morph conformations were generated using the UCSF Chimera (Pettersen *et al*, 2004) package from the Resource for Biocomputing, Visualization, and Informatics at the University of California, San Francisco (supported by NIH P41 RR-01081). For this purpose, we applied the corkscrew interpolation method with 40 interpolation steps and used two crystal structures of XfOhr in its closed (1ZB8) and open states (4XX2) to generate the first set of morph conformations. Subsequently, the first, the average and the last snapshots of the XfOhr-SS trajectory (see below) were used to generate the second set of morph conformations.

2.4.8 – MD simulations

The XfOhr structure in the closed conformation (PDB entry 1ZB8, 2.4 Å resolution) was subjected to MD simulation studies in two conditions: (1) in the reduced form (C_p as thiolate, Cys61) with 12 crystal water molecules, having B-factors < 25 $Å^2$ and (2) with an artificial intramolecular disulfide between C_p and Cys125, which was built with SYBYL [29]. After the disulfide bond formation, the neighboring residues had their geometry optimized using Tripos force field and the Powell method [30,31]. The XfOhr trajectories in the reduced and oxidized forms were named XfOhr-S^- and XfOhr-SS, respectively. Furthermore, an XfOhr trajectory with C_p as a protonated thiol (named

XfOhr-SH) was similarly built and subjected to MD simulation. To evaluate the roles of the Arg19 and Glu51 residues in the conformational change of XfOhr, the R19A and E51A XfOhr mutants were built *in silico* using SYBYL-X [32]. The wild-type residues were replaced by alanine, and their neighboring residues were minimized, as described above.

Finally, the open conformation of XfOhr described here (PDB entry 4XX2) was also used as a starting point for MD simulation, having, however, its C_p reduced to thiolate by breaking the disulfide bond and deprotonated using SYBYL-X [32]. Subsequently, the geometry of the C_p neighboring residues was optimized as described for XfOhr-SS, and the minimized structure was named Open-S^-. Arginine and lysine were protonated, whereas aspartic and glutamic acids were deprotonated. Histidine was protonated at its ε-nitrogen atoms.

All MD simulations were performed using GROMACS 4.6.3 [31,32] and G54a7 force field [33]. Force field parameters for cysteine as thiolate were taken from those available for Cys without adding a hydrogen atom to the Sγ atom. Partial charges for Sγ and Cβ atoms were assigned as -0.7 and -0.3, respectively, which correspond to the mean values calculated using the Gasteiger Marsili, Huckel, Pullman, MMFF94, Gasteiger Huck methods available in SYBYL-X (SYBYL, 2013). The starting structure was initially minimized in vacuum, using the steepest descent method and the conjugated gradient algorithm (2000 steps each). The minimized structure was placed in a 100 Å cubic box, solvated with simple point-charge (SPC) water [36] and neutralized by adding sodium ions. Periodic boundary conditions were applied, and all covalent bonds containing hydrogen were fixed at equilibrium lengths using the LINCS algorithm [37]. The particle-mesh Ewald method [38,39] was used and a 9 Å cutoff value was applied for van der Waals interactions. The system energy was further minimized using the steepest descent method and the conjugate gradient method (2000 steps each). Subsequently, a position restraint dynamics simulation was performed for 2.5 ps at 200 K, keeping rigid all protein atom positions. The whole system was heated from 100 K to 300 K over 37 ps, followed by a period of 100 ps of equilibration. The temperature and pressure were kept at 300 K and 1 atm, respectively, by the V-rescale [40] and Berendsen [41] approaches. Subsequently, MD simulations were carried out for 50/150 ns at 300 K. A 2 fs integration time step was used, and configurations were collected every 2 ps.

VMD [42] was used to align all trajectories to their corresponding starting structures. The root-mean-square deviation (RMSD) values of all backbone atoms with respect to the initial conformation were calculated by VMD [42], and their average values were used to determine the overall backbone dynamics. The snapshot closest to the average structures was used as a representative of each simulation. The root-mean-square fluctuation (RMSF) of all protein residues with respect to their average position was calculated with VMD [42] and used to analyze protein residue flexibility. The conformational change of XfOhr in the simulation was followed by measuring the distance between the Arg19-Cα and C_p-Cα/Glu51-Cα atoms throughout the simulation time using VMD [42]. For the residues Arg19, Glu51 and C_p, the stability of the hydrogen bond interactions was measured by

hydrogen bond (Hbond) occupancy throughout the entire trajectory using the default parameters of the VMD hydrogen bond tool (donor-acceptor distance and angle values of 3.0 Å and 20 °, respectively). The stability of the salt-bridge interactions between these residues was measured considering the distance between all N – O/S pairs throughout the simulation using VMD [42]. These distances were analyzed by Tukey box-plots generated by R (R Core Team, 2015), and only residues having at least one N – O/S pair whose median distance value was lower than 4 Å [43,45] were considered to be stable. PyMOL [26] and VMD [42] were used for visualization of both the trajectories and the representative structures. MD simulation movies were generated using the UCSF Chimera (Pettersen *et al*, 2004) package from the Resource for Biocomputing, Visualization, and Informatics at the University of California, San Francisco (supported by NIH P41 RR-01081).

3.5 – Results

3.5.1 – Crystal structure of XfOhr as a disulfide in its open form

Ohr proteins contain a distinct α/β fold, and there are currently only six structures deposited in the Protein Data Bank. Therefore, it is relevant to make new Ohr crystal structures available for comparative studies. Two of these structures are of XfOhr, and both are in the closed state [11]. A new structure of XfOhr in the open state is described here.

XfOhr was crystallized by the hanging drop vapor diffusion method, and the corresponding crystal belongs to space group C2 (**Table 1**). A complete data set was collected up to 2.15 Å resolution. The molecular replacement solution contained three monomers in the asymmetric unit. As expected from the previous characterizations [6,11], the overall structure of XfOhr in the disulfide state is an elliptically shaped homodimer. The superposition of the two XfOhr structures (PDB entries 4XX2 and 1ZB8/1ZB9) resulted in an RMSD = 1.21 Å. The XfOhr open-state structure was obtained in the oxidized state (disulfide bond) despite the presence of a reducing agent (dihydrolipoamide) in the solution. It is possible that the growth of the crystal started after the oxidation of dihydrolipoamide. Nevertheless, the same phenomenon occurred with DrOhr, but in this case, DTT instead of dihydrolipoamide was used as the reducing agent [15]. It is well documented that the efficacy of thiols as reductants decreases over time [46].

Table 1. Data collection and refinement statistics parameters for the XfOhr open-state.

Parameter	XfOhr open state
I. Data Collection	
Space group	C2
Unit-cell dimensions (Å)	a = 87.81; b = 83.69; c = 60.76
Unit-cell angles (°)	α = γ = 90 and β = 93.67
Resolution limits (Å)	43.81 – 2.15
Total no. reflections	229678
No. unique reflections	25723
Completeness (%)	99.9 (99.9)
Multiplicity	3.1 (3.0)
R sym (%)	0.088 (0.349)
< I/σ(I)>	13.9 (3.0)
II. Refinement statistics	
Reflections	23868
Working	22647
Test	1221
Non-hydrogen atoms	3394
No. of water molecules	435
R_{factor}	0.176
R_{free}	0.223
RMDS values	
Bonds	0.001
Angles	1.539
Average B-factor	
Main chain	20.24
Side chains and water molecules	22.44
Ramachandran analysis (%)	
Favored regions	91.9
allowed regions	8.1
PDB code	4XX2

In the XfOhr open-state structure, the two fully conserved Cys residues are linked by a disulfide bond (Cys61-S-S-Cys125, **S1 Fig**), and the Arg19 loop is displaced far away from C_p (Cys61) in an open configuration (**Fig 1A**), in contrast to the reported XfOhr closed-state structure (**Fig 1B**) [9]. Other differences between the two XfOhr states are: (i) the α-helix that contains C_p is slightly bent in the open form and (ii) a Gly-rich loop containing residues 35 to 46 (**Fig 1B**), which is referred herein as the Gly-rich loop. In spite of these differences, the overall fold of XfOhr is quite similar to that of other Ohr structures (**Fig 1C**).

The main chains of the Arg19 loops of the XfOhr open state and of DrOhr overlapped well (**Fig 1C**). In the case of DrOhr, it was not possible to assign electronic densities to the side chains of the Arg19 loop [15], whereas the corresponding assignment for XfOhr was possible (**S1 Fig**), probably due to crystal contacts (**S2 Fig**). Possibly, the Arg19 side chain position observed in the XfOhr open structure

may differ from the biological structure. Nevertheless, the XfOhr open state structure shares several structural features with DrOhr.

In the other structure, XfOhr is in the closed state and Arg19 makes polar interactions with Glu51 and with C_p (**Fig 1D**). The opening of the loop would probably then be facilitated by the loss of

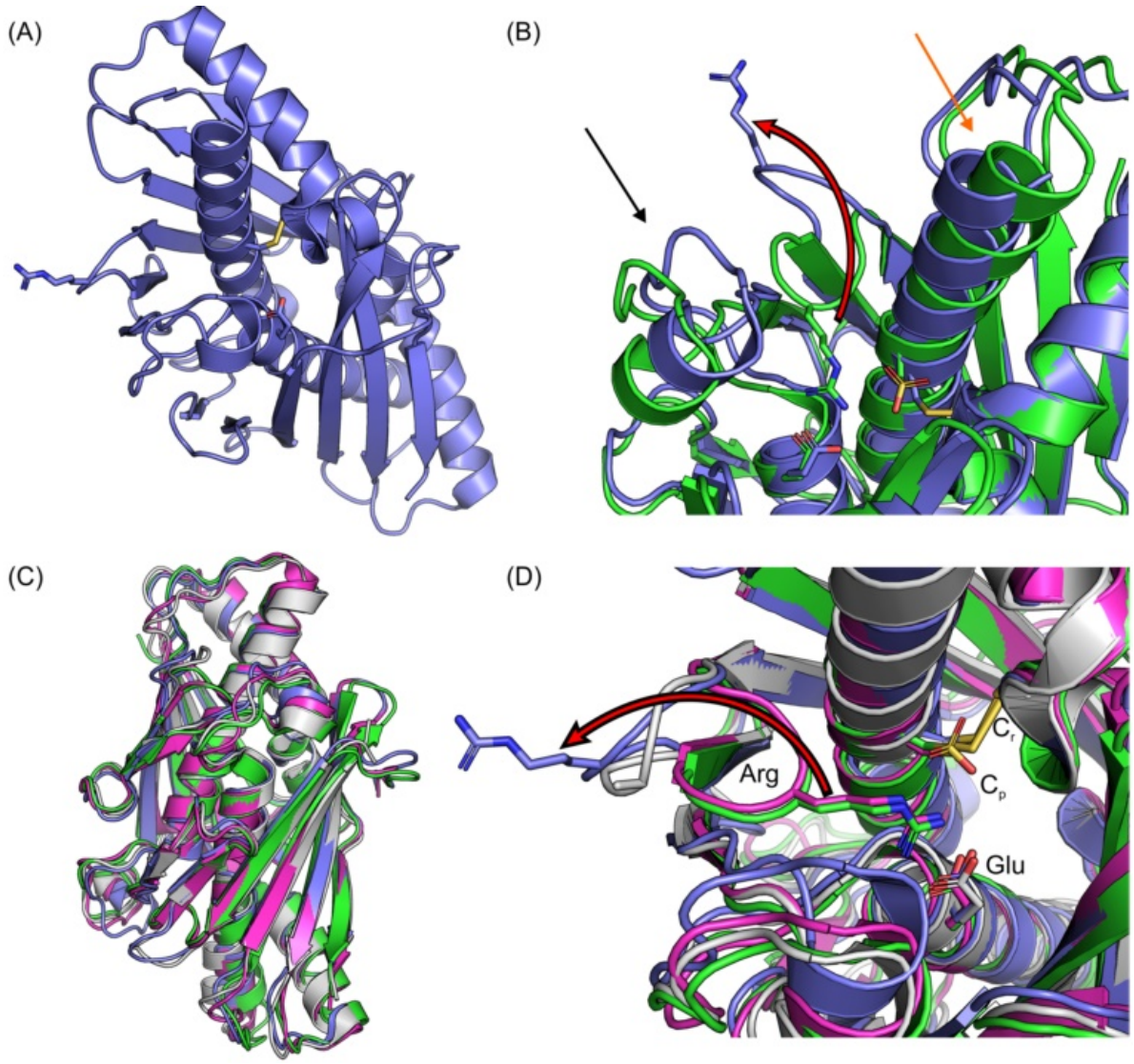

Fig 1. Comparison of different crystal structures of Ohr (A) XfOhr open-state crystal structure in its oxidized form (Arg19 loop exposed to the solvent). (B) Superposition of the XfOhr open (green) and closed (blue marine) structures. The red arrow shows a shift between the open and closed conformations of the alpha helix containing C_p (moves approximately 2.1 Å), and the black arrow shows the superposition of the loop containing residues 33 to 48 (Gly-rich loop). (C) Superposed structures of XfOhr closed (blue marine); XfOhr open (green); PaOhr closed (pink) and DrOhr open (gray). (D) Active site of the XfOhr open (blue marine) and closed (green) states superimposed onto PaOhr closed (pink) and DrOhr open (gray) states. All backbone atoms are shown in cartoon representation, and the active site Arg (Arg19 in XfOhr), Glu (Glu51 in XfOhr), C_p (Cys61 in XfOhr) and C_r (Cys125 in XfOhr) residues are shown in stick representation. PDB entries: XfOhr closed (1ZB8); XfOhr open (4XX2); PaOhr closed (1N2F) and DrOhr open (1USP) states.

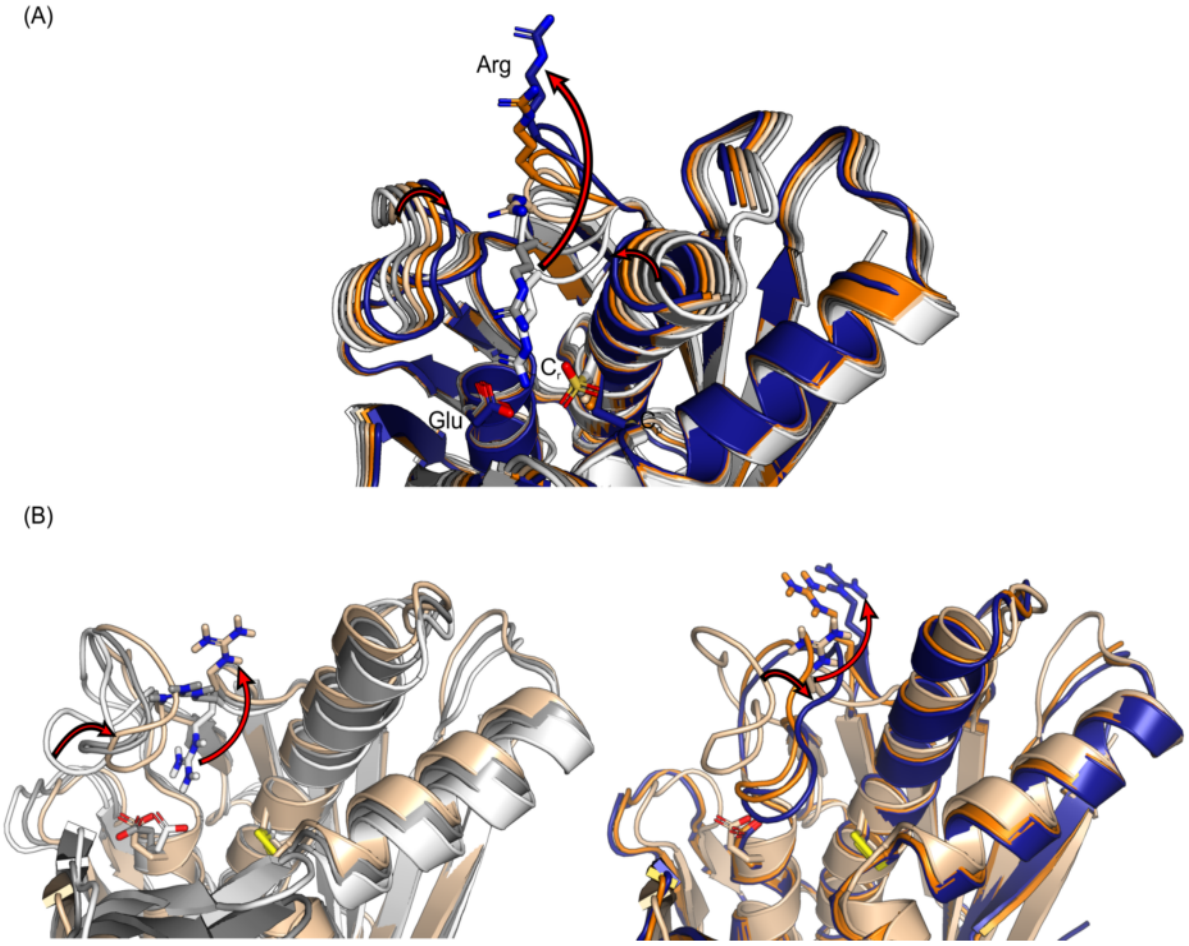

Fig 2. Morph conformations superimposed to the closed and open states of XfOhr. (A) Morph conformations generated using the two crystal structures of XfOhr in its closed (1ZB8) and open states (4XX2). The XfOhr crystal structure in its closed and open states is shown in white and blue, respectively. Gray, beige and orange structures correspond to some of the morph conformations generated by Chimera. (B) Morph conformations generated using the first, the average and the last snapshots of the XfOhr-SS trajectory. The XfOhr first and last snapshots are shown in white and blue, respectively. Gray, beige and orange structures correspond to some of the morph conformations generated by Chimera. This figure was divided in two, which represents two views in distinct orientations of the same movements. The red arrows indicate the major movements observed from the closed to the open state, namely, the Arg19 loop moves away from the active site, the Gly-loop moves into the active site and the shift of the alpha helix containing C_p.

some of the polar interactions that occurred when C_p was oxidized to Cys-SOH, subsequently forming an intramolecular disulfide bond with the C_r (**Fig 1A**).

To gain insights into the conformational changes between the open and closed states, we made a morph conformations movie using 1ZB8 (open) and 4XX2 (closed) as the reference XfOhr crystal structures (see **Fig 2A** and **S1 Video**). This morph conformations movie suggested a concerted movement involving the Arg19 and Gly-rich loops. While the Arg19 loop moved far away from the XfOhr active site, the Gly-rich loop occupied this space, which is near the active site.

3.5.2 – Molecular dynamics of XfOhr: from closed to open states

To evaluate the role of polar interactions in the structural movements of the Arg19 loop, MD simulations were performed after "*in silico*" reconstruction of the disulfide bond between its C_p and C_r in

Table 2. Average backbone RMSD (Å) and standard deviation values with respect to the corresponding starting structures calculated for each simulation.

Backbone atoms of	Simulation					
	XfOhr–S^-	XfOhr-SS	XfOhr-SH	E51A	R19A	Open-S^-
All protein	2.14 ± 0.31	3.24 ± 0.50	2.37 ± 0.43	3.07 ± 0.54	2.81 ± 0.44	3.12 ± 0.37

the XfOhr closed state structure. With this disulfide bond, no polar interactions between C_p and Arg19 can occur, and therefore, some of the constraints on the dynamics of the Arg19 loop were relieved (**S3 Fig**). As a control, the XfOhr closed state in the reduced form (Cys61 as thiolate) was also subjected to MD simulation. Both of these simulations were performed for 150 ns. These two XfOhr simulations in the oxidized and reduced forms of the closed state structure are referred to herein as XfOhr-SS and XfOhr-S^-, respectively. The XfOhr-S^- trajectory displayed an average RMSD = 2.14 ± 0.31 Å, indicating that its overall fold was stable [47] throughout the entire simulation (Table 2). In contrast, the average RMSD value for XfOhr-SS was 3.24 ± 0.50 Å, which was consistent with some conformational changes taking place. Notably, the RMSD values of the XfOhr-SS structure increased rapidly in the first 30 ns, reaching values up to 4 Å (**S4 Fig**).

Next, we calculated the per-residue Cα RMSF to measure more localized fluctuations along the simulations. For the Arg19 residue, the values were approximately 1.0 and 1.8 Å during the XfOhr-S^- and XfOhr-SS trajectories, respectively (**Fig 3A**). The higher values observed for the XfOhr-SS trajectory than those of the XfOhr-S^- trajectory indicated that the Arg19 loop underwent conformational movements in the first case (Fig 3A-C). Notably, the X-ray diffraction data (B-factors) also indicated that the Arg19 loop displayed a higher mobility in the open state than in the closed state (**Fig 3D**). Although the correlation of the intensities between the MD simulations and the X-ray data is not perfect, the overall profile of peaks and valleys displayed high correspondence (**Fig 3A, D**). The Arg19 loop was not the region that presented the highest RMSF values. Instead, the residues from positions 33 to 48 (KLSVPQGLGGPGGSGT) in both simulations displayed the highest RMSF values, which is consistent with the fact that this loop (the Gly-rich loop) is mainly composed of short side chain residues (**Fig 3A-C**). Residues 71 to 82 and 88 to 98 also displayed a higher mobility than the Arg19 loop (**Fig 3A-C**). Moreover, the high flexibility of these three regions was also experimentally observed (*c.f.*, B-factors of **Fig 3D**).

For further analysis of the dynamics of these loops along the XFOhr-SS trajectory, we made a morph conformations movie using the starting, the average and final conformation observed during this trajectory (**Figs 2B**, **2C** and **S2 Video**). From this analysis, we again observed a concerned movement

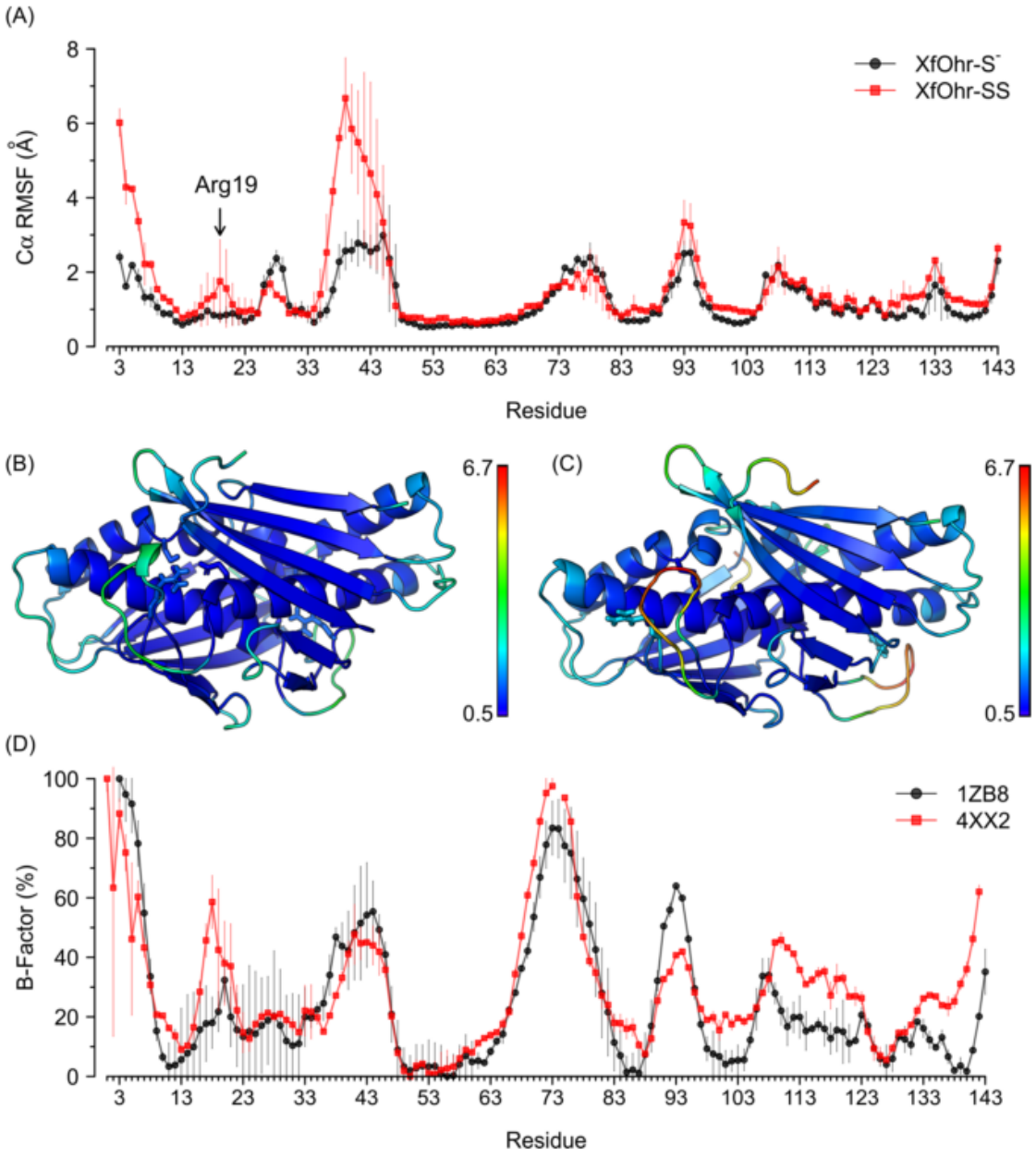

Fig 3. Localized fluctuations for XfOhr in the reduced and oxidized states. (A) Plot of Cα RMSD per-residue average values (Å) of both chains for XfOhr-S- (black) and XfOhr-SS (red) trajectories; standard deviations are shown as vertical lines. (B) XfOhr-S- representative structure. (C) XfOhr-SS representative structure. In (B) and (C), the protein backbone atoms and the Arg19, Glu51, Cys61 and Cys125 residue side chains are shown in cartoon and in stick representations, respectively. All protein atoms are colored by their corresponding Cα RMSF values, ranging from 0.5 Å (blue) to 6.7 Å (red), as indicated by the right side bars. The snapshot closest to the average structure of each simulation was used as its representative structure. (D) Plot of normalized per-residue B-factors for the 1ZB8 (black) and 4XX2 (red) structures. Per-residue B-factors were calculated by averaging all Cα atom B-factors for both structures, separately. These total averages were normalized, where 0 and 100 % correspond to the smallest and the largest averages, respectively. The vertical lines depict the corresponding standard deviations. The Cα atom B-factors for 1ZB8 and 4XX2 were determined using two monomers of each homodimer.

between Arg19 and the Gly-rich loops. According to the previous results (**Fig 3**), the Gly-rich loop movement was more pronounced than the Arg19 loop movement.

Due to its importance for catalysis, the movement of the Arg19 loop was further analyzed by measuring the distances of the Arg19-Cα atom to the C_p-Cα and Glu51-Cα atoms throughout the simulations (**Fig 4**). For comparison, the average distance of Arg19-Cα to Glu51-Cα was 10 Å in the closed-state crystal structure and 18 Å in the open-state crystal structure. Likewise, the average distance

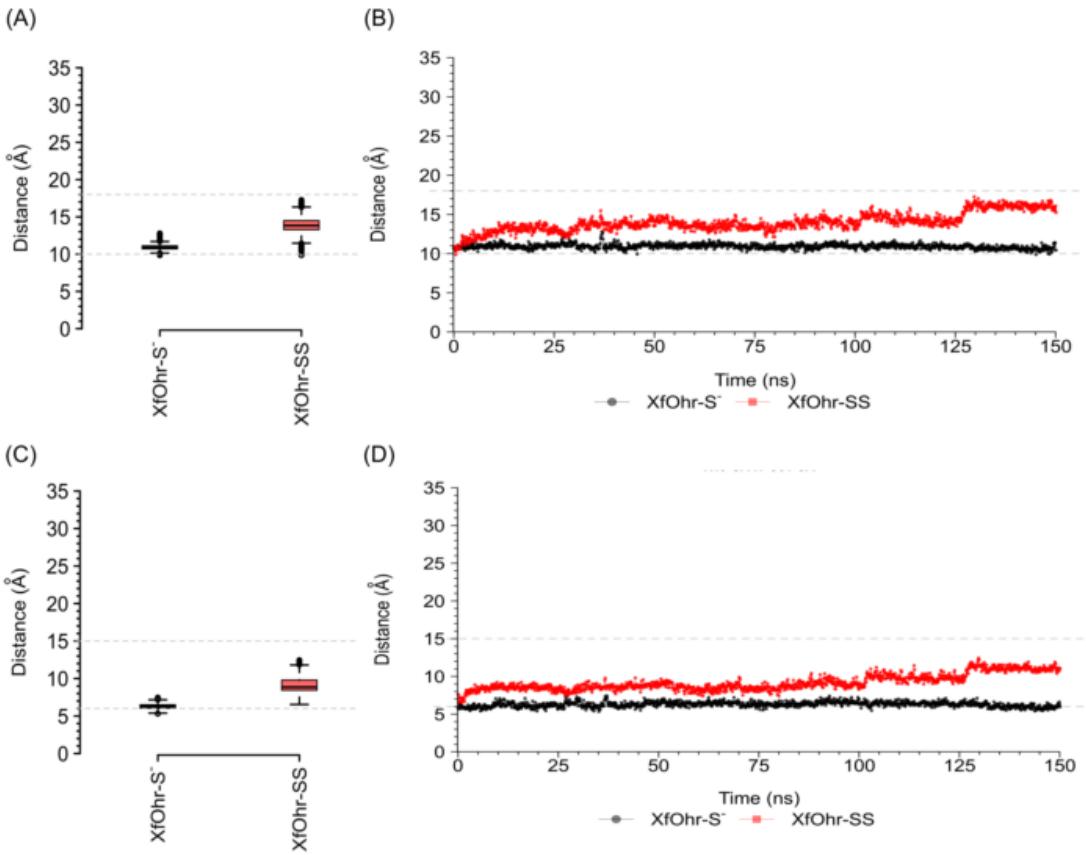

Fig 4. Distance values between Arg19-Cα and Glu51-Cα atoms (A and B) and between Arg19-Cα and Cp-Cα atoms (C and D) for the XfOhr-S- (black) and XfOhr-SS (red) trajectories (150 ns each). Distance value distributions are shown as Tukey box-plots for Arg19 - Glu51 (A) and Arg19 - Cp (C) distances. In the Tukey box-plots (A and C), boxes indicate the interquartile distances, black lines show the median values, whiskers extend the box to 1.5 times the interquartile distance and circles represent outliers (values higher/lower than the whiskers). The box size shows the spread of the distance values, i.e., small boxes indicate less spread in the distance values. XfOhr-S- (black) Arg19 - Glu51 and Arg19 - Cp median distance values are equal to 11 and 6 Å, respectively. XfOhr-SS (red) Arg19 - Glu51 and Arg19 - Cp median distance values are equal to 14 and 9 Å, respectively. The distance values are also shown as a function of simulation time for Arg19 - Glu51 (B) and Arg19 - Cp (D) distances. The average distance values between Arg19 - Glu51 and Arg19 - Cp Cα atoms obtained for the closed state (PDB entry = 1ZB8) and the open state (PDB entry = 4XX2) are shown as gray dashed lines at 10/6 and 18/15 Å, respectively.

between Arg19-Cα and C_p-Cα was 6 Å and 15 Å in the crystals structures in the closed and open states, respectively. The XfOhr-S^- trajectory appears to be more stable in a conformation more similar to the closed-state crystal structure of XfOhr, whereas the XfOhr-SS trajectory displayed more freedom with intermediate distances between the two crystal structures (**Fig 4**). These findings further suggested that the Arg19 loop was less constrained in the XfOhr-SS state, being able to move away from the active site. In contrast, the Arg19 loop kept its position close to C_p throughout the entire XfOhr-S^- simulation.

The polar interactions among C_p - Arg19 - Glu51 residues were further investigated by analyzing the distances involving atoms of the side chains (**Fig 5A**, **B**). As expected, the Arg19 - Glu51 and Arg19 - Cys61 salt-bridge interactions were stable in the XfOhr-S^- trajectory (median values <4 Å for nearly all N – O/S pairs, *c.f.*, Material and Methods). Likewise, the Arg19 - Glu51 and Arg19 - Cys61 hydrogen bond (Hbond) interactions were observed throughout the XfOhr-S^- trajectory, with occupancy values equal to 65 and 37 %, respectively (**Fig 5C**). In contrast, these interactions were

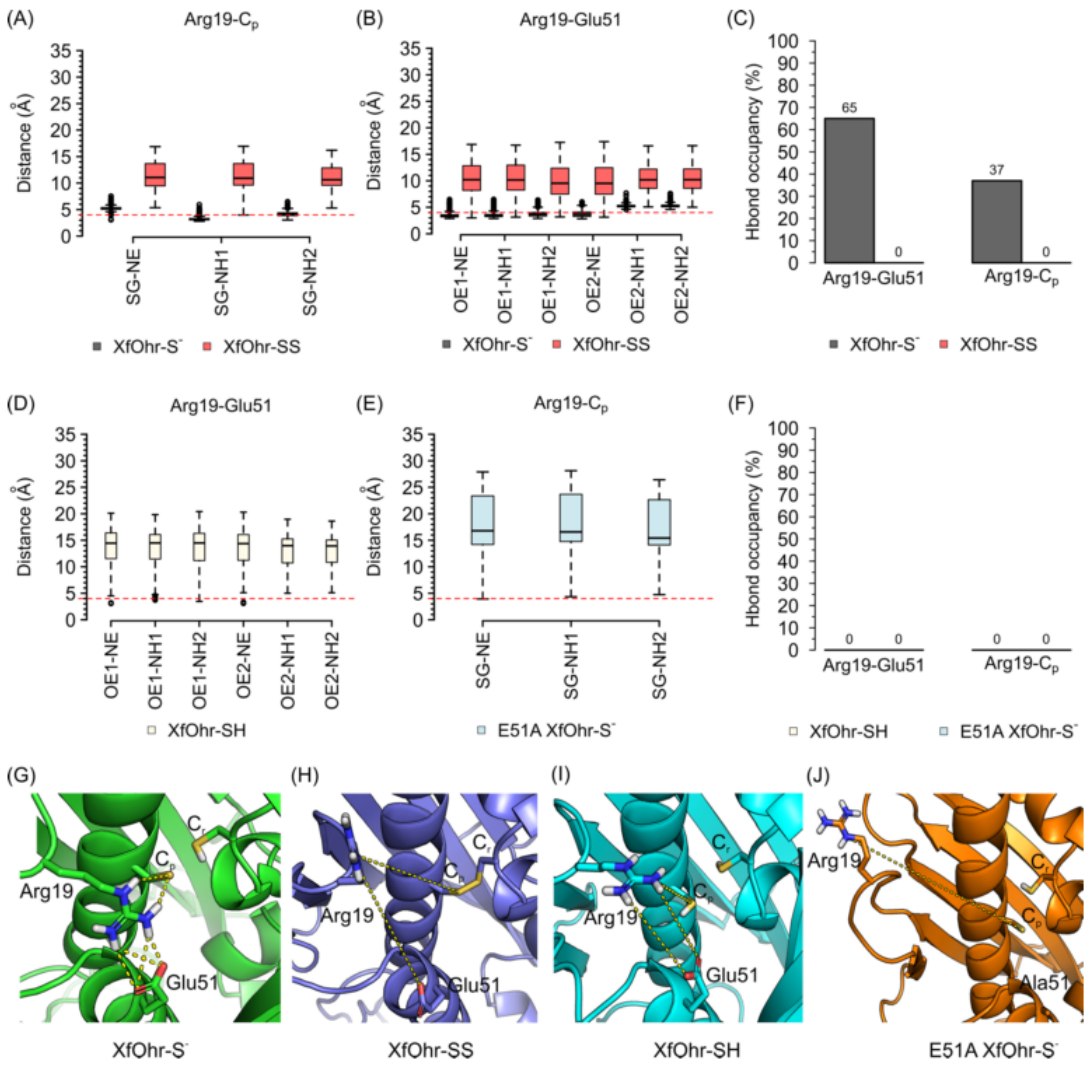

Fig 5. Salt-bridge and Hbond interactions of Arg19 with Cp and with Glu51 during XfOhr-S- (black), XfOhr-SS (red), XfOhr-SH (beige) and E51A XfOhr-S- (light blue) simulations. Distance value distributions are shown as a Tukey box-plots (A,B,D,E), in which boxes indicate the interquartile distances, black lines show the median values, whiskers extend the box to 1.5 times the interquartile distance and circles represent outliers (values higher/lower than the whiskers). The box size shows the sp**Fig 7.** Representative structures of XfOhr-SH, XfOhr mutants from MD simulations.nce values. The red dashed lines show the 4 Å cutoff value used as the criterion to define stable salt-bridge interactions [45]. The occupancy values for the Hbond interactions throughout the simulations are presented as bar plots (C,F). (A) Distances between the gamma sulfur atom (SG) of Cp and the nitrogen (NE, NH1, NH2) atoms of the Arg19 guanidinium group for XfOhr-S- (black) and XfOhr-SS (red) simulations. (B) Distances between the oxygen atoms of Glu51 (OE1, OE2) and nitrogen (NE, NH1, NH2) atoms of the Arg19 guanidinium group for Xf.

unstable or even absent during the XfOhr-SS trajectory (median values > 4 Å for all N – O/S pairs and hydrogen bond occupancy values = 0 %, **Fig 5C**). Indeed, the corresponding median values of the Arg19 - Glu51 and Arg19 - Cys61 distances for XfOhr-SS trajectories were high, reaching values of approximately 10 Å (**Fig 5A, B**).

The snapshot closest to the average structure throughout each MD simulation was used to represent the entire XfOhr-SS and XfOhr-S⁻ trajectories (**Fig 6**). No significant difference in the overall structure was observed between the two average structures (**Fig 6A**, with RMSD = 1.93 Å). Despite these similarities, their Arg19 loops adopted two different conformations. In the XfOhr-S⁻ representative structure, the Arg19 loop adopted a closed orientation in both chains, which were very

similar to the closed crystal structure (**Fig 6B** and **S3 Video**). Furthermore, Arg19 kept stable hydrogen bond and salt-bridge interactions with Glu51 and C_p (both identified as stable during the entire XfOhr-S^- simulation). In contrast, the Arg19 loop of the XfOhr-SS representative structure underwent a conformational change, moving away from the active site, which was similar to the conformation observed in the open crystal structure (**Fig 6C** and **S4 Video**). Both chains adopted this open state; however, their Arg19 loop orientations were somewhat different (**S5 Fig**). Another difference observed between the XfOhr-SS and XfOhr-S^- representative structures is the Glu51 side chain orientation. In the XfOhr-S^- representative structure, the Glu51 side chain is oriented toward the guanidinium group of Arg19, establishing polar contacts (**Fig 6B**). On the other hand, in the XfOhr-SS representative structure, the Glu51 side chain is oriented toward the Gly-rich loop (**Fig 7C**). From a visual inspection of the Glu51 side chain movement along the XfOhr-SS trajectory, we observed that Glu51 initially formed polar contacts with Arg19. However, as Arg19 moved away from the XfOhr active site, the Arg19 - Glu51 interactions were lost. As a result, the Glu51 side chain was less constrained, being able to establish hydrogen bond interactions with other residues, in particular with those of the Gly-rich loop. Probably, these changes observed in the Glu51 conformations are part of the concerted movement between the Arg19 and Gly-rich loop described previously (**S2** and **S4 Videos**).

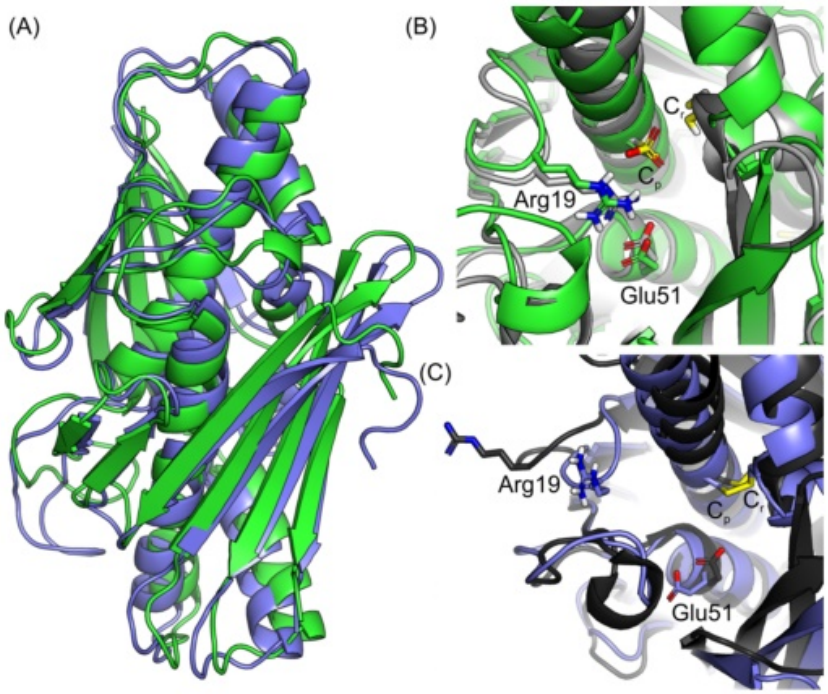

Fig 6. XfOhr-S- and XfOhr-SS representative structures from MD simulations. (A) Comparison between the overall representative structures of XfOhr-S- (green) and XfOhr-SS (blue marine). (B) Active site of the XfOhr-S- representative structure (green) superposed to the XfOhr crystal structure (light gray) in its closed state (PDB entry 1ZB8). (C) Active site of the XfOhr-SS representative structure (blue marine) superimposed to the XfOhr crystal structure (dark gray) in its oxidized form and open state (PDB entry 4XX2, described in this paper). Each representative structure corresponds to the MD simulation snapshot closest to the average structure calculated throughout the entire trajectory (150 ns). The protein backbone atoms are shown in cartoon representation, and the side chains atoms of Arg19, Glu51, Cp and Cr are shown in the stick representation.

Next, we investigated whether the polar interactions between the Arg19 and C_p residues could restrict the movement of the corresponding loop. Therefore, another MD simulation (50 ns) was performed, again with XfOhr in the closed state, but now having both thiols artificially protonated. This simulation is referred to herein as XfOhr-SH. Since the Arg19 loop movement started immediately after the initial 30 ns in the XfOhr-SS trajectory (**S4 Fig**), we assumed that 50 ns of simulation would be

enough to observe similar movement in the XfOhr-SH trajectory. Indeed, the Arg19 loop of both chains moved away from the active site, leaving the Arg19 side chain highly exposed to the solvent (**Figs 5D**, **5F**, **5I** and **7** and **S5 Video**). Furthermore, the Arg19 – Glu51 salt-bridges and hydrogen bond interactions were unstable during the XfOhr-SH trajectory (**Figs 5D** and **5F**, respectively). Moreover, the distances between Arg19-Cα and Glu51-Cα were comparable with those observed for the XfOhr-SS simulation, with values up to 19 Å (**S6 Fig**). These findings further support the notion that the salt-bridge interaction between Arg19 and the negatively charged C_p (Cys61-S^-) plays a relevant role in stabilizing the Arg19 loop near the active site. Thus, our simulations indicated that the Arg19 loop movement is constrained by polar interactions between C_p-S^- and Arg19. Considering the overall XfOhr-SH simulation, the average RMSD values were in between those observed for the XfOhr-S^- and XfOhr -SS trajectories (**Table 2**).

Subsequently, we addressed whether Glu51 could also contribute to the stabilization of the

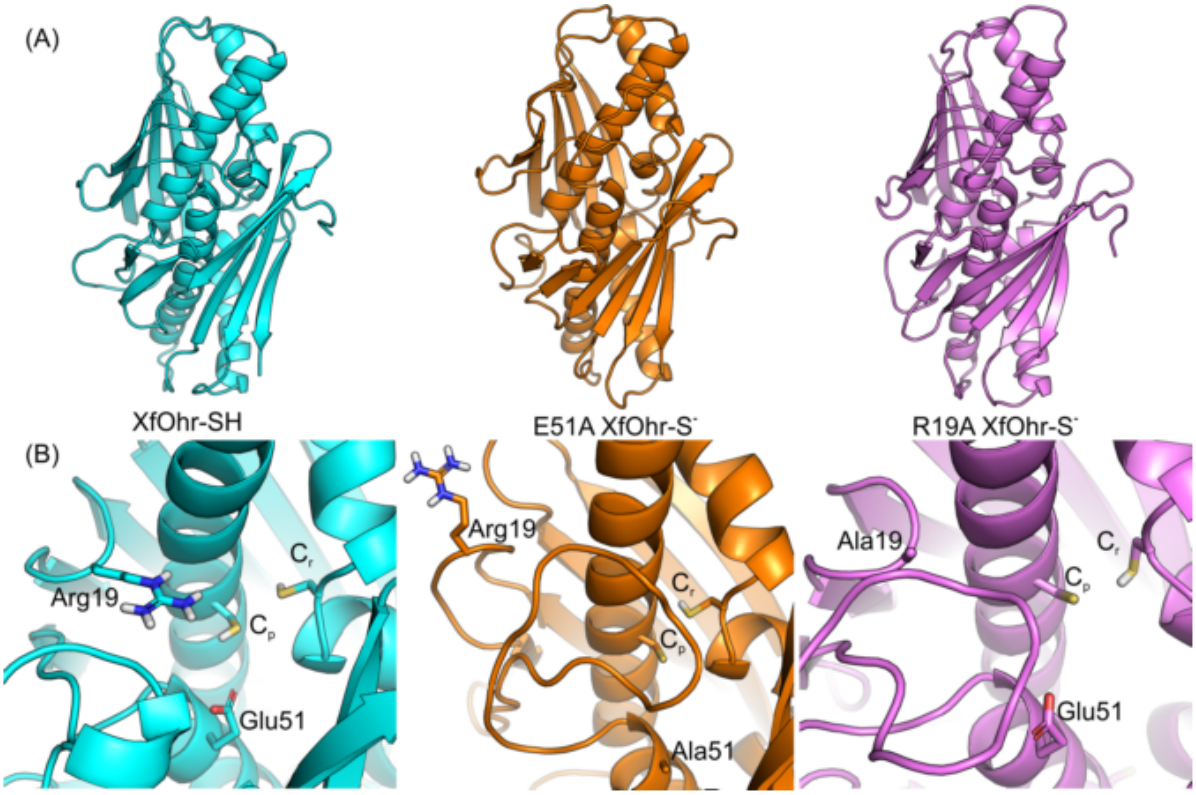

Fig 7. Representative structures of XfOhr-SH, XfOhr mutants from MD simulations. (A) Overall representative structure of the XfOhr-SH (cyan), E51A-XfOhr (orange) and R19A-XfOhr (purple) simulations. (B) Active sites of representative structure of the XfOhr-SH (cyan), E51A-XfOhr (orange) and R19A-XfOhr (purple) simulations. Each representative structure corresponds to the MD simulation snapshot closest to the average structure calculated for its trajectory (50 ns). The protein backbone atoms are show in cartoon representation and Arg19/Ala19, Glu51/A1a51, Cp and Cr side chain atoms are shown in stick representation.

XfOhr structure in the closed state [9]. Thus, the E51A XfOhr-S^- mutant was artificially built and subjected to MD simulations (50 ns). Again, the Arg19 loop moved away from the active site (**Figs 5E, 5F, 5J, 7** and **S6 Video**). In this case, the movement occurred in an even shorter interval than those observed for the XfOhr-SS and XfOhr-SH trajectories. The highest Arg19-Cα to Ala51-Cα distance observed during the E51A XfOhr-S^- trajectory was 27 Å (**S7 Fig**). Furthermore, the Arg19 – C_p salt-

bridge and hydrogen bond interactions were also unstable during this trajectory (**Figs 5E, F**). Therefore, Glu51 is also crucial for stabilizing the Arg19 loop close to the active site, in this case independently of the C_p oxidative state.

Finally, we artificially built a R19A substitution in the XfOhr-S^- structure in the closed state. According to our hypothesis, the mutated "Ala19" loop would move away from the active site. The median distance values for Ala19-Cα - Glu51-Cα and Ala19- Cα - C_p- Cα distance values were equal to 16 and 12 Å, respectively (**S8 Fig** and **S7 Video**). Interestingly, these values were slightly shorter than those obtained for the E51A XfOhr-S^- mutant. The more restricted behavior of the R19A mutant could be related to the aliphatic side chain that confers hydrophobic properties to the Ala residue. As a consequence, polar interactions between the Ala19 side chain and solvent water molecules are not favorable, destabilizing the open-state conformation (**S9 Fig**).

2.5.3 – Molecular dynamics of XfOhr: from the open to closed states

Since our MD simulations indicated that upon C_p oxidation, XfOhr could move from the closed to the open state, we decided to verify whether the opposite process could occur, *i.e.*, if the reduction of the Cys61-Cys125 bond would lead to the reverse movement (from the open to the closed state). In this case, the XfOhr open state was used as a starting point for MD simulation (150 ns), being named the Open XfOhr-S^- trajectory. Thus, the disulfide bond was artificially reduced, considering C_p (Cys61) and C_r (Cys125) as a thiolate (RS^-) and a thiol (RSH), respectively.

Unexpectedly, the Arg19 loop did not undergo major movements but remained in its open state throughout the entire trajectory (**S8 Video**). Indeed, the observed distances of the Open XfOhr-S^- structure were similar to those measured in the XfOhr open-state crystal structure (**S10 Fig**). One hypothesis for this is that the crystal packing contacts in the crystal structure of the XfOhr open state (4XX2) artificially kept the Arg19 loop orientation more exposed to the solvent than in its native condition. Therefore, the starting structure used for the Open XfOhr-S^- trajectory would have the Arg19 loop orientation more distant from the active site than the biological one, preventing the closure of the Arg19 loop. Alternatively, entropic factors related to the dehydration of the Arg19 loop may have also prevented XfOhr from assuming the closed state. Indeed, the Ohr active site is surrounded by hydrophobic residues [11]. Furthermore, the Gly-rich loop (comprising residues 33 – 48) might have impaired the closure of the Arg19 loop. Our MD simulations are consistent with this possibility, as the Gly-rich loop appears to prevent the movement of the Arg19 loop back to the active site by steric hindrance effects (**S8 Video**), at least during the simulation time employed (150 ns). Further studies are required to understand the possible roles of the Gly-rich loop in catalysis.

2.5.4 – Biochemical Analysis of XfOhr mutants (R19A and E51A)

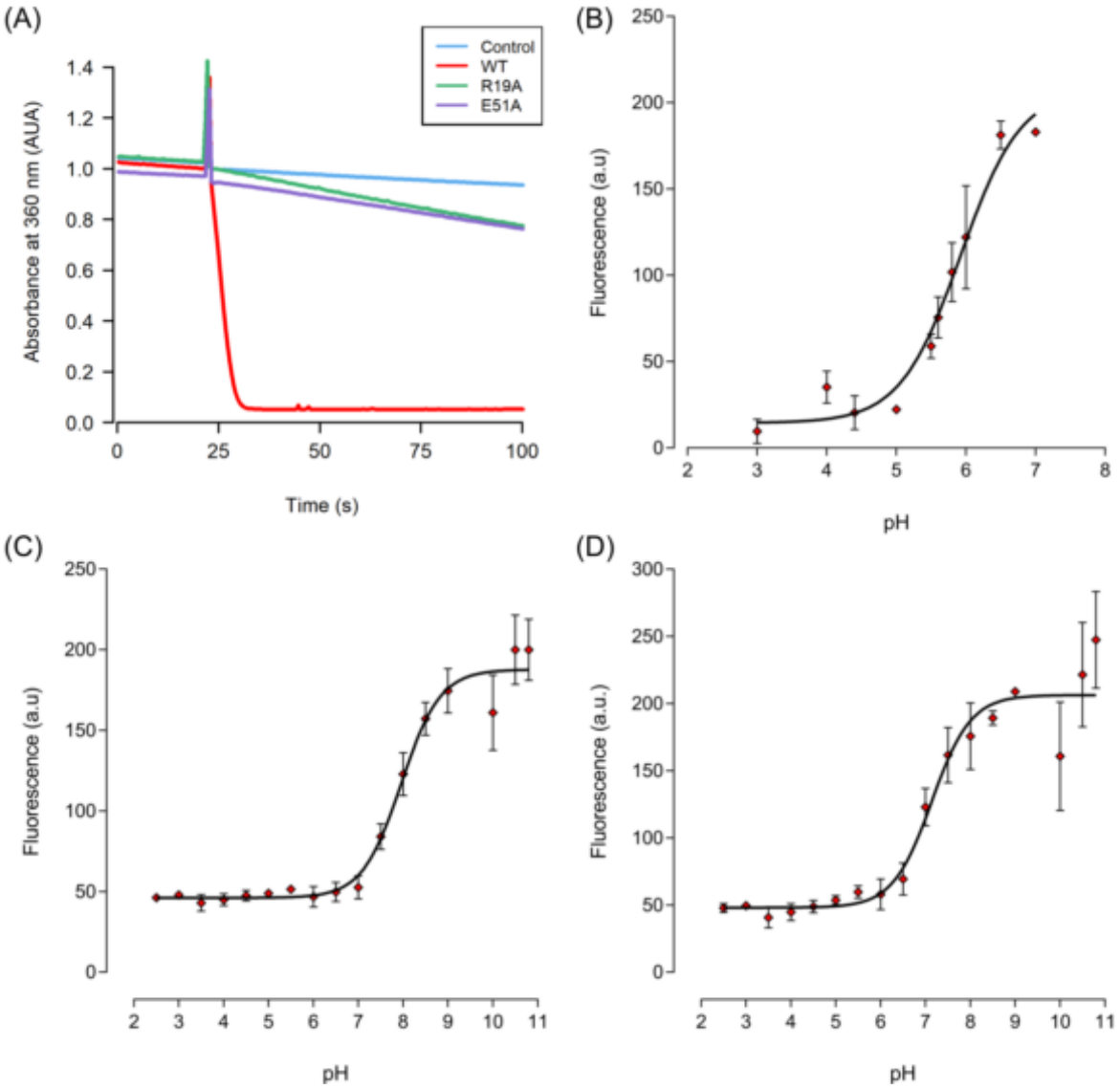

Fig 8. Comparative analyses of wild-type XfOhr and two mutants (R19A and E51A). (A) Lipoamide-lipoamide dehydrogenase peroxidase-coupled assay of wild-type XfOhr, R19A and E51A. The peroxidase activities were monitored by the oxidation of NADH at 340 nm in the presence of XfOhr (0.05 μM), lipoamide dehydrogenase from X. fastidiosa (XfLpD, 0.5 μM), and lipoamide (50 μM) in sodium phosphate buffer (20 mM, pH 7.4) and DTPA (0.1 mM). Cys61 (Cp) pKa determination of wild-type XfOhr and two mutants (R19A and E51A) by the monobromobimane method; plots of fluorescence as a function of pH for wild-type XfOhr (B), R19A XfOhr (C) and E51A XfOhr (D). The red points show the mean values of at least two independent experiments. The error bars indicate the SEM. All pKa values were determined using the Henderson-Hasselbach equation of GraphPad®Prism4.

It is well accepted that the presence of Arg and Glu in the active site of Ohr in close proximity to C_p are important factors for the high reactivity of this peroxidase toward hydroperoxides [1,6,11]. Furthermore, our MD simulation data presented here indicate that Glu51 and C_p are required to stabilize the Arg19 loop in the closed state. Therefore, two mutations (R19A and E51A) were generated by site-directed mutagenesis into the XfOhr recombinant protein to experimentally validate these *in silico* findings. As expected, compared with the wild-type protein, XfOhr R19A and XfOhr E51A presented only residual dihydrolipoamide-dependent peroxidase activity (**Fig 8A**). Moreover, these mutations

resulted in significant changes in the pK_a of the catalytic Cys thiolate 8.09 (± 0.11) for R19A and 7.20 (± 0.11) for E51A) compared that observed in the wild-type protein (5.92 ± 0.11; **Fig 8B** to **8D**). Previously, we also observed that wild-type XfOhr displays an acidic pK_a [48]. Here, we show for the first time that mutation of the catalytic Glu impairs the enzymatic activity of Ohr. Previously, the relevance of the catalytic Arg was analyzed by mutation in PaOhr [6]. Therefore, these results are consistent with the proposed roles of Arg19 and Glu51 in catalysis, as well as with our MD simulations. Indeed, the thiolate pK_a values for the R19A and E51A mutants are more similar to that of free cysteine [46] than the pK_a values corresponding to the wild-type protein. Circular dichroism spectra of the wild-type and mutant proteins in the reduced and oxidized states were very similar, excluding the hypothesis that the R19A and E51A mutations might provoke major problems to the overall structure of XfOhr (**S11 Fig**).

3.6 – Discussion

A working hypothesis for the catalytic mechanism of Ohr enzymes is presented in **Fig 9**. Most likely, the catalytic cycle of Ohr enzymes is more complex, and additional steps occur between the closed (**Fig 9**, **i**) and open (**Fig 9**, **iv**) states.

There are six crystal structures of Ohr enzymes deposited in the RSCB Protein Data Bank, and all of them are either in the open or in the closed state that corresponds either to snapshot (i) or (iv) in **Fig 9**, respectively. The closed state appears to be an optimal conformation for hydroperoxide reduction,

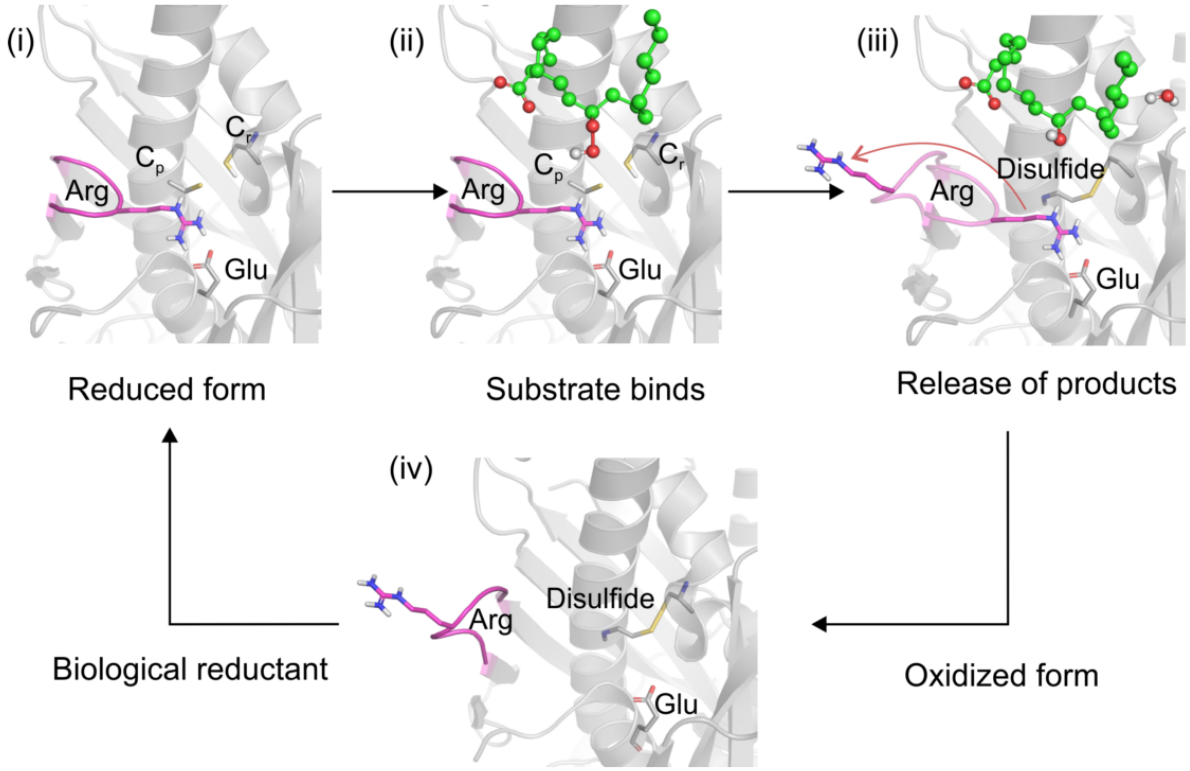

Fig 9. Proposed model for fatty acid hydroperoxide reduction by Ohr. (i) In the reduced form of Ohr (Cp-S-, Cys61 of XfOhr), the thiolate anion (Sγ of Cp) makes an Hbond with the guanidinium group of the conserved Arg (Arg19 of XfOhr), which also makes a salt-bridge with the conserved Glu (Glu51 of XfOhr). (ii) The lipid hydroperoxide (LHP) is placed over the hydrophobic moiety of the Arg side chain, being also stabilized by other hydrophobic interactions. (iii) After peroxide reduction, Cp is oxidized to sulfenic acid (SOH), which is then attacked by the sulfhydryl group of the resolving Cys (Cys125 of XfOhr), forming an intra-molecular disulfide. Our working hypothesis is that this condensation reaction releases constraints for Arg19 loop movements. (iv) The last step involves the reduction of the disulfide by a lipoylated protein and a rearrangement of the loop to the close state (taken from [11]). Steps (ii) and (iii) are hypothetical, as substrate and product (respectively) were inserted based on the co-crystallization of PEG with XfOhr [11].

as the catalytic Arg (Arg19 in XfOhr) is near to C_p, which probably results in increased C_p nucleophilicity and ROOH electrophilicity. Indeed, in peroxiredoxins (another type of Cys-based peroxidase), a catalytic Arg plays a similar role [50]. In the open state, the entrance of the active site is wider [10], which might better accommodate lipoylated proteins that are the reducing agent of XfOhr [15]. Prior to this work, no information on intermediate states was available.

Initially, the opening of the Arg19 loop was investigated by MD simulations. The overall fold was stable throughout the XfOhr-SS simulation, but the Arg19 loop underwent an opening movement,

among other conformational changes. In contrast, the Arg19 loop was stabilized in the closed form when C_p was reduced and unprotonated (**Figs 4-6** and **S3 video**), which is consistent with a pK_a for the thiolate group of C_p equivalent to 5.92 (**Fig 9 B**). In contrast, when the thiol group of C_p was oxidized or protonated (Figs 4-8 and **S6 Fig**), Arg19 displayed greater freedom, moving away from the active site (**Figs 6** and **7**, and **S4** and **S5 Videos**). Therefore, according to our hypothesis, the stability of the Arg19 loop depends on the oxidative state of C_p.

However, other factors also contribute to the stability of the Arg19 loop in the closed state, and a major one is the polar interaction of Arg19 with Glu51. Indeed, the mutation of Glu51 to Ala resulted in increased mobility of the Arg19 loop (**Figs 5** and **7**; **S7 Fig** and **S6 Video**), even when C_p was in the thiolate form. Therefore, the disruption of either the Arg19 - C_p or the Arg19 - Glu51 polar interaction facilitated the opening of the Arg19 loop.

We also performed MD simulations starting from the structure with the Arg19 loop in the open form in an attempt to investigate the closing of this loop. Contrary to our expectations, the Arg19 loop did not return to the closed state in any of the conditions and intervals analyzed (**S10** and **S8 video**). Possibly, the removal of water molecules solvated to the Arg19 loop is required prior to the approximation of this region toward C_p. One hypothesis is that the reducing agent (lipoylated proteins) might assist the closing process of the Arg19 loop. Another possibility is that this movement would require much longer simulation time (>150 ns) or would be better observed using a different *in silico* technique, such as Normal Mode analysis [51]. Investigations in these directions are underway.

This is the first report that describes a biochemical feature associated with the Gly-rich loop (comprising residues from position 35 to 48) that was part of the XfOhr, which exhibited the greatest flexibility (**Fig 3A**). Hydrophobicity is another feature of the Gly-rich loop that is highly conserved among Ohr family members [7,12,14]. Remarkably, some of these residues interact with polyethylene glycol by hydrophobic interactions [11]. Indeed, docking studies [1] have indicated that the hydrophobic interactions are major factors for lipid hydroperoxide binding within the XfOhr active site. Interestingly, the position of the catalytic Arg considerably differs between Ohr and OsmC proteins that comprise two of the major sub-families in the Ohr/OsmC superfamily [14]. The catalytic Arg is in the Gly-rich loop in OsmC proteins. Therefore, our studies open new perspectives in the understanding of enzyme-substrate interactions in proteins belonging to the Ohr/OsmC superfamily, which may foster investigations aiming to identify inhibitors of these enzymes.

Furthermore, this study contributes information to help distinguish Ohr from other Cys-based peroxidases, such as Prx. Indeed, we have previously reported that Ohr and Prx display distinct biochemical and structural properties [1]. For instance, Ohr and Prx are not homologous proteins, as they do not share amino acid sequence or structural similarities [7,12,52]. For most Prx enzymes, the reductant is Trx, whereas for Ohr, the reductants are probably lipoylated proteins [10]. In this report, we present other features that distinguish Ohr from Prx enzymes. For instance, it is well known that Prx enzymes switch back and forth between the so-called fully folded and locally unfolded states when

catalytic Cys residues undergo large movements to allow disulfide formation, as these two residues are far apart in the reduced state [53]. In contrast, the catalytic Arg remains relatively static throughout the catalytic cycle of Prx. In the case of XfOhr, the two catalytic Cys residues remain relatively static throughout the catalytic cycle, whereas the catalytic Arg19 undergoes movement between the closed and open states. Therefore, distinct mechanisms were selected throughout evolution that allowed for the development of two different systems, operating with extraordinary efficiency in hydroperoxide reduction and attaining rates in the 10^7-10^8 M^{-1} s^{-1} range [1,53,54].

Finally, it is important to emphasize that the high correspondence between the crystallographic and simulation data and the biochemical characterizations indicate the robustness of our analysis. Understanding catalytic cycle dynamics might be relevant for the development of Ohr inhibitors. Since Ohr enzymes are present in pathogenic bacteria and fungi [7] but are absent in their hosts, such as plants and animals, these enzymes might be promising targets for drug design.

Accession codes

The crystal structure in this paper has been deposited in the Protein Data Bank as 4XX2.

Acknowledgements

We would like to thank the Fundação de Amparo à Pesquisa no Estado de São Paulo (FAPESP), Brazil, and Conselho Nacional de Desenvolvimento Científico e Tecnológico (CNPq), Brazil, for the grants to support this study. A.T-do A., L.E.S.N., and M.A.O. are members of the CEPID Redoxoma (No. 2013/07937-8) and of the NAP Redoxoma (PRPUSP). T.G.P.A., K.F.D., J.R.R.C., E.P. and A.T-do.A were recipients of fellowships from FAPESP (2008/07971-3; 2009/12885-1; 2005/50056-6; 2014/01614-5 and 2012/06633-2 and 2016/12392-9).

Supplementary material

Supplementary data associated with this article can be found in the online version at doi.org/10.1371/journal.pone.0196918.

3.7 – References

1. Alegria TGP, Meireles DA, Cussiol JRR, Hugo M, Trujillo M, de Oliveira MA, et al. Ohr plays a central role in bacterial responses against fatty acid hydroperoxides and peroxynitrite. Proc Natl Acad Sci. 2017;114: E132–E141. doi:10.1073/pnas.1619659114
2. Tobin DM, Ramakrishnan L. TB: the Yin and Yang of lipid mediators. Curr Opin Pharmacol. 2013;13: 641–645. doi:10.1016/j.coph.2013.06.007
3. Serhan CN, Chiang N. Resolution phase lipid mediators of inflammation: agonists of resolution. Curr Opin Pharmacol. 2013;13: 632–640. doi:10.1016/j.coph.2013.05.012
4. Prost I. Evaluation of the Antimicrobial Activities of Plant Oxylipins Supports Their Involvement in Defense against Pathogens. PLANT Physiol. 2005;139: 1902–1913. doi:10.1104/pp.105.066274
5. Cussiol JRR, Alves SV, De Oliveira MA, Netto LES. Organic hydroperoxide resistance gene encodes a thiol-dependent peroxidase. J Biol Chem. 2003;278: 11570–11578. doi:10.1074/jbc.M300252200
6. Lesniak J, Barton W a, Nikolov DB. Structural and functional characterization of the Pseudomonas hydroperoxide resistance protein Ohr. EMBO J. 2002;21: 6649–6659. doi:10.1093/emboj/cdf670
7. Meireles DA, Domingos RM, Gaiarsa JW, Ragnoni EG, Bannitz-Fernandes R, da Silva Neto JF, et al. Functional and evolutionary characterization of Ohr proteins in eukaryotes reveals many active homologs among pathogenic fungi. Redox Biol. Elsevier B.V.; 2017;12: 600–609. doi:10.1016/j.redox.2017.03.026
8. Baldi P, La Porta N. Xylella fastidiosa: Host Range and Advance in Molecular Identification Techniques. Front Plant Sci. 2017;8. doi:10.3389/fpls.2017.00944
9. Mongkolsuk S, Praituan W, Loprasert S, Fuangthong M, Chamnongpol S. Identification and characterization of a new organic hydroperoxide resistance (ohr) gene with a novel pattern of oxidative stress regulation from Xanthomonas campestris pv. phaseoli. J Bacteriol. 1998;180: 2636–2643.
10. Cussiol JRR, Alegria TGP, Szweda LI, Netto LES. Ohr (organic hydroperoxide resistance protein) possesses a previously undescribed activity, lipoyl-dependent peroxidase. J Biol Chem. 2010;285: 21943–21950. doi:10.1074/jbc.M110.117283
11. Oliveira MA, Guimarães BG, Cussiol JRR, Medrano FJ, Gozzo FC, Netto LES. Structural Insights into Enzyme–Substrate Interaction and Characterization of Enzymatic Intermediates of Organic Hydroperoxide Resistance Protein from Xylella fastidiosa. J Mol Biol. 2006;359: 433–445. doi:10.1016/j.jmb.2006.03.054
12. Atichartpongkul S, Loprasert S, Vattanaviboon P, Whangsuk W, Helmann JD, Mongkolsuk S. Bacterial Ohr and OsmC paralogues define two protein families with distinct functions and patterns of expression. Microbiology. 2001;147: 1775–1782. doi:10.1099/00221287-147-7-1775
13. Lesniak J, Barton WA, Nikolov DB. Structural and functional features of the Escherichia coli hydroperoxide resistance protein OsmC. Protein Sci. 2003;12: 2838–43. doi:10.1110/ps.03375603
14. Shin DH, Choi IG, Busso D, Jancarik J, Yokota H, Kim R, et al. Structure of OsmC from Escherichia coli: A salt-shock-induced protein. Acta Crystallogr Sect D Biol Crystallogr. 2004;60: 903–911. doi:10.1107/S0907444904005013
15. Meunier-Jamin C, Kapp U, Leonard GA, McSweeney S. The structure of the organic hydroperoxide resistance protein from Deinococcus radiodurans: Do conformational changes facilitate recycling of the redox disulfide. J Biol Chem. 2004;279: 25830–25837. doi:10.1074/jbc.M312983200
16. Flohé L. The impact of thiol peroxidases on redox regulation. Free Radic Res. 2016;50: 126–142. doi:10.3109/10715762.2015.1046858
17. Leslie AGW. Joint CCP4 EESF-EACMB Newsletter on Protein Crystallography. Daresbury Lab Warrington, UK. 1993;29.
18. Kabsch W. Evaluation of single-crystal X-ray diffraction data from a position-sensitive detector. J Appl Crystallogr. International Union of Crystallography; 1988;21: 916–924. doi:doi:10.1107/S0021889888007903
19. Blessing RH. An empirical correction for absorption anisotropy. Acta Crystallogr Sect A Found Crystallogr. 1995;51: 33–38. doi:10.1107/S0108767394005726
20. Winn MD, Ballard CC, Cowtan KD, Dodson EJ, Emsley P, Evans PR, et al. Overview of the CCP4 suite and current developments. Acta Crystallogr Sect D Biol Crystallogr. International Union of Crystallography; 2011;67: 235–242. doi:10.1107/S0907444910045749
21. Adams PD, Afonine P V., Bunkóczi G, Chen VB, Davis IW, Echols N, et al. PHENIX: A comprehensive Python-based system for macromolecular structure solution. Acta Crystallogr Sect D Biol Crystallogr. 2010;66: 213–221. doi:10.1107/S0907444909052925
22. Emsley P, Lohkamp B, Scott WG, Cowtan K. Features and development of Coot. Acta Crystallogr Sect D Biol Crystallogr. International Union of Crystallography; 2010;66: 486–501. doi:10.1107/S0907444910007493
23. Murshudov GN, Vagin AA, Dodson EJ. Refinement of macromolecular structures by the maximum-likelihood method. Acta Crystallogr Sect D Biol Crystallogr. 1997;53: 240–255.

doi:10.1107/S0907444996012255
24. Laskowski R a., MacArthur MW, Moss DS, Thornton JM. PROCHECK: a program to check the stereochemical quality of protein structures. J Appl Crystallogr. 1993;26: 283–291. doi:10.1107/S0021889892009944
25. Hooft RWW, Vriend G, Sander C, Abola EE. Errors in protein structures. Nature. 1996;381: 272–272. doi:10.1038/381272a0
26. Schrödinger L. The PyMOL Molecular Graphics System. 2013.
27. Sardi F, Manta B, Portillo-Ledesma S, Knoops B, Comini MA, Ferrer-Sueta G. Determination of acidity and nucleophilicity in thiols by reaction with monobromobimane and fluorescence detection. Anal Biochem. 2013;435: 74–82. doi:10.1016/j.ab.2012.12.017
28. Pettersen EF, Goddard TD, Huang CC, Couch GS, Greenblatt DM, Meng EC, et al. UCSF Chimera - A visualization system for exploratory research and analysis. J Comput Chem. 2004;25: 1605–1612. doi:10.1002/jcc.20084
29. SYBYL. SYBYL. 1699 South Hanley Rd., St. Louis, Missouri, 63144, USA: Tripos International; 2009.
30. Clark M, Cramer RD, Van Opdenbosch N. Validation of the general purpose tripos 5.2 force field. J Comput Chem. 1989;10: 982–1012. doi:10.1002/jcc.540100804
31. Powell MJD. Restart procedures for the conjugate gradient method. Math Program. 1977;12: 241–254. doi:10.1007/BF01593790
32. SYBYL. SYBYL-X. 1699 South Hanley Rd., St. Louis, Missouri, 63144, USA: Tripos, a Certara Companie; 2013.
33. Pronk S, Páll S, Schulz R, Larsson P, Bjelkmar P, Apostolov R, et al. GROMACS 4.5: A high-throughput and highly parallel open source molecular simulation toolkit. Bioinformatics. 2013;29: 845–854. doi:10.1093/bioinformatics/btt055
34. Berendsen HJC, van der Spoel D, van Drunen R. GROMACS: A message-passing parallel molecular dynamics implementation. Comput Phys Commun. 1995;91: 43–56. doi:10.1016/0010-4655(95)00042-E
35. Schmid N, Eichenberger AP, Choutko A, Riniker S, Winger M, Mark AE, et al. Definition and testing of the GROMOS force-field versions 54A7 and 54B7. Eur Biophys J. 2011;40: 843–856. doi:10.1007/s00249-011-0700-9
36. Berendsen HJC, Postma JPM, van Gunsteren WF, Hermans J. Interaction Models for Water in Relation to Protein Hydration. In: Pullman B, editor. Intermolecular Forces. Dordrecht: Springer Netherlands; 1981. pp. 331–342. doi:10.1007/978-94-015-7658-1_21
37. Hess B, Bekker H, Berendsen HJC, Fraaije JGEM. LINCS: A linear constraint solver for molecular simulations. J Comput Chem. 1997;18: 1463–1472. doi:10.1002/(SICI)1096-987X(199709)18:12<1463:AID-JCC4>3.0.CO;2-H
38. Essmann U, Perera L, Berkowitz ML, Darden T, Lee H, Pedersen LG. A smooth particle mesh Ewald method. J Chem Phys. 1995;103: 8577–8593. doi:10.1063/1.470117
39. Lange OF, Van Der Spoel D, De Groot BL. Scrutinizing molecular mechanics force fields on the submicrosecond timescale with NMR Data. Biophys J. Biophysical Society; 2010;99: 647–655. doi:10.1016/j.bpj.2010.04.062
40. Bussi G, Donadio D, Parrinello M. Canonical sampling through velocity rescaling. J Chem Phys. 2007;126: 14101. doi:10.1063/1.2408420
41. Berendsen HJC, Postma JPM, van Gunsteren WF, DiNola a, Haak JR. Molecular dynamics with coupling to an external bath. J Chem Phys. 1984;81: 3684–3690. doi:10.1063/1.448118
42. Humphrey W, Dalke A, Schulten K. VMD: Visual molecular dynamics. J Mol Graph. 1996;14: 33–38. doi:10.1016/0263-7855(96)00018-5
43. Piccirillo E, Merget B, Sotriffer CA, Do Amaral AT. Conformational flexibility of DENV NS2B/NS3pro: From the inhibitor effect to the serotype influence. J Comput Aided Mol Des. Springer International Publishing; 2016;30: 251–270. doi:10.1007/s10822-016-9901-8
44. R Core Team. R: A Language and Environment for Statistical Computing [Internet]. Vienna, Austria; 2015. Available: https://www.r-project.org/
45. Barlow DJ, Thornton JM. Ion-pairs in proteins. J Mol Biol. 1983;168: 867–885. doi:10.1016/S0022-2836(83)80079-5
46. Weichsel A, Gasdaska JR, Powis G, Montfort WR. Crystal structures of reduced, oxidized, and mutated human thioredoxins: evidence for a regulatory homodimer. Structure. 1996;4: 735–751. doi:10.1016/S0969-2126(96)00079-2
47. Sippel M, Sotriffer CA. Molecular dynamics simulations of the HIV-1 integrase dimerization interface: Guidelines for the design of a novel class of integrase inhibitors. J Chem Inf Model. 2010;50: 604–614. doi:10.1021/ci900403s
48. Meireles D de A, Alegria TGP, Alves SV, Arantes CRR, Netto LES. A 14.7 kDa Protein from Francisella tularensis subsp. novicida (Named FTN_1133), Involved in the Response to Oxidative Stress Induced by Organic Peroxides, Is Not Endowed with Thiol-Dependent Peroxidase Activity. Abu Kwaik Y, editor. PLoS One. 2014;9: e99492. doi:10.1371/journal.pone.0099492
49. Benesch RE, Benesch R. The Acid Strength of the -SH Group in Cysteine and Related Compounds. J Am Chem Soc. 1955;77: 5877–5881. doi:10.1021/ja01627a030
50. Hall A, Nelson K, Poole LB, Karplus PA. Structure-

based insights into the catalytic power and conformational dexterity of peroxiredoxins. Antioxid Redox Signal. 2011;15: 795–815. doi:10.1089/ars.2010.3624

51. Costa MGS, Batista PR, Bisch PM, Perahia D. Exploring Free Energy Landscapes of Large Conformational Changes: Molecular Dynamics with Excited Normal Modes. J Chem Theory Comput. 2015;11: 2755–2767. doi:10.1021/acs.jctc.5b00003
52. Nelson KJ, Knutson ST, Soito L, Klomsiri C, Poole LB, Fetrow JS. Analysis of the peroxiredoxin family: Using active-site structure and sequence information for global classification and residue analysis. Proteins Struct Funct Bioinforma. 2011;79: 947–964. doi:10.1002/prot.22936
53. Nelson KJ, Perkins A, Van Swearingen AED, Hartman S, Brereton AE, Parsonage D, et al. Experimentally Dissecting the Origins of Peroxiredoxin Catalysis. Antioxid Redox Signal. 2017; ars.2016.6922. doi:10.1089/ars.2016.6922
54. Tairum-Jr CA, Santos MC, Breyer C., Geyer R, Ferrer-Suetta G, Nieves C, et al. Catalytic Thr or Ser residue modulates structural switches in 2-Cys peroxiredoxin by distinct mechanisms. Sci Reports. 2016;6: 1–12. doi:10.1038/srep331

CHAPTER 4 – UNIQUE STRUCTURAL SWITCHES ALONG THE CATALYTIC CYCLE OF OHR ARE ASSISTED BY SUBSTRATES AND PRODUCTS

Unique structural switches along the catalytic cycle of Ohr are assisted by substrates and products

Renato M. Domingos[1]; Raphael D. Teixeira[2#]; Ari Zeida[3]; William A. Agudelo[3]; Thiago G.P. Alegria[1]; Plínio P.S. Vieira[4]; Mario T. Murakami[4]; Dario A. Estrin[3]; Chuck S. Farah[2]; Luis E.S. Netto[1]

[1]*Dep. Genetics and Evolutive Biology – IB, USP, São Paulo, Brazil;*
[2]*Instituto de Química - Universidade de São Paulo, Brazil*
[3]*Dep. of Inorganic Chemistry, Analytical and Physical Chemistry – FCEyN, UBA, Buenos Aires, Argentina;*
[4]*Brazilian Center for Research in Energy and Materials, Campinas, Brazil.*

[#] *currently at Biozentrum – UB, Basel, Switzerland;*
*To whom correspondence may be addressed. Email: nettoles@ib.usp.br or mdomingos@ib.usp.br

Key words: Ohr/OsmC; thiol-dependent peroxidases; Dihydrolipoamide

This Chapter is in preparation for submission in 2018

4.1 – Main contribution by Renato M. Domingos

I was the main researcher during this work, performing both the experimental work and the computational analyses. This expertise was gained through my participation in specialized courses in X-ray crystallography, MM and hybrid QM-MM simulations and in redox chemistry and thiols. In this paper, I obtained six crystallographic structures and several molecular dynamics simulations which together with *in vitro* evaluations of Ohr point mutations, represented a solid framework where the catalytic mechanism of Ohr could be built.

4.2 – Abstract

Organic Hydroperoxide Resistance (Ohr) proteins play central roles in the bacterial response to fatty acid peroxides and peroxynitrite, presenting unique structural and biochemical features in comparison with mammalian Cys-based peroxidases. The molecular events associated with the high reactivity of Ohr enzymes towards hydroperoxides and its reducibility by the dihydrolipoamide moiety, present in lipoylated proteins, are still elusive. Here, six crystallographic structures are reported, including the complex between Ohr and its reducing substrate, which together with MM and hybrid QM-MM simulations indicated that Ohr undergoes unique structural switches to allow an intermittent movement of the loop containing the catalytic Arg, which is stabilized in the closed state when the catalytic Cys is reduced. Interestingly, dihydrolipoamide (DHL) directly assisted the closing the Arg-loop and thereby the turning over of the enzyme. The awareness of the molecular dynamics is a crucial information to apply structure-based drug discovery approaches for searching for Ohr inhibitors.

4.3 – Introduction

Ohr (Organic Hydroperoxide Resistance) are essential players in the bacterial defense against fatty acid hydroperoxides and peroxynitrite, two important oxidants at host-pathogen interface (Alegria *et al*, 2017). Ohr proteins were first described for their involvement in the defense of *Xanthomonas campestris* towards organic hydroperoxides, but not hydrogen peroxide (Mongkolsuk *et al*, 1998a). Later, similar phenotype (specific sensitivity to organic hydroperoxides) was described for other bacteria, was associated with the Cys-based, thiol-dependent activity of Ohr enzymes (Cussiol *et al*, 2003; Lesniak *et al*, 2002).

Ohr was associated with the virulence of some pathogenic bacteria, raising the potential of this peroxidase as a drug target. For instance, *ohr* from *Actinobacillus pleuropneumoniae*, the causative agent of porcine pleuropneumonia, is specifically up-regulated during infection (Shea & Mulks, 2002; Wolfram *et al*, 2009). Moreover, Ohr from *Listeria monocytogenes* and *mycobacterium smegmatis* (facultative intracellular bacterial pathogens) is relevant for bacterial survival in the host phagosomes (Saikolappan *et al*, 2015; Reniere *et al*, 2016).

OhrR, the sensor that regulates *ohr* transcription has also been implicated in virulence of some bacteria (Atichartpongkul *et al*, 2010). OhrR belongs to the MarR, a family of Cys-based transcriptional regulators (Previato-Mello *et al*, 2017; Garnica *et al*, 2017). Ohr and OhrR are crucial to the successful adaptation of *Bacillus cereus* to the gastrointestinal (GI) tract environment (Clair *et al*, 2012).

Ohr displays a very distinct folding from other important peroxidases present in the hosts, such as peroxiredoxins and glutathione peroxidase (Lesniak *et al*, 2002; Oliveira *et al*, 2006) and can only be reduced by lipoylated proteins and not by thioredoxin, glutaredoxin or glutathione (Cussiol *et al*, 2003; Meunier-Jamin *et al*, 2004; Cussiol *et al*, 2010), which is another unique characteristic of these enzymes. Ohr active site architecture is composed by two cysteines. The peroxidatic cysteine (C_p) directly reacts with peroxides, generating a sulfenic acid (C_p - SOH), which then condenses with the resolution cysteine (C_r-SH) leading to the formation of an intra-molecular disulfide. Besides C_p and C_r, the catalytic arginine (R_c) and glutamate (E_c) are relevant in the enzymatic activity of Ohr (**Fig. 1b**). In the so-called close state (CS), the C_p, R_c and E_c (the catalytic triad) interacted through polar interactions, thereby stabilizing C_p in the thiolate state, thus, increasing its nucleophilicity. In contrast, when Ohr is in the open state (OS), the loop containing the R_c (Arg-loop) is opened, the C_p, R_c and E_c network of interactions is disrupted and exposing R_c to solvent (**Fig. 1c**). This OS was previously suggested to be the most appropriated to allow the reduction of Ohr by lipoylated proteins (Lesniak *et al*, 2002; Cussiol *et al*, 2003; Meunier-Jamin *et al*, 2004; Oliveira *et al*, 2006; Cussiol *et al*, 2010). Recently, our group showed by MD that when Ohr from *Xylella fastidiosa* was oxidized to disulfide, the opening of the R_c loop was favored. However, the closing of the R_c loop was not observed under the analyzed conditions (Piccirillo *et al*, 2018).

Here, we analyzed in deep the Ohr catalytic cycle, employing X-ray crystallography, classical mechanics (MM), steered molecular dynamics (SMD), hybrid quantum mechanics (QM-MM) and *in*

vitro evaluations of point mutations. Remarkably, we described the structure of Ohr in complex with its reducing substrate, DHL. Furthermore, we present strong evidence that substrates and products assist the catalysis, by facilitating structural switches.

4.4 – Results

Table 1 - Data collection and refinement statistics

	OhrB (PDB$_{ID}$=6EB4)	OhrB_DTT (PDB$_{ID}$=6EBC)	OhrB_C60A_DHL (PDB$_{ID}$=6EBD)	OhrB_C60S_DHL (PDB$_{ID}$=6EBG)	OhrA (PDB$_{ID}$=6ECY)	OhrA_C61S (PDB$_{ID}$= 6ED0)
Data collection						
Space group	$P6_1$	$P6_1$	$P6_1$	$P6_1$	$P3_221$	$P3_2$
Cell dimensions						
a, *b*, *c* (Å)	87.27, 87.27, 178.78	88.16, 88.16, 169.92	87.67, 87.67, 179.61	88.65, 88.65, 180.11	138.09, 138.09, 45.12	41.96, 41.96, 123.59
a, b, g (°)	90.0, 90.0, 120.0	90.0, 90.0, 120.0	90.0, 90.0, 120.0	90.0, 90.0, 120.0	90.0, 90.0, 120.0	90.0, 90.0, 120.0
Resolution (Å)	34.81–2.10 (2.16–2.10)	34.8–1.85 (1.89–1.85)	43.84–2.61 (2.73–2.61)	39.77–2.10 (2.16–2.10)	36.01–1.35 (1.37–1.35)	36.34–1.42 (1.44–1.42)
*R*merge	0.07 (2.60)	0.108 (2.92)	0.327 (4.71)	0.223 (5.406)	0.056 (5.07)	0.033 (3.261)
I / s*I*	22.9 (1.29)	18.5 (1.28)	10.6 (1.26)	13.2 (1.24)	24.2 (1.29)	24.9 (1.29)
$CC_{1/2}$	0.999 (0.363)	0.999 (0.311)	0.997 (0.407)	0.999 (0.327)	1.000 (0.391)	1.000 (0.314)
Completeness (%)	97.5 (89.3)	100.0 (99.8)	99.9 (99.6)	93.0 (99.7)	97.7 (100.0)	96.8 (73.1)
Multiplicity	14.3 (8.5)	17.0 (9.1)	20.8 (20.9)	19.9 (14.3)	19.7 (19.9)	10.0 (8.0)
Refinement						
Resolution (Å)	34.83–2.10	34.85–1.85	35.00–2.61	35.00–2.10	35.00–1.35	35.00–1.42
No. reflections	41419	60416	22527	41170	100160	42161
*R*work / *R*free	0.189 / 0.223	0.167 / 0.217	0.198 / 0.250	0.205 / 0.227	0.148 / 0.179	0.193 / 0.213
No. atoms						
Protein	4088	4128	4076	4104	2125	2083
Ligand/ion	28	16	36	36	-	5
Water	159	215	10	61	302	93
B factors						
Protein	58.28	42.83	73.50	58.93	35.68	37.55
Ligand/ion	73.12	73.15	94.18	86.07	-	47.99
Water	51.18	41.12	44.49	46.16	47.62	42.91
r.m.s. deviations						
Bond lengths (Å)	0.018	0.015	0.013	0.015	0.025	0.012
Bond angles (°)	1.700	1.563	1.662	1.730	2.146	1.434

Values in parentheses are for highest-resolution shell.

4.4.1 – Available Ohr structure conformations

In an attempt to obtain distinct snapshots throughout catalysis, we performed several crystallization trials of two Ohr paralogues from *Chromobacterium violaceum* (*Cv*OhrA and *Cv*OhrB) that share 58% amino acid sequence identity (da Silva Neto *et al*, 2012). *C. violaceum* is an opportunist pathogen present in tropical and subtropical areas (Lima-Bittencourt *et al*, 2007). Six crystallographic structures were elucidated, which is highly relevant as the characterization of this Cys-based peroxidase is still poor. Indeed, there are only 10 structures available in Protein Data Bank at this moment. In all cases, the egg-shaped dimeric protein was observed as expected (**Fig 1a**). Initially, the structures of *Cv*OhrA in the closed (**Fig. 1b**) and open (**Fig. 1c**) states were elucidated at 1.42 and 1.35 Å resolution, respectively (**Table 1**). These CS and OS structures are highly similar to others previously described (**Fig. S1**). Notably, these two crystallographic structures present very high resolution and are among the

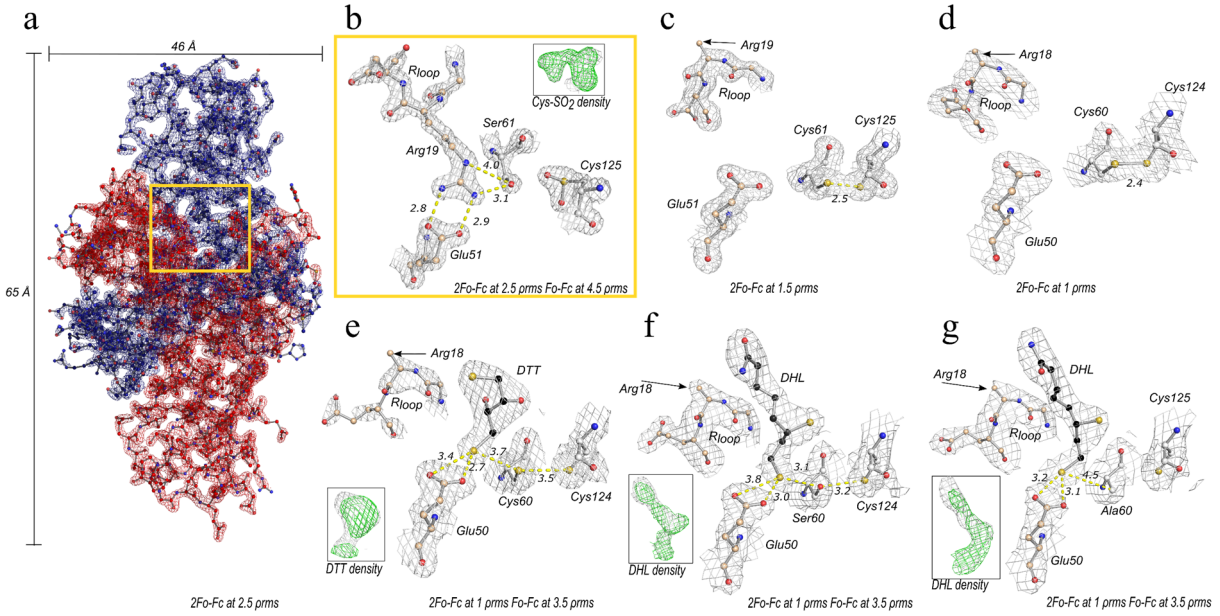

Fig. 1 – Six crystallographic structures, including the complexes of Ohr enzymes with DTT and DHL. 2Fo-Fc electron density maps are represented as blue, red or grey blue mesh (contour between 1-2.5 ρrms), whereas Fo-Fc electron density maps are represented as green mesh (contour between 3.5-4.5ρrms). Spheres are colored by atom (oxygen = red, nitrogen = blue, sulfur = yellow, carbon = white or beige, depending on chain, A or B, respectively, or black if substrate). (**a**) Overview of the Ohr dimer, using *Cv*OhrA_C61S (PDB_{ID}=6ED0) as the representative crystal structure in the close state. Red and blue densities represent each one of the two monomers. (**b**) Active site of *Cv*OhrA_C61S in the close state (PDB_{ID}=6ED0), showing the highly conserved salt bridge interactions between R19 and E51 atoms, together with the electrostatic interaction between Oγ from S61 and Nε from R19. All these polar interactions are depicted in yellow. (**c**) WT *Cv*OhrA in the open state (PDB_{ID}=6ECY), showing the R-loop (R19 sidechain not shown) pointing out from the active site, while C_p and C_r are not linked. (**d**) WT *Cv*OhrB in the open state (PDB_{ID}=6EB4), while C_p and C_r are linked through a disulfide bond. (**e**) Structure of WT *Cv*OhrB in the open state and in complex with DTT (PDB_{ID}=6EBC), where C_p and C_r are detached. (**f**) *Cv*OhrB_C60S_ in the open state and in complex with dihydrolipoamide (PDB_{ID}=6EBG). (**g**) *Cv*OhrB_C60A in the open conformation and in complex with dihydrolipoamide (PDB_{ID}=6EBD). This figure was generated using PyMOL.

highest resolution representatives for the Ohr opened and closed states. The OS structure of *Cv*OhrA was achieved in a mutant, where a serine residue replaced the C_p. In this case, C_r unexpectedly appeared hyperoxidized as a sulfinic acid (**Fig. 1b**) by an unknown mechanism. We also elucidated the OS structure of *Cv*OhrB (**Fig 1d**). In both cases, the distance between the Sγ between C_p and C_r is somehow, larger than the expected for a disulfide bond (**Fig. 1c & d**), probably due to X-ray radiation damage (De

La Mora *et al*, 2011; Weik *et al*, 2002). These two structures join a group of another six available structures that display the OS (**Fig. S1**). Noteworthy, the position of the Arg-loop in the structure of OhrB from *Bacillus subtilis* (Cooper *et al*, 2007) is intermediate between the CS and OS (Cooper et al, 2007). This structure also displays the catalytic triad disrupted, but the Arg-loop is not as open as in other OS representants ($_{C\alpha}$Rc-$_{C\alpha}$Ec ~ 18 Å, in OS structures and $_{C\alpha}$Rc-$_{C\alpha}$Ec ~ 12 Å with triat network disrupted, in IS and $_{C\alpha}$Rc-$_{C\alpha}$Ec ~ 10 Å with tria network intact, in CS structures) see (**Fig. S2c**) . Despite that, the Arg-loop showed high B-factor values (**Fig. S2a**) as in other OS structures. Indeed, the electronic density for the arginine side-chain is not present (**Fig. S2b**). Here, we defined this structure as an intermediate state (IS).

Next, we successfully obtained the structure of *Cv*OhrB in complex with DTT by soaking the crystals of this peroxidase in the disulfide state (**Fig 1d**) with this reducing agent (**Fig. 1e**). The increased distance between the two Sγ atoms indicated the reduction of the disulfide bond by DTT (**Fig 1e**). DTT appeared in the active site in its reduced state probably due to the high concentrations of this reduced agent (50mM) employed in this experiment (**Fig.1e**).

4.4.2 – The Structure of Ohr in complex with its biological reductant (DHL)

The elucidation of the complex structure between Ohr and reduced DTT was probably facilitated by its high solubility in water. In contrast, DHL is poorly soluble in water (~2 mM) making the soaking experiments more difficult. Nevertheless, we successfully obtained the structures of *Cv*OhrB in complex DHL after several attempts, when Cp was replaced by serine (**Fig. 1f**) or by alanine (**Fig. 1g**). Remarkably, these two structures are the first representatives of the Ohr in complex with its biological substrate (Cussiol *et al*, 2010). The distal sulfur atom of DHL interacts with E_c atoms through H-bonds (**Figs. 1f & 1g**), similarly to one of the sulfur atoms of DTT (**Fig 1e**). In fact, similar interactions between the ligands and *Cv*OhrB were observed in these three structures, discarding artefacts due to crystal packing. In the *Cv*OhrB_C60S mutant (**Fig. 1f**), the distal sulfur atom of DHL slightly shifted towards the Oγ Ser60, which might be mimicking an intermediate state just prior to the formation of a mixed disulfide between the peroxidase and its substrate (DHL).

4.4.3 – A hydrophobic collar is conserved and relevant for Ohr-substrates interactions

The strong association between the two identical subunits (**Fig. 1a**) is a typical feature among Ohr structures (Lesniak *et al*, 2002; Oliveira *et al*, 2006). Notably, more than 50% of all the Ohr residues are at the monomer-monomer interface. These residues promote strong stabilization by intertwining the two chains through hydrogen bonds, hydrophobic and salt bridge interactions (**Table S1** and **Fig. 2a**). Indeed, hydrophobicity is a common characteristic of Ohr substrates; both fatty acid hydroperoxides (as oxidants) (Oliveira *et al*, 2006; Alegria *et al*, 2017) and the lipoyl groups (as reductants) (Cussiol *et al*, 2010). Hence, we investigated whether this hydrophobic collar would emerge as a major conserved

feature in the Ohr active site from the alignment of 200 amino acid sequences and from the superposition of all the available structures. 10 cluster positions surrounding the active site (H-1 to H-10, **Fig. 2a** & **b**) are available for hydrophobic interactions, all of them belonging to the hydrophobic collar (**Fig. 2b & c**). Interestingly, although the residues in these regions are not identical, their hydrophobic properties are highly conserved (**Fig. 2a**).

Some of the residues previously proposed to be involved with the interaction with Ohr hydroperoxide substrates (Oliveira *et al*, 2006; Alegria *et al*, 2017) take part of the hydrophobic collar described here (**Fig. 2f**). In fact, from 13 hydrophobic interactions between Ohr and a PEG molecule (proposed to be similarly occupying the position of Ohr hydroperoxide substrate), 8 are placed at the hydrophobic collar (**Fig. 2b** & **f**). Moreover, we identified 10 hydrophobic interactions and 8 of them

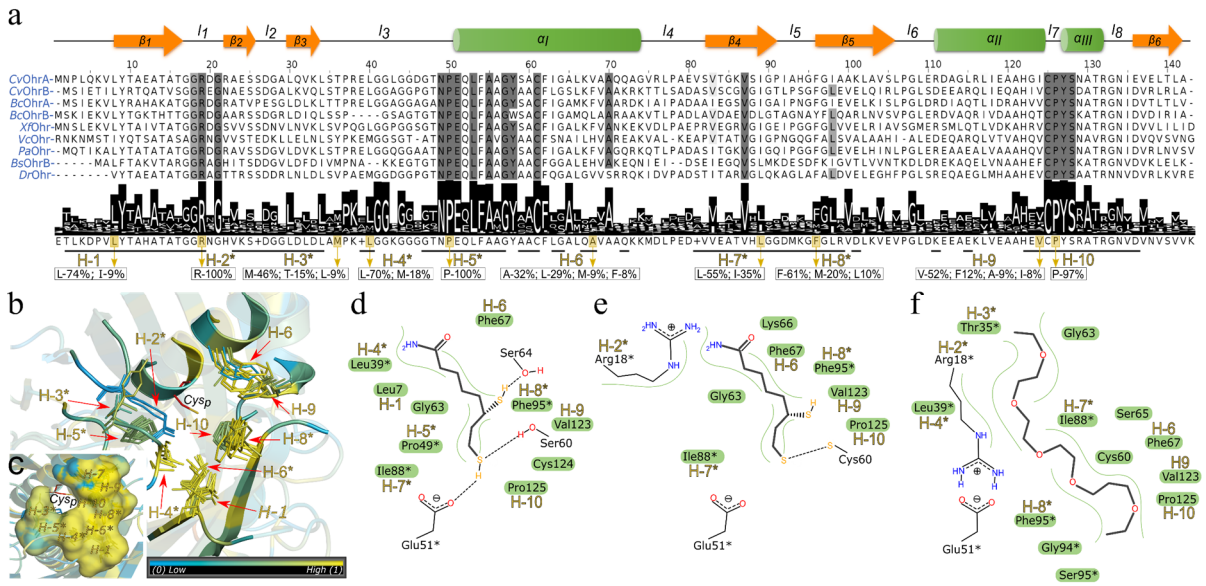

Fig. 2 – Hydrophobic cradle underlies interactions between Ohr enzymes with their substrates. (a) Multiple sequence alignment of 200 selected Ohr enzymes (Meireles *et al*, 2017). Emphasis was given to proteins with structures available in PDB (1USP, 1ZB8, 2BJO, 3LUS, 4MH4, 4NOZ, 6ECY, 6EB4 and 1N2F), which were used as reference for the assignment of the secondary structures. α=α-helix, β=β-sheet and l=loop. Residues highlighted by a yellow box (named here as H-1 to H-10, asterisks indicate the residues that belong to chain B) compose the conserved hydrophobic cradle (shown in (b) and (c)). Underlined residues are located at the interface between chains A and B. (b) Surface representation of the hydrophobic cradle, where yellow represents highly hydrophobic portions according to the scale in the bottom (adapted from Black and Mould, 1991). All the available Ohr structures were employed for the superposition, using Coot software. (c) Surface representation of the conserved hydrophobic cradle. In (d), (e) and (f), asterisks indicate the residues that belong to chain B; green lines and boxes indicate hydrophobic interactions; H-n indicate the residues that take part of the hydrophobic cradle. (d) 2D-scheme representation based on (PDB_{ID}=6EBG), showing the most relevant *Cv*OhrB-dihydrolipoamide interactions. (e) 2D-scheme representation based on a structure taken from the MD1 (a snapshot of the molecular dynamics). (f) 2D-scheme representation based on (PDB_{ID}=1ZB9), adapted from Oliveira *et al*, 2006, which represents the interaction between Ohr and PEG molecule, a putative substrate mimic. This figure was generated using Jalview, Coot, PyMOL and LigPlot^{+} softwares.

are at the hydrophobic collar (**Fig. 2b** & **d**). Therefore, probably the hydrophobic collar is involved in the Ohr specificity for elongated and hydrophobic substrates. Therefore, we decided to analyze enzyme-substrate interactions in the two major Ohr states (OS and CS).

4.4.4 – Flexible regions surrounding Ohr active site

Recently, we identified 5 different flexible regions (F-1 to F-5) in Ohr from *Xylella fastidiosa* (Piccirillo *et al*, 2018). Here, by comparing the C_α B-factors in all the available in OS and in CS structures, we show that this flexibility is consistently present in the active sites of all Ohr enzymes (**Fig. 3a, c, d & e**). Noteworthy, B-factors indicated that the Arg-loop is more intensely flexible when Ohr is in OS than in CS (**Fig. 3a, c & d).** Four of these five conserved flexible regions surround the active site and could have a role in accommodating structurally different substrates (**Fig. 3e**). Previously, short-ranged MM simulations (150 ns) indicated that C_p thiolate state stabilizes the Arg-loop near the active site, however, the transition from OS to CS was not observed in any of the systems analyzed (Piccirillo *et al*, 2018). Therefore, longer simulations (1000 ns) were performed and polar

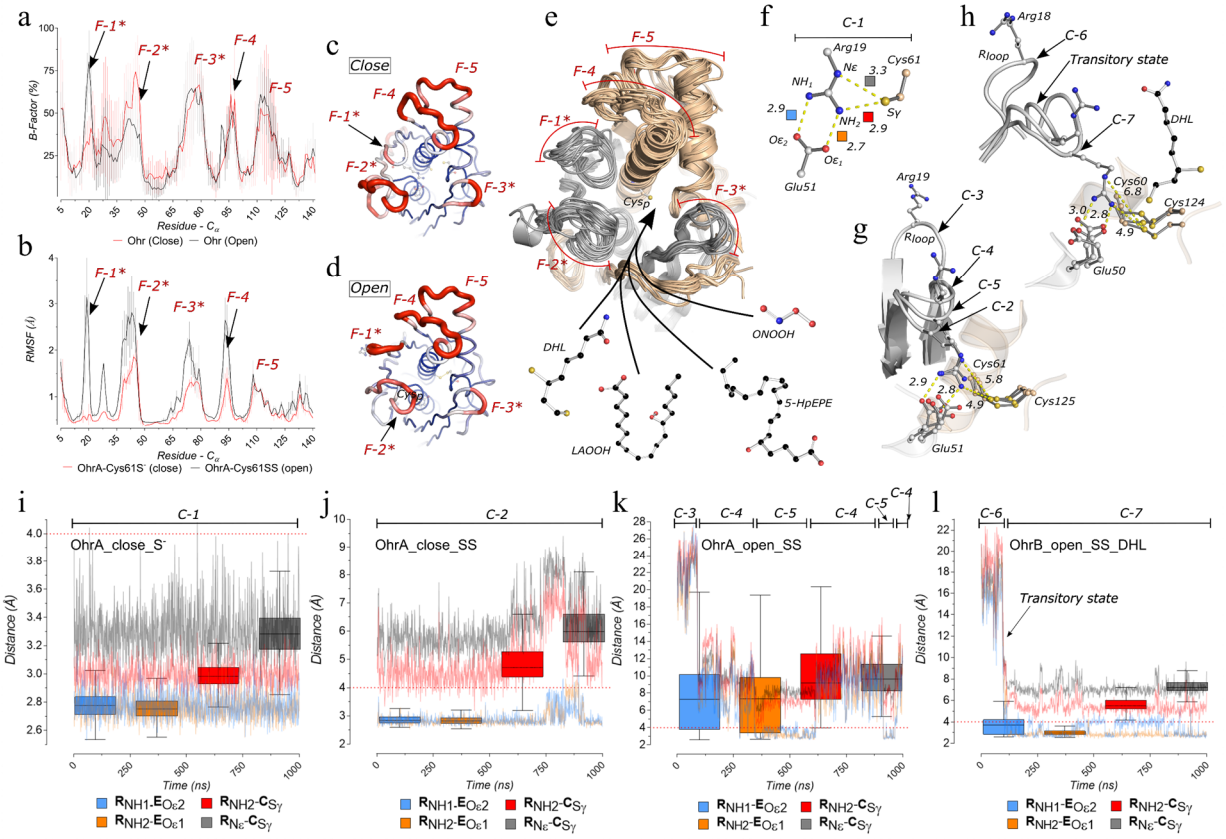

Fig. 3 – Insights into the Ohr dynamics by crystallography and molecular dynamics. From (a) to (e), F-1 to F-5 indicate the five most flexible regions in Ohr enzymes, asterisks point out opposite chains, standard deviations are shown as vertical lines. (a) Normalized Cα B-factors (%) along the primary sequences from all the Ohr crystallographic structures (every monomer) available in PDB (n=15). Structures in the open (black) and close (red) states were analyzed separately. (b) Cα RMSF (Å) for the OhrA_Open_SS (black, n=2 monomers) and for the OhrA_close_S- (red, n=2 monomers) trajectories that were calculated from the first 200 ns of MM simulation. Wire representations of Ohr flexible regions in the closed (c) and open (d) states. The more red and wider structures correspond to higher B-factors. (e) Superposition of all the available Ohr monomers. Beige and grey correspond to chain A and B, respectively. Examples of tested Ohr substrates are shown. (f) Representation of the conserved salt-bridge interactions among R19 atoms with Cp (C61) and E51 atoms. Same color representation for each one of the four salt bridges (squares) were maintained during MM simulations for 4 different systems (from i to l). (g) and (h) are conformational representatives showing distinct R-loop positions during MM of the OhrA_SS trajectory (R-loop opened and closed) and of the OhrB SS trajectory in presence of DHL (R-loop opened), respectively. C-1 to C-7 represent 7 different clusters of the R19 position during the MM trajectories of four different systems (i) OhrA_close_S-, (j) OhrA_close_SS, (k) OhrA_open_SS and (l) OhrA_open_SS_DHL. Distance value distributions are shown as Tukey box-plots, in which boxes indicate the interquartile distances, black lines show the median values and whiskers extend the box to 1.5 time the interquartile distance. The red dash lines show the 4 Å cut-off value.

interactions of residues belonging to the catalytic triad were analyzed by following distance variations among side-chain atoms of R_c, E_c or C_p (**Fig. 3f**) along 1000ns simulations (**Fig. 3i, j, k**, **l**). The following systems were analyzed: OhrA_close_S^- (From PDB_{ID}=6ED0, with C_p in its thiolate form, **Fig 3f** & **i**); OhrA_close_SS (From PDB_{ID}=6ED0, with disulfide bridge between C_p and C_r, **Fig 3g** & **j**); OhrA_open_S^- (From PDB_{ID}=6ECY, with C_p in its thiolate form, (data not shown); OhrA_open_SS (From PDB_{ID}=6ECY, with disulfide bridge between C_p and C_r, **Fig 3g** & **k**); OhrB_open_SS_DHL (From PDB_{ID}=6EBG, with disulfide bridge between C_p and C_r and DHL-S^-_2, **Fig 3h** & **l**).

Arg-loop was always nearby the active site during the OhrA_close_S^- MM trajectories and the polar network of interactions remained stable (**Fig. 3i & f)**. In contrast, the R_{NH}-$E_{O\varepsilon}$ interaction along the OhrA_close_SS system trajectories were stable for around 750ns, then distances reached values close to the 4 Å threshold for few moments (**Fig 3j & g).** This data suggested the absence of the $R_{NH\&N\varepsilon}$-C_{SY} interaction due to disulfide bond formation, facilitates disruption of the R_{NH}-$E_{O\varepsilon}$ interaction. Previously, we observed that a second loop (the so-called Gly-loop) blocked the closing of the Arg-loop (Piccirillo *et al*, 2018), precluding the turn-over of Ohr. Again, the Gly-loop prevented the closing of the Arg-loop, ever at much longer simulation intervals in one of the monomers for both OhrA_open_SS and OhrA_open_S^- systems (data not shown). Yet, we could observe the transition from OS to CS, in the opposite monomer (**Fig 3k**). In between the OS and CS, an intermediate state, similar to PDB_{ID}=2BJO, had a relatively long-life time, lasting at least 300 ns (**Fig. S2c** and **C-4** in **Fig 3k** & **g**). At the IS, R_c only gets partially exposed to solvent (**Fig. S2c** and **C-4** in **Fig 3k** & **g**), and intermittently shifts between IS and CS (**C-4** & **C-5** in **Fig 3k** & **g**), yet it still never achieved OS back again**.**

4.4.5 – Oxidized Ohr is more prone to undergo Arg loop opening

To gain more insights on the structural switch from CS to OS when Ohr was in the reduced or in the oxidized forms, SMD were performed, applying the Jarzynski equality (see methods) (**Fig. 4a**). SMD were performed for OhrB_close_S^- (**Fig. 4b** & **e**) and OhrB_close_SS systems (**Fig.4 c** & **f**). The absence of the thiolate negative charge in OhrB_close_SS (**Fig. S4**) greatly facilitated the opening of the Arg-loop, since, the energy required to disrupt the R_{NH2}-$E_{O\varepsilon 2}$ interaction was around 3kcal/mol lower, when comparing with the OhrB_close_S^- system (4.37 kcal/mol for disulfide, 7.14 kcal/mol for thiolate) (**Fig 4 b** & **c** blue region and **Fig. S4**). Furthermore, even when the R_{NH2}-$E_{O\varepsilon 2}$ interaction was lost, the thiolate of C_p still kept interacting with R_c, until reaching a maximum of energy (14.3 kcal/mol) in the OhrB_close_S^- trajectory (**Fig. 4b** & **e**). In contrast, the maximum energy achieved in the OhrB_close_SS system was 10.2 kcal/mol. Probably, this energy was required to disrupt hydrophobic interactions between the hydrophobic collar and the side chain of R_c, among other forces (*i.e.* electrostatic). Moreover, at the end of the reaction coordinate (RC_{max} = 16.5 Å) the distance reached, between R_{NH2}-$E_{O\varepsilon 2}$ was around 4 Å higher in the OhrB_close_SS system (16 Å) than in the

OhrB_close_S$^-$ system (12 Å) (see upper panels in **Fig 4b & c)**. It clearly suggests Arg-loop stabilization in the CS is greatly decreased when C_p and C_r are linked.

These free energy profiles indicated that the OS are always more unstable than CS (**Fig. 4b & c**) and are unlikely to be an intermediate during Ohr catalysis. Instead, an IS such as C-4 (**Fig. 3k & g)** and the transitory state (**Fig. 3i & h**) could be intermittently achieved with relatively long life-time when

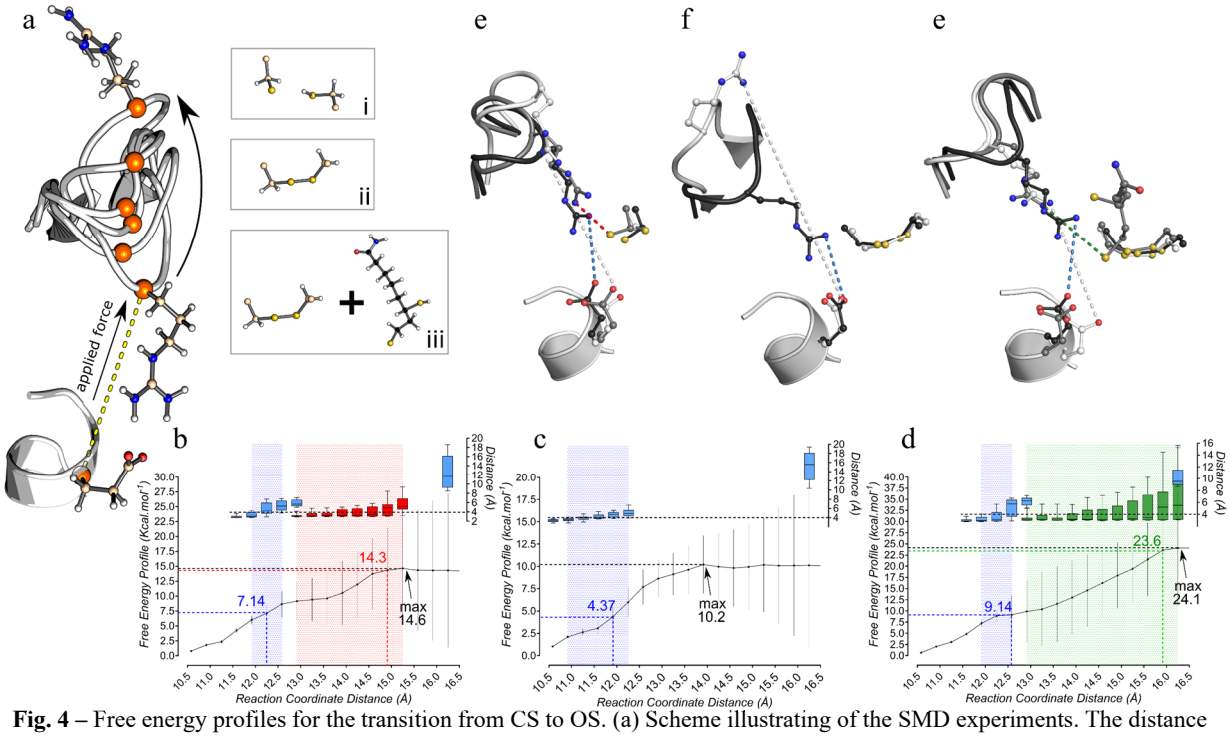

Fig. 4 – Free energy profiles for the transition from CS to OS. (a) Scheme illustrating of the SMD experiments. The distance between Cα Glu50 and Cα Arg18 of OhrB (orange spheres) was followed along the reaction coordinate. The distance between these atoms was increased by an external force at constant rate of 0.33 Å/ns, from 10.5 Å to 19.5 Å. These simulations were replicated at least 46 times for each one of the three systems: (i) OhrB_S$^-$, (ii) OhrB_SS and (iii) OhrB_SS_DHL. (b) (c) and (d) are the free energy profiles for the OhrB_close_S$^-$, OhrB_close_SS and OhrB_close_SS_DHLS$_2^-$ trajectories, respectively. The colored backgrounds indicate the regions where the R_{NH1}-$E_{O\varepsilon1}$ (blue), R_{NH1}-$C_{S\gamma}$ (red) and R_{NH1}-DHL_{S2} (green) distances are overcoming the 4Å cut-off for salt bridge interactions. The blue, red and green dashed lines indicate the energy required to increase the R_{NH1}-$E_{O\varepsilon1}$, R_{NH1}-$C_{S\gamma}$ and R_{NH1}-DHL_{S2} distances (median) to values that exceed the 4Å threshold. The Tukey box-plot on top of each one of the three free energy profile plots represent the distribution of distances involving the side chain of Arg18: blue = R_{NH1}-$E_{O\varepsilon1}$, red = R_{NH1}-$C_{S\gamma}$ and green = RNH1-DHL_{S2}. Once the values overcome the 4Å threshold (indicated by black dashed lines), they were omitted for sake of clarity. The maximum R_{NH1}-$E_{O\varepsilon1}$ distances attained in each of the experiments were indicated by white asterisks. (e), (f) and (g) are representations of the intermediate positions of the Arg-loo (blue (breaking of R_{NH1}-$E_{O\varepsilon1}$), red (breaking of R_{NH1}-$C_{S\gamma}$), green (breaking of R_{NH1}-DHL_{S2}) and white (maximum distance acheaved for R_{NH1}-$E_{O\varepsilon1}$) dashes) according to (b), (c) and (d) trajectories, respectively.

Ohr is oxidized. Longer openings of the Arg-loop, such as C-3 and C-6 (**Fig. 3k, i, g & h**), might only be achieved and stabilized during crystallographic experiments, where proteins are in a very crowded environment, sensing many external forces. Additionally, during MM simulations performed for the OhrA_open_SS system, the Arg-loop opened even more than the crystallographic structures when in the C-3 cluster position (**Fig. 3k & g**), increasing the chance of permanently interacting with external regions of the protein.

4.4.6 – Alcohol release assisted the Arg-loop opening

We further hypothesized that the product of Ohr, the alcohol derived from the reduction of the lipid hydroperoxide might assist structural opening switches as this compound probably hydrophobically interacts with the R_c side chain. This hypothesis was tested by modeling a fatty acid carbon chain based on the PEG molecule present in an Ohr structure (PDB_{ID}=1ZB9) previously described (Oliveira *et al*, 2006). Thus, we performed SMD by pulling the carbon chain out from the active pocket and following the R_{NH}-$E_{O\varepsilon}$ interaction disruption (**Fig. S3**). Remarkably, the disruption of the Arg-Glu salt bridge was facilitated when the fatty acid alcohol was present in the molecular simulation (**Fig. S3**). Probably, hydrophobic interactions between the carbon chain of the alcohol and the R_c side chain could assist the opening of the Arg loop.

4.4.7 – DHL induces the fast closing switch

Next, we analyzed the closing of the Arg-loop in the presence of DHL (OhrB_open_SS_DHL system), taking advantage of our structure complex (**Fig. 3h** & **l)**. Remarkably, the Arg-loop transition from OS to CS passed through the IS, only as a transient transitory state (**Fig. 3h** & **l**). In contrast, in the OhrB_open_SS system, the IS lasted a relatively long life-time (**C-4** in **Fig. 3k**). Such result agrees with the idea that DHL interacts with Ohr when Arg-loop is at the IS, and while it is moving towards the disulfide bond to react and reduce Ohr, the Arg-loop could be attracted to regain its CS (**C-7** in **Fig.4 h** & **l**). To further support that DHL could help Arg-loop to close, we also performed SMD with OhrB_close_SS_DHL (**Fig. 4c** & **g**), by also pulling the $R_{C\alpha}$ and $E_{C\alpha}$ apart from each other and, again, we applyed then the Jarzynski equality in order to obtain the free energy profile of the reversible conformational switch. This system showed the highest energy required to break R_{NH2}-$E_{O\varepsilon 2}$ interactions (around 9.14 kcal/mol). Furthermore, once arginine lost its interaction with glutamate, it kept directly interacting with the thiolate from of DHL-S_2, until reaching the energetic barrier of around 24 kcal/mol. Such high energetic barriers indicate the system would tend to quickly go to the state of lower energy. Corroborating, thus, with the idea that DHL actually induces the fast closing and reactivation of Ohr.

4.4.8 – Catalytic arginine is not required for the reduction of Ohr by DHL

R_c and E_c are associated with the activation of C_P for hydroperoxide reduction (Lesniak et al., 2002; Oliveira et al., 2006). As new structural information on Ohr reduction by DHL was described above, we decided to evaluate the reducing step of Ohr catalysis by mutating either R_c or E_c. First, we evaluated the effects of mutations on the entire cycle through the lipoamide/lipoamide dehydrogenase coupled assay (**Fig 5b** & **a**). As previously described (Lesniak *et al*, 2002; Oliveira *et al*, 2006; Alegria *et al*, 2017), the residues that comprise the catalytic triad (R_c, E_c and C_p) are relevant for peroxidase activity (**Fig. 5b)**. Furthermore, the absence of C_r was also crucial for catalysis (**Fig 5b)**. We then dissected the reaction into oxidative and reductive steps, in order to determine where the mutants were

specifically interfering. First, we evaluated the oxidation of Ohr (reduction of peroxide) which ends up with the formation of a disulfide bond between C_p and C_r (**Fig 5c** & **a)**. By a competition assay employing AhpE, a peroxiredoxin with known rate constants with distinct peroxides (Alegria *et al*, 2017), we determined the second order rates for the Ohr oxidation by oleic hydroperoxide (reaction **I** in **Fig. 5a** & **a**). As expected, mutation of R_c and E_c strongly inhibited the ability of Ohr to reduce the

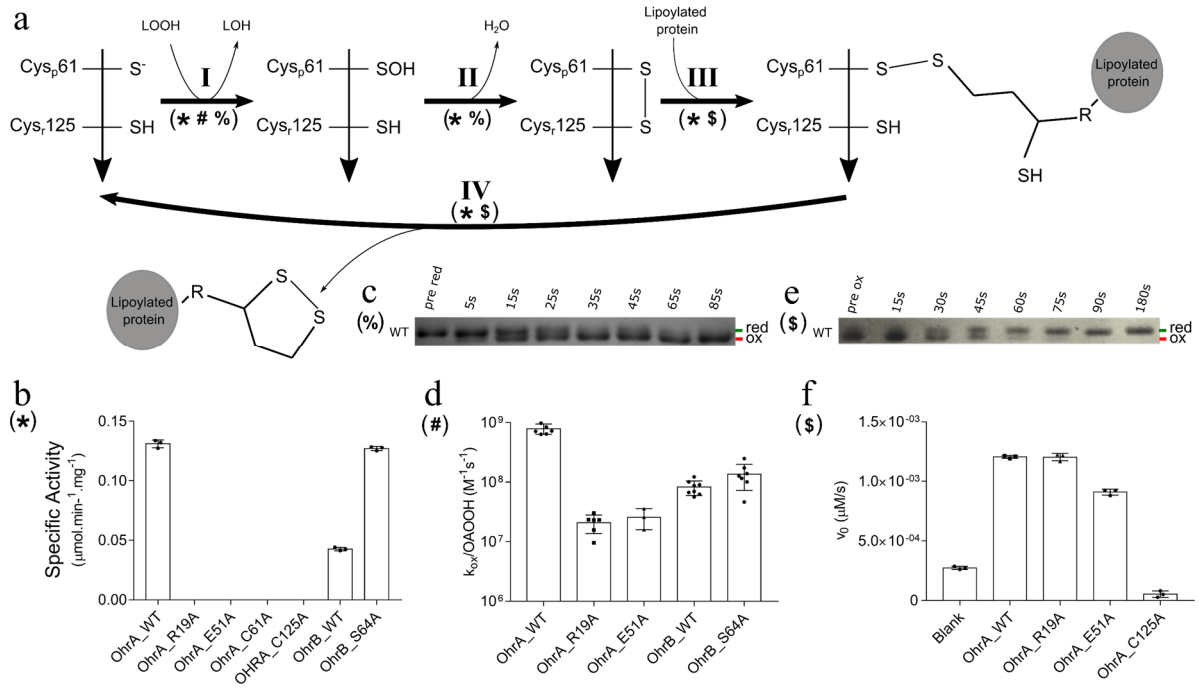

Fig. 5 – Ohr Kinetics evaluating arginine role during hydroperoxide reduction and DHL oxidation. (a) Scheme of the reactions that take place along the overall catalytic cycle. (Step I) Reactive thiolate (C_p-S^-) of Ohr reacts with lipid peroxides (LOOH), giving rise to a sulfenic acid intermediate (Cp- SOH). (Step II) condensation reaction between Cp- SOH and Cr, generating an intramolecular disulfide bond. (Step III) First thiol-disulfide exchange reaction between Ohr and a lipoylated protein, giving rise to a mixed disulfide between Cp and the lipoylated protein. (Step IV) Second thiol-disulfide exchange reaction between the second thiol of the dihydrolipoic acid moiety and the mixed disulfide bridge, allowing the turnover of Ohr. (b) Specific activity for the reduction of tBOOH by Ohr, determined through the lipoamide/lipoamide dehydrogenase coupled assay. NADH = 300 μM; Lpd = 1 μM; lipoamide = 50 μM; tBOOH = 200 μM (c) Analysis of disulfide bond formation by non-reducing SDS PAGE. The band migrating faster corresponds to the disulfide (Oliveira *et al*, 2006). Ohr was pre-reduced with excess DTT (50 mM). The reaction was initiated by adding H_2O_2 50 μM and it was stopped at different times with 20% of TCA and 50 mM of NEM. (d) Rate constants for the reaction of oleic acid hydroperoxide (OAOOH) with wild-type and mutants of CvOhrA. (e) and (f) analysis of disulfide bond reduction by non-reducing SDS PAGE and by determining the initial velocities through the lipoamide/lipoamide dehydrogenase coupled assay. Ohr was pre-oxidized with H_2O_2 (proportion 1:10 enzyme:peroxide) and the reduction of Ohr (50 μM) was performed in presence of NADH = 175 μM; Lpd = 1 μM; lipoamide = 0.2 μM. For the gel, the reaction was initiated adding the lipoamide and it was stopped as in (c). Details can be found in "Methods".

hydroperoxide (from around $8.0x10^8$ to $2.0x10^7$ M^{-1} s^{-1}) (**Fig. 5d**).

Then, we evaluated the reduction of Ohr by DHL after pre-oxidizing the Cys-based peroxides with H_2O_2. Two reactions represent the process by which Ohr disulfide bond is reduced (reactions **III** and **IV** of **Fig. 5a**), restoring its capacity to reduce hydroperoxides (**Fig. 5c**). R_c mutation did not decrease the ability of Ohr to be reduced by DHL, while the E_c mutation only slightly inhibited Ohr reduction (**Fig. 5f**). Additionally, the C_r mutant showed no activity, indicating either DHL is not able to reduce C_p in the sulfenic acid state, or C_p became irreversibly overoxidized into sulfinic or sulfonic acid states (**Fig. 5f**) when pre-oxidized by H_2O_2. Therefore, R_c is not required for Ohr reduction, making it

plausible that the Arg-loop could leave its close position to accommodate DHL. Thus, we hypothesize that two things could be happening: 1- the reducing step could either occur with an opened or closed Arg-loop as arginine does not interfere in either conformation; 2- Arginine would negatively interfere if closed, so, DHL only fits and reacts when the triad network is disrupted during IS.

4.4.9 – Catalytic triad disruption is crucial for Ohr reduction by DHL

In an attempt to obtain some insights on which situation could actually be happening during the reducing step, we studied the chemical reactivity of DHL (reaction **III** in **Fig. 5a**) in both situations (intact and disrupted catalytic triad) through hybrid QM-MM analysis (Senn & Thiel, 2009). Thereby,

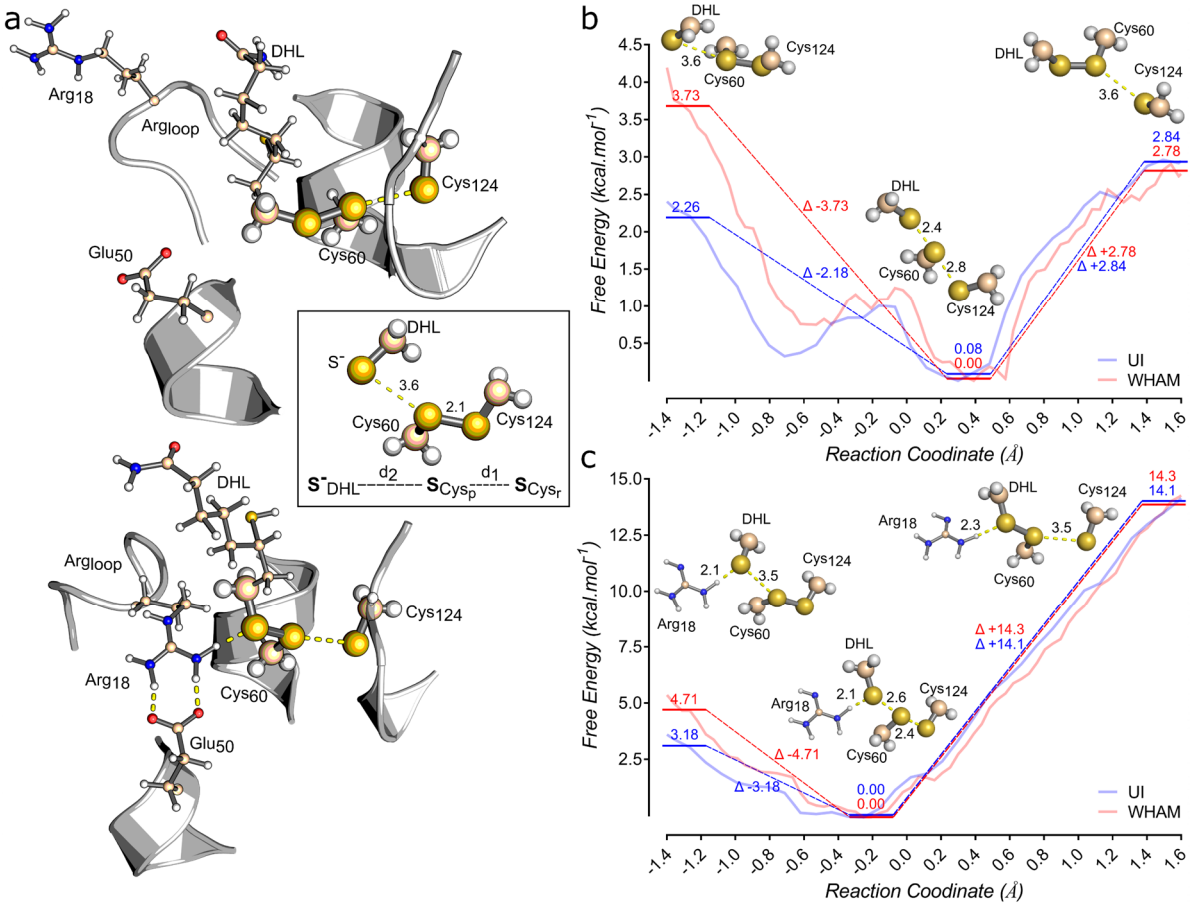

Fig. 6 – Hybrid QM-MM analysis comparing the intramolecular disulfide bond attack by DHL (reaction III, figure 5) in open and close states. (a) illustrative representation of the OhrB experimental system (emphasis in the active site) in open (top) and close (below) states, with mixed disulfide bridge with DHL (product of reaction III, figure 5), with a schematic view (black box) of the quantum subsystem, i.e. H_2CS of Cys60 and Cys124 and the H2CS- moiety of DHL. QM atoms are shown in a larger size (oxygen = red, nitrogen = blue, sulfur = yellow, carbon = beige). The reaction coordinate was followed by the difference between the S-DHL-SCycp (d2) and the SCysp-SCysr (d1) distances. (b) and (c) are the free energy profiles obtained by QM-MM umbrella sampling for the intramolecular disulfide bond reduction when Ohr is in the opened (top) or in the closed (below) state. Representations of the QM atoms positions are shown for the following reaction coordinates: -1.2 (DHL approximation), -0.2 (free energy minimum, Ohr close conformation), 0.4 (free energy minimum, Ohr open conformation), and 1.6 (DHL-Ohr mixed disulfide formation). Weighted histogram analysis method (WHAM) and umbrella integration method (UI) analysis are shown in the graphics in red and blue, respectively.

two initial systems were prepared as classical (MM): with Ohr in OS (**Fig. 6a** top) and CS (**Fig. 6a** bottom), both with DHL at the active site. Umbrella sampling QM-MM simulations were performed

from the initial systems, where only the three sulfurs involved in the reaction and their adjacent methylene groups were considered as quantum atoms (**Fig. 6a** (box)), and all the rest was treated as a classical system. The reaction was considered as a nucleophilic substitution (S_N2) and the reaction coordinate was chosen to be the difference between the $\mathbf{S}_{Cysp}$-$\mathbf{S}_{Cysr}$ (d1) and $\mathbf{S}^{-}_{DHL}$-$\mathbf{S}_{Cycp}$ (d2) distances (**Fig. 6a** (box)). In order to facilitate the interpretation of the free energy profiles for OS (**Fig. 6b**) and CS (**Fig. 6c**), we divided the reaction into three different stages: **Step 1** is related with the approaching of DHL towards the C_p, which is slightly exergonic for both systems (up to -3.73 kcal/mol for OS and -4.71 kcal/mol for CS). These results suggested that once DHL is nearby the active site, all the surrounding environment guides the reducing molecule towards the C_p. Such fact agrees with the idea that lipoylated compounds could actually be the reducing agent of Ohr proteins (Cussiol *et al*, 2010). Then, in **step 2** the system reaches an energetic minimum state. The CS reaches this minimum faster than the OS, probably because R_c provides an extra contribution in stabilizing the DHL distal sulfur in a closer position to the C_p sulfur. **Step 3** is related with the formation of the mixed disulfide bridge between DLH and C_p. This thiol/disulfide exchange is endergonic for both CS and OS. However, the reaction energetic profile in presence of R_c at the active site was at least 5 times more endergonic than when R_c is far away from the active site (up to +2.84 and +14.2 kcal/mol for OS and CS, respectively). Such difference is probably correlated with the exacerbated stability of the DHL in the thiolate form by the interaction with R_c in the CS (**Fig. 6c**). The opening of the Arg-loop would prevent this interaction, decreasing energetic barrier for the Ohr mixed disulfide formation with DHL and, therefore, making it more favorable on thermodynamics grounds. Then in the second step of the reaction (**Step IV** in **Fig. 5a**) the oxidized DHL would leave the reduced Ohr. This proposal is consistent with the finding that wild type Ohr is equally reducible by DHL as the protein mutant for R_c (**Fig 5f**).

4.5 – Discussion

Despite lipoic acid is mostly associated to its ability to act as electron acceptors in oxidative pathways (Cronan, 2016), it has been proposed that lipoic acid, normally associated to proteins (as lipoylated proteins) also act as electron donors supporting the redox cycling of some enzymes (Bryk *et al*, 2002; Eser *et al*, 2009; Cronan, 2016)). Remarkably the ability of lipoylated proteins to interact and reduce Ohr enzymes has been previously described, both, by Co-Immunoprecipitation (Co-IP) and *in vitro* reconstitution coupled with kinetic assays (Cussiol *et al*, 2010). Furthermore, it was suggested that the reducing agents would interact with oxidized Ohr proteins in OS (Oliveira *et al*, 2006). Despite some evidences that Ohr oxidation could be associated with the opening of the Arg-loop (Piccirillo *et al*, 2018), there is no cohesive mechanistic evidences on the Ohr conformational exchange during enzymatic turnover. Moreover, there was no clear understanding into how the DHL moiety in proteins would interact with Ohr enzymes. Thus, our high-resolution X-ray structures representatives of Ohr in OS and CS, together with the first available model for Ohr-dihydrolipoamide complex allowed us to build a cohesive model consistent with the experimental and theoretical findings described here.

Invariably, Ohr achieves its unique architecture characteristics of efficient organic hydroperoxidase by rapidly dimerizing and structurally assembling a hydrophobic collar at active site surroundings. Ohr enzyme specificity to interact and reduce elongated organic hydroperoxides would be due to a larger set of conserved characteristics. The hydrophobic interaction between Ohr and the lipidic hydroperoxides was previously proposed to be important when, specifically, *Xylella fastidiosa* Ohr was co-crystalized with a PEG molecule that would be mimicking the substrate (Oliveira *et al*, 2006). Further docking experiments supported the hypothesis that PEG would probably be similarly accommodated at the active site as lipid hydroperoxides are (**Fig. 2f**) (Oliveira *et al*, 2006; Alegria *et al*, 2017). Here, we correlated the interface regions of interaction between Ohr monomers with the highest conserved regions in Ohr enzymes (**Fig 2a**). *Cv*OhrA analysis showed that more than 50% of the residues are at the monomer-monomer interface (**Table S1**). Our results further support that the enzyme quickly assembles together the catalytic triad, but also the intrinsic hydrophobic characteristic conservation (**H-1 to H-10, Fig. 2a**), which surrounds Ohr active site, (hydrophobic collar) (**Fig.2b & c**).

Consistent with early studies showing that elongated lipid hydroperoxides would interact with hydrophobic residues (Oliveira *et al*, 2006), Ohr reduction by DHL was also depend on hydrophobic interactions, which overlap the conserved hydrophobic collar. The structure of the complex between *Cv*OhrB and DHL allowed us, for the first time, to map the interactions between Ohr and its biological reductant (**Fig 1f & g & 2d**). Structural analysis of the DHL accommodation at the active site suggested its linkage with a lysine residue from lipoylated proteins are long enough to fit at the active pocket without much additional disturbances. Furthermore, *Cv*OhrB provided an extra hydrogen bond interaction not present in most of the other Ohr proteins. *Cv*OhrB exceptionally contains a Ser at

position 64, while an Ala is preferentially present in more than 80% of Ohr proteins (**Fig 2a & d**). Possibly this extra hydrogen bond provides too much stability to the reductant, delaying the reducing step in *Cv*OhrB, in agreement with our kinetic data (**Fig 5b & d**). These results strengthen the importance of the hydrophobic collar conservation for both substrates: elongated organic hydroperoxides or DHL.

The long openings of the Arg-loop such as those represented in C-3 and C-6 (**Fig. 3g** and **6h**) that are similar to most crystallographic structure in OS are probably not achieved during Ohr catalysis. Indeed, no closing of the Arg-loop was observed in MM analyses when investigating proteins starting in an OS with the Arg-loop highly exposed (Piccirillo *et al*, 2018). It was then proposed that crystal packing contacts would artificially expose R_c. Here, we present strong evidences that such long Arg-loop openings are very hard to be achieved (**Fig.** 4**c & f**). First, in all simulations where the starting structure was found in such openings, at least one of the monomers could not sample the closing switch, due to interactions of R_c with external residues. Moreover, the free energy profiles associated to the opening switch displayed a great energetic barrier of at least 10Kcal/mol. (**Fig 4c** & **f**).

Notably, our data indicated that the structural switch between CS and IS is influenced either by the reductant substrate or by the alcohol, product derived from the reduction of lipid hydroperoxides. Recent findings, described evidences that Arg-loop in CS is destabilized when Ohr becomes oxidized, as the active site loses the thiolate electronegative charge (reaction **3** and stage **IV** in **Fig. 7 & Fig. S4**) (Piccirillo *et al*, 2018). In fact, the free energy profile associated to CS to OS switch, confirm that oxidized Ohr displays a relatively lower energetic barrier than reduced Ohr (**Fig 4b** & **c).** Moreover, we describe that the release of the product derived from the reduction of lipid hydroperoxides cause an additional disturbance in Arg-loop stability, triggering the switch from CS to IS (IV & V in Fig. 7, **video, Fig 3k & Fig. S3**). Furthermore, MM simulations of OhrB_SS_DHL showed a direct transition from OS to CS, briefly crossing the IS, in contrast to the system where DHL was absent (**Fig 3k & i**). Furthermore, the high free energy barrier (around 24 kcal/mol) linked to the conformational change from CS to IS in presence of DHL suggests that the system has strong thermodynamic tendency to close when DHL is present in the active site (**Fig 4d**). Therefore, these findings are consistent with the idea that substrates and products accelerate structural switches and thus, potentially contributing for Ohr efficient peroxidase activity. These structural switches depend on the oxidative state of Ohr.

For instance, our data indicated that the disruption of the catalytic triad is required for a favorable thermodynamic attack of the Ohr intramolecular disulfide bond by DHL. First, our kinetics with mutant proteins ensured us that R_c is irrelevant for Ohr reduction (**Fig. 5f & a**). Therefore, moving R_c away from the active site would not impair the reduction of the Ohr disulfide by DHL. However, only through the hybrid QMMM analyses we could really exclude the hypothesis that the maintenance or disruption of the network of interactions among the residues of the catalytic triad would be equally thermodynamically favorable for the Ohr reduction by DHL. Hybrid QM-MM unveiled that Ohr OS/IS structure is thermodynamically, over five times, more prone to be reduced by DHL than in Ohr close

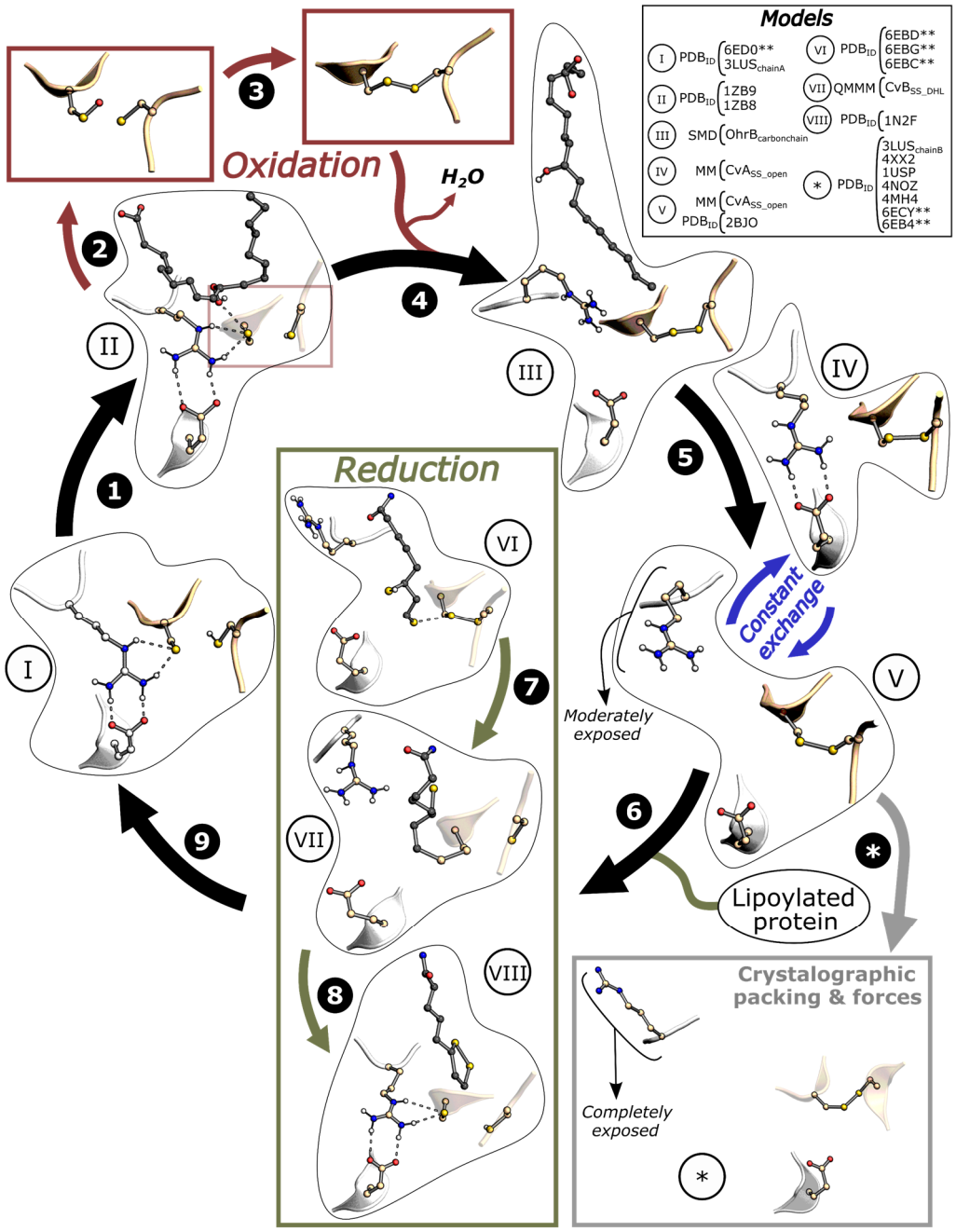

Fig. 7 – Proposed detailed scheme for Ohr enzymatic mechanism. 1) Thiolate form of peroxidatic cysteine attacks lipid hydroperoxide in an electronegative environment (red background). 2) Peroxidatic cysteine is oxidized to sulfenic acid and (3) resolution cysteine would attack oxidized peroxidatic cysteine forming a disulfide bridge, with the release of water, providing an electrostatic shift at the active site surroundings becoming electropositive (blue background). 4) Electropositivity decreases Arg-loop stability and it opens while interacting with the alcohol (product) which leaves the active site. 5) Arg-loop initiates a constant exchange between moderately opened and closed conformations. 6) Dihydrolipoamide would then interact with Ohr while arginine is moderately opened. 7) as dihydrolipoamide gets covalently bond to Cp, arginine hydrophobic interactions with dihydrolipoamide carbon chain induce the Ohr conformational change and 8) once lipoamide completely restores thiolate form of Cp and leaves the active site, electronegativity is regained and the Arg-loop quickly restores catalytic triad interactions. 9) Ohr is reactivated and prompt to reduce another hydroperoxide. * represent crystallographic environment conditions, where very high concentration of protein, would provide arginine loop external interactions and crystallographic packing and forces would allow Arg-loop stabilization at exaggerated apertures. The models which approximately represent the different structural states (I to VIII) are suggested. ** represent PDB structures elucidated in this work

conformation (**Fig.6b & c**). Probably, such negative influence of the arginine presence at close proximity to DHL-S^- is due to an over stabilization of the DHL thiolate. Thus, our findings cohesively

suggest that DHL would optimally fit and react with Ohr in an IS conformation.

The unique Ohr structural properties associated with: the strong sensitive of *Δohr* cells for pathogenic bacteria exposed to organic peroxides (Mongkolsuk *et al*, 1998b; da Silva Neto *et al*, 2012; Alegria *et al*, 2017); the Ohr involvement in bacterial virulence (Shea & Mulks, 2002; Wolfram *et al*, 2009; Clair *et al*, 2012; Saikolappan *et al*, 2015; Liu *et al*, 2016; Reniere *et al*, 2016); and its absence in mammals and vascularized plants (Meireles *et al*, 2017) raise the possibility of Ohr as a promising drug target. In fact, several reports described the production of oxidants as mechanism of action of some antibiotics (Dwyer *et al*, 2014; Belenky *et al*, 2015; Ladjouzi *et al*, 2015; Van Acker & Coenye, 2017). Our studies provide a comprehensive evaluation into the conserved features of residues surrounding the active site of Ohr and its dynamic behavior during the enzymatic turnover (**Fig. 7**). However, this work is relevant not only on biochemical grounds (including six crystal structures), but also because these studies are coupled to theoretical computation dynamics analyses. This approach turns out to be especially important when employing promising virtual methodologies for searching for bioactive compounds (Ruiz-Carmona *et al*, 2017; Ozbuyukkaya *et al*, 2013; Scior *et al*, 2012). As, frequently, drug design and screening is performed based on X-ray protein structures and enzyme active site available interactional properties (Lionta *et al*, 2014). Our work is an example where previous in deep analyses are required to evaluate the most prevalent conformations a protein can adopt in solution, as crystal packing can restrain and induce different conformational stabilization than those most prevalent in solution. In fact, despite the fact that most Ohr X-ray structures are in OS, we show the most prevalent conformation in solution are the CS. Moreover, Ohr available interactions (hydrogen donor and receptor and hydrophobic) at the active site are massively conformational dependent (**Fig. S5**). Thus, when applying virtual modern methods to search for inhibitors, we suggest that only the CS must be considered, for both reduced and oxidized states.

4.6 – Methods

4.6.1 – Cloning procedures and site-directed mutations of *Cv*OhrA and *Cv*OhrB

Wild type coding region of the *C. violaceum ohrA* (CV0209) and *ohrB* (CV2493) genes were PCR amplified using appropriate primers for *Cv*OhrAwt and *Cv*OhrBwt (NdeI/BamHI, for both) (**Table S2**). The fragments were then cloned into the vector pET15b (novagen) to express the proteins with N-terminal histidine tag. *E. coli* DH5α was transformed with pET15b containing the cloned genes by electroporation. Primers designed to construct the site-directed mutant proteins are described in **Table S2**. The mutations were obtained using the mutagenesis kit "*QuikChange II Site-Directed Mutagenesis*" from *Agilent Technologies* as described by the manufacturer.

4.6.2 – Protein expression and purification

Gene expression was induced in *Escherichia coli* BL21 (*DE3*) or AD494 (DE3) strains through by the addition of isopropyl 1-thio-β-D-galactopyranoside (IPTG) in the exponential phase (OD_{600nm} 0.6-1). Cells were grown in a shaker/incubator at 37 °C in LB broth until the exponential phase. IPTG concentrations, times and temperatures of induction and antibiotics added are described in the **Table S3**. Cells were collected by centrifugation (5000rpm/20 min, 4 °C) then resuspended and sonicated in 500 mM of NaCl, 20 mM of sodium phosphate pH 7.4, 0.2 mg/mL of lysozyme, 1x SigmaFAST Protease Inhibitor Tablet (Sigma) 30% Sucrose and 1% Glycerin (and 1 mM of DTT for *Mt*AhpE). 1 %w/v of Streptomycin was added to the lysate and it was incubated on ice for 20min. The lysate was then centrifuged (17,000rpm/40 minutes, at 4 °C), and the soluble proteins were filtered using a 0.45 µm pore membrane. The target proteins were purified by affinity chromatography (Ni-NTA Agarose column, Qiagen) using the ÄKTA Protein Purification system (GE Health Care Life Sciences). The 5 ml Column was washed with 3 column volumes of 500 mM NaCl, 20 mM sodium phosphate pH 7.4, 50 mM and then with 100 mM of imidazole. An imidazole gradient (100-500 mM) was used for protein elution. Fractions were analyzed by 14% SDS-PAGE. Buffer exchange and concentration of purified proteins were performed in HiTrap® Desalting Columns (GE Healthcare) and Amicon Centrifugal device (sizes according each protein) (Millipore ®), respectively.

4.6.3 – Protein quantification

Protein quantification was performed on basis of direct protein 280 nm absorbance using the molecular weight and extinction coefficient (Ɛ) prediction in *protoparam* tools (Gasteiger *et al*, 2005).

4.6.4 – Lipoamide reduction to dihydrolipoamide

Lipoamide was incubated with sodium borohydride (10 lipoamide:1 $NaBH_4$) for 1 hour at 37 ºC. HCl (1-2 M) was added to react with the excess of borohydride. 1 volume of dichloromethane was used to separate the organic (collected) from aqueous phases. The collected organic phase was mixed

with sodium sulfate (powder of, Na_2SO_4) to dehydrate the solution. Finally, the supernatant was transferred to a clean eppendorf and dried by a N_2 flux, and then absolute ethanol was used to resuspend the dihydrolipoamide.

4.6.5 – Crystallization.

All crystals were grown at 18 °C using the hanging-drop vapor diffusion method. *Cv*OhrB wildtype and mutants were grown by adding 10mg/ml of 6xHis-protein (diluted in 5mM Tris-HCl pH 7.4, for *Cv*OhrBwt, *Cv*OhrB_C60A and C60S or diluted in 5mM Tris-HCl pH 7.4 and 10 mM DTT for *Cv*OhrBwt-DTT complex in an equal volume with the reservoir solution containing Magnesium Chloride 200mM, BIS-TRIS 100mM pH 5.5 and PEG 3,350 25%w/v. *Cv*OhrB_C60A_DHL and CvOhrB_C60S_DHL complexes were obtained by soaking the previous described grown crystals in the reservoir solution with 5% ethanol and 5 mM dihydrolipoamide during 10 minutes and 16 hours, respectively. *Cv*OhrA wildtype crystals were grown by adding 10mg/ml of 6xHis-protein (diluted in 5mM Tris-HCl pH 7.4) in an equal volume with the reservoir solution containing Potassium Sodium Tartrate 200mM, Tri-Sodium Citrate 100mM pH 5.5, Ammonium Sulfate 2M. *Cv*OhrA_C61S mutant crystals were grown by adding 10mg/ml of 6xHis-protein (diluted in 5mM Tris-HCl pH 7.4 and 50mM NaCl) in an equal volume with the reservoir solution containing Ammonium sulfate 200mM, Sodium acetate 100 mM pH 4, PEG 2,000 30 %w/v. The crystals were all flash frozen in liquid nitrogen and collected at beamline MX2 at Brazilian Synchrotron Light Laboratory (LNLS) for *Cv*OhrBwt and *Cv*OhrBwt-DTT complex. *Cv*OhrAwt, *Cv*OhrB_C60A-DHL and *Cv*OhrB_C60S-DHL crystals were collected at beamline 12.2, and *Cv*OhrA_C60S at beamline 9.2, both at Stanford Synchrotron Radiation Lightsource (SSRL).

4.6.6 – Structural determination

All data were integrated with XDS (Kabsch, 2010) and scaled using AIMELESS from CCP4 program suite (Winn *et al*, 2011). Initial phases were obtained by molecular replacement with PHASER (McCoy *et al*, 2007) using *Pa*Ohr from PDB 1N2F as the search models. Four copies of all the four structures derived from *Cv*OhrB were found in the asymmetric unit. In respect to the two structures derived from *Cv*OhrA, two copies were found in the asymmetric unit. Models were built in COOT (Emsley & Cowtan, 2004) and refined using REFMAC (Vagin *et al*, 2004) and Phenix (Adams *et al*, 2010). Details of the refinement statistics are shown in Table 1. Figure models were generated using PYMOL (Schrödinger) LigPlot+ (Laskowski & Swindells, 2011).

4.6.7 – Crystallographic B-factors and structures superposition

Proteins available in PDB belonging to Ohr subfamily were divided into open or close confirmations. The opened Ohr proteins used were: PDB_{ID} = 4XX2(3 monomers); PDB_{ID} = 6ECY(2 monomers); PDB_{ID} = 6EB4(4 monomers); (PDB_{ID} = 1USP (2 monomers); (PDB_{ID} = 2BJO (2

monomers); (PDB_{ID} = 4NOZ (2 monomers); (PDB_{ID} = 4MH4(2 monomers); (PDB_{ID} = 3LUS (1 monomer (B)) with a total of 18 monomers (*n*). The closed Ohr proteins used were: (PDB_{ID} = 1ZB8(2 monomers); (PDB_{ID} = 1N2F (2 monomers); (PDB_{ID} = 3LUS (1 monomers); PDB_{ID} = 6ED0 (2 monomers) with a total of 7 monomers (*n*). Residue C_α B-factors values were aligned according protein primary structure. Ohr structure monomer superposition was obtained by using the secondary structure matching method for superposition from Coot (Emsley & Cowtan, 2004).

4.6.7 – Parameterization of new molecules for MD simulations

Molecules such as oxidized (sulfenic acid) cysteine, reduced dihydrolipoamide (S_1-H and S^-_2), Dihydrolipoamide forming mixed disulfide with Cys_p (S^-_1 and S_2-S_{cys}) and oxidized lipoamide (S_1-S_2), were all parameterized using the software *Gaussian 09* (Frisch *et al*, 2016). Partial charges were computed using the restricted electrostatic potential (RESP) method (Bayly *et al*, 1993) and the density function theory (DFT) for electronic structure calculations was computed with the PBE functional and dzvp basis set. Equilibrium distances and angles, as well as force constants and VdW parameters were assigned using antechamber (Case *et al*, 2016).

4.6.8 – System preparation for classical MD

The structure of the PDB files were edited to remove all crystallographic waters and change the peroxydatic and resolution cysteines, according to the desired oxidative state. The system was solvated using a default method, with a octahedral box of 12 Å in radius with TIP3P water molecules, and protein parameters correspond to the ff14SB Amber force field (Jorgensen *et al*, 1983; Case *et al*, 2016).

4.6.9 – Classical Molecular Dynamics Simulations

The systems were first subjected to a total of 1000 steps of minimization (10 steps of steepest descent and 990 steps of conjugate gradient minimization). Then, they were slowly heated from 100 to 300 K for 200 picoseconds (ps) at constant pressure, with Berendsen thermostat, with the protein held fixed by using position restraints with a force constant of 200 kcal mol^{-1} $Å^{-2}$. Finally, pressure was equilibrated at 1 bar for 50 ps. Then, free molecular dynamics at NVT ensemble at 300 K, using periodic boundary conditions with a 10 Å cutoff and particle mesh Ewald (PME) summation method for treating the electrostatic interactions was performed. The hydrogen bond lengths were kept at their equilibrium distance by using the SHAKE algorithm. Temperature was kept with Berendsen thermostat. Simulations were performed for the following initial structures: OhrA_close_S^-: Ohr (close conformation) with Cys_p reduced (thiolate) (prepared from PDB_{ID}=6ECY); OhrA_close_SS: Ohr (close conformation) forming disulfide bridge between Cys_p and Cys_r (prepared from PDB_{ID}=6ECY); OhrA_open_S^-: Ohr (open conformation) with Cys_p reduced (thiolate) (prepared from PDB_{ID}=6ED0); OhrA_open_SS: Ohr (open conformation) forming disulfide bridge between Cys_p and Cys_r (prepared from PDB_{ID}=6ED0);

OhrB_open_SS_DHL: Ohr (open conformation) forming disulfide bridge between Cys_p and Cys_r with reduced dihydrolipoamide (S_1H and S_2^-) (prepared from PDBID=6EBG); OhrB_close_S^-: Ohr (close conformation) with Cys_p reduced (thiolate) (prepared from MD of OhrB_open_SS_DHL); OhrB_close_SS: Ohr (close conformation) forming disulfide bridge between Cys_p and Cys_r (prepared from MD of OhrB_open_SS_DHL). For the last system, we observed the Arg-loop kept bending to the opposite direction of the active site, thus restrains were applied preventing the exaggerated Arg-loop opening.

4.6.10 – Steered Molecular Dynamics (SMD)

In SMD simulations, a time-dependent external force is applied to the system to facilitate the achievement of a desired conformational exchange, which could not be achieved by standard MD simulations (Park *et al*, 2003). In particular, the transition between the closed and opened states were achieved by adding to the standard Hamiltonian a harmonic time-dependent potential acting on a defined reaction coordinate (RC). Three systems (OhrB_close_S^-, OhrB_close_SS and OhrB_close_SS_DHL) were tested. The RC was defined as the distance between $C\alpha_{Glu50}$ and $C\alpha_{Arg18,}$ and all systems were previously submitted to a 30 ns MD simulation restraining the RC atoms to maintain a distance from 9.5 to 10.5 Å between them (**Fig. 4a**). Then the SMD simulation was performed increasing the RC distance from 10 to 19 Å, at velocity of 0.33 Å per ns. The experiment was performed at least 46 times. During the transition, we could calculate the exerted force as well as the external work performed on the system. Thus, through the Jarzynski equality: $\boldsymbol{e^{-\Delta G/kT} = \langle e^{-\omega/kT} \rangle}$, where $\boldsymbol{k}$ is Boltzeman constant, $\boldsymbol{T}$ is temperature at equilibrium state and $\boldsymbol{w}$ is the work done by the system due to the external force applied to move the equilibrium state to another, we were able to calculate ΔG for this process (Jarzynski, 1997). For the experiment pulling the lipid carbon chain out form the active site, the distance between $C\alpha_{Glu50}$ and $C10_{carbon\ chain}$ (orange spheres) was followed along the RC. The distance between these atoms was increased by an external force at constant rate of 0.5 Å/ns, from 8.5 Å to 23.5 Å (**Fig. S3**)

4.6.11 – Kinetics of oleic acid hydroperoxide (OAOOH) reduction by *Cv*OhrA

*Mt*AhpE competition assay – *Cv*OhrA (wt and mutants) and *Mt*AhpE were overnight pre-reduced with 50 and 1 mM of DTT, respectively. DTT was then removed using 2 HiTrap® Desalting Columns (5ml) with 50 mM of NaCl and 20 mM of sodium phosphate pH 7.4 (previously purged with N_2). The DTNB reactant was used to confirm protein thiol reduction. The rate constants for the reduction of OAOOH *Cv*OhrA were calculated according to the competitive assay described in (Alegria *et al*, 2017). The assay is based on the redox-dependent changes in the intrinsic fluorescence of the Cys-based peroxidase from *Mycobacterium tuberculosis* (*Mt*AhpE) (Reyes *et al*, 2011; Hugo *et al*, 2009). The experiments ran in 100 mM of sodium phosphate pH 7.4 previously purged with N_2 and the

concentrations of *Mt*AhpE, Ohr, and hydroperoxide used were 2 μM, 2–14 μM, and 1.8 μM, respectively. All measurements were performed in a stopped-flow spectrophotometer (Applied Photophysics SX-18MV) at 25.0±0.5 °C using the sequential mixing mode.

4.6.12 – Ohr specific activities for tBOOH reduction

The specific activities of *Cv*OhrA (wt and mutants) were measured taking advantage of the Absorbance decay due to consumption of NADH measured at A_{340}(ε = 6290 $M^{-1}.cm^{-1}$) in an assay adaptation from (Oliveira *et al*, 2006; Cussiol *et al*, 2010). In this assay, the initial rates were obtained from reaction performed at different enzyme concentrations (0.01 – 0.25 μM) and initiated by adding the same concentration of t-BOOH. Concentration of all other reactants can be found in **figure 5**.

4.6.13 – Hybrid Quantum Molecular Dynamics (QM-MM)

The QM-MM simulations were carried out using the software combination of LIO (for QM) and AMBER (MM) (Nitsche *et al*, 2014; Case *et al*, 2016). The Protein was embedded in an octahedral box of 12 Å in radius with explicit TIP3P water molecules. All used residue parameters correspond to the ff14SB Amber force field, the parameters for reduced, oxidized dihydrolipoamide. As we employed an umbrella sampling scheme, we first defined the reaction coordinate the difference between the S_{Cysp}-S_{Cysr} and the S_{LPA}-S_{Cysp} distances, which was sampled from −2.2 to 2.2 Å in 23 windows sections. The harmonic potentials used had spring constants of about 9.5 $kcal.mol^{-1}$. For each window, several steps of QM calculations were performed for all atoms selected to be treated as QM atom. Final free energy profiles were constructed using the umbrella integration (UI) and weighted histogram analysis method (WHAM) and umbrella integration methods (Kumar *et al*, 1992; Souaille & Roux, 2001; Kästner & Thiel, 2005; Kästner, 2011)

4.7 – References

Van Acker H & Coenye T (2017) The Role of Reactive Oxygen Species in Antibiotic-Mediated Killing of Bacteria. ***Trends Microbiol.*** 25**:** 456–466

Adams PD, Afonine P V., Bunkóczi G, Chen VB, Davis IW, Echols N, Headd JJ, Hung LW, Kapral GJ, Grosse-Kunstleve RW, McCoy AJ, Moriarty NW, Oeffner R, Read RJ, Richardson DC, Richardson JS, Terwilliger TC & Zwart PH (2010) PHENIX: A comprehensive Python-based system for macromolecular structure solution. ***Acta Crystallogr. Sect. D Biol. Crystallogr.*** 66**:** 213–221

Alegria TGP, Meireles DA, Cussiol JRR, Hugo M, Trujillo M, de Oliveira MA, Miyamoto S, Queiroz RF, Valadares NF, Garratt RC, Radi R, Di Mascio P, Augusto O & Netto LES (2017) Ohr plays a central role in bacterial responses against fatty acid hydroperoxides and peroxynitrite. ***Proc. Natl. Acad. Sci.*** 114**:** E132–E141

Atichartpongkul S, Fuangthong M, Vattanaviboon P & Mongkolsuk S (2010) Analyses of the regulatory mechanism and physiological roles of Pseudomonas aeruginosa OhrR, a transcription regulator and a sensor of organic hydroperoxides. ***J. Bacteriol.*** 192**:** 2093–2101

Bayly CI, Cieplak P, Cornell WD & Kollman PA (1993) A well-behaved electrostatic potential based method using charge restraints for deriving atomic charges: The RESP model. ***J. Phys. Chem.*** 97**:** 10269–10280

Belenky P, Ye JD, Porter CBM, Cohen NR, Lobritz MA, Ferrante T, Jain S, Korry BJ, Schwarz EG, Walker GC & Collins JJ (2015) Bactericidal Antibiotics Induce Toxic Metabolic Perturbations that Lead to Cellular Damage. ***Cell Rep.*** 13**:** 968–980

Bryk R, Lima CD, Erdjument-Bromage H, Tempst P & Nathan C (2002) Metabolic enzymes of mycobacteria linked to antioxidant defense by a thioredoxin-like protein. ***Science (80-.).*** 295**:** 1073–1077

Case DA, Betz RM, Cerutti DS, T.E. Cheatham I, Darden TA, Duke RE, Giese TJ, Gohlke H, Goetz AW, Homeyer N, Izadi S, Janowski P, Kaus J, Kovalenko A, Lee TS, LeGrand S, Li P, Lin C, Luchko T, Luo R, et al (2016) Amber 2016.

Clair G, Armengaud J & Duport C (2012) Restricting Fermentative Potential by Proteome Remodeling: AN ADAPTIVE STRATEGY EVIDENCED IN BACILLUS CEREUS. ***Mol. Cell. Proteomics*** 11**:** M111.013102

Cooper DR, Surendranath Y, Devedjiev Y, Bielnicki J & Derewenda ZS (2007) Structure of the Bacillus subtilis OhrB hydroperoxide-resistance protein in a fully oxidized state. ***Acta Crystallogr. Sect. D Biol. Crystallogr.*** 63**:** 1269–1273

Cronan JE (2016) Assembly of Lipoic Acid on Its Cognate Enzymes: an Extraordinary and Essential Biosynthetic Pathway. ***Microbiol. Mol. Biol. Rev.*** 80**:** 429–50

Cussiol JRR, Alegria TGP, Szweda LI & Netto LES (2010) Ohr (organic hydroperoxide resistance protein) possesses a previously undescribed activity, lipoyl-dependent peroxidase. ***J. Biol. Chem.*** 285**:** 21943–50

Cussiol JRR, Alves SV, de Oliveira MA & Netto LES (2003) Organic hydroperoxide resistance gene encodes a thiol-dependent peroxidase. ***J. Biol. Chem.*** 278**:** 11570–8

Dwyer DJ, Belenky PA, Yang JH, MacDonald IC, Martell JD, Takahashi N, Chan CTY, Lobritz MA, Braff D, Schwarz EG, Ye JD, Pati M, Vercruysse M, Ralifo PS, Allison KR, Khalil AS, Ting AY, Walker GC & Collins JJ (2014) Antibiotics induce redox-related physiological alterations as part of their lethality. ***Proc. Natl. Acad. Sci.*** 111**:** E2100–E2109

Emsley P & Cowtan K (2004) Coot: Model-building tools for molecular graphics. ***Acta Crystallogr. Sect. D Biol. Crystallogr.*** 60**:** 2126–2132

Eser M, Masip L, Kadokura H, Georgiou G & Beckwith J (2009) Disulfide bond formation by exported glutaredoxin indicates glutathione's presence in the E. coli periplasm. ***Proc. Natl. Acad. Sci. U. S. A.*** 106**:** 1572–1577

Frisch MJ, Trucks GW, Schlegel HB, Scuseria GE, Robb MA, Cheeseman JR, Scalmani G, Barone V, Petersson GA, Nakatsuji H, Li X, Caricato M, Marenich A, Bloino J, Janesko BG, Gomperts R, Mennucci B, Hratchian HP, Ortiz J V., Izmaylov AF, et al (2016) Gaussian 09, Revision A.02. ***Inc., Wallingford***

Garnica OA, Das K & Dhandayuthapani S (2017) OhrR of Mycobacterium smegmatis senses and responds to intracellular organic hydroperoxide stress. **:** 1–12

Gasteiger E, Hoogland C, Gattiker A, Duvaud S, Wilkins MR, Appel RD & Bairoch A (2005) The Proteomics Protocols Handbook - Chapter 52: Protein Identification and Analysis Tools on the ExPASy Server

Hugo M, Turell L, Manta B, Botti H, Monteiro G, Netto LES, Alvarez B, Radi R & Trujillo M (2009) Thiol and Sulfenic Acid Oxidation of AhpE, the One-Cysteine Peroxiredoxin from *Mycobacterium tuberculosis* : Kinetics, Acidity Constants, and Conformational Dynamics. ***Biochemistry*** 48**:** 9416–9426

Jarzynski C (1997) A nonequilibrium equality for free energy differences. 78**:** 0–3

Jorgensen WL, Chandrasekhar J, Madura JD, Impey RW & Klein ML (1983) Comparison of simple potential functions for simulating liquid water. ***J. Chem. Phys.*** 79**:** 926–935

Kabsch W (2010) *XDS*. ***Acta Crystallogr. Sect. D Biol. Crystallogr.*** 66**:** 125–132

Kästner J (2011) Umbrella sampling. ***Wiley Interdiscip. Rev. Comput. Mol. Sci.***

Kästner J & Thiel W (2005) Bridging the gap between thermodynamic integration and umbrella sampling provides a novel analysis method: 'umbrella integration'. ***J. Chem. Phys.*** 123**:**

Kumar S, Rosenberg JM, Bouzida D, Swendsen RH & Kollman PA (1992) THE weighted histogram analysis method for free-energy calculations on biomolecules. I. The method. ***J. Comput. Chem.*** 13**:** 1011–1021

De La Mora E, Carmichael I & Garman EF (2011) Effective scavenging at cryotemperatures: Further increasing the dose tolerance of protein crystals. ***J. Synchrotron Radiat.*** 18**:** 346–357

Ladjouzi R, Bizzini A, van Schaik W, Zhang X, Rincï¿½ A, Benachour A & Hartke A (2015) Loss of antibiotic tolerance in sod-deficient mutants is dependent on the energy source and arginine catabolism in enterococci. ***J. Bacteriol.*** 197**:** 3283–3293

Laskowski RA & Swindells MB (2011) LigPlot + : Multiple Ligand À Protein Interaction Diagrams for Drug Discovery. **:** 2778–2786

Lesniak J, Barton W a & Nikolov DB (2002) Structural and functional characterization of the Pseudomonas hydroperoxide resistance protein Ohr. ***EMBO J.*** 21**:** 6649–59

Lima-Bittencourt CI, Astolfi-Filho S, Chartone-Souza E, Santos FR & Nascimento AMA (2007) Analysis of Chromobacterium sp. natural isolates from different Brazilian ecosystems. ***BMC Microbiol.*** 7**:** 1–9

Lionta E, Spyrou G, Vassilatis DK & Cournia Z (2014) Structure-based virtual screening for drug discovery: principles, applications and recent advances. ***Curr. Top. Med. Chem.*** 14**:** 1923–1938

Liu Z, Wang H, Zhou Z, Naseer N, Xiang F, Kan B, Goulian M & Zhu J (2016) Differential Thiol-Based Switches Jump-Start Vibrio cholerae Pathogenesis. ***Cell Rep.*** 14**:** 347–354

McCoy AJ, Grosse-Kunstleve RW, Adams PD, Winn MD, Storoni LC & Read RJ (2007) Phaser crystallographic software. ***J. Appl. Crystallogr.*** 40**:** 658–674

Meireles DA, Domingos RM, Gaiarsa JW, Ragnoni EG, Bannitz-Fernandes R, da Silva Neto JF, de Souza RF & Netto LES (2017) Functional and evolutionary characterization of Ohr proteins in eukaryotes reveals many active homologs among pathogenic fungi. ***Redox Biol.*** 12**:** 600–609

Meunier-Jamin C, Kapp U, Leonard G a & McSweeney S (2004) The structure of the organic hydroperoxide resistance protein from Deinococcus radiodurans. Do conformational changes facilitate recycling of the redox disulfide? ***J. Biol. Chem.*** 279**:** 25830–7

Mongkolsuk S, Praituan W, Loprasert S, Fuangthong M & Chamnongpol S (1998a) Identification and Characterization

of a New Organic Hydroperoxide Resistance (ohr) Gene with a Novel Pattern of Oxidative Stress Regulation from Xanthomonas campestrispv . phaseoli Identification and Characterization of a New Organic Hydroperoxide Resi. ***J. Bacteriol.*** 180**:** 2636–2643

Mongkolsuk S, Praituan W, Loprasert S, Fuangthong M & Chamnongpol S (1998b) Identification and Characterization of a New Organic Hydroperoxide Resistance (ohr) Gene with a Novel Pattern of Oxidative Stress Regulation from Xanthomonas campestrispv . phaseoli. ***J. Bacteriol.*** 180**:** 2636–2643

Nitsche MA, Ferreria M, E.Mocskos E & Lebrere MCG (2014) GPU Accelerated Implementation of Density Functional Theory for Hybrid QM / MM Simulations. ***J. Chem. Theory Comput.*** 10**:** 959–967

Oliveira M a, Guimarães BG, Cussiol JRR, Medrano FJ, Gozzo FC & Netto LES (2006) Structural insights into enzyme-substrate interaction and characterization of enzymatic intermediates of organic hydroperoxide resistance protein from Xylella fastidiosa. ***J. Mol. Biol.*** 359**:** 433–45

Ozbuyukkaya G, Ozkirimli Olmez E & Ulgen KO (2013) Discovery of YopE Inhibitors by Pharmacophore-Based Virtual Screening and Docking. ***ISRN Bioinforma.*** 2013**:** 1–12

Park S, Khalili-Araghi F, Tajkhorshid E & Schulten K (2003) Free energy calculation from steered molecular dynamics simulations using Jarzynski's equality. ***J. Chem. Phys.*** 119**:** 3559–3566

Piccirillo E, Alegria TGP, Discola KF, Cussiol JRR, Domingos RM, De Oliveira MA, de Rezende L, Netto LES & do Amaral AT (2018) Structural insights on the efficient catalysis of hydroperoxide reduction by Ohr: Crystallographic and molecular dynamics approaches. ***PLoS One*** 13**:** 1–23

Previato-Mello M, Meireles D de A, Netto LES & Neto JF da S (2017) Global transcriptional response to organic hydroperoxide and the role of OhrR in the control of virulence traits in Chromobacterium violaceum. ***Infect. Immun.*** 85**:** 1–18

Reniere ML, Whiteley AT & Portnoy DA (2016) An In Vivo Selection Identifies Listeria monocytogenes Genes Required to Sense the Intracellular Environment and Activate Virulence Factor Expression. ***PLoS Pathog.*** 12**:** 1–27

Reyes AM, Hugo M, Trostchansky A, Capece L, Radi R & Trujillo M (2011) Oxidizing substrate specificity of Mycobacterium tuberculosis alkyl hydroperoxide reductase E: Kinetics and mechanisms of oxidation and overoxidation. ***Free Radic. Biol. Med.*** 51**:** 464–473

Ruiz-Carmona S, Schmidtke P, Luque FJ, Baker L, Matassova N, Davis B, Roughley S, Murray J, Hubbard R & Barril X (2017) Dynamic undocking and the quasi-bound state as tools for drug discovery. ***Nat. Chem.*** 9**:** 201–206

Saikolappan S, Das K & Dhandayuthapani S (2015) Inactivation of the organic hydroperoxide stress resistance regulator OhrR enhances resistance to oxidative stress and isoniazid in Mycobacterium smegmatis. ***J. Bacteriol.*** 197**:** 51–62

Scior T, Bender A, Tresadern G, Medina-Franco JL, Martínez-Mayorga K, Langer T, Cuanalo-Contreras K & Agrafiotis DK (2012) Recognizing pitfalls in virtual screening: A critical review. ***J. Chem. Inf. Model.*** 52**:** 867–881

Senn HM & Thiel W (2009) QM/MM methods for biomolecular systems. ***Angew. Chemie - Int. Ed.*** 48**:** 1198–1229

Shea RJ & Mulks MH (2002) ohr , Encoding an Organic Hydroperoxide Reductase , Is an In Vivo-Induced Gene in Actinobacillus pleuropneumoniae. 70**:** 794–802

da Silva Neto JF, Negretto CC & Netto LES (2012) Analysis of the Organic Hydroperoxide Response of Chromobacterium violaceum Reveals That OhrR Is a Cys-Based Redox Sensor Regulated by Thioredoxin. ***PLoS One*** 7**:**

Souaille M & Roux B (2001) Extension to the weighted histogram analysis method: Combining umbrella sampling with free energy calculations. ***Comput. Phys. Commun.*** 135**:** 40–57

Vagin AA, Steiner RA, Lebedev AA, Potterton L, McNicholas S, Long F & Murshudov GN (2004) *REFMAC* 5 dictionary: organization of prior chemical knowledge and guidelines for its use. ***Acta Crystallogr. Sect. D Biol. Crystallogr.*** 60**:** 2184–2195

Weik M, Berge J, Gros P, Mcsweeney S, Silman I, Joel L, Houe C, Curie ÂPM & Jussieu P (2002) radiation damage workshop Evidence for the formation of disul ® de radicals in protein crystals upon X-ray. **:** 342–346

Winn MD, Ballard CC, Cowtan KD, Dodson EJ, Emsley P, Evans PR, Keegan RM, Krissinel EB, Leslie AGW, McCoy A, McNicholas SJ, Murshudov GN, Pannu NS, Potterton EA, Powell HR, Read RJ, Vagin A & Wilson KS (2011) Overview of the *CCP* 4 suite and current developments. ***Acta Crystallogr. Sect. D Biol. Crystallogr.*** 67**:** 235–242

Wolfram TJ, LeVeque RM, Kastenmayer RJ & Mulks MH (2009) Ohr, an in vivo-induced gene in Actinobacillus pleuropneumoniae, is located on a genomic island and requires glutathione-S-transferase for activity. ***FEMS Immunol. Med. Microbiol.*** 57**:** 59–68

CHAPTER 5 – ORGANIC HYDROPEROXIDE RESISTANCE PROTEIN AS A POTENTIAL DRUG TARGET – SEARCH FOR INHIBITOR COMPOUNDS

Organic Hydroperoxide resistance protein as a Potential Drug Target – Search for Inhibitor Compounds

Renato M. Domingos[1]; Lucas G. Viviani[2]; Andressa Y. S. Sakugawa[1]; Jademilson C. dos Santos[3]; Marcio V.B. Dias[3]; Antonia T. do Amaral[2]; Luis E.S. Netto[1]

[1]Dep. Genetics and Evolutive Biology – IB, USP, São Paulo, Brazil
[2]Instituto de Química - Universidade de São Paulo, Brazil
[3]Instituto de Ciências Biomédicas – Universidade de São Paulo, Brazil

*To whom correspondence may be addressed. Email: nettoles@ib.usp.br or mdomingos@ib.usp.br

Key words: Ohr/OsmC; thiol-dependent peroxidases; Dihydrolipoamide.

This Chapter still needs further preparation in order to be submitted

5.1 – Main contribution by Renato M. Domingos

I was the main researcher during this work, performing both the experimental work and the computational analysis. The pharmacophore modeling and the differential scanning fluorimetry (DSF) experiments were performed under the guidance of Lucas G. Viviani and Jademilson C. dos Santos, respectively. Although our work needs further experimental procedures to reach final conclusions, it represents the first initial trials for search and rationally design bioactive molecules with potentiality to specifically target Ohr proteins.

5.2 – Abstract

Ohr unique structural and biochemical properties; the strong sensitivity of the Ohr mutants (*Δohr*) to oxidative stress and its absence in mammals and vascularized plants suggest the possibility that Ohr might be a promisor drug target. Indeed, there are some evidences that Ohr enzymes might be implicated with the virulence of some pathogenic bacteria. Therefore, inhibition of Ohr could in principle decrease bacterial chances to cope oxidants released by the host or boost ROS-mediated antibiotic action. To our knowledge, no search for compounds that specifically interact with Ohr is upgoing. Here, we describe the identification of two compounds (C-31 & C-42), which could represent a framework for further studies attempting to find specific Ohr inhibitors. Compound C-42 was selected from *ab initio* design, whereas C-31 was selected from a virtual screening using pharmacophoric models to filters databases containing over 30 million of compounds. Pharmacophoric models were designed considering *Xf*Ohr crystallographic structure (PDB_{ID}=1ZB9). To validate these *in silico* analysis, inhibition of Ohr was measured by the lipoamide-lipoamide dehydrogenase (Lpd) coupled system assay, using *tert*-butyl-hydroperoxide (*t*-BOOH) as the oxidizing substrate. The IC_{50} calculated for C-31 and C-42 were 120-240 μM and 240-320 μM, respectively. Other assays must be performed to understand if any of these two compounds might also be inhibiting the activity of Lpd. Differential scanning fluorimetry (DSF) experiments were also initiated to find fragment of molecules which could physically interact with Ohr protein and consequently changing its melting temperature. Seven different fragments increased Ohr melting temperature (~ 55.98 °C). With these fragments, we intend to perform further soaking experiments with *Cv*OhrA crystals in an attempt to obtain structural information by X-ray crystallography. Although this work needs further experimental procedures, it represents the first trials for search of molecules to specifically target Ohr proteins.

5.3 – Introduction

Organic Hydroperoxide Resistance (Ohr) proteins are antioxidant enzymes which belong to the superfamily of proteins Ohr/OsmC and are present in several pathogenic bacteria, such as *Xylella fasidiosa* (*Xf*) and *Chromobacterium violceum* (*Cv*) and fungi (Mongkolsuk *et al*, 1998a; Lesniak *et al*, 2002; Cussiol *et al*, 2003; Meireles *et al*, 2017). Ohr enzymes display several properties appropriate for a target for drug design: (i) unique structural and biochemical features; (ii) high sensitivity of the Ohr mutants (*Δohr*) to oxidative stress; and (iii) its absence in mammals and vascularized plants (potential hosts). There are also some evidences that Ohr enzymes might be implicated with the virulence of some pathogenic bacteria. For instance, *ohr* gene from *Actinobacillus pleuropneumoniae*, the causative agent of porcine pleuropneumonia, is specifically up-regulated during infection (Shea & Mulks, 2002; Wolfram *et al*, 2009). Moreover, studies in *Listeria monocytogenes* and *mycobacterium smegmatis*, facultative intracellular bacterial pathogens, showed *ohr* played a crucial role for bacteria survival into the phagosomes in the host macrophages (Saikolappan *et al*, 2015; Reniere *et al*, 2016).

ohr expression is frequently controlled by the redox sensor OhrR, which responds to organic hydroperoxide. OhrR belongs to the MarR family of transcription factors, which contains many other thiol-based redox-sensing regulators that respond to redox active compounds (Previato-Mello *et al*, 2017; Garnica *et al*, 2017). Studies also pointed Ohr and its transcriptional repressor OhrR being crucial to the successful adaptation of *Bacillus cereus* to the gastrointestinal (GI) tract environment (Clair *et al*, 2012). Ohr displays a unique folding, very distinct from other important peroxidases, such as peroxiredoxins and glutathione peroxidase (Lesniak *et al*, 2002; Oliveira *et al*, 2006). Another differential characteristic of Ohr sub-family is the nature of its reducing agent. Contrary to other well-known peroxidases, evidences show that Ohr can only be reduced by lipoylated proteins and not by thioredoxin, glutaredoxin or glutathione (Cussiol *et al*, 2003; Meunier-Jamin *et al*, 2004; Cussiol *et al*, 2010). These unique characteristics and the emergence of data showing Ohr involvement in virulence make these Cys-based proteins very promissing drug targets.

Frequently, drug design and screening are procedures based on X-ray protein structures and on the available interactional properties of the enzyme active site. These techniques are known as structure-based drug discovery (SBDD), which are raising as tools for fast and low cost drug design (Lionta *et al*, 2014). Together, these virtual methodologies for bioactive compounds identification are raising in efficiency as computational power and tools also increase (Ruiz-Carmona *et al*, 2017; Ozbuyukkaya *et al*, 2013; Scior *et al*, 2012). In this work, we took advantage of our previous in-dept analyses (Domingos *et al,* 2018; **Chapter 4** of this thesis) evaluating the dynamics and biochemical environment at the active site of Ohr, which is highly conformational dependent. Indeed, Ohr was shown to be most stable in its closed state. Therefore, here we described studies taking advantage of the Ohr structure from the important plant pathogen *X. fastidiosa* (PDB_{ID}=1ZB9) in the closed state. We performed *ab initio, in silico* and *in vitro* approaches for searching compounds that could inhibit Ohr activity. We found two promising compounds: C-42 from *ab initio* design and C-31 from a virtual screening performed against

pharmacophore models. To validate these *in silico* studies, lipoamide-Lpd coupled assays were performed using t-BOOH as the final reactant. The calculated IC_{50} values were within the 120-240 μM and 240-320 μM ranges for C-31 and C-42, respectively. Furthermore, we initiated DSF in an attempt to find fragment compounds, which could interact at different regions of the Ohr active site. If successful, this approach would allow us to perform organic chemistry synthesis of larger molecules, containing the fragments that we found that supposedly interact with multiple regions of Ohr active site.

5.4 – Results

5.4.1 – Pharmacophore Model

As previously mentioned, the pharmacophore model was built considering the *Xf*Ohr structure (PDB_{ID} = 1ZB9) obtained by our group (Oliveira *et al*, 2006). This structure was co-crystalized with a PEG molecule into the active, which was postulated to be mimicking the Ohr substrates. Thus, Ohr-

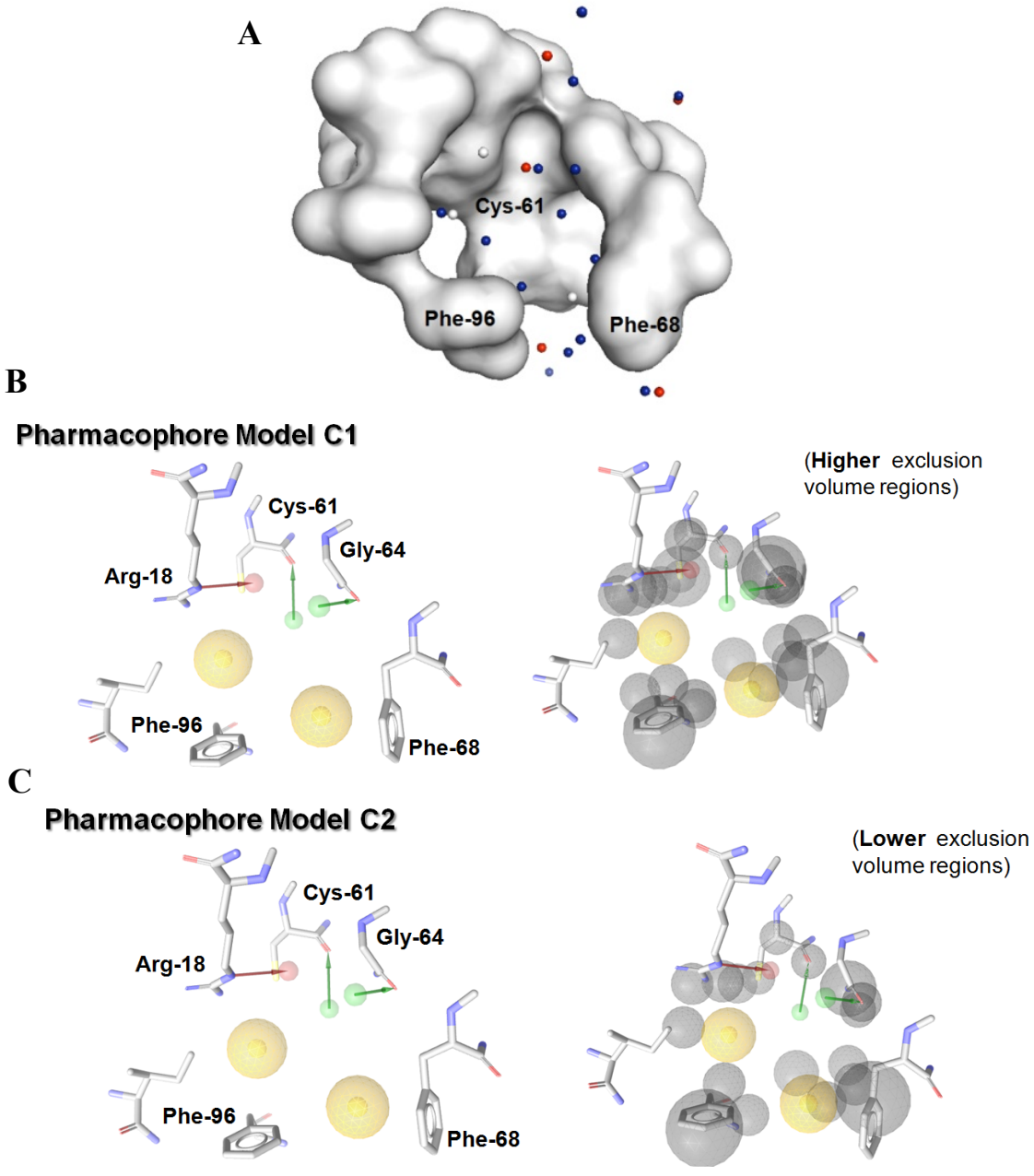

Fig. 1 – Pharmacophore model design. **A** represents the spatial representation of molecular interactions at XfOhr active site (PDB_{ID}=1ZB9), (●) hydrophobic interactions; (●) hydrogen bond acceptors; (●) Hydrogen bond donors. **B** & **C**, Pharmacophore models: atoms: (●) Carbon; (●) oxygen (●) nitrogen. "Hot spots": (●) hydrophobic; (●) hydrogen acceptors (●) hydrogen donors. **Model C1** was designed considering interactions with conserved residues with low mobility. **Model C2** is identical to C1 but the exclusion volume was reduced in order to apply less restricting during compound selection by virtual screening.

PEG interactions were considered when the pharmacophore model was created. Another important point to consider is that the *Xf*Ohr structure (PDB_{ID} = 1ZB9) is in the close state, which is the most prevalent conformation in solution (Domingos *et al*, 2018, at **Chapter 4**). Initially, we determined energetically favorable binding sites at the active pocked of *Xf*Ohr taking advantage of the GRID 22C software (Goodford, 1985). Potential proton donors and receptors were identified as well as hydrophobic interaction regions (**Fig. 1A**). Then, two pharmacophore models were developed **(Fig. 1B & C**), employing the Ligandscout 3.01 software (Wolber & Langer, 2005). Both models were similar and contained two hydrogen donors; one hydrogen acceptor and two hydrophobic regions. However, model 1 presented a higher exclusion volume than model 2, so the selection of compounds was differently restricted when applying both models (**Fig. 1B & C**). The virtual screening was then performed applying the pharmacophore models against the ZINC virtual compound data base (over 35 million compounds) (Irwin & Shoichet, 2005). 47 compounds were selected, 4 from model 1 and 43 from model 2. From all, 33 compounds were commercially available and acquired for enzymatic assays (**Table S1**).

5.4.2 – Electrophilic ligand design

It is well known that nucleophilicity of thiols (RSH) increases when they are ionized into thiolates (RS^-). These nucleophiles can irreversibly react with electrophilic compounds, which in the case of thiol-based enzymes, such as Ohr, would fully inhibit their enzymatic activity (Otto &

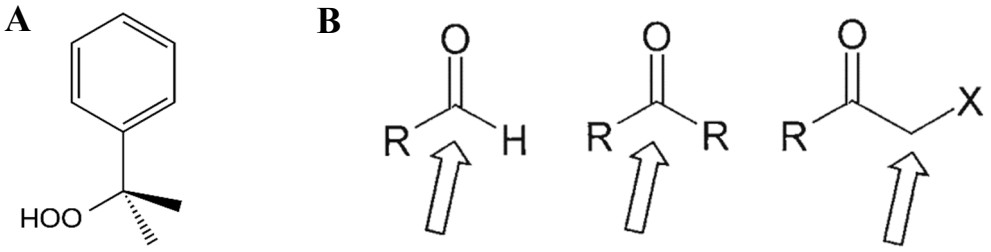

Fig. 2 – Electrophilic functional groups with susceptibility to attack the peroxidatic cysteine sulphur at Ohr active site. **A** Structure of cumene hydroperoxide, a synthetic organic hydroperoxide towards which Ohr shows reactivity. **B** Electrophilic groups considered to design a rational inhibitor for Ohr (aldehyde, ketone and α-halo methyl ketone). Arrows points the electrophilic atom which would suffer the nucleophilic attack by the cysteine thiolate.

Schirmeister, 1997; Lopachin & Gavin, 2017). Thus, we attempt to rationally design potential inhibitors for Ohr by considering the core structure of a synthetic organic hydroperoxide towards which Ohr could react, such as cumene hydroperoxide (**Fig.2 A**). Therefore, we searched in the ZINC virtual compound database for compounds structurally similar with cumene but containing an electrophilic moiety (**Fig.2 B**). Three different compounds were selected and purchased for further enzymatic assays (**Table S1**).

5.4.3 – Experimental conditions standardization of the inhibitor activity assay

Prior to the tests of the purchased compounds, optimization of the lipoamide/Lpd coupled assay was performed (Cussiol *et al*, 2010). We tried several concentrations of either Lpd (1.0, 2.5 and 5.0 µM)

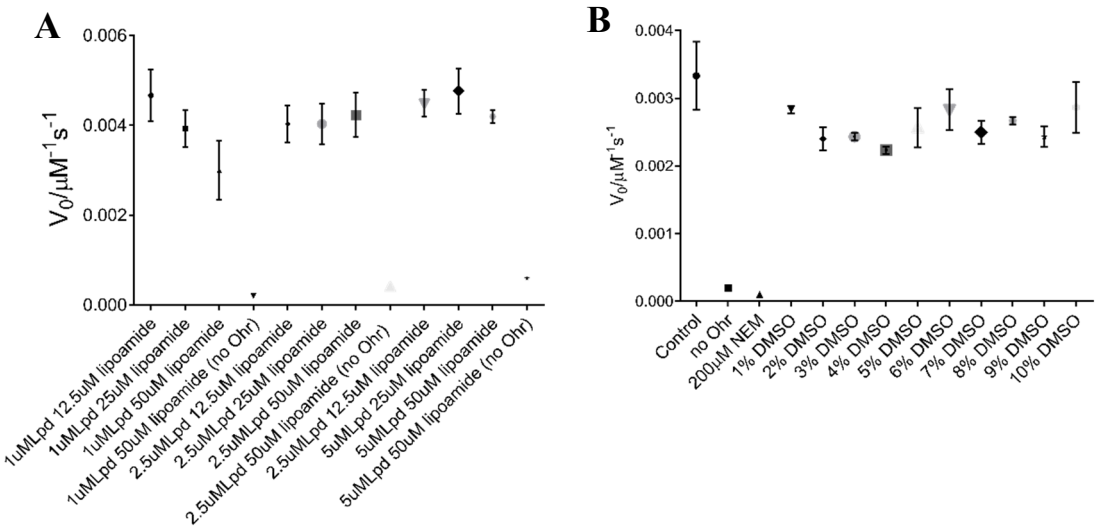

Fig. 3 – Reaction system standardization for the evaluation of the potential inhibitor activity for the selected compounds. **A** and **B** correspond to the assay standardization where the concentrations of LpD, lipoamide and DMSO where evaluated. The experimental conditions: 50 mM Sodium phosphate buffer (pH 7.4), 100 µM DTPA, 350 µM NADH, lipoamide (variable concentrations), Lpd (variable concentration), DMSO (variable concentrations, when present), 200 µM t-BOOH at 37°C.

and lipoamide (12.5, 25 and 50 µM), since these compounds also contain thiol groups (**Fig. 3A**). We would like to use the minimal amount of Lpd and lipoamide that did not limit the reaction rate. The assay conditions were then set to be performed with lipoamide 12.5 µM and Lpd 1 µM. Considering the wide range of solubilities, all the compounds to be tested were dissolved in 100% dimethyl sulfoxide (DMSO). Therefore, we evaluated the DMSO interference by itself in the Ohr enzymatic activity (**Fig. 3B**). Then, we chose 1 mM as the initial concentration to test the inhibitory potency of the compounds to be tested. This concentration corresponded to more than ten times dilution, therefore, we evaluated

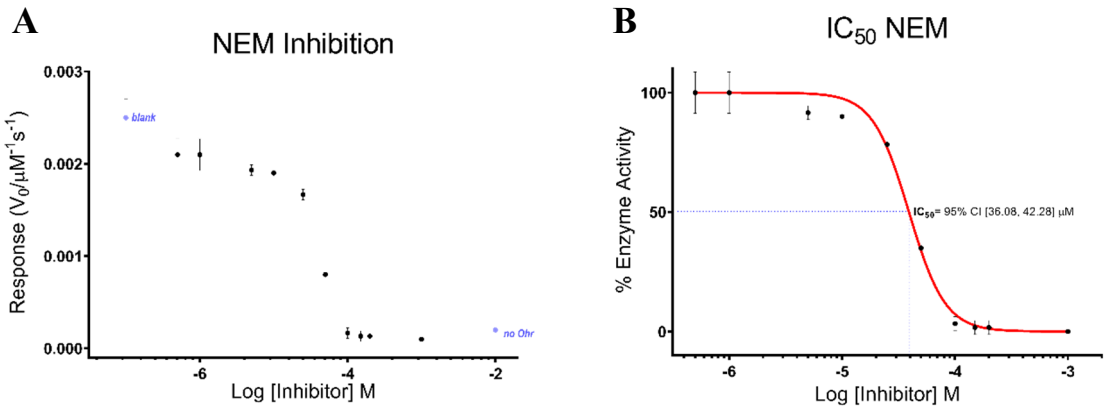

Fig. 4 – IC50 standardization assay. **A** & **B** represent the IC_{50} determination using the N-Ethylmaleimide (NEM) irreversible inhibitor of thiol-enzymes. Experimental conditions: 50 mM Sodium phosphate buffer (pH 7.4), 100 µM DTPA, 350 µM NADH, 12.5 µM lipoamide, 1 µM Lpd, 10% DMSO, 200 µM t-BOOH and 1 mM of target compound, and the assay was performed at 37°C.

the interference of 1 to 10% of DMSO on the Ohr activity (**Fig. 3B**). Not much interference was detected

for 10% DMSO, thus we decided to use 10% DMSO as it would allow us to test a very high concentration of compound for the initial screenings (1 mM).

Once we standardized the experimental test conditions, we performed an IC_{50} control assay with a well-known irreversible inhibitor of thiol proteins: N-Ethylmaleimide (NEM). The corresponding IC_{50} value was within the 36.0-42.0 µM range, in the 95% confidence (**Fig. 4A & B**). This IC_{50} value in the µM range indicated that the employed experimental conditions were sensitive enough to identify the inhibitory capacity of the target compounds.

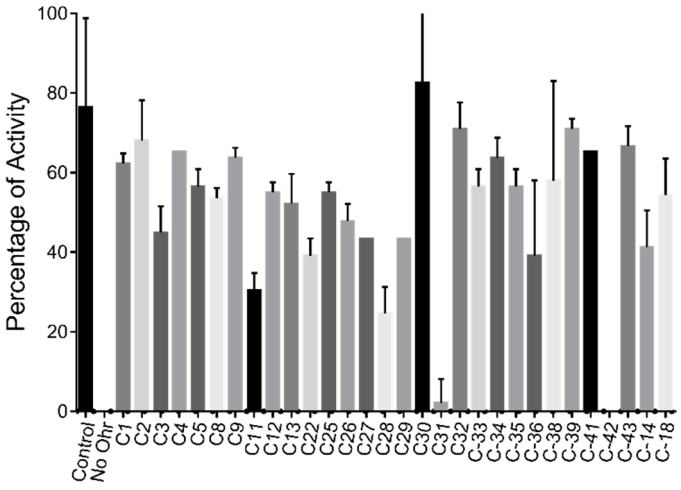

Fig. 5 – Screening of the Inhibitory capacity for the selected compounds. Experimental conditions: 50 mM Sodium phosphate buffer (pH 7.4), 100 µM DTPA, 350 µM NADH, 12.5 µM lipoamide, 1 µM Lpd, 10% DMSO, 20 µM t-BOOH and 1 mM of target compound, and the assay was performed at 37°C.

Then, we performed an initial evaluation of the inhibitory potencies of the target compounds. Initially the assay was performed at the same conditions as the assays shown in **figure 4**. However, the high concentration of peroxide (200 µM) employed in those assays might outcompete the target compounds for the interaction with Ohr. Indeed, no inhibition was detected in such conditions (results not shown). Therefore, several concentrations of peroxide were tested, until we achieved 20 µM as the

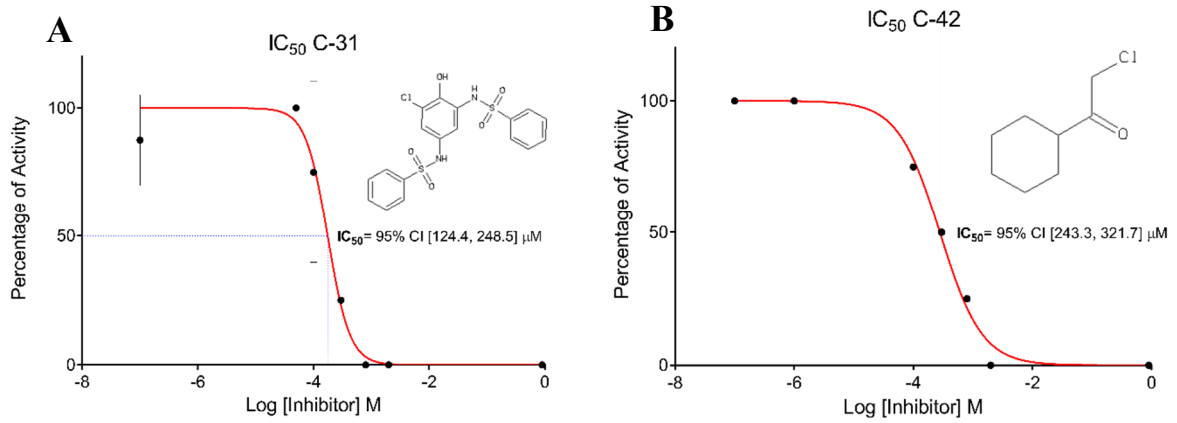

Fig. 6 – IC50 determination. **A** IC_{50} determination for the virtual screening selected compound. **B** IC_{50} determination for the theoretically designed compound. The IC_{50} determination was performed by fitting the equation (*log(inhibitor) vs. response*) from *GraphPad Prism 7 in*to the data. Experimental conditions: 50 mM Sodium phosphate buffer (pH 7.4), 100 µM DTPA, 350 µM NADH, 12.5 µM lipoamide, 1 µM Lpd, 10% DMSO, 20 µM t-BOOH at 37°C. The target compounds concentration varied from 2 to 0.0005 mM.

ideal concentration to detect the inhibitory activity for some of the target compounds at 1 mM concentration (**Fig. 5**).

5.4.4 – IC_{50} determination for the inhibitor compounds

From the previous analysis, two compounds showed inhibitory capacity of near 100% of the Ohr activity (**figure 5)**. Compound C-42 was rationally designed by adapting in the structure of cumene an electrophilic α-halo methyl ketone moiety (**Fig. 6B**). Compound C-31 was selected by the virtual screening, applying the pharmacophoric model 2 (**Fig. 6A**). The IC_{50} values for the inhibition of Ohr were 120-240 µM for C-31 compound and 240-320 µM for C-42, both considering the 95% confidence range.

5.4.5 – DSF approach

In order to get additional experimental information about the Ohr active site physicochemical microenvironment and increase the efficiency of our inhibitor compounds search, we decide to use an experimental technique widely applied in the pharmaceutical industry: the DSF (**Fig. 7A**) (Niesen *et al*, 2007). This technique is based on the identification of small fragments of molecules with the capacity of interacting with enzymatic cavities. A library containing 500 fragments of compounds belonging to our collaborator Dr. Marcio Dias (ICB – USP) was screened to search for fragments that might induce a shift in the Ohr melting temperature (Tm) (**Fig. 7B**). The structure and respective Ohr Tm associated to each of the fragment molecules, which showed positive increase in the Ohr Tm, are shown in **figure 8**. It is expected that each one of these molecular fragments may have distinct preferences for different

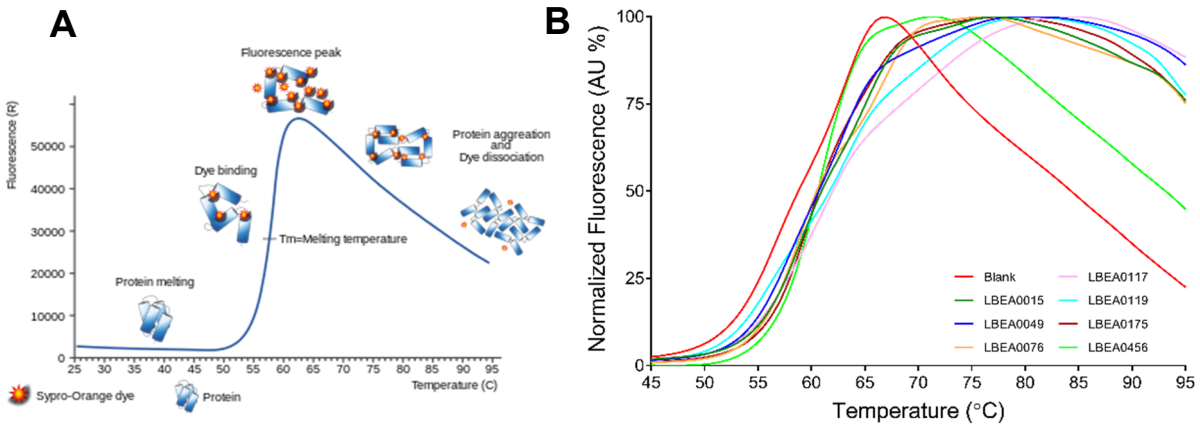

Fig. 7 – DSF assay – The assay was performed with 5mg/ml *Xf*Ohr diluted in 20mM Phosphate buffer and 50mM NaCl. 12 mM of target compound dissolved in DMSO 100% was added to the protein. The DSF was performed following the method described in Niesen *et al*, 2007. **A** illustrative graphic explaining the DSF method. **B** The screening was performed with around 500 compounds, however there are only shown some positive hits. The curves were normalized and melting temperatures (Tm) were determine by fitting the Boltzmann equation from *GraphPad Prism 7* into the data.

regions of the Ohr active site. Thus, we intended to map the region of interaction of each fragment by biophysical methodologies, such as soaking experiments with Ohr protein crystals. We intended to take advantage of the well standardized crystal growth of *Cv*OhrA protein in the close conformation (most

prevalent in solution) for these soaking experiments. The additional information from the fragment structures and the tridimensional location of interaction with the protein, would allow us to rationally synthetize a larger molecule by merging the structure characteristics of the interacting fragments, aiming the increase of the number of interactions between molecule and protein, which in turn would increase their affinity and the molecule inhibitory potency.

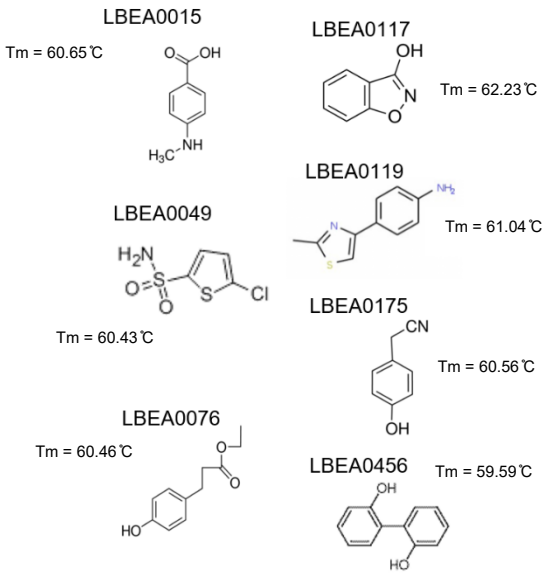

Fig. 8 – DSF-derived compounds with substantial Tm shifts. There is represented the structure of the compounds which presented Tm shifts comparing with the Tm control (~ 55.98 °C). Melting temperatures are indicated in the figure.

5.5 – Discussion

Despite all evidence suggesting that the Ohr targeting could contribute to fight infections, to date, there are no successful efforts in finding specific inhibitors for Ohr. Our work represents the first effort with some promising results, in this direction. Here, we designed potential Ohr inhibitors through pharmacophoric modeling and further application of virtual screening towards a virtual compound database. Furthermore, by knowing that Ohr is a Cys-based protein that depend on the thiolate nucleophilicity for its activity, we designed some electrophilic compounds, which could inhibit Ohr activity by irreversible reaction with the peroxidatic cysteine. From these two approaches, two compounds were selected through enzymatic assays. Moreover, an experimental technique was also carried out: the DSF. By applying these three different techniques, we intended to increase our chances of designing potential inhibitors with great specificity for Ohr active cavity.

Several Ohr inhibitory compounds were selected by applying our pharmacophoric model on the virtual screening applied against the ZINC compound database. The pharmacophoric models were designed based on the closed state of Ohr protein from *X. fastidiosa*, an important pathogenic bacterium (Simpson *et al*, 2000). An initial evaluation of the possible interaction found in the active cavity of the protein showed several regions of hydrogen acceptors and donors' interactions and regions with strong potential for hydrophobic interactions (**Fig. 1A**). Our model was designed considering two hydrogen donors; one hydrogen receptor and two hydrophobic interaction regions (**Fig. 1A & B**). All these interactions are provided by conserved residues, positioned at relatively stable positions. After *in vitro* evaluation of the selected compounds (**Fig. 5**), one of them (**C-31** in **Table S1**) showed promising inhibitory activity when added at 1 mM concentration.

In another approach, three different electrophilic moieties were placed in the core structure of a known synthetic Ohr substrate, the cumene hydroperoxide, in an attempt to specifically and irreversibly cease Ohr activity. Cumene hydroperoxide is a synthetic hydroperoxide, which is known to rapidly react with Ohr (10^6-10^7 M^{-1} s^{-1}). Thus, we rationally selected some electrophilic moieties well known know to react with the thiolate in Cys-based proteins, in an attempt to specifically target Ohr. Aldehyde, ketone and α-halo methyl ketone electrophilic derivatives of cumene-based compounds are commercially available and were purchased (**Fig. 2B**). After *in vitro* evaluations, the α-halo methyl ketone derivative (**C-42** in **Table S1**) displayed promising inhibitory activity (**Fig. 5**).

IC_{50} were in the following ranges 120-240 and 240-320 μM at a 95% confidence range for compounds C-31 and C-42, respectively (**Fig. 6**). These values were considerably higher than the IC_{50} obtained for NEM (36 – 42 μM) (**Fig. 4**). Yet, the NEM inhibition capacity gets even superior, when consideration that 10 times less hydroperoxide was used in the conditions of Figure 6 (C-31 and C-42) than similar experiment in Figure 4 (NEM), the substrate (hydroperoxide) can compete with the inhibitor for Ohr. However, the NEM molecule is very small and promiscuous, and it could easily react with all available thiols.

Although at this point we did not succeed in finding a specific inhibitor for Ohr, the selection of the compounds described here revealed several biophysical properties (hydrophobicity region and larger size) that could be considered in further development. Further assays must be carried out to evaluate if any of the compounds is inhibiting the activity of Lpd or lipoamide and not specifically Ohr. For instance, it should be verified if the selected compounds can inhibit the reduction of DTNB by Lpd-lipoamide, using NADH as electron donor.

Through DSF we selected seven fragment compounds which would physically interact and stabilize Ohr (**Fig. 7B**). Fragment molecules selected with DSF require further biophysical analysis to better understand how the physical contacts provoke changes in the melting temperatures. This information is crucial to experimentally find different hot spot regions in the protein active cavity, allowing further synthesis of stronger and more specific inhibitors. One way of mapping these regions would be performing soaking experiments with Ohr crystals. The *Xf*Ohr (PDB_{ID}=1ZB9) crystal conditions were unsuccessfully reproduced. Then, we intend to use the very well standardized crystal conditions for easily grow *Cv*OhrA crystals. Although *Cv*OhrA was not the protein used in DSF, it shares all the conserved physicochemical properties in the active site with *Xf*Ohr. Due to a lack of time, we could not perform such experiments.

Due to Ohr unique physicochemical properties: the strong sensitive Ohr mutants of important pathogenic bacteria to oxidative stress (Mongkolsuk *et al*, 1998b; da Silva Neto *et al*, 2012; Alegria *et al*, 2017); the Ohr involvement in bacterial virulence (Shea & Mulks, 2002; Wolfram *et al*, 2009; Clair *et al*, 2012; Saikolappan *et al*, 2015; Liu *et al*, 2016; Reniere *et al*, 2016); and its absence in mammals and vascularized plants (Meireles *et al*, 2017), raise Ohr as targets for drug development. The Ohr inhibition could decrease bacterial chances in overcoming the host defenses. Moreover, the fact that several reports have described the production of oxidants as mechanism of action of some antibiotics, suggests that the discovery of bioactive compound with the ability to inhibit Ohr peroxidase activity could also work as a new antibiotic boosting molecule (Dwyer *et al*, 2014; Belenky *et al*, 2015; Ladjouzi *et al*, 2015; Van Acker & Coenye, 2017). Although our work needs further experimental procedures to reach final conclusions, it represents the first initial trials for search and rationally design bioactive molecules with potentiality to specifically target Ohr proteins.

5.6 – Methods

5.6.1 – Pharmacophore model and virtual screening

The Ohr structure (PDB_{ID} = 1ZB9) was previously, energetically minimized, using *SYBYL 8.0*, (Tripos International). The energetic favorable binding sites used for the designing of the pharmacophore models were determined by using the software package *GRID 22C* (Goodford, 1985). The pharmacophoric models were generated though *LIGANSCOUT 3.01* (Wolber & Langer, 2005), taking into account residues with less mobility (Piccirillo *et al*, 2018) and high level of conservation (Meireles *et al*, 2017) at the active site. Two pharmacophore models were designed (**Fig. 1**) and used to filter the ZINC virtual database containing over 30 million of compounds (Irwin & Shoichet, 2005).

5.6.2 – Peroxidatic activity assay for screening and IC_{50} determination

The reaction was initiated by addition of hydroperoxide (200 μM for IC_{50} of NEM and 20 μM for screening and IC_{50} of selected compounds) and followed though the NADH consumption (ε340nm = 6290 $M^{-1}.cm^{-1}$). The assay was performed at the following conditions: 50 mM Sodium phosphate buffer (pH 7.4), 100 μM DTPA, 350 μM NADH, 12.5 μM lipoamide, 1 μM Lpd, 10% DMSO, at 37°C. The target compounds concentration was 1 mM for the compound activity screening and varied from 2 to 0.0005 mM for IC_{50} determination. IC_{50} was calculated by fitting the equation (*log(inhibitor) vs. response*) from *GraphPad Prism 7* into the data.

5.6.3 – DSF experiments

The DSF analysis was performed as described in (Niesen *et al*, 2007) with 5 mg/ml of XfOhr diluted in 20 mM Sodium phosphate buffer (pH 7.4) and 50 mM of NaCl in presence of 12 mM of screening compound. dissolved in 100% of DMSO. The compounds were part of the over 500 fragment compounds library belonging to our collaborator Dr. Marcio Dias (ICB – USP). The curves were normalized and melting temperatures (Tm) were determine by fitting the Boltzmann equation from *GraphPad Prism 7* into the data.

5.7 – References

Van Acker H & Coenye T (2017) The Role of Reactive Oxygen Species in Antibiotic-Mediated Killing of Bacteria. ***Trends Microbiol.*** 25**:** 456–466

Alegria TGP, Meireles DA, Cussiol JRR, Hugo M, Trujillo M, de Oliveira MA, Miyamoto S, Queiroz RF, Valadares NF, Garratt RC, Radi R, Di Mascio P, Augusto O & Netto LES (2017) Ohr plays a central role in bacterial responses against fatty acid hydroperoxides and peroxynitrite. ***Proc. Natl. Acad. Sci.*** 114**:** E132–E141

Belenky P, Ye JD, Porter CBM, Cohen NR, Lobritz MA, Ferrante T, Jain S, Korry BJ, Schwarz EG, Walker GC & Collins JJ (2015) Bactericidal Antibiotics Induce Toxic Metabolic Perturbations that Lead to Cellular Damage. ***Cell Rep.*** 13**:** 968–980

Clair G, Armengaud J & Duport C (2012) Restricting Fermentative Potential by Proteome Remodeling: AN ADAPTIVE STRATEGY EVIDENCED IN BACILLUS CEREUS. ***Mol. Cell. Proteomics*** 11**:** M111.013102

Cussiol JRR, Alegria TGP, Szweda LI & Netto LES (2010) Ohr (organic hydroperoxide resistance protein) possesses a previously undescribed activity, lipoyl-dependent peroxidase. ***J. Biol. Chem.*** 285**:** 21943–50

Cussiol JRR, Alves SV, de Oliveira MA & Netto LES (2003) Organic hydroperoxide resistance gene encodes a thiol-dependent peroxidase. ***J. Biol. Chem.*** 278**:** 11570–8

Dwyer DJ, Belenky PA, Yang JH, MacDonald IC, Martell JD, Takahashi N, Chan CTY, Lobritz MA, Braff D, Schwarz EG, Ye JD, Pati M, Vercruysse M, Ralifo PS, Allison KR, Khalil AS, Ting AY, Walker GC & Collins JJ (2014) Antibiotics induce redox-related physiological alterations as part of their lethality. ***Proc. Natl. Acad. Sci.*** 111**:** E2100–E2109

Garnica OA, Das K & Dhandayuthapani S (2017) OhrR of Mycobacterium smegmatis senses and responds to intracellular organic hydroperoxide stress. **:** 1–12

Goodford P (1985) A Computational Procedure for Determining Energetically Favourable Binding Sites on Biologically Important Macromolecules. ***J. Med. Chem.*** 28**:** 849–857

Irwin JJ & Shoichet BK (2005) ZINC - A free database of commercially available compounds for virtual screening. ***J. Chem. Inf. Model.*** 45**:** 177–182

Ladjouzi R, Bizzini A, van Schaik W, Zhang X, Rincï¿½ A, Benachour A & Hartke A (2015) Loss of antibiotic tolerance in sod-deficient mutants is dependent on the energy source and arginine catabolism in enterococci. ***J. Bacteriol.*** 197**:** 3283–3293

Lesniak J, Barton W a & Nikolov DB (2002) Structural and functional characterization of the Pseudomonas hydroperoxide resistance protein Ohr. ***EMBO J.*** 21**:** 6649–59

Lionta E, Spyrou G, Vassilatis DK & Cournia Z (2014) Structure-based virtual screening for drug discovery: principles, applications and recent advances. ***Curr. Top. Med. Chem.*** 14**:** 1923–1938

Liu Z, Wang H, Zhou Z, Naseer N, Xiang F, Kan B, Goulian M & Zhu J (2016) Differential Thiol-Based Switches Jump-Start Vibrio cholerae Pathogenesis. ***Cell Rep.*** 14**:** 347–354

Lopachin RM & Gavin T (2017) Thiolate Sites : Relevance To Pathophysiological. 50**:** 195–205

Meireles DA, Domingos RM, Gaiarsa JW, Ragnoni EG, Bannitz-Fernandes R, da Silva Neto JF, de Souza RF & Netto LES (2017) Functional and evolutionary characterization of Ohr proteins in eukaryotes reveals many active homologs among pathogenic fungi. ***Redox Biol.*** 12**:** 600–609

Meunier-Jamin C, Kapp U, Leonard G a & McSweeney S (2004) The structure of the organic hydroperoxide resistance protein from Deinococcus radiodurans. Do conformational changes facilitate recycling of the redox disulfide? ***J. Biol. Chem.*** 279**:** 25830–7

Mongkolsuk S, Praituan W, Loprasert S, Fuangthong M & Chamnongpol S (1998a) Identification and Characterization of a New Organic Hydroperoxide Resistance (ohr) Gene with a Novel Pattern of Oxidative Stress Regulation from Xanthomonas campestrispv . phaseoli. ***J. Bacteriol.*** 180**:** 2636–2643

Mongkolsuk S, Praituan W, Loprasert S, Fuangthong M & Chamnongpol S (1998b) Identification and Characterization of a New Organic Hydroperoxide Resistance (ohr) Gene with a Novel Pattern of Oxidative Stress Regulation from Xanthomonas campestrispv . phaseoli Identification and Characterization of a New Organic Hydroperoxide Resi. ***J. Bacteriol.*** 180**:** 2636–2643

Niesen FH, Berglund H & Vedadi M (2007) The use of differential scanning fluorimetry to detect ligand interactions that promote protein stability. ***Nat. Protoc.*** 2**:** 2212–2221

Oliveira M a, Guimarães BG, Cussiol JRR, Medrano FJ, Gozzo FC & Netto LES (2006) Structural insights into enzyme-substrate interaction and characterization of enzymatic intermediates of organic hydroperoxide resistance protein from Xylella fastidiosa. ***J. Mol. Biol.*** 359**:** 433–45

Otto H-H & Schirmeister T (1997) Cysteine Proteases and Their Inhibitors. ***Chem. Rev.*** 97**:** 133–172

Ozbuyukkaya G, Ozkirimli Olmez E & Ulgen KO (2013) Discovery of YopE Inhibitors by Pharmacophore-Based Virtual Screening and Docking. ***ISRN Bioinforma.*** 2013**:** 1–12

Piccirillo E, Alegria TGP, Discola KF, Cussiol JRR, Domingos RM, De Oliveira MA, de Rezende L, Netto LES & do Amaral AT (2018) Structural insights on the efficient catalysis of hydroperoxide reduction by Ohr: Crystallographic and molecular dynamics approaches. ***PLoS One*** 13**:** 1–23

Previato-Mello M, Meireles D de A, Netto LES & Neto JF da S (2017) Global transcriptional response to organic hydroperoxide and the role of OhrR in the control of virulence traits in Chromobacterium violaceum. ***Infect. Immun.*** 85**:** 1–18

Reniere ML, Whiteley AT & Portnoy DA (2016) An In Vivo Selection Identifies Listeria monocytogenes Genes Required to Sense the Intracellular Environment and Activate Virulence Factor Expression. ***PLoS Pathog.*** 12**:** 1–27

Ruiz-Carmona S, Schmidtke P, Luque FJ, Baker L, Matassova N, Davis B, Roughley S, Murray J, Hubbard R & Barril X (2017) Dynamic undocking and the quasi-bound state as tools for drug discovery. ***Nat. Chem.*** 9**:** 201–206

Saikolappan S, Das K & Dhandayuthapani S (2015) Inactivation of the organic hydroperoxide stress resistance regulator OhrR enhances resistance to oxidative stress and isoniazid in Mycobacterium smegmatis. ***J. Bacteriol.*** 197**:** 51–62

Scior T, Bender A, Tresadern G, Medina-Franco JL, Martínez-Mayorga K, Langer T, Cuanalo-Contreras K & Agrafiotis DK (2012) Recognizing pitfalls in virtual screening: A critical review. ***J. Chem. Inf. Model.*** 52**:** 867–881

Shea RJ & Mulks MH (2002) ohr , Encoding an Organic Hydroperoxide Reductase , Is an In Vivo-Induced Gene in Actinobacillus pleuropneumoniae. 70**:** 794–802

da Silva Neto JF, Negretto CC & Netto LES (2012) Analysis of the Organic Hydroperoxide Response of Chromobacterium violaceum Reveals That OhrR Is a Cys-Based Redox Sensor Regulated by Thioredoxin. ***PLoS One*** 7**:**

Simpson AJ, Reinach FC, Arruda P, Abreu FA, Acencio M, Alvarenga R, Alves LM, Araya JE, Baia GS, Baptista CS, Barros MH, Bonaccorsi ED, Bordin S, Bove JM, Briones MR, Bueno MR, Camargo AA, Camargo LE, Carraro DM, Carrer H, et al (2000) The genome sequence of the plant pathogen Xylella fastidiosa. The Xylella fastidiosa Consortium of the Organization for Nucleotide Sequencing and Analysis. ***Nature*** 406**:** 151–159

Wolber G & Langer T (2005) LigandScout : 3-D Pharmacophores Derived from Protein-Bound Ligands and Their Use as Virtual Screening Filters. ***J. Chem. Inf. Model.*** 45**:** 160–169

Wolfram TJ, LeVeque RM, Kastenmayer RJ & Mulks MH (2009) Ohr, an in vivo-induced gene in Actinobacillus pleuropneumoniae, is located on a genomic island and requires glutathione-S-transferase for activity. ***FEMS Immunol. Med. Microbiol.*** 57**:** 59–68

CHAPTER 6 – DISCUSSION AND GENERAL CONCLUSIONS

6.1 – Discussion

Ohr proteins were initially, exclusively associated to prokaryotic organisms (Mongkolsuk *et al*, 1998b; Chuchue *et al*, 2006; da Silva Neto *et al*, 2012; Alegria *et al*, 2017). For a long time, they were described as a crucial enzymatic system involved in bacterial defense against organic hydroperoxide. In the work presented in **chapter 2**, through *in silico* analyses, we identified the presence of Ohr proteins in several eukaryotic organisms, including in fungi (**Chapter 2**, **Fig. 2**). *In silico* predictions demonstrated that the large majority of eukaryotic Ohr proteins possesses a N-terminal signal sequence, which probably targets the proteins towards mitochondria or other organelle, such as peroxisome or chloroplasts (**Chapter 2**, **Table S1**). We biochemically characterized the Ohr homolog from the ascomycete fungus *Mycosphaerella fijiensis*, the causative agent of Black Sigatoka disease in banana plants, and concluded it shared several biochemical properties with the prokaryotic Ohr, as their high reactivity towards linoleic acid hydroperoxides (k_{obs} = 3.18 (± 2.13) $\times 10^8$ $M^{-1}.s^{-1}$) (**Chapter 2**, **Fig. 7**). Then, through subcellular fractionation of *M. fijiensis* protoplast cells followed by western blot analysis, we confirmed the *in silico* prediction that MfOhr is a mitochondrial protein. The presence of lipoylated proteins (proposed reducing system for Ohr) from α-ketoacid dehydrogenase complexes (Cussiol *et al*, 2010), in mitochondria, supports Ohr peroxidase activity in one of the major sources of endogenous oxidants (Murphy, 2009). Thus, for eukaryotes, Ohr is probably associated with detoxification of endogenous sources of hydroperoxides and might be not associated in defense toward exogenous oxidative insults, as it is proposed for bacteria (Alegria *et al*, 2017; Reniere *et al*, 2016; Liu *et al*, 2016).

The molecular events associated with the highly effective reduction of hydroperoxides by Ohr enzymes and their specific reducibility by the DHL (present in lipoylated proteins) were elusive before this work. The previously proposed hypothesis suggested that interaction among the catalytic triad of Ohr (C_p, R_c and a E_c) by a salt bridge network was important to stabilize the reduced form of the enzyme (the so-called closed state). The MM simulations presented in the **chapter 3**, represent the first evidence that the disruption of this catalytical triad network, once C_p and C_r condense into a disulfide bridge, is directly associated with the greater gain of freedom and consequent opening of the Arg-loop (**Chapter 3**, **Fig. 5)**. Therefore, according to the hypothesis of Oliveira *et al*, 2006, the stability of the Arg-loop depends on the oxidative state of C_p.

Although, MM simulations also pointed that the polar interactions between C_p, R_c and E_c are crucial to stabilize the CS of Ohr proteins. Still, the Arg-loop return to the CS could not be sampled, during the time scale analyzed, this made us to hypothesize either that a longer time scale was needed, or the reducing agent was required to assist the closing switch. The developments presented in **Chapter 4** represent important contributions addressing those remaining questions. By correlating the monomer-

monomer interface with the highest conserved regions in Ohr enzymes, we observed that a great area of interaction is responsible for a quick dimerization, which assembles together not only the catalytic triad, but also an intrinsic hydrophobic structure region that surrounds Ohr active site and was refered here as the hydrophobic collar (**Chapter 4**, **Fig. 2)**. Consistent with early studies showing that elongated lipid hydroperoxides would interact with hydrophobic residues (Oliveira *et al*, 2006), our crystallographic structure of the complex between Ohr and its biological reductant (DHL) suggested Ohr reduction by DHL, also depend on the hydrophobic interactions that overlap with the conserved hydrophobic collar (**Chapter 4**, **Fig. 2)**. Through SMD, by pulling the Arg-loop from its CS to its OS, we were able to determine the corresponding free energy profiles for the conformational swith (**Chapter 4**, **Fig. 4)**. The results supported the idea that the opeing of the Arg-loop is easier to happen, when Ohr is oxidized (**Chapter 4**, **Fig. 3 & 4)**. However, our data also supported the idea that the high openings of crystallographic OS structures would hardly be reached during catalysis. Moreover, through SMD and MM simulations we show that either the reducing substrate and the product (alcohol) derived from the hydroperoxide reduction, are responsible to accelerate the closing and the opening switch, respectively (**Chapter 4**, **Fig. 3, 4 & S3)**. Finally, by evaluating the kinetics of Ohr point mutations (R_c and E_c) (**Chapter 4**, **Fig. 5)** and by comparative thermodynamics analysis (**Chapter 4**, **Fig. 6)**, we present cohesive evidence that the catalytic triad has to necessarily be disrupted for a favorable Ohr reduction by DHL. In fact, hybrid QM-MM unveiled that Ohr OS/IS structures are thermodynamically over five times more prone to be reduced by DHL than in Ohr close conformation (**Chapter 4**, **Fig. 6)**.

The work presented in **chapter 3** and **4** represent an important contribution addressing main features that distinguish Ohr from other very well characterized peroxidases, such as Prx. For instance, peroxiredoxins switch between a fully folded and a locally unfolded states, where the catalytic Cys residues undergo great movements to allow disulfide formation, as in the reduced form these two amino acids are far apart from each other. In contrast, their catalytic Arg residue remains relatively static during Prx turnover (Nelson *et al*, 2017). Furthermore, the active cavity in Ohr is much deeper and well defined, and conformational and micro physicochemical environment exchanges unveil to be crucial in different stages of catalysis, both directing the substrate towards the reactive cysteine or inducing faster conformational exchanges, as the oxidant and the reactant substrates would require it to efficiently fit and react (**Chapter 4**, **Fig. 7)**. Interestingly, despite the mechanism of action is very distinct, both systems operate with extraordinary efficiency in hydroperoxide reduction and attaining rates in the 10^7-10^8 $M^{-1}s^{-1}$ range (Alegria *et al*, 2017; Nelson *et al*, 2017; Tairum *et al*, 2016)

The unique characteristics that distinguish Ohr proteins support the ideia of Ohr as a target for drug development. **Chapter 5** represents the first effort with some promising results for searching for bioactive compounds to target Ohr proteins. We describe the identification of two compounds (C-31 & C-42), which could represent a framework for further studies attempting to find specific Ohr inhibitors (**Chapter 5**, **Fig. 5**). Compound C-42 was selected from *ab initio design* where we considered that electrophilic compounds irreversibly react with Cys-based enzymes by reacting with their nucleophilic

thiolate (Otto & Schirmeister, 1997; Lopachin & Gavin, 2017). In fact, the compound showed an IC_{50} of 243.3-321.7 μM at a 95% confidence range (**Chapter 5**, **Fig. 6B**). C-31 was selected from a virtual screening using pharmacophoric models designed by considering the close conformation of the crystallographic structure of XfOhr (PDB_{ID}=1ZB9). The models were then applied against the ZINC database containing over 30 million of compounds. C-31 showed an IC_{50} of 124.4-248.5 μM at a 95% confidence range (**Chapter 5**, **Fig. 6A**). Despite both compounds showed promising IC_{50} values, we could not yet specifically corelate their inhibition specificity towards Ohr, further analysis must be done. Additional efforts were made applying differential scanning fluorimetry were several fragment compounds (Niesen *et al*, 2007), with potentiality to interact with the Ohr active site, were selected (**Chapter 5**, **Fig. 8**), nonetheless due to a limitation of time, we could not further analyses them.

Concluding, the results presented in this thesis represent important contributions for the understanding of the enzymatic mechanistic, the importance and distribution of the Ohr enzymes, peroxidases that display highly efficient catalysis, comparable to other very important hydroperoxide removing enzymes, such as GSH peroxidase and peroxiredoxin. The optimistic outcome of targeting Ohr proteins in pathogenic bacteria is becoming promisor and although it needs further analysis, we present the first initial trials for search and rationally design bioactive molecules with potentiality to specifically target Ohr proteins.

6.2 – References

Alegria TGP, Meireles DA, Cussiol JRR, Hugo M, Trujillo M, de Oliveira MA, Miyamoto S, Queiroz RF, Valadares NF, Garratt RC, Radi R, Di Mascio P, Augusto O & Netto LES (2017) Ohr plays a central role in bacterial responses against fatty acid hydroperoxides and peroxynitrite. ***Proc. Natl. Acad. Sci.*** 114**:** E132–E141

Chuchue T, Tanboon W, Prapagdee B, Dubbs JM, Vattanaviboon P & Mongkolsuk S (2006) ohrR and ohr Are the Primary Sensor / Regulator and Protective Genes against Organic Hydroperoxide Stress in Agrobacterium tumefaciens. ***J. Bac*** 188**:** 842–851

Cussiol JRR, Alegria TGP, Szweda LI & Netto LES (2010) Ohr (organic hydroperoxide resistance protein) possesses a previously undescribed activity, lipoyl-dependent peroxidase. ***J. Biol. Chem.*** 285**:** 21943–50

Liu Z, Wang H, Zhou Z, Naseer N, Xiang F, Kan B, Goulian M & Zhu J (2016) Differential Thiol-Based Switches Jump-Start Vibrio cholerae Pathogenesis. ***Cell Rep.*** 14**:** 347–354

Lopachin RM & Gavin T (2017) Thiolate Sites : Relevance To Pathophysiological. 50**:** 195–205

Mongkolsuk S, Praituan W, Loprasert S, Fuangthong M & Chamnongpol S (1998) Identification and Characterization of a New Organic Hydroperoxide Resistance (ohr) Gene with a Novel Pattern of Oxidative Stress Regulation from Xanthomonas campestrispv . phaseoli Identification and Characterization of a New Organic Hydroperoxide Resi. ***J. Bacteriol.*** 180**:** 2636–2643

Murphy MP (2009) How mitochondria produce reactive oxygen species. ***Biochem. J.*** 417**:** 1–13

Nelson KJ, Perkins A, Van Swearingen AED, Hartman S, Brereton AE, Parsonage D, Salsbury FR, Karplus PA & Poole LB (2017) Experimentally Dissecting the Origins of Peroxiredoxin Catalysis. ***Antioxid. Redox Signal.*:** ars.2016.6922

Niesen FH, Berglund H & Vedadi M (2007) The use of differential scanning fluorimetry to detect ligand interactions that promote protein stability. ***Nat. Protoc.*** 2**:** 2212–2221

Oliveira M a, Guimarães BG, Cussiol JRR, Medrano FJ, Gozzo FC & Netto LES (2006) Structural insights into enzyme-substrate interaction and characterization of enzymatic intermediates of organic hydroperoxide resistance protein from Xylella fastidiosa. ***J. Mol. Biol.*** 359**:** 433–45

Otto H-H & Schirmeister T (1997) Cysteine Proteases and Their Inhibitors. ***Chem. Rev.*** 97**:** 133–172

Reniere ML, Whiteley AT & Portnoy DA (2016) An In Vivo Selection Identifies Listeria monocytogenes Genes Required to Sense the Intracellular Environment and Activate Virulence Factor Expression. ***PLoS Pathog.*** 12**:** 1–27

da Silva Neto JF, Negretto CC & Netto LES (2012) Analysis of the Organic Hydroperoxide Response of Chromobacterium violaceum Reveals That OhrR Is a Cys-Based Redox Sensor Regulated by Thioredoxin. ***PLoS One*** 7**:**

Tairum CA, Santos MC, Breyer CA, Geyer RR, Nieves CJ, Portillo-Ledesma S, Ferrer-Sueta G, Toledo JC, Toyama MH, Augusto O, Netto LES & De Oliveira MA (2016) Catalytic Thr or ser Residue Modulates Structural Switches in 2-Cys Peroxiredoxin by Distinct Mechanisms. ***Sci. Rep.*** 6**:** 1–12

CHAPTER 7 – ABSTRACT

7.1 – Abstract

Organic hydroperoxide resistance (Ohr) proteins are highly efficient thiol-based peroxidases that play central roles in bacterial response towards organic hydroperoxides. In Fungi, Ohr frequently presents a N-terminal extension, which is predicted to target them to mitochondria. The catalytic triad of Ohr comprises the peroxidatic Cys (C_p), the catalytic Arg (R_c) and a Glu (E_c) are fully conserved and interact among themselves by a salt bridge network in a reduced form of the enzyme (the so-called closed state). After getting oxidized to sulfenic acid (Cys-SOH), C_p condenses with the sulfhydryl group of resolution Cys (C_r) in a disulfide bond. The absence of negativity of the thiolate (RS^-) in C_p facilitates the opening of the Arg-loop (containing the R_c) away from the active site, generating the so-called open state. However, the molecular events associated with the high reactivity of Ohr enzymes towards hydroperoxides and its specific reducibility by the dihydrolipoamide (DHL) or by lipoylated proteins were still elusive before this work.

Additionally, several factors support the idea of Ohr as a target for drug development: (i) Ohr displays unique physicochemical properties; (ii) bacteria mutant for Ohr (Δ*ohr*) are highly sensitive to oxidative stress; (iii) the indications that Ohr might be involved in bacterial virulence; and (iv) its absence in mammals and vascularized plants.

In this thesis, several aspects of Ohr enzymes were evaluated. In **chapter 2**, we biochemically characterized the Ohr homologs from the ascomycete fungus *Mycosphaerella fijiensis* Mf_1 (MfOhr), the causative agent of Black Sigatoka disease in banana plants, which presented extraordinary reactivity towards linoleic acid hydroperoxides (k_{obs} = 3.18 (± 2.13) $\times 10^8$ $M^{-1}.s^{-1}$). Furthermore, through subcellular fractionation of *M fijiensis* protoplast cells followed by western blot analysis, we confirmed the *in silico* prediction that MfOhr is a mitochondrial protein. In **chapter 3** and **4**, we described seven new crystallographic structures from two opportunistic pathogen, one from *Xylella fastidiosa* and six from *Chromobacterium violaceum* (including the first representative of the complex between Ohr and its biological reductant, DHL). Taken together these structures might represent new snapshots along the catalysis. Furthermore, several molecular modelling approaches, such as classical mechanics (MM), steered molecular dynamics (SMD), hybrid quantum mechanics (QM-MM) and together with enzymatic assays of point mutations, indicated that Ohr underwent unique structural switches to allow an intermittent opening (oxidized state) and returning to a more stable closed form (reduced state) of an Arg-loop along catalysis. Remarkably, dihydrolipoamide directly assisted the closing the Arg-loop and thereby the turnover of the enzyme. In **chapter 5**, we describe the identification of two compounds (C-31 & C-42) that could represent a framework for further studies attempting to find specific Ohr inhibitors, either through *ab initio* design of chemical compounds and virtual screening using

pharmacophoric models. The IC_{50} calculated for C-31 and C-42 were 124.4-248.5 µM and 243.3-321.7 µM, respectively.

Finally, this thesis highlights several new aspects related to Ohr function: **1** – evidence that eukaryotic Ohr are preferentially located in mitochondria and share several biochemical properties with the prokaryotic ones; **2** – the network of polar interactions among residues of the catalytic triad (C_p, R_c and E) strongly contributed to stabilize Ohr in the closed state, in an optimum configuration for hydroperoxide reduction; **3** – evidence that disulfide bond formation and the product release (alcohol derived from hydroperoxide reduction) facilitate the opening of the R_c loop to an intermediate state (probably not to the excessively open state presented in crystallographic structures); **4** – mapping the interactions between the biological reductant (DHL) and the Ohr active site; **5** – strong indications that DHL is not able to fit and react with Ohr in the close conformation; **6** – the first trials for search of molecules to specifically target Ohr proteins, although further assays must be performed to verify the specificity of the selected compounds to target Ohr. Therefore, we describe relevant new information for an antioxidant protein that displays highly efficient catalysis, comparable to other very important hydroperoxide removing enzymes, such as GSH peroxidase and peroxiredoxin.

7.2 – Resumo

As proteínas Ohr (*Organic hydroperoxide resistance*) são peroxidases dependente de tiól extremamente eficientes e têm um papel central na resposta das bactérias contra peróxidos orgânicos. Em fungos, as proteínas Ohr apresentam uma extensão N-terminal, cujo predições *in silico* apontam estar associada ao direcionamento da proteína para a mitocôndria. A tríade catalítica é composta pela cisteína peroxidatic (C_p), a arginina (R_c) e o glutamato (E_c) catalíticos que são totalmente conservados e interagem entre eles por uma rede de interações de ponte salina, na forma reduzida da proteína (conformação fechada). Após se tornarem oxidadas em ácido sulfênico (Cis-SOH), a C_p condensa com o grupo sulfidrila da cisteína de resolução (C_r) numa ligação disulfeto. A ausência da carga negativa do tiolato (RS^-) da C_p facilita a abertura da alça que contem a R_c para longe do centro ativo, gerando a conformação aberta. No entanto, os eventos moleculares associados a alta reatividade das enzimas Ohr contra hidroperóxidos e a sua redução pela dihydrolipoamida (presente em proteínas lipoiladas), ainda está descrita de forma bem superficial.

Adicionalmente, vários fatores suportam a ideia de que a Ohr seria um potencial alvo para o desenvolvimento de drogas: (i) a Ohr exibe propriedade físico-químicas únicas; (ii) as bactérias mutantes para Ohr (Δ*ohr*) são fortemente sensíveis ao stress oxidativo; (iii) indicações de que a Ohr poderá está envolvida na virulência de várias bactérias; e (iv) a ausência de Ohr em mamíferos e plantas vascularizadas. Nesta tese, vários aspetos relacionados com as enzimas Ohr foram avaliados. No Capitulo 2, foi caracterizada bioquimicamente a proteína Ohr homologa de fungo ascomiceto, *Mycosphaerella fijiensis* Mf_1 (MfOhr), o agente causador da doença de bananas, Sigatoka-negra. A enzima apresentou eficiente atividade contra peroxido de ácido linoleico (k_{obs} = 3.18 (± 2.13) $\times 10^8$ $M^{-1}.s^{-1}$). Além disso, através do fracionamento sub celular de protoblasto de *M fijiensis* seguido de *western blot*, foram confirmadas as predições *in silico* de que a MfOhr é uma proteína mitocondrial. No capítulo 3 e 4, foram descritas sete estruturas cristalográficas oriundas de dois patógenos oportunistas, uma de *Xylella fastidiosa* e seis de *Chromobacterium violaceum* (incluindo o primeiro representante do complexo entre a Ohr e o seu redutor biológico, DHL). Estas estruturas poderão representar diferentes conformações ao longo do ciclo catalítico. Adicionalmente, várias abordagens de modelagem molecular, tais como mecânica clássica (MM), mecânica molecular direcionada (SMM) e mecânica quântica híbrida (QM-MM), juntamente com ensaios experimentais com mutações pontuais, indicaram que a Ohr sofre várias mudanças conformacionais para permitir uma abertura intermitente (estado oxidado) e o retorno para uma conformação fechada mais estável (estado reduzido) da alça da arginina ao longo da catálise. Notavelmente, a dihydrolipoamide assistiu diretamente o fechamento da alça da arginina e por consequência o turnover da enzima. No capítulo 5, foi descrita a identificação de dois compostos (C-31 e C-42) que representam estudos iniciais com a finalidade de encontrar inibidores específicos para a enzima Ohr. Estes compostos foram encontrados por *ab initio design* e por varrimento virtual com o uso de modelos farmacofóricos. Os IC_{50} calculados para o C-31 e C-42 foram de 124.4-248.5 μM e 243.3-321.7 μM, respectivamente.

Finalmente, esta tese descreve vários aspetos relacionados com a função da Ohr: 1 – evidências que as Ohr de eucariotos estão preferencialmente localizadas na mitocôndria e partilham várias propriedades bioquímicas com as Ohr de bactéria; 2 – a rede de interações polares entre os resíduos da tríade catalítica (C_p, R_c e E_c) contribuem fortemente para a estabilização do estado fechado, a configuração ótima para a redução de hydroperoxidos; 3 – evidências de que a formação da ligação disulfeto e a liberação do produto (álcool derivado da redução do hydroperoxido) facilitam a abertura da alça da arginina até um estado intermediários (provavelmente não o estado totalmente exposto apresentado nas estruturas cristalográficas) 4 – o mapeamento das interações entre o redutor biológico no centro ativo da Ohr; 5 – fortes indicações de que a DHL não é capaz de interagir e reagir com a Ohr na conformação fechada; 6 – os primeiros ensaios para a procura por moléculas que especificamente interajam com a Ohr, apesar de que futuros ensaios terão de ser executados para verificar a especificidade dos compostos selecionados. Assim, nós descrevemos nova informação relevante sobre uma proteína antioxidante que exibe uma alta eficiência catalítica, comparável com outras importantes enzimas removedores de hydroperoxidos, tais como glutationa peroxidases e peroxiredoxinas.

APPENDIX 1 – SUPPLEMENTARY DATA

Ap1.1 – Chapter 4 (supplementary)

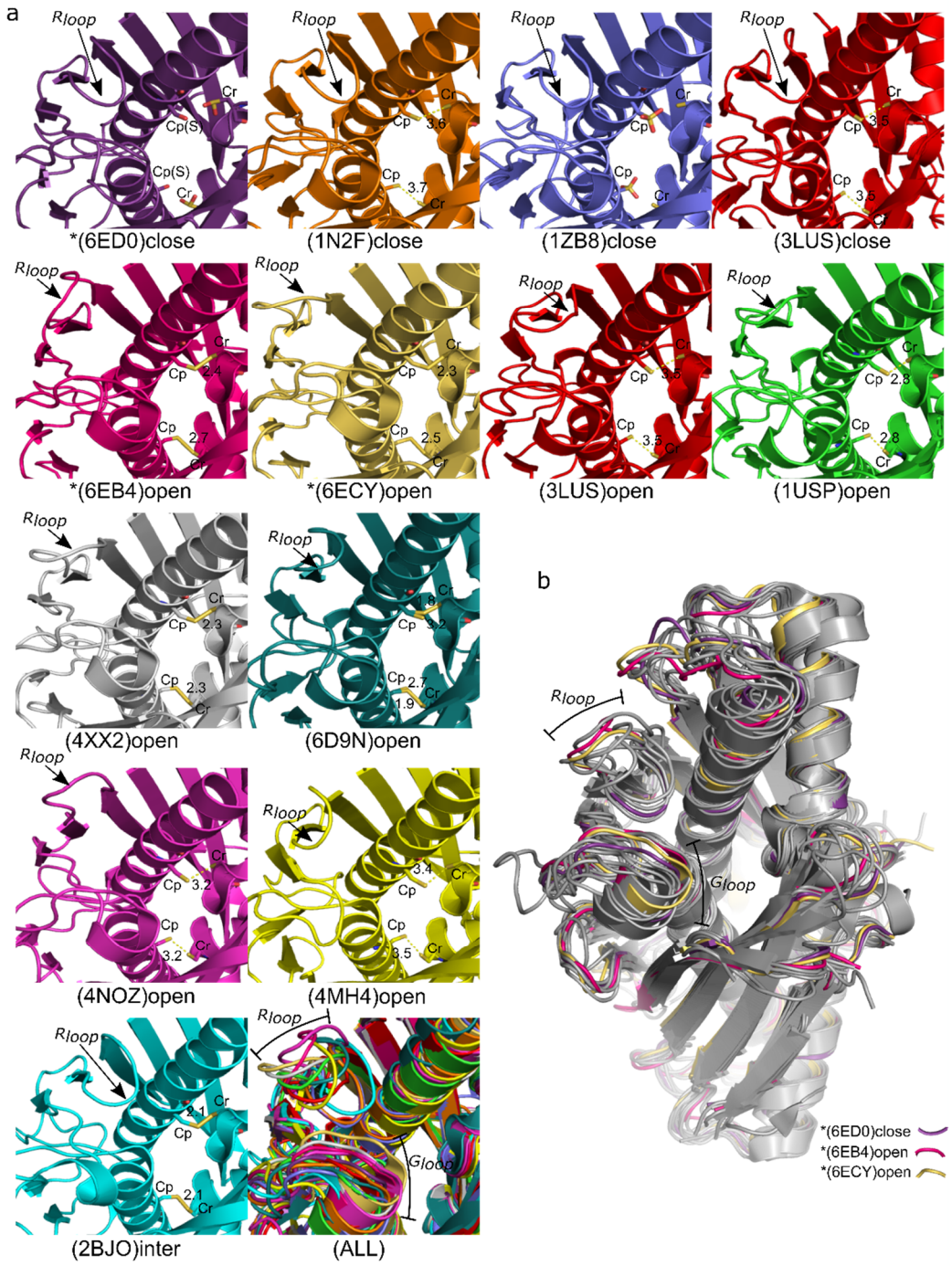

Fig. S1 – Comparison of Arg-loop openings. (a) Ohr Arg-loop conformations available at the protein database (PDD): CS, OS and IS. Asterix represent structures from this work. (b) Superposition of the structures solved at this work with the other structures present in PDB.

Table S1 – Ohr dimer interface hydrogen interactions

*Cv*OhrA_C61S (Close conformation)
PDB: 6ED0

Interface Summary		
Atoms in the interface	346 (34.2%)	347 (34.3%)
on the surface	743 (73.3%)	753 (74.3%)
total	1013 (100.0%)	1013 (100.0%)
Residues in the interface	83 (58.5%)	83 (58.5%)
on the surface	137 (96.5%)	138 (97.2%)
total	142 (100.0%)	142 (100.0%)

Hydrogen bonds

	Structure 1			Dist.	Structure 1		
1	A:ASN	2	[ND2]	2.7	B:ASN	134	[O]
2	A:GLN	5	[N]	2.8	B:PRO	91	[O]
3	A:LEU	8	[N]	2.9	B:ILE	89	[O]
4	A:TYR	9	[N]	3.5	B:ILE	89	[O]
5	A:THR	10	[OG1]	2.8	B:SER	88	[OG]
6	A:ALA	11	[N]	2.8	B:VAL	87	[O]
7	A:ALA	13	[N]	2.9	B:GLY	85	[O]
8	A:THR	14	[OG1]	2.8	B:THR	84	[OG1]
9	A:ALA	15	[N]	2.8	B:VAL	83	[O]
10	A:GLY	17	[N]	3.1	B:VAL	81	[O]
11	A:ARG	19	[NH1]	3.1	B:SER	61	[OG]
12	A:ASN	49	[ND2]	3	B:TYR	9	[OH]
13	A:GLN	52	[NE2]	3.6	B:TYR	9	[OH]
14	A:GLN	52	[NE2]	3	B:ASP	27	[OD2]
15	A:GLN	52	[NE2]	3.1	B:ASP	27	[OD1]
16	A:LYS	67	[NZ]	2.8	B:GLY	17	[O]
17	A:SER	82	[OG]	3	B:ALA	15	[O]
18	A:SER	82	[OG]	3	B:THR	16	[OG1]
19	A:VAL	83	[N]	2.9	B:ALA	15	[O]
20	A:THR	84	[OG1]	2.9	B:THR	14	[OG1]
21	A:GLY	85	[N]	2.8	B:ALA	13	[O]
22	A:VAL	87	[N]	2.9	B:ALA	11	[O]
23	A:SER	88	[OG]	2.9	B:THR	10	[OG1]
24	A:ILE	89	[N]	3	B:TYR	9	[O]
25	A:PHE	96	[N]	3.1	B:ILE	124	[O]
26	A:TYR	127	[OH]	2.7	B:GLU	51	[OE1]
27	A:ASN	129	[ND2]	3.4	B:HIS	94	[O]
28	A:ASN	129	[ND2]	2.8	B:PHE	96	[O]
29	A:ASN	134	[ND2]	2.9	B:ARG	132	[O]
30	A:ASN	134	[ND2]	3	B:ALA	130	[O]
31	A:ILE	135	[N]	3.9	B:MET	1	[SD]
32	A:ASN	134	[O]	3.2	B:ASN	2	[N]
33	A:PRO	91	[O]	2.9	B:GLN	5	[N]
34	A:ILE	89	[O]	2.9	B:LEU	8	[N]
35	A:ILE	89	[O]	3.4	B:TYR	9	[N]
36	A:VAL	87	[O]	2.8	B:ALA	11	[N]
37	A:GLY	85	[O]	2.9	B:ALA	13	[N]
38	A:VAL	83	[O]	2.8	B:ALA	15	[N]
39	A:VAL	81	[O]	3	B:GLY	17	[N]
40	A:SER	61	[OG]	3.2	B:ARG	19	[NH2]
41	A:TYR	9	[OH]	2.9	B:ASN	49	[ND2]
42	A:TYR	9	[OH]	3.7	B:GLN	52	[NE2]
43	A:ASP	27	[OD1]	3.2	B:GLN	52	[NE2]
44	A:ASP	27	[OD2]	3.1	B:GLN	52	[NE2]
45	A:GLY	17	[O]	2.8	B:LYS	67	[NZ]
46	A:ALA	15	[O]	3.1	B:SER	82	[OG]
47	A:ALA	15	[O]	3	B:VAL	83	[N]
48	A:ALA	13	[O]	2.8	B:GLY	85	[N]
49	A:ALA	11	[O]	2.9	B:VAL	87	[N]
50	A:TYR	9	[O]	3	B:ILE	89	[N]
51	A:ILE	124	[O]	3.1	B:PHE	96	[N]
52	A:GLU	51	[OE1]	2.7	B:TYR	127	[OH]
53	A:HIS	94	[O]	3.4	B:ASN	129	[ND2]
54	A:PHE	96	[O]	2.9	B:ASN	129	[ND2]
55	A:ALA	130	[O]	3	B:ASN	134	[ND2]
56	A:ARG	132	[O]	2.7	B:ASN	134	[ND2]
57	A:MET	1	[O]	3.7	B:GLU	136	[N]

*Cv*OhrA_WT (Open conformation)
PDB: 6ECY

Interface Summary		
Atoms in the interface	331 (32.7%)	325 (32.1%)
on the surface	738 (73.0%)	752 (74.4%)
total	1011 (100.0%)	1011 (100.0%)
Residues in the interface	80 (56.3%)	81 (57.0%)
on the surface	135 (95.1%)	138 (97.2%)
total	142 (100.0%)	142 (100.0%)

Hydrogen bonds

	Structure 1			Dist.	Structure 1		
1	A:ASN	2	[ND2]	2.9	B:ASN	134	[O]
2	A:GLN	5	[N]	2.9	B:PRO	91	[O]
3	A:LEU	8	[N]	2.8	B:ILE	89	[O]
4	A:TYR	9	[N]	3.6	B:ILE	89	[O]
5	A:THR	10	[OG1]	2.8	B:SER	88	[OG]
6	A:ALA	11	[N]	2.9	B:VAL	87	[O]
7	A:ALA	13	[N]	3	B:GLY	85	[O]
8	A:THR	14	[OG1]	2.7	B:THR	84	[OG1]
9	A:ALA	15	[N]	2.9	B:VAL	83	[O]
10	A:GLY	17	[N]	3	B:VAL	81	[O]
11	A:ASN	49	[ND2]	3	B:TYR	9	[OH]
12	A:GLN	52	[NE2]	3	B:ASP	27	[OD1]
13	A:GLN	52	[NE2]	3.4	B:GLU	12	[O]
14	A:SER	59	[OG]	3.8	B:ALA	13	[O]
15	A:SER	82	[OG]	3.6	B:ALA	15	[O]
16	A:VAL	83	[N]	3	B:ALA	15	[O]
17	A:THR	84	[OG1]	2.8	B:THR	14	[OG1]
18	A:GLY	85	[N]	2.8	B:ALA	13	[O]
19	A:VAL	87	[N]	2.9	B:ALA	11	[O]
20	A:ILE	89	[N]	2.9	B:TYR	9	[O]
21	A:PHE	96	[N]	3.4	B:ILE	124	[O]
22	A:TYR	127	[OH]	2.7	B:PRO	50	[O]
23	A:ASN	129	[ND2]	3.4	B:HIS	94	[O]
24	A:ASN	129	[ND2]	2.8	B:PHE	96	[O]
25	A:ASN	134	[ND2]	3	B:ALA	130	[O]
26	A:ASN	134	[ND2]	2.9	B:ARG	132	[O]
27	A:GLU	136	[N]	3.7	B:MET	1	[SD]
28	A:ASN	134	[O]	3.1	B:ASN	2	[N]
29	A:PRO	91	[O]	3	B:GLN	5	[N]
30	A:ILE	89	[O]	2.8	B:LEU	8	[N]
31	A:ILE	89	[O]	3.6	B:TYR	9	[N]
32	A:VAL	87	[O]	2.8	B:ALA	11	[N]
33	A:GLY	85	[O]	3	B:ALA	13	[N]
34	A:VAL	83	[O]	2.8	B:ALA	15	[N]
35	A:TYR	9	[OH]	2.9	B:ASN	49	[ND2]
36	A:TYR	9	[OH]	3.6	B:GLN	52	[NE2]
37	A:ALA	13	[O]	3.8	B:SER	59	[OG]
38	A:GLY	18	[O]	3.9	B:LYS	67	[NZ]
39	A:ALA	15	[O]	2.9	B:VAL	83	[N]
40	A:ALA	13	[O]	2.8	B:GLY	85	[N]
41	A:ALA	11	[O]	2.8	B:VAL	87	[N]
42	A:TYR	9	[O]	3	B:ILE	89	[N]
43	A:ILE	124	[O]	3.1	B:PHE	96	[N]
44	A:PRO	50	[O]	2.7	B:TYR	127	[OH]
45	A:PHE	96	[O]	3	B:ASN	129	[ND2]
46	A:ALA	130	[O]	3	B:ASN	134	[ND2]
47	A:ARG	132	[O]	2.9	B:ASN	134	[ND2]
48	A:MET	1	[O]	3.6	B:GLU	136	[N]

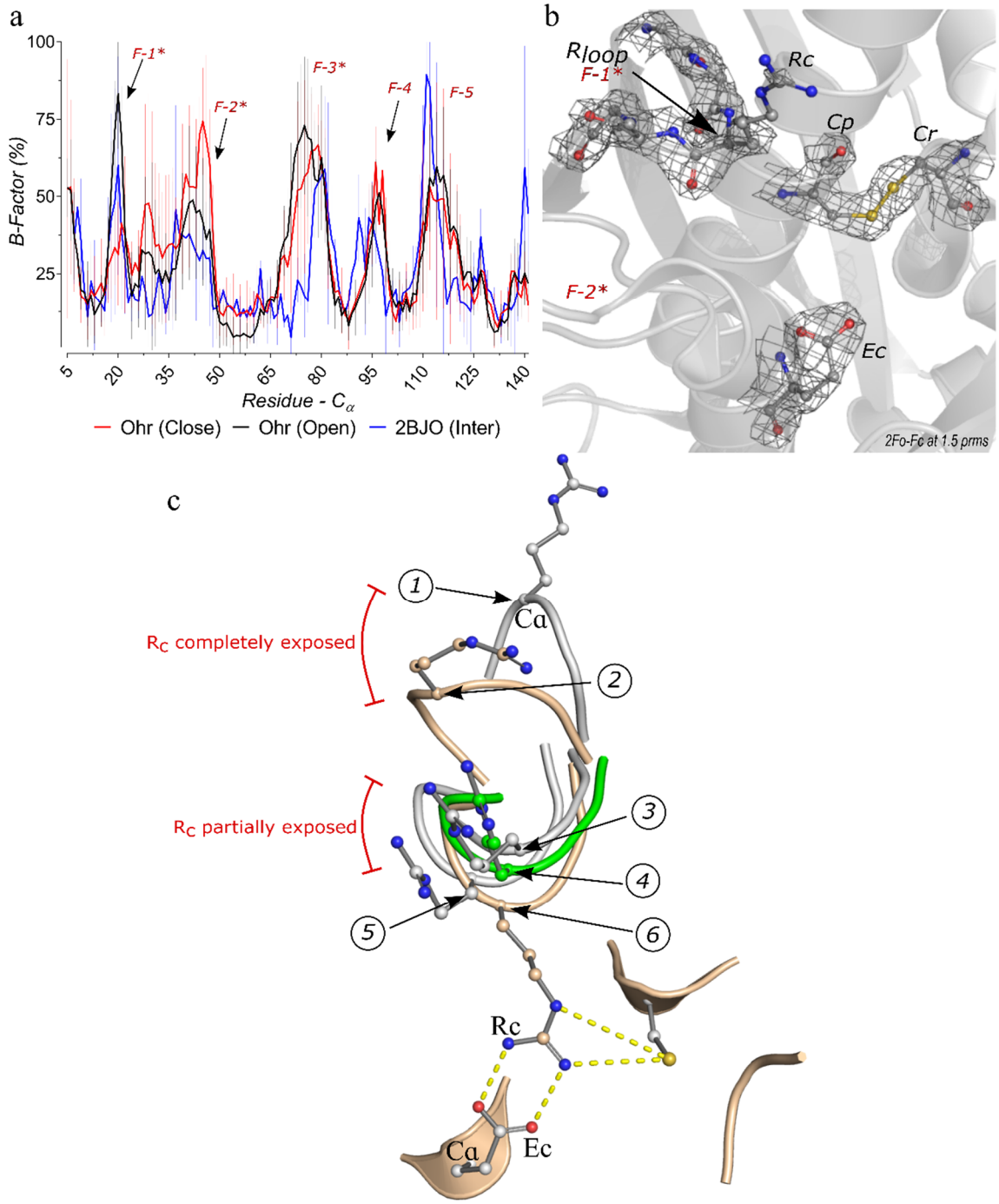

Fig. S2 – Flexibility of the Arg-loop in the IS present in the BsOhrB (PDBID=2BJO). F-1 to F-5 indicate the five most flexible regions in Ohr enzymes, asterisks point out opposite chains. Standard deviations are shown as vertical lines. (a) Normalized Cα B-factors (%) (blue) along the primary sequences of the *Bs*OhrB crystallographic structure (both monomers) (n=2), open (red) and close (red) plots derive from **Fig. 3a**. (b) Electronic density of the Arg loop, E_c and catalytic Cys residues of *Bs*OhrB. (c) Structural representatives of OS, IS and CS, comparing with *Bs*OhrB: **1** – MM-OhrA_open_SS (C-3) (**C-3** in **Fig. 3g**), distance $R_{C\alpha}$-Ecα = 22.3 Å; **2** – CvOhrA (6ECY), distance $R_{C\alpha}$-Ecα = 18.4 Å; **3** - MM-OhrA_open_SS (C-4) (**C-4** in **Fig. 3g**) distance $R_{C\alpha}$-Ecα = 11.9 Å; **4** – MM-OhrB_open_SS_DHL (TS) (**TS** in **Fig. 3h**) distance $R_{C\alpha}$-Ecα = 10.6 Å; **5** – *Bs*OhrB (PDB_{ID}=2BJO) distance $R_{C\alpha}$-Ecα = 12.0 Å; **6** – CvOhrA_C61S (6ED0) = distance $R_{C\alpha}$-Ecα = 10.3 Å.

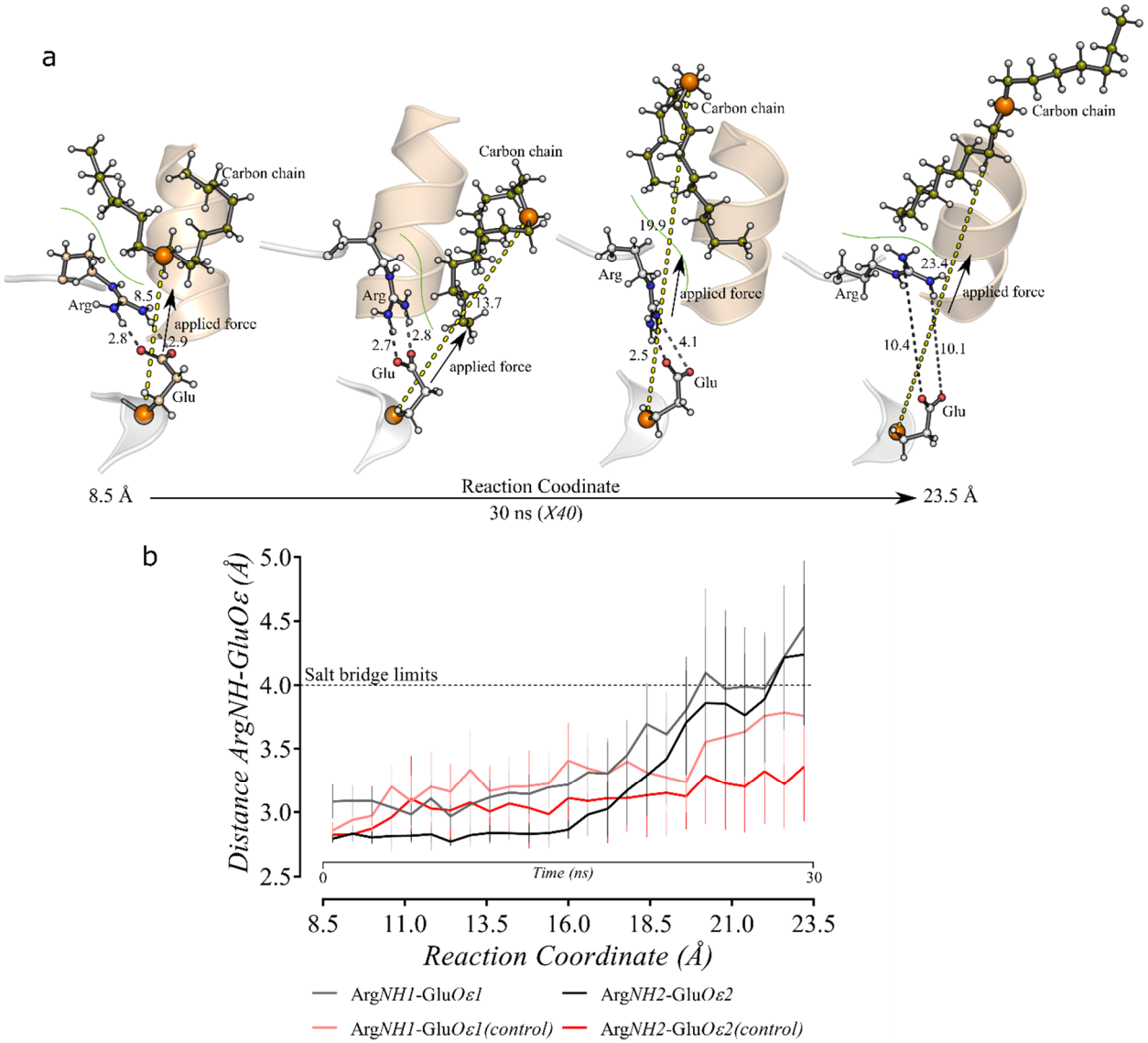

Fig. S3 – Carbon chain release assisted the disruption of the R_c and E_c (R_{NH}-$E_{O\varepsilon}$) interaction. A carbon chain mimicking a alcohol derived from fatty acid was modeled on the structure derived from the MM of OhrB_SS_DHL (close conformation) considering the position of the PEG molecule in the *Xf*Ohr (PDB_{ID}=1ZB9). (a) Scheme of the SMD simulations performed to evaluate the interference of the carbon chain release on the R_c and E_c (R_{NH}-$E_{O\varepsilon}$) interaction disruption. The distance between Cα Glu50 and C_{10} carbon chain (orange spheres) was followed along the reaction coordinate. The distance between these atoms was increased by an external force at constant rate of 0.5 Å/ns, from 8.5 Å to 23.5 Å. These simulations were replicated 40 times. R_{NH}-$E_{O\varepsilon}$ distances of the opposite monomer (with no carbon chain) were used as control. Green line represents hydrophobic interaction between the carbon chain and Arg side chain. (b) The graphic represents the R_{NH1}-$E_{O\varepsilon1}$ and R_{NH2}-$E_{O\varepsilon2}$ distances while pulling the carbon chain out from the active site (Black lines) the same interaction distances at the opposite active site (absence of carbon chain) were used as control (Red lines). Control distances were obtained in the opposite active site where a carbon chain was absent. 4Å cut-off for salt bridge interactions is represented as black dash lines. Vertical lines represent erros at 95% Cl.

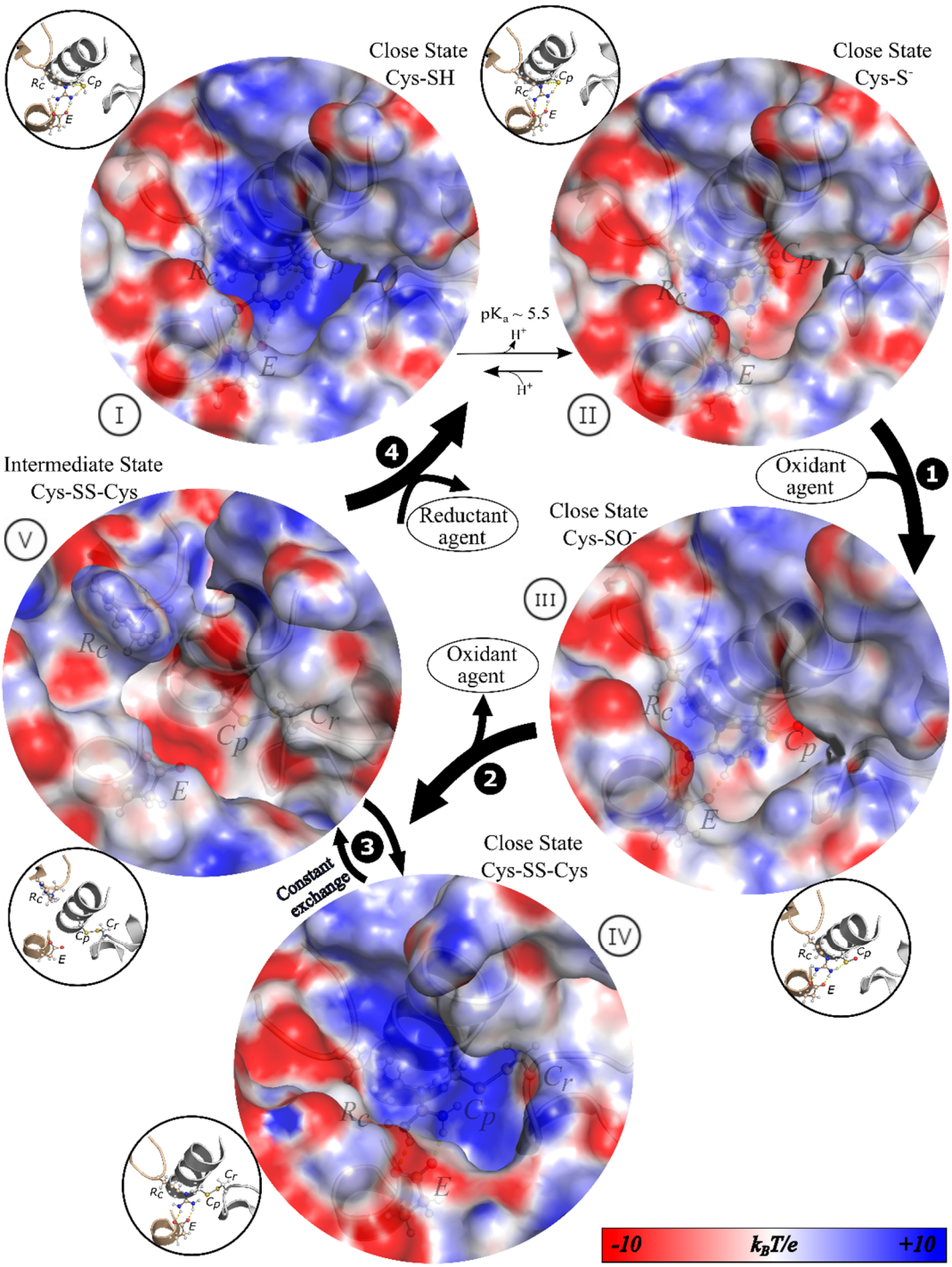

Fig. S4 – Electrostatic surface during key stages of Ohr catalysis. Ohr is constantly exchanging between states I and II, however as the pKa for Cp was determined to be around 5.5 (Meireles *et al*, 2017; Piccirillo *et al* 2018) it is mostly found at state II. Once the oxidant oxidizes the enzyme (Step 1) in the state III, C_r reacts and forms a disulfide bond with C_p (state IV) and while the oxidant leaves the active site (Step 2), Ohr intermittently exchanges from CS (IV) and IS (V). Once DHL interacts with the IS of Ohr, the enzymes regains its CS and is reactivated. The electrostatic potentials were calculated through the software *APBS* and the images generated with *PyMOL*.

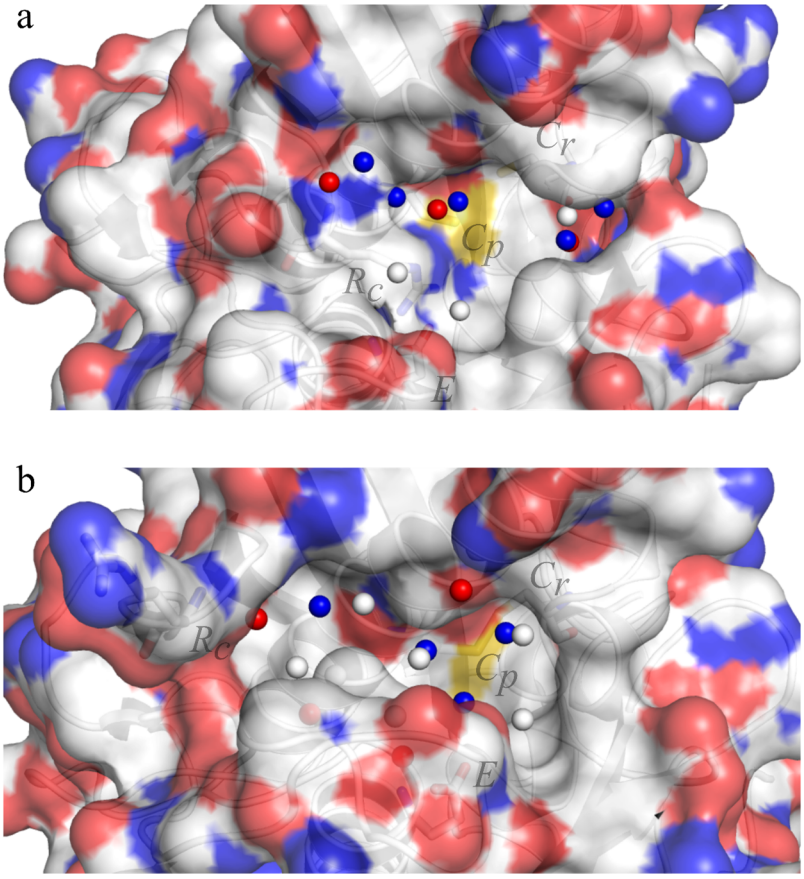

Fig. S5 – Spatial representation of available molecular interactions at XfOhr active site (PDB_{ID}=1ZB9). (a) represents interactions at CS. (b) represents interactions at OS. (⚪) hydrophobic interactions; (🔴) hydrogen bond acceptors; (🔵) Hydrogen bond donors. Molecular interactions were calculated through the software *GRID*.

Table S2 – Primers for site-directed mutation

Primer sequence (5'→3')*	Primer names
GTACCACATATGAACCCTCTGCAAAAAGTAC	*Cv*OhrAwt_fw
TTGGGATCCTTACGCCAACGTCAGCTCC	*Cv*OhrAwt_rv
GTACCACATATGTCGATTGAAACCATTCTGTAC	*Cv*OhrBwt_fw
TTGGGATCCTCACGCCAGGCGCAGGCGTA	*Cv*OhrBwt_rv
CCACCGGGGGCGCGGACGGCCGGGC	*Cv*OhrA_R19Afw
GCCCGGCCGTCCGCGCCCCCGGTGG	*Cv*OhrA_R19Arv
GCACCAATCCGGCGCAGCTGTTCGC	*Cv*OhrA_E51Afw
GCGAACAGCTGCGCCGGATTGGTGC	*Cv*OhrA_E51Arv
CGGCTATTCCGCCGCGTTCATCGGCGCG	*Cv*OhrA_C61Afw
CGCGCCGATGAACGCGGCGGAATAGCCG	*Cv*OhrA_C61Arv
GGCTATTCCGCCAGCTTCATCGGCG	CvOhrA_C61Sfw
CGCCGATGAAGCTGGCGGAATAGCC	CvOhrA_C61Srv
CGCGCACGGCATCGCCCCGTATTCCAAC	*Cv*OhrA_C125Afw
GTTGGAATACGGGGCGATGCCGTGCGCG	*Cv*OhrA_C125Arv
CGGTTACGCCGCCGCGTTTCTCGGATCGC	CvOhrB_C60Afw
GCGATCCGAGAAACGCGGCGGCGTAACCG	CvOhrB_C60Arv
GGTTACGCCGCCAGCTTTCTCGGATC	CvOhrB_C60Sfw
GATCCGAGAAAGCTGGCGGCGTAACC	CvOhrB_C60Srv

Table S3 – Expressing conditions of recombinant proteins

Gene	Vector	bacteria	Antibiotics	Induction condition
MtAhpE	pDEST	BL21 (DE3)	Ampicillin (100 µg/ml)	0.5 mM IPTG, 5h, 30ºC
CvOhrA WT & mutants	pET-15b	BL21 (DE3)	Ampicillin (100 µg/ml)	1 mM IPTG, 4h, 30ºC
CvOhrB WT & mutants	pET-15b	BL21 (DE3)	Ampicillin (100 µg/ml)	1 mM IPTG, 4h, 30ºC
XfLpd	pET-15b	AD494(DE3)	Ampicillin (100 µg/ml) Kanamycin (15 µg/ml)	0.5 mM IPTG, overnight, 20°C

Ap1.2 – Chapter 5 (supplementary)

Table S1 – Molecules from Virtual screening

Compounds selected from Pharmacophore 1		
Nº	Compound (#ZINC)	Structure
39	ZINC30603842	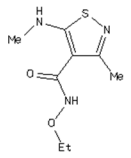

Compounds selected from Pharmacophore 2		
Nº	Compound (#ZINC)	Structure
1	ZINC49547779	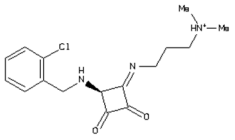
2	ZINC00071549	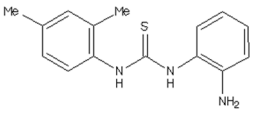
3	ZINC36387124	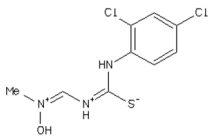
4	ZINC49548396	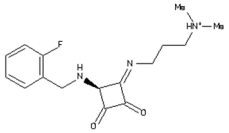
5	ZINC20458476	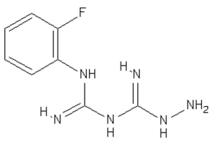
8	ZINC12111719	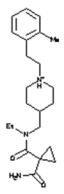
9	ZINC20730335	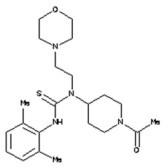

11 ZINC06007372

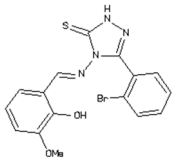

12 ZINC12189047

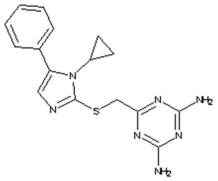

13 ZINC20996195

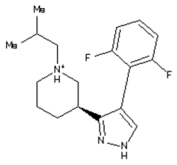

14 ZINC00814215

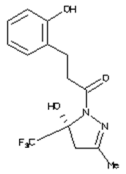

18 ZINC01275149

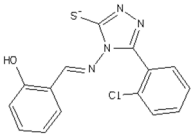

22 ZINC23074792

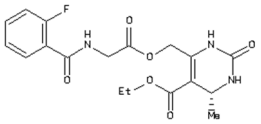

25 ZINC12535527

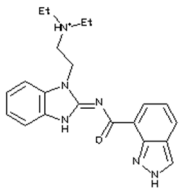

26 ZINC23339753

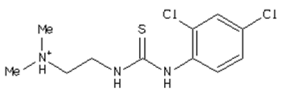

27 ZINC12854257

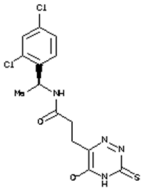

28 ZINC24257742

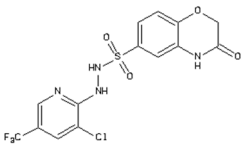

29 ZINC06566370

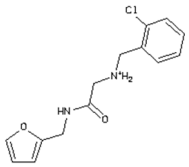

30 ZINC13370159

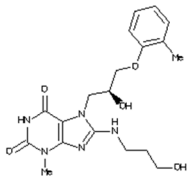

31 ZINC02996799

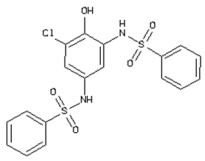

32 ZINC07051195

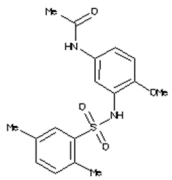

33 ZINC13635395

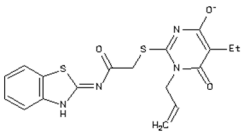

34 ZINC08992977

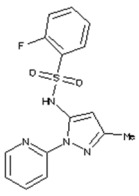

35 ZINC48302855

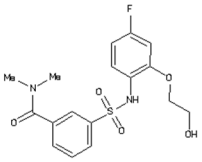

36 ZINC09329817

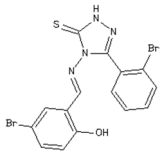

38 ZINC09421768

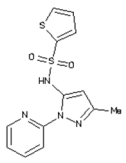

Molecules with electrophilic moieties

Nº	Compound (#ZINC)	Structure
		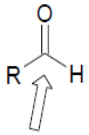
41	ZINC01695170	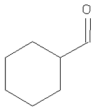
		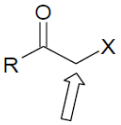
42	ZINC32005992	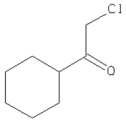
		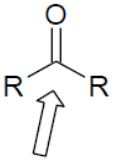
43	ZINC12358900	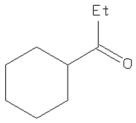

APPENDIX 2 – CONFERENCE PROCEEDINGS, COURSES, INTERNSHIPS & AWARDS

Ap2.1 – Abstracts in Conference proceedings and workshops (the presenter was always the first author)**:**

Ap2.1.1 – Oral Presentation:

- 2016, **V Latin American Protein Society Meeting (LAPSM)**, Rio de Janeiro, RJ, Brazil
  - **Domingos, RM**; Meireles, DA; Teixeira, RD; Alegria, TGP; Netto, LES ***"Dimerization of Organic Hydroperoxide Resistance Proteins is Required for Proper Architecture of Amino Acids in the Active Site: Analysis of a High-Resolution Structure of OhrA from Chromobacterium violaceum"***, eventoexpress.com.br/anais/laps2016/listaresumosoral_1.htm

- 2016, **23rd Annual Meeting of Society for Redox Biology and Medicine, a joint meeting with the Society for Free Radical Research International (SfRBM||SFRRI)**, San Francisco CA, US
  - Meireles, DA; **Domingos, RM**; Alegria, TGP; Netto, LES ***"Analyses of amino acid sequences and tertiary structures among Ohr enzymes revealed a catalytic role for Y126"***, Free Radical Biology and Medicine, Vol.100, p.S27, doi.org/10.1016/j.freeradbiomed.2016.10.067

- 2014, **I Workshop of Redox Signaling and Oxidative Stress Response**, Institute of Biosciences, USP, São Paulo, Brazil
  - **Renato M. Domingos** ***"Comparative Research on Ohr/OsmC Protein Family as Potential Drug Targets"***

Ap2.1.2 – Poster Presentation:

- 2018, **19th Meeting of the Society for Free Radical Research International (SFRRI)**, Lisboa, Portugal
  - **Renato M. Domingos**; Raphael D. Teixeira; Ari Zeida; William A. Agudelo; Thiago G.P. Alegria; Mario T. Murakami; Dario A. Estrin; Luis E.S. Netto ***"Substrate Triggered Structural Movements in Ohr: Dihydrolipoamide Accelerates the Approximation of Catalytic Arg Towards the Active Site"*** Free Radical Biology and Medicine, Vol.120, p.S93, doi.org/10.1016/j.freeradbiomed.2018.04.308

- 2017, **46th Brazilian Society for Biochemistry and Molecular Biology (SBBq)**, Águas de Lindóia, SP, Brazil.
  - **Domingos, RM**; Teixeira, RD; Zeida, A; Alegria TGP.; Estrin, DA; Netto, LES "***First Crystallographic Structure of the Interaction Between an Organic Hydroperoxide Resistance Protein and its Biological Reductant: Structural and Molecular Dynamic Analyses***"

- 2017, **42nd Brazilian Society for Biophysics (SBBf)**, Santos, SP, Brazil.

- **Domingos, RM**; Teixeira, RD; Zeida, A; Agudelo, WA; Alegria TGP; Murakami, MT; Estrin, DA; Netto, LES "***The unique reducing step of organic hydroperoxide resistance proteins: is the catalytic arginine important to activate the reducing agent?***"

- 2015, **23rd International Union of biochemistry and Molecular Biology (IUBMB) || 44th Brazilian Society for Biochemistry and Molecular Biology (SBBq)**, Foz do Iguaçu, PR, Brazil
  - **Renato M Domingos**; Diogo A Meireles; Jose F da Silva Neto; Thiago GP Alegria; Raphael D Teixeira; Luis ES Netto "***The First Structural and Biochemical Comparative analysis of two Organic Hydroperoxide Resistance Paralogues: The Chromobacterium violaceum OhrA and OhrB***" www.sbbq.org.br/iubmb2015/cdrom/resumos/R08839-1.pdf
  - Meireles, DA; **Domingos, RM**; Gaiarsa, JW; Alegria, TGP; Souza, RF; Netto, LES "***Use of residue conservation analysis to identify functional and structural conserved residues of Ohr/OsmC family***"

- 2015, **22nd Annual Meeting of Society for Redox Biology and Medicine (SFRBM)**, Boston, MA, US
  - **Renato M Domingos**, Diogo A Meireles, José F da Silva Neto, Thiago GP Alegria, Mário T Murakami, Raphael D Teixeira, and Luis ES Netto ***"Structural and Biochemical Analysis of the Open Conformation of OhrA & OhrB from Chromobacterium Violaceum, Two Cys-Based Peroxidases with Extraordinary Reactivity Towards Organic Peroxides"*** Free Radical Biology and Medicine, Vol.87, p.S146-147, doi.org/10.1016/j.freeradbiomed.2015.10.377
  - Meireles, D.A.; **Domingos, RM**.; Gaiarsa, J.W.; Souza, R.; Netto, L.E.S. ***"Functional and Biochemical Characterization of the First Ohr Peroxidase Identified in Eukaryotes"*** Free Radical Biology and Medicine, Vol.87, p.S150, doi.org/10.1016/j.freeradbiomed.2015.10.387

- 2014, **21st Annual Meeting of Society for Redox Biology and Medicine (SFRBM)**, Seattle, WA, US
  - **Domingos, RM**; Meireles, DA; da Silva Neto, JF; Viviani, LG; Alegria, TGP; do Amaral, AT; Netto, LES ***"Structural & Biochemical Comparative Analysis Among Cys-based Ohr/OsmC Protein Family: Insight on their High Reactivity towards Hydroperoxides"*** Free Radical Biology and Medicine, Vol.76, p.S156-S157, doi.org/10.1016/j.freeradbiomed.2014.10.061
  - Meireles, DA; **Domingos, RM**.; Souza, R; Netto, LES ***"Distribution and Classification of Cys-Based Proteins of the Ohr/OsmC Family"*** Free Radical Biology and Medicine, Vol.76, p.S142, doi.org/10.1016/j.freeradbiomed.2014.10.118

Ap2.2 – Specialized Courses:

- 2015, ***Redox Chemistry and Biology of Thiols*****,** Institut Pasteur de Montevideo, Montevideo, Uruguay

- 2016, ***CCP4 2016: Macromolecular Crystallography School*** - From data processing to structure refinement and beyond, Instituto de Física de Sao Carlos da Universidade de São Paulo (IFSC-USP), São Carlos, Brazil
- 2016, ***RapiData: Data collection and Structure Solving***, Stanford Synchrotron Radiation Lightsource (SSRL), Stanford, CA, US
- 2016, ***Crystallization: micro and nano-crystals and high throughput methods***, Stanford Synchrotron Radiation Lightsource (SSRL), Stanford, CA, US
- 2017, ***Fundaments in molecular simulation of biomolecules,*** Facultad de Ciencias Exactas y Naturales, Universidad de Buenos Aires (FCEN-UBA), Buenos Aires, Argentina

$_{Ap}$2.3 – Internships:

- 2017 (10 weeks), ***Computational tools on hybrid classical/quantum molecular dynamics***, Dario Estrin laboratory at Facultad de Ciencias Exactas y Naturales, Universidad de Buenos Aires (FCEN-UBA), Buenos Aires, Argentina

$_{Ap}$2.4 – Awards:

- 2017, ***SBBq Award 2017*** for the best poster presented during SBBq. ***"First Crystallographic Structure of the Interaction Between an Organic Hydroperoxide Resistance Protein and its Biological Reductant: Structural and Molecular Dynamic Analyses***". Águas de Lindóia, SP, Brazil
- 2016, ***Young Scientist Travel Award*** during ***"RapiData 2016: Data collection and Structure Solving"***. Stanford Linear Accelerator Center, SLAC, Stanford, CA, US.
- 2016, ***Young Scientist Travel Award*** during ***"Crystallization: micro and nanocrystals and high throughput methods"***. Stanford Linear Accelerator Center, SLAC, CA, Stanford, US.
- 2015, ***Best Poster Award*** during IUBMB||SBBq. ***"The First Structural and Biochemical Comparative analysis of two Organic Hydroperoxide Resistance Paralogues: The Chromobacterium violaceum OhrA and OhrB"***. Foz do Iguaçu, PR, Brazil.